STRENGTH BEHAVIOUR OF JOINTED ROCKS REINFORCED WITH PASSIVE BOLTS

Ph.D. THESIS

by

LOK PRIYA SRIVASTAVA

DEPARTMENT OF CIVIL ENGINEERING
INDIAN INSTITUTE OF TECHNOLOGY ROORKEE
ROORKEE – 247 667 (INDIA)
FEBRUARY, 2015

STRENGTH BEHAVIOUR OF JOINTED ROCKS REINFORCED WITH PASSIVE BOLTS

A THESIS

Submitted in partial fulfilment of the requirements for the award of the degree

of

DOCTOR OF PHILOSOPHY

in

CIVIL ENGINEERING

by

LOK PRIYA SRIVASTAVA

DEPARTMENT OF CIVIL ENGINEERING
INDIAN INSTITUTE OF TECHNOLOGY ROORKEE
ROORKEE – 247 667 (INDIA)
FEBRUARY, 2015

ABSTRACT

Rocks encountered in civil and mining engineering structures are generally intersected by joints. The joints introduce planes of weakness, and sliding of blocks can occur easily along joint planes. Consequently, the jointed rock offers relatively little resistance against failure and strength of rock is considerably reduced. Strength behaviour of jointed rocks (unreinforced) is a complex phenomenon and various studies have been conducted during past to understand the strength behaviour. The studies can be grouped into two major groups. Group I comprises of studies where analysis is conducted in σ, τ space (Patton, 1966; Ladayni and Archambault, 1970; Jaeger, 1971; Barton, 1973). The group II involves those studies where analysis is done in terms of σ_3, σ_1 space (Hoek and Brown, 1980, 1997, 2002; Ramamurthy, 1993; Ramamurthy and Arora, 1994; Singh et al., 2011; Singh and Singh, 2012). Rock bolts are extensively used to enhance strength of jointed rocks, however assessment of strength enhancement in jointed rocks due to provision of bolts is still a challenging task faced by designers. Based on studies available on reinforced rock, it is understood that the strength behaviour of reinforced rock depends on various factors like the strength of the parent rock (Dight, 1982; McHugh and Signer, 1999; Sakurai, 2010), joint orientation, angle of inclination between joint and bolt and diameter of bolt (Bjurström, 1974; Ludvig, 1983; Grasselli et al., 1999, Grasselli, 2005). Further pre tensioning of the bolt has also been an important factor (Dight, 1982; Ferrero, 1995; Jalalifar and Aziz, 2010). An excellent discussion on the difference in the strength behavior of "individual bolt placed to reinforce single joint" and "interaction between bolts and rock mass" has been presented by Ferrero (1995) and Ferrero et al. (1997). Ferrero et al. (1997) emphasized that the assessment of enhancement in the engineering properties of a rock mass is very difficult since it involves complex failure mechanisms, the interaction between different materials and the characteristics of joints. In addition, the complexities of interactions between a large numbers of blocks add to the difficulties. Though several studies have been conducted during past on rocks reinforced with bolts, these studies focused on strength behaviour of single joint rather than a mass. In field, the rock mass comprises of intact rock blocks separated by discontinuities. The strength behaviour of such a

blocky mass is substantially different from single joint due to complex interaction of blocks and scale effect.

The first major objective of the present study has been to investigate the strength behaviour of a blocky mass under un-reinforced and reinforced (with bolts) cases. The objective was achieved by conducting direct shear tests on large sized jointed block mass (750 mm x 750 mm x 900 mm) specimens. Passive rock bolts were used to investigate strength enhancement due to reinforcement. The outcome of this part is applicable in designing rock bolt reinforcement in situations like rock slopes where analysis is done σ, τ space. The another area where rock bolts are frequently used is underground openings in jointed rocks. The analysis in such conditions is done in σ_3, σ_1 space, and a failure criterion is used to assess the strength of unreinforced or reinforced rock subjected to given confining pressure. The stress conditions may vary from almost uniaxial loading condition to very high confining pressure range ($\sigma_3 \gg 0$). The second part of the present study has focused on assessment of strength of reinforced rock under uniaxial and triaxial loading conditions. It is envisaged that if uniaxial compressive strength of jointed rock (reinforced or unreinforced) is assessed with confidence, the additional effect of confining pressure could be incorporated through a suitable strength criterion (Hoek and Brown, 1980, 2002; Ramamurthy, 2001; Singh and Singh, 2012). Uniaxial and triaxial tests were conducted on intact and jointed specimens of synthetic and natural rocks. Tests were also conducted on reinforced specimens. The results were analysed and an approach for assessing the strength of reinforced rock has been suggested. In the following sections, a brief abstract of the study is presented.

As a part of first objective, the direct shear tests were conducted on blocky mass specimens of size 750 mm x 750mm x 900 mm (height). For this purpose a specially designed and fabricated direct shear test apparatus was used. The size of shear box in the apparatus is 750 mm x 750mm x 1000 mm (height). To form the elemental blocky mass, concrete blocks of size 150 mm x150 mm x150 mm were used. About 150 blocks of concrete were required for conducting one test. The uniaxial compressive strength of intact material is about 42 MPa. Formed blocky mass consists of three orthogonal joint sets spaced at 150 mm centre to centre. To

reinforce the mass, six mm diameter steel bars having tensile strength 550 MPa were used. The bolts were installed perpendicular to the shearing direction, and were grouted with cement mortar. Three different configurations of bolts were used in which numbers of bolts and bolt spacing were varied. Tests were performed for a normal stress range of 0 to 2 MPa. In case of unreinforced blocky mass, sliding of blocks was observed at all the normal stress levels. When bolts were installed, the sliding through the joint plane was restricted. The results indicated increase in shear strength with increase in normal stress for unreinforced as well as reinforced specimens. The shear stress (τ) vs horizontal shear displacement (δ_H) plots of reinforced blocky mass exhibit two distinct segments. The first part of the plot was relatively flat and second part was steep. The first part indicates the mobilization of shear stress due to the interaction of the blocks, while second part indicates the mobilization of shear stress through the bolts. It is found that for all the normal stress levels, provision of bolts enhances the shear strength of blocky mass. The main reasons for enhancement in shear strength are improved interlocking by bolts, and generation of additional normal stress on joint surfaces due to development of tensile stress in the bolt. Due to improved interlocking produced by the bolts, the stiffness of the mass enhances. The rock mass, therefore, becomes stiffer and stronger. Installation of bolts enhances the cohesion (c_{j_mass}) of blocky mass whereas the friction angle (ϕ_{j_mass}) remains almost constant (with some scatter). For practical purpose, it may be assumed that the friction angle of series of joints in mass ϕ_{j_mass} is equal to the friction angle of a single joint ϕ_j and effect of reinforcement may be considered through enhanced value of cohesion. The enhanced value of c_{j_mass} is always less then intact rock cohesion (c_i). The enhancement in shear strength depends on amount of reinforcement, spacing between joints, spacing between bolts and imposed normal stress. Increase in amount of reinforcement and reduction in bolt spacing results in increase in the shear strength of blocky mass at all normal stress levels. However, the change in shear strength enhancement per unit change in normal stress decreases with increasing normal stress for each configuration of reinforced mass. Based on the results of direct shear tests the following correlation has been developed to assess the shear strength of a reinforced mass subjected to a given normal stress (σ_n)

$$\tau_f = c_i \left(0.04 \; ln \left(\frac{A_r}{N} \right) + \; 0.24 \right) + c_j + \sigma_n \; tan\phi_j$$

where τ_f = shear strength of reinforced mass; c_i = cohesion of intact rock material; A_r = percent area ratio, N = spacing ratio, c_j = cohesion of a single joint and ϕ_j = friction angle of single joint. The proposed correlation may be used in the field to assess shear strength of mass where analysis is done in τ - σ_n space like slopes. The correlation may also be used to optimise the number of bolts to reinforce the slopes.

The designer needs an understanding of triaxial strength behaviour of rock for designing structure in rocks. For assessing triaxial strength of reinforced rock, a suitable strength criterion may be used. The starting point of the strength criterion is the uniaxial compressive strength (UCS). If an accurate assessment of UCS could be made, triaxial strength can also be predicted accurately. Experimental studies have been conducted to get insight into UCS of jointed unreinforced and reinforced rocks. As second objective of the study, uniaxial compression tests were performed on the prismatic specimens of synthetic rocks (size 150 mm x 150 mm x 300 mm (height)). Two different grades of concrete (referred to T2 and T3) were used as model material. The uniaxial compressive strength of cylindrical specimens of the model material was 84 MPa and 127 MPa for T2 and T3 types of synthetic rock respectively. The jointed specimens of synthetic rocks consist of one smooth joint orientated at 0° to 90° with the base of the specimen. For preparing reinforced jointed specimens, two steel bars of diameter 6 mm were installed in the specimens, and were grouted with 2 mm thick cement-mortar. Bolts were installed perpendicular to loading direction and spaced at 50 mm c/c. The results of uniaxial compression tests were obtained in the form of uniaxial compressive strength (σ_{ci}) and tangent modulus (E_{t50}) and failure modes were recorded. In general, the specimens of unreinforced and reinforced synthetic rocks (both T2 and T3) failed due to splitting. Sliding failure was observed only for unreinforced specimens having θ = 45° and 60°. Due to installation of bolts, the sliding failure mode was altered to splitting. It was found that the strength as well as modulus of jointed rocks were enhanced due to provision of bolts. The enhancement in strength and modulus was mainly due to improved interlocking produced by the bolts. The maximum enhancement was found at orientations where sliding mode of

failure was observed (θ = 45° and 60°) in unreinforced specimens and reinforcement altered the failure mode.

The third part of study involves laboratory tests for evaluating failure criteria for reinforced rock. Triaxial compression tests were performed on the specimens of natural jointed rocks (cylindrical specimens of NX size) without and with bolt. The uniaxial compressive strength of intact material was about 87 MPa. The height to diameter ratio of the prepared specimens was about 2. The joint orientation (θ) of specimens was varied from 0° to 90° with respect to base of the specimens. To reinforce the rock, 4 mm diameter bolt was installed perpendicular to loading direction. The bolt was grouted with 1 mm thick cement mortar. The ends of the bolt were tightened by nut washer system. The specimens were tested at confining pressure of 0, 5, 20, and 40 MPa respectively. Load, displacement and failure modes were recorded. It is observed that the unreinforced jointed rocks exhibit splitting, shearing, and sliding or a combination of these failure modes. In case of reinforced specimens, only sliding and shearing or combination of theses failure modes were observed. Sliding failure was observed only between θ = 30° to 80° at σ_3 = 0 MPa for unreinforced jointed rocks. Provision of bolt altered the sliding mode of failure into splitting or shearing. The results of triaxial tests were plotted in the form of σ_1 vs σ_3. For both unreinforced and reinforced jointed rocks, an increase in confining stress (σ_3) results in increase in the strength (σ_1). The variation of σ_1 with σ_3 is found to be non-linear for all the cases. Results also indicate that the provision of bolt enhances the strength of rocks at all the confining stress levels and reduces the anisotropy ratio. However, increase in confining pressure reduces the bolt contribution toward strength enhancement. The value of strength parameters (c and ϕ) were also altered due to installation of bolt.

The results obtained from uniaxial compression tests on natural and synthetic rocks were plotted on Deere-Miller (1966) classification chart. It was observed that strength and modulus of intact, unreinforced and reinforced rocks are uniquely correlated with each other and assessment of UCS can be done if modulus is available. The following correlations were obtained

$$\frac{\sigma_{cju}}{\sigma_{ci}} = \left[\frac{E_{ju}}{E_i}\right]^{0.67}$$

$$\frac{\sigma_{cjr}}{\sigma_{ci}} = \left[\frac{E_{jr}}{E_i}\right]^{0.67}$$

where σ_{ci} and E_i = uniaxial compressive strength and modulus of intact rock; σ_{cju} and E_{ju} = uniaxial compressive strength and modulus of unreinforced jointed rock; σ_{jr} and E_{jr} = uniaxial compressive strength and modulus of reinforced jointed rock. In the field, it is relatively easy to get modulus of the mass either through testing or through back analysis. Using the modulus of rock mass and laboratory value of strength and modulus of intact rock, a reasonable estimate can be made on UCS of reinforced rock.

Analysis of triaxial results suggested that for sliding failure in jointed rocks the single plane of weakness theory associated with Barton (1976) criterion could be used with confidence. For non-sliding failure the criterion proposed by Singh and Singh (2012) can be used if effect of *JCS* and *JRC* are incorporated. The following criterion is proposed for non-sliding failure of unreinforced rock as well as for reinforced rocks

$$\sigma_1 = \sigma_{cj} \ (or \ \sigma_{cr}) + \left(\frac{2 \sin(\phi_{i0}+JRC)}{1-\sin(\phi_{i0}+JRC)} + 1\right)\sigma_3 - \frac{1}{JCS}\frac{\sin(\phi_{i0}+JRC)}{1-\sin(\phi_{i0}+JRC)}\sigma_3^2 \quad for \ \frac{\sigma_3}{JCS} \leq 0.3$$

and

$$\sigma_1 = \sigma_{cj} \ (or \ \sigma_{cr}) + \left(\frac{2 \sin(\phi_{i0})}{1-\sin(\phi_{i0})} + 1\right)\sigma_3 - \frac{1}{JCS}\frac{\sin(\phi_{i0})}{1-\sin(\phi_{i0})}\sigma_3^2 \quad\quad for \ \frac{\sigma_3}{JCS} > 0.3$$

where σ_{cj} and σ_{cr} is the uniaxial compressive strength of unreinforced and reinforced jointed rock respectively. The above-proposed criterion can be used for assessing the strength of reinforced rock subjected to a given σ_3.

ACKNOWLEDGEMENTS

APPENDIX I

AXIAL STRESS VS AXIAL STRAIN PLOTS OF INTACT (PRISMATIC), UNREINFORCED AND REINFORCED SYNTHETIC ROCKS (T2 AND T3)
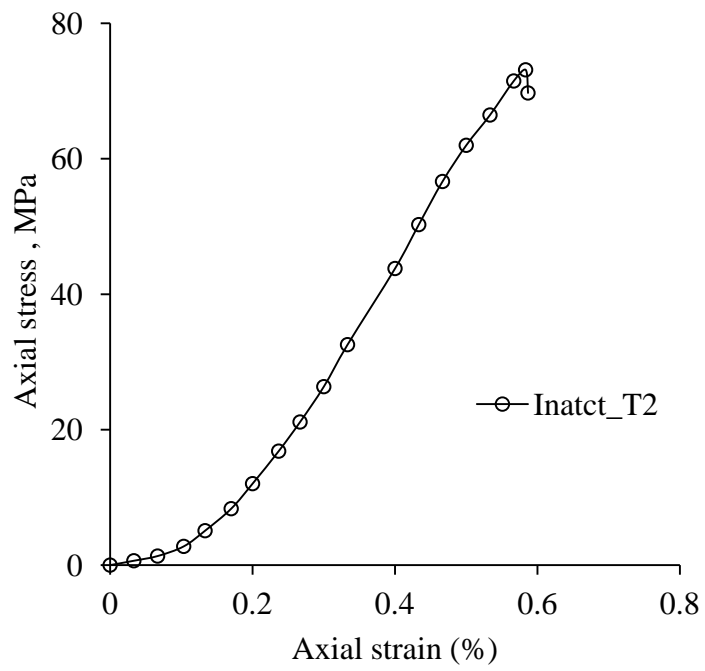
Fig.A-I.1 Axial stress vs axial strain plot of intact (prismatic section) synthetic

rock (T2)

Observations

Peak stress	73.13 MPa
Axial strain at failure	0.583 %
Mode of failure	Splitting
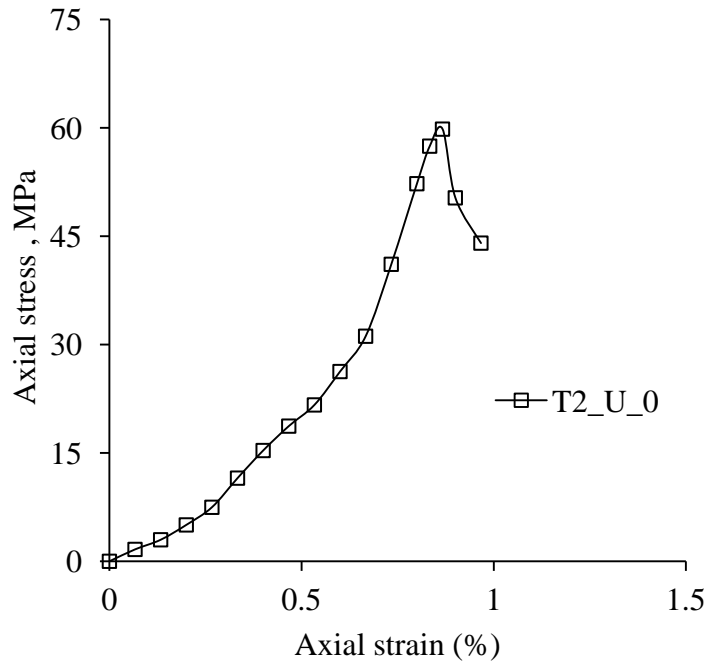
Fig.A-I.2 Axial stress vs axial strain plot of unreinforced jointed synthetic rock

(T2) at $\theta = 0°$

Observations

Peak stress	59.82 MPa
Axial strain at failure	0.867 %
Mode of failure	Splitting

Fig.A-I.3 Axial stress vs axial strain plot of unreinforced jointed synthetic rock

(T2) at $\theta = 15°$

Observations

Peak stress	52.62 MPa
Axial strain at failure	0.70 %
Mode of failure	Splitting

Fig.A-I.4 Axial stress vs axial strain plot of unreinforced jointed synthetic rock

(T2) at θ = 30°

Observations

Peak stress	44.36 MPa
Axial strain at failure	0.90 %
Mode of failure	Splitting

Fig.A-I.5 Axial stress vs axial strain plot of unreinforced jointed synthetic rock

(T2) at $\theta = 45°$

Observations

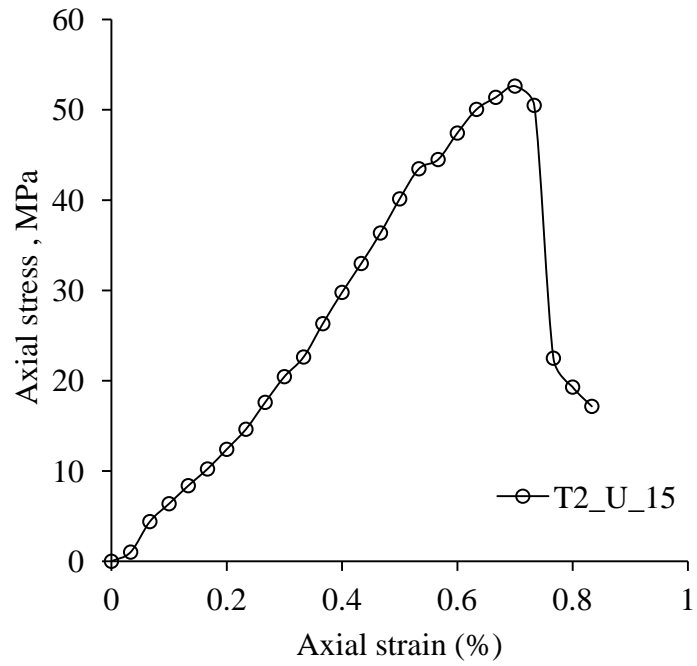|	
Peak stress	0.19 MPa
Axial strain at failure	1.093 %
Mode of failure	Sliding

Fig.A-I.6 Axial stress vs axial strain plot of unreinforced jointed synthetic rock

(T2) at $\theta = 60°$

Observations

Peak stress	0.10 MPa
Axial strain at failure	1.807 %
Mode of failure	Sliding

Fig.A-I.7 Axial stress vs axial strain plot of unreinforced jointed synthetic rock

(T2) at θ = 75°

Observations

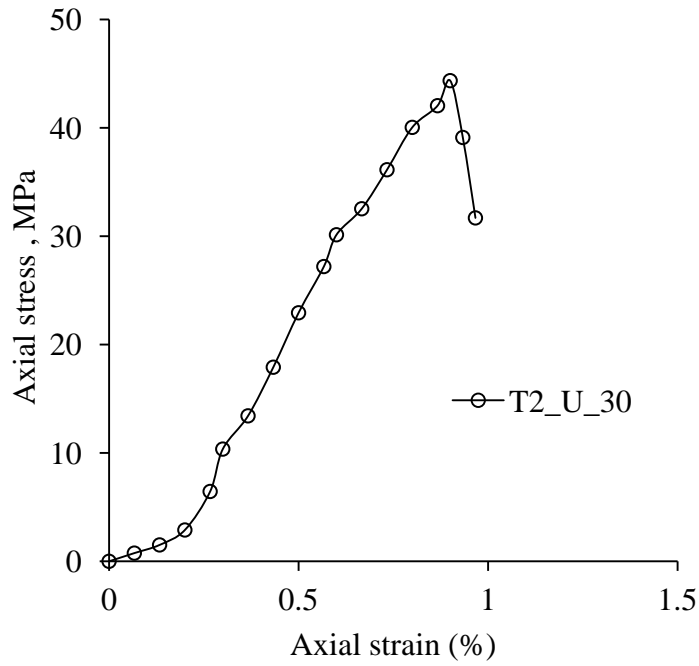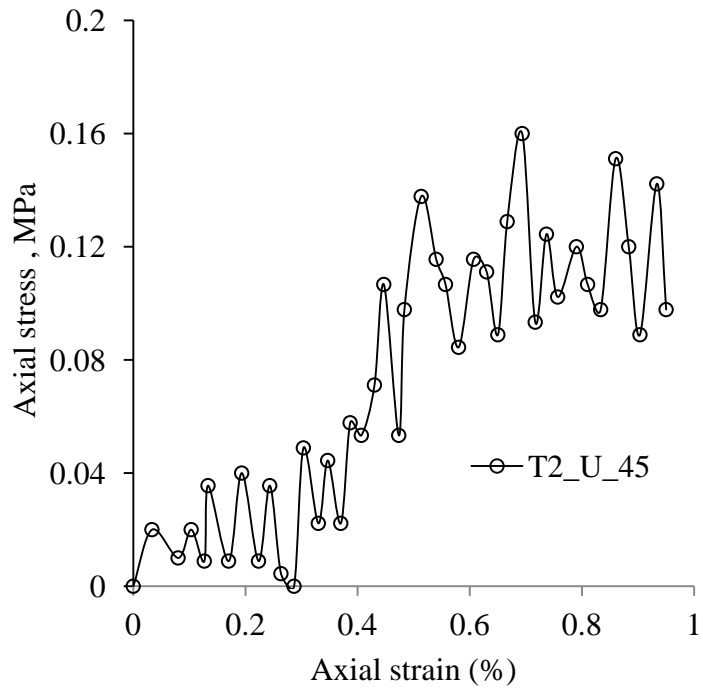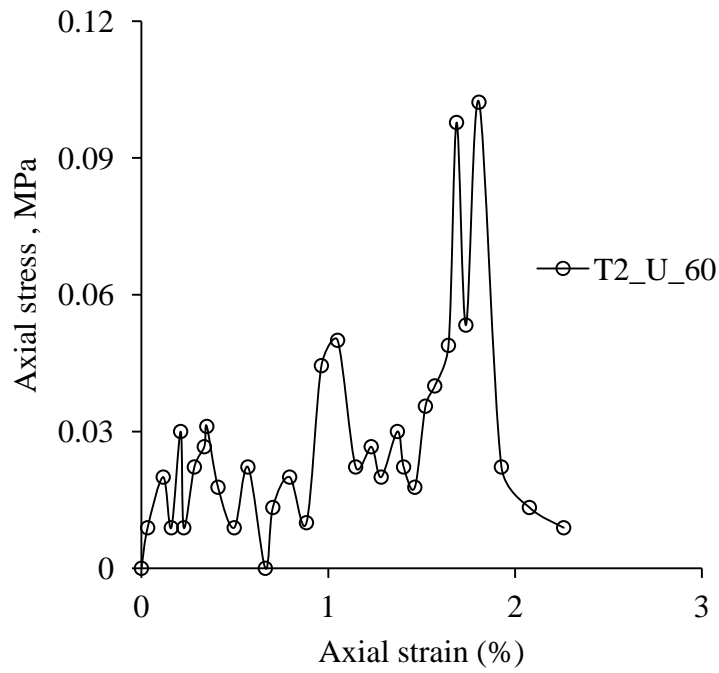|	
Peak stress	40.93 MPa
Axial strain at failure	0.80 %
Mode of failure	Splitting

Fig.A-I.8 Axial stress vs axial strain plot of unreinforced jointed synthetic rock

(T2) at $\theta = 90°$

Observations

Peak stress   45.96 MPa

Axial strain at failure   1.067 %

Mode of failure   Splitting

Fig.A-I.9 Axial stress vs axial strain plot of reinforced jointed synthetic rock (T2)

at $\theta = 15°$

Observations

Peak stress	55.02 MPa
Axial strain at failure	0.633 %
Mode of failure	Splitting
Deformation in bolt	No

Fig.A-I.10 Axial stress vs axial strain plot of reinforced jointed synthetic rock

(T2) at $\theta = 30°$

Observations

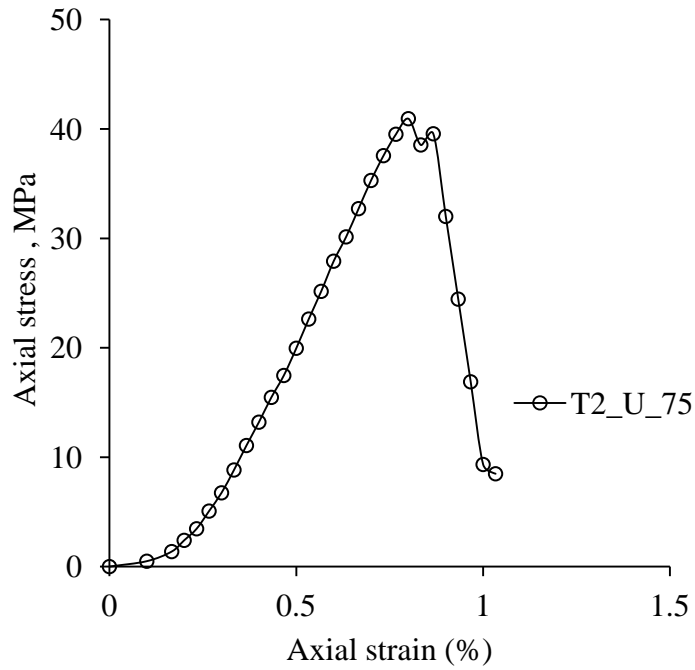|	
Peak stress	54.93 MPa
Axial strain at failure	0.767 %
Mode of failure	Splitting
Deformation in bolt	No

Fig.A-I.11 Axial stress vs axial strain plot of reinforced jointed synthetic rock

(T2) at $\theta = 45°$

Observations

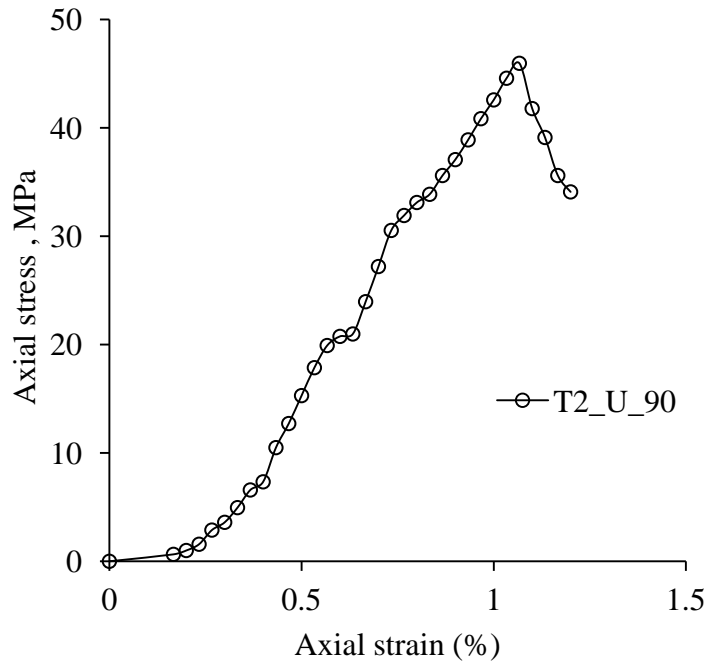|	
Peak stress	9.57 MPa
Axial strain at failure	1.073 %
Mode of failure	Splitting
Deformation in bolt	Slight

Fig.A-I.12 Axial stress vs axial strain plot of reinforced jointed synthetic rock

(T2) at $\theta = 60°$

Observations

Peak stress	4.97 MPa
Axial strain at failure	1.550 %
Mode of failure	Splitting
Deformation in bolt	Slight

Fig.A-I.13 Axial stress vs axial strain plot of reinforced jointed synthetic rock
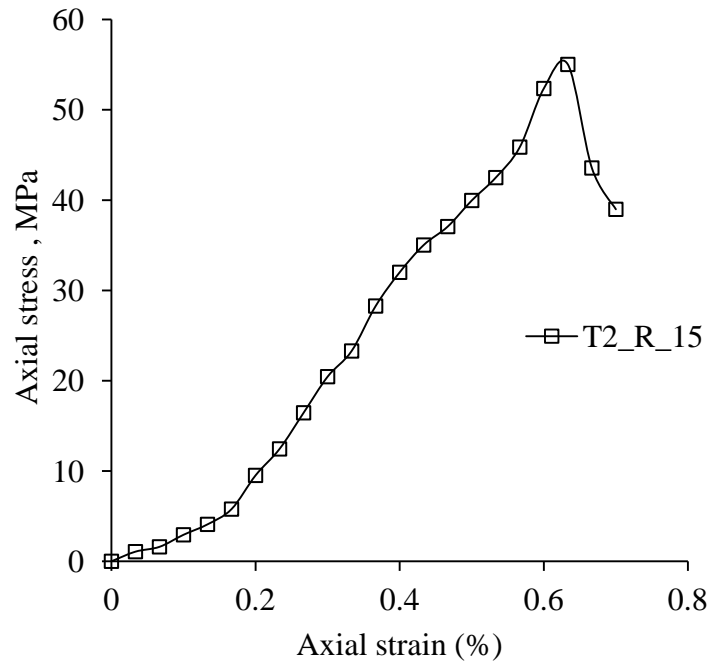
(T2) at $\theta = 75°$

Observations

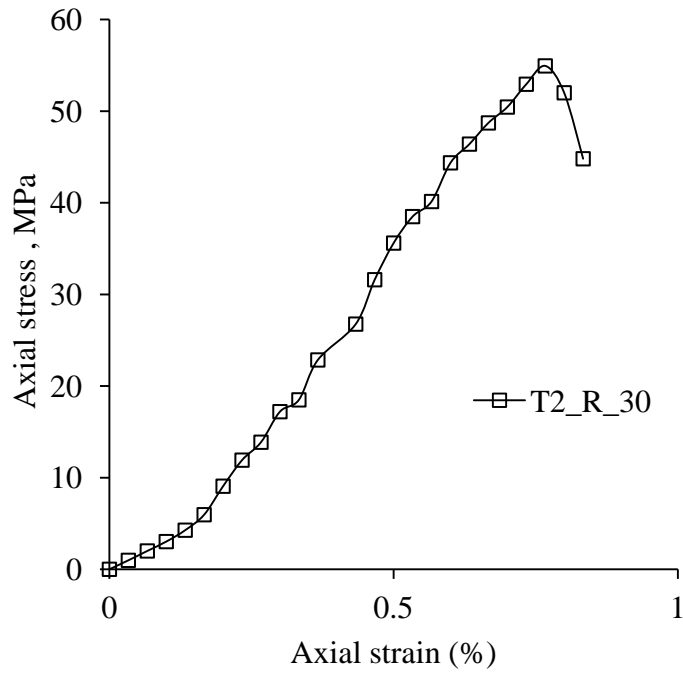|	
Peak stress	43.14 MPa
Axial strain at failure	0.60 %
Mode of failure	Splitting
Deformation in bolt	No

Fig.A-I.14 Axial stress vs axial strain plot of reinforced jointed synthetic rock

(T2) at $\theta = 90°$

Observations

Peak stress	50.40 MPa
Axial strain at failure	0.90 %
Mode of failure	Splitting
Deformation in bolt	No

Fig.A-I.15 Axial stress vs axial strain plot of intact (prismatic) synthetic rock

(T3)

Observations

Peak stress	97.56 MPa
Axial strain at failure	0.467 %
Mode of failure	Splitting

Fig.A-I.16 Axial stress vs axial strain plot of unreinforced jointed synthetic rock

(T3) at *θ* = 0°

Observations

Peak stress	86.00 MPa
Axial strain at failure	0.650 %
Mode of failure	Splitting

Fig.A-I.17 Axial stress vs axial strain plot of unreinforced jointed synthetic rock
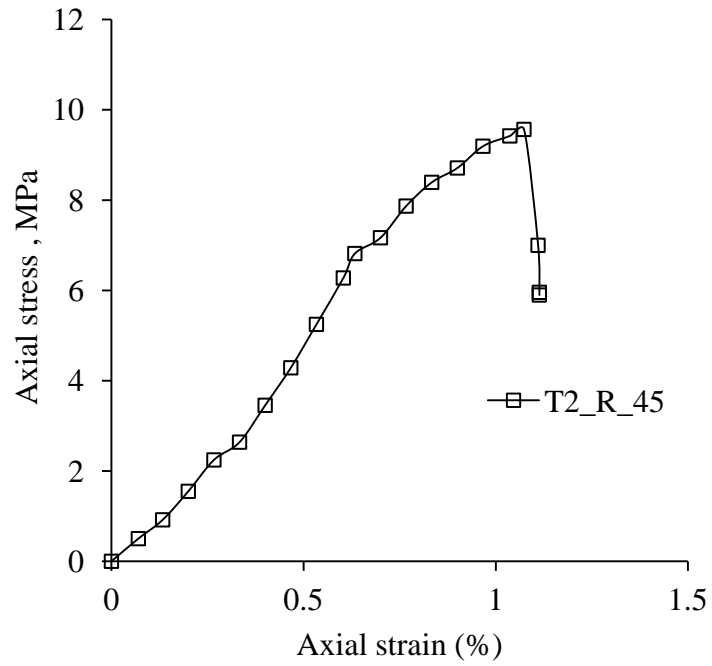
(T3) at $\theta = 15°$

Observations

Peak stress	74.76 MPa
Axial strain at failure	0.800 %
Mode of failure	Splitting

Fig.A-I.18 Axial stress vs axial strain plot of unreinforced jointed synthetic rock
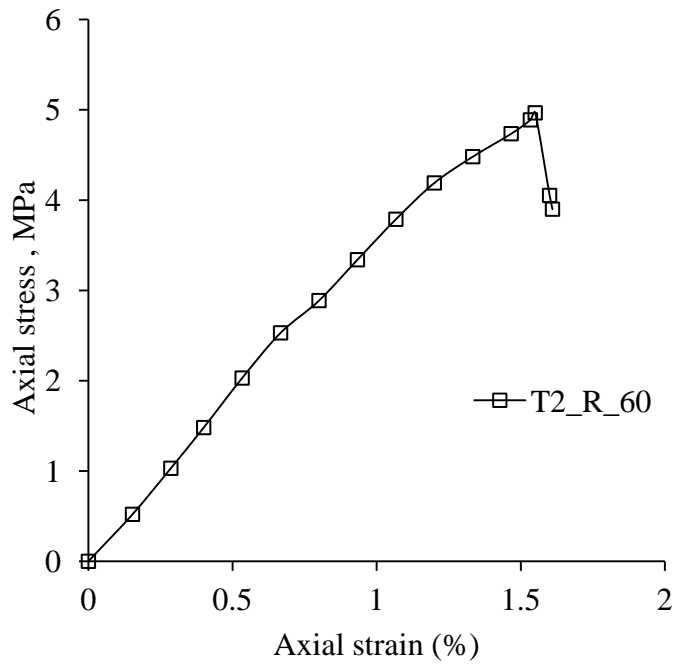
(T3) at $\theta = 30°$

Observations

Peak stress	73.69 MPa
Axial strain at failure	0.867 %
Mode of failure	Splitting

Fig.A-I.19 Axial stress vs axial strain plot of unreinforced jointed synthetic rock

(T3) at $\theta = 45°$

Observations

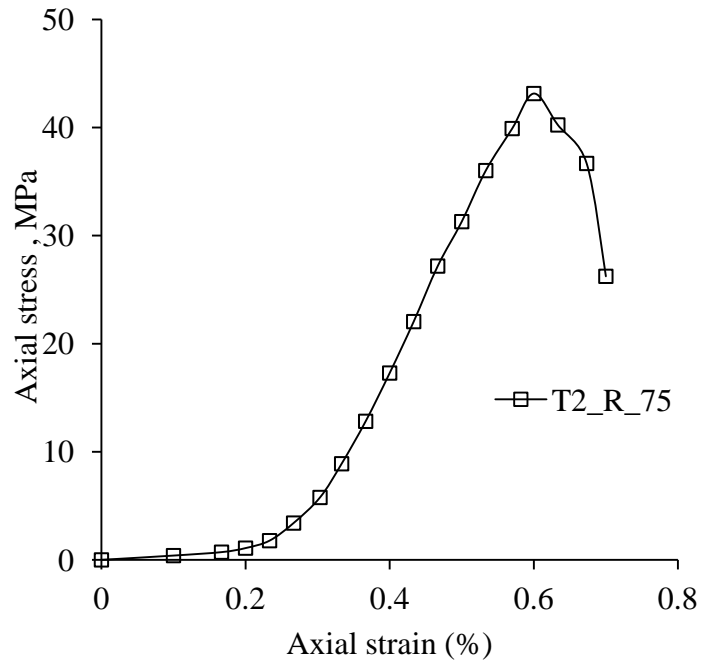|	
Peak stress	0.13 MPa
Axial strain at failure	1.197 %
Mode of failure	Sliding
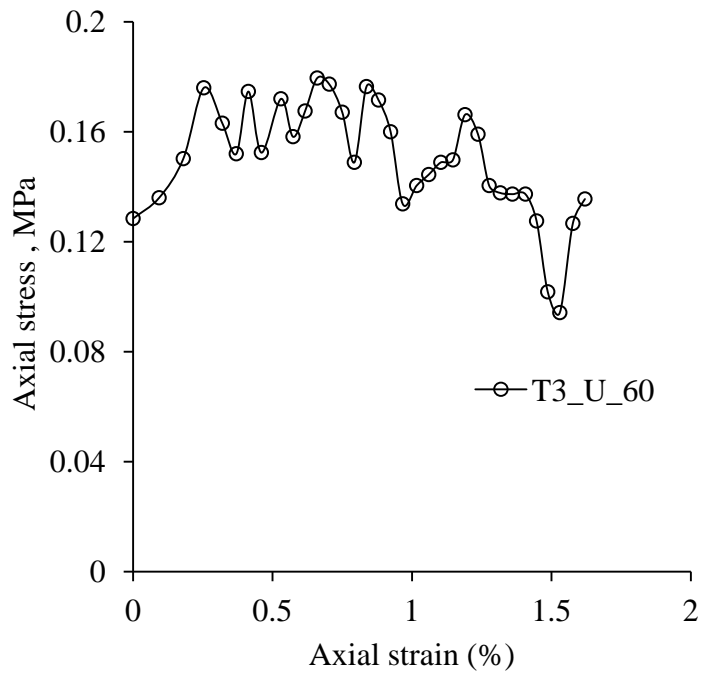
Fig.A-I.20 Axial stress vs axial strain plot of unreinforced jointed synthetic rock

(T3) at $\theta = 60°$

Observations

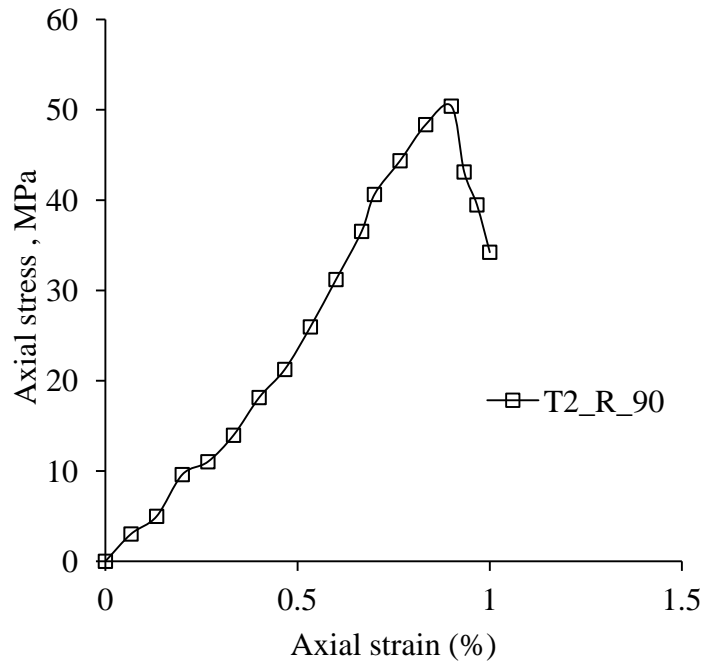|	
Peak stress	0.18 MPa
Axial strain at failure	0.680 %
Mode of failure	Sliding
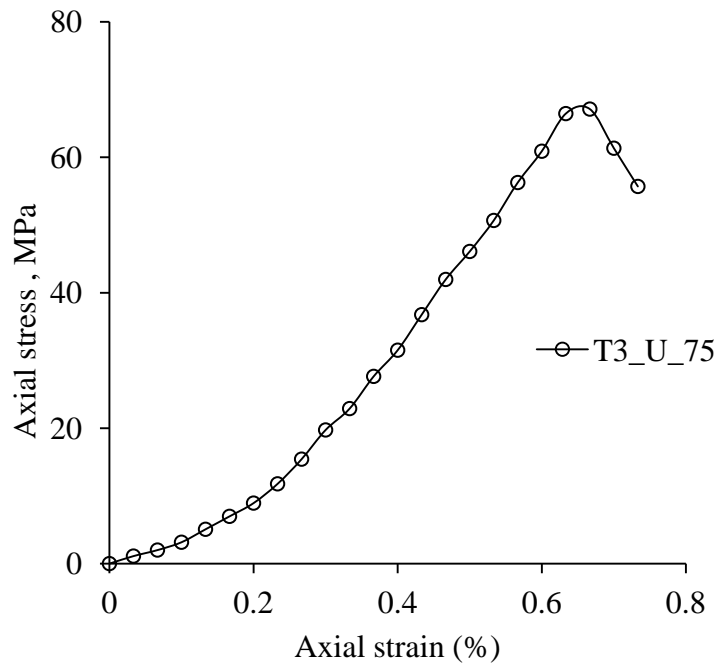
Fig.A-I.21 Axial stress vs axial strain plot of unreinforced jointed synthetic rock

(T3) at $\theta = 75°$

Observations

Peak stress	67.11 MPa
Axial strain at failure	0.667 %
Mode of failure	Splitting
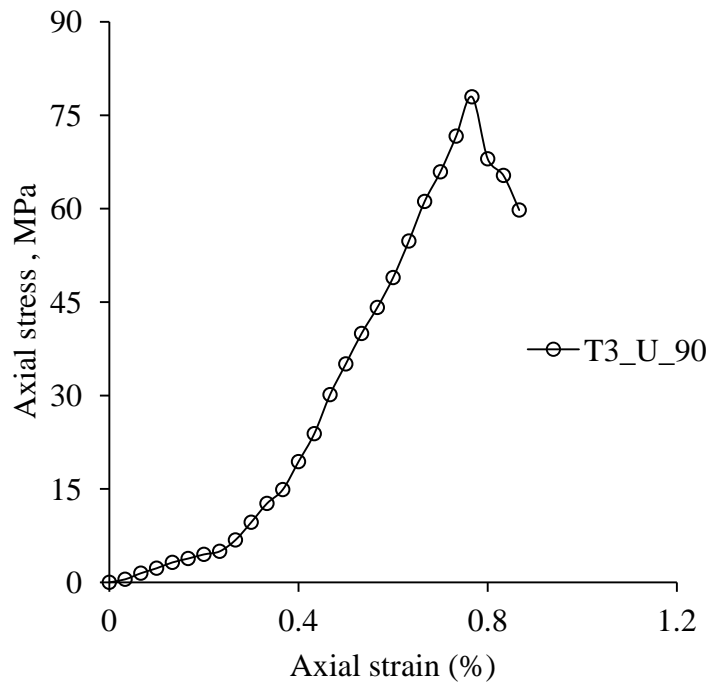
Fig.A-I.22 Axial stress vs axial strain plot of unreinforced jointed synthetic rock

(T3) at *θ* = 90°

Observations

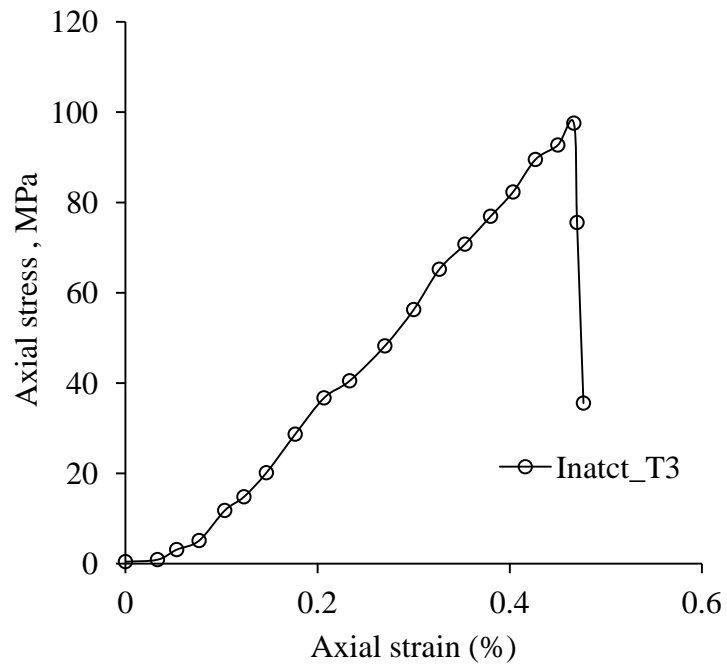|	
Peak stress	77.96 MPa
Axial strain at failure	0.767 %
Mode of failure	Splitting
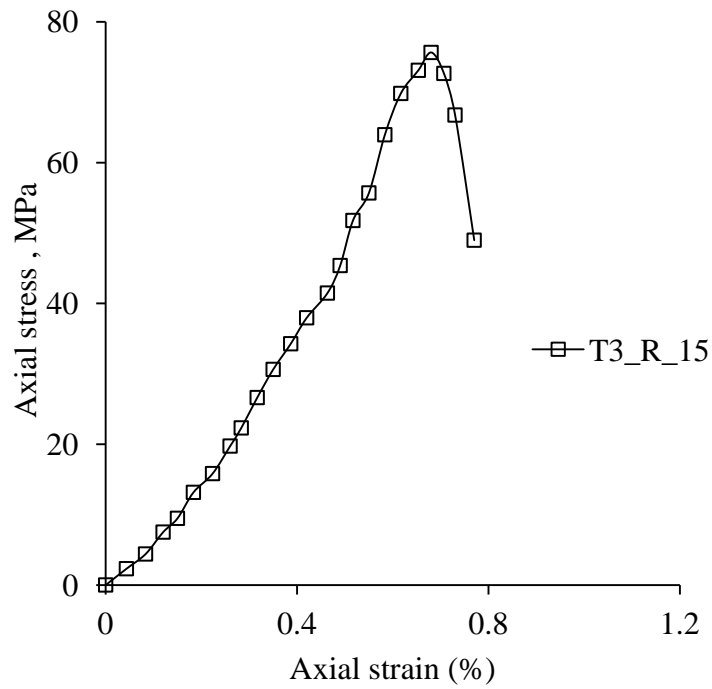
Fig.A-I.23 Axial stress vs axial strain plot of reinforced jointed synthetic rock

(T3) at $\theta = 15°$

Observations

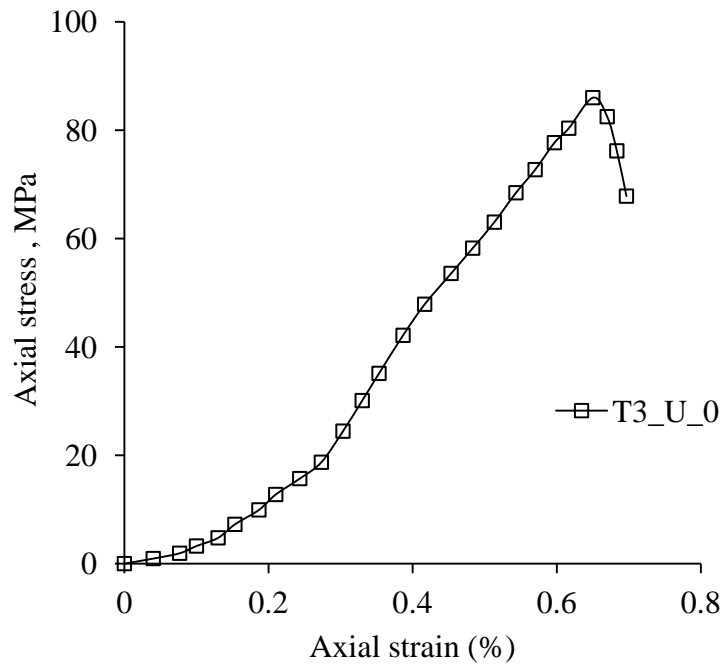|	
Peak stress	75.64 MPa
Axial strain at failure	0.680 %
Mode of failure	Splitting
Deformation in bolt	No

311
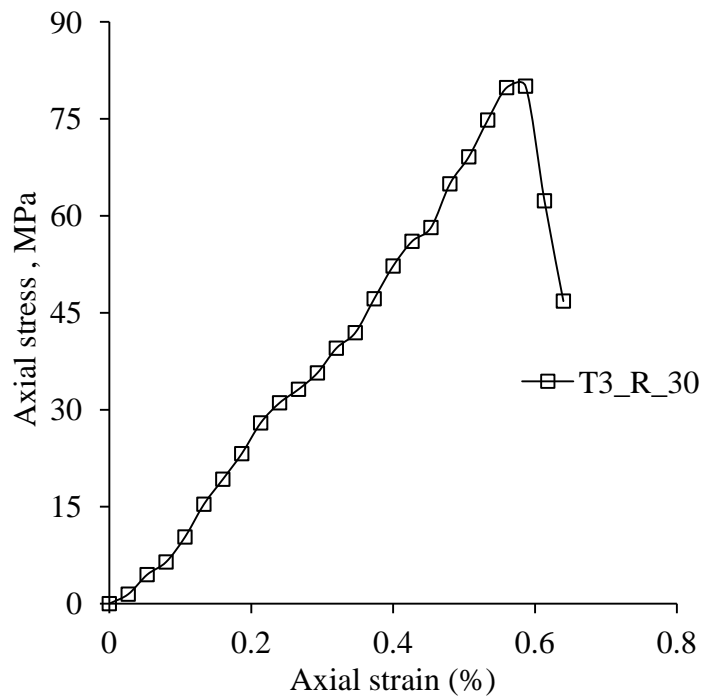
Fig.A-I.24 Axial stress vs axial strain plot of reinforced jointed synthetic rock

(T3) at $\theta = 30°$

Observations

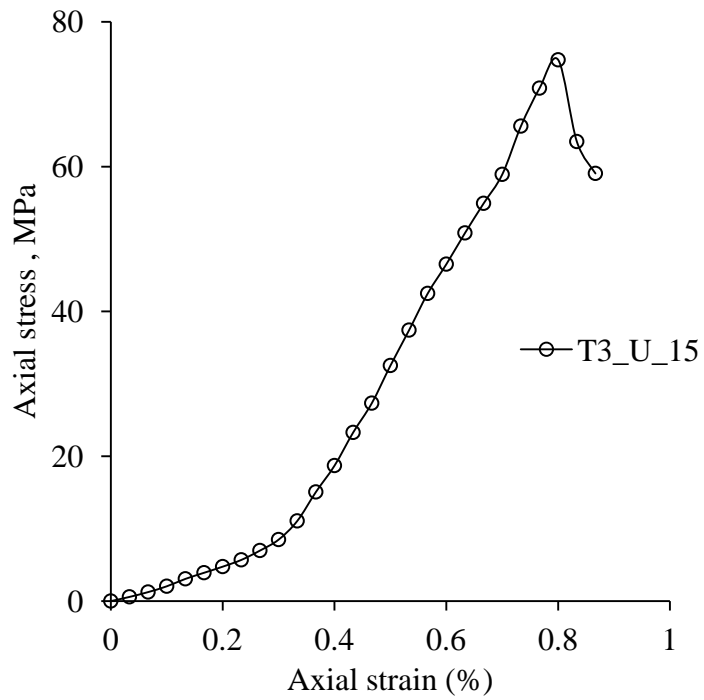|	
Peak stress	80.04 MPa
Axial strain at failure	0.587 %
Mode of failure	Splitting
Deformation in bolt	No
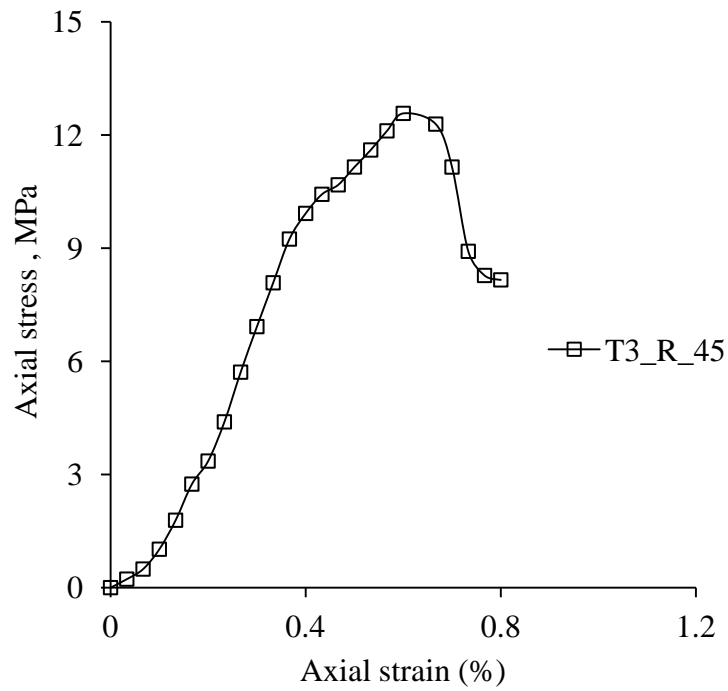
Fig.A-I.25 Axial stress vs axial strain plot of reinforced jointed synthetic rock

(T3) at $\theta = 45°$

Observations

Peak stress	12.57 MPa
Axial strain at failure	0.60 %
Mode of failure	Splitting
Deformation in bolt	Slight
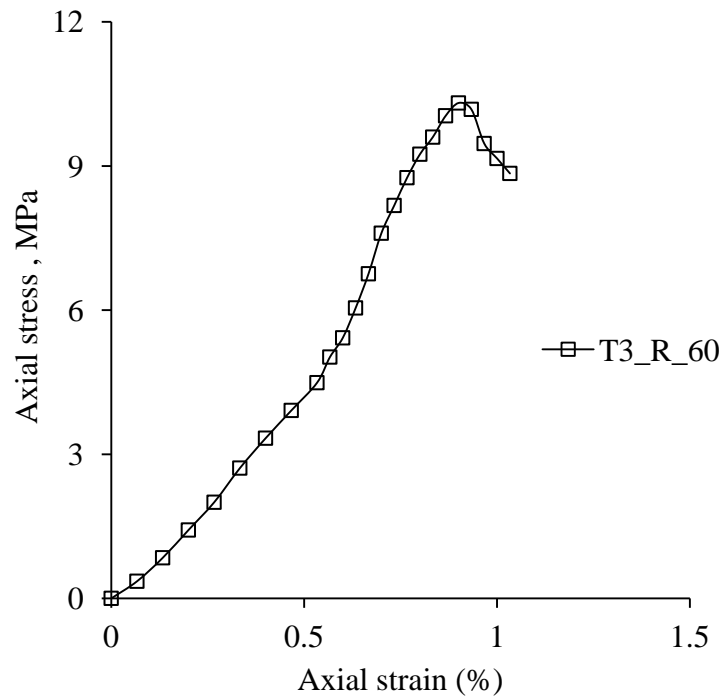
Fig.A-I.26 Axial stress vs axial strain plot of reinforced jointed synthetic rock
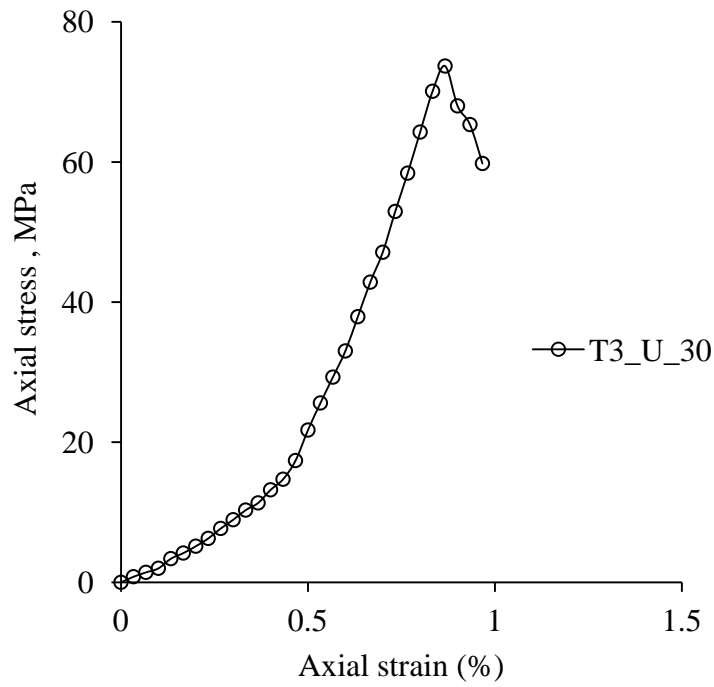
(T3) at *θ* = 60°

Observations

Peak stress	10.31 MPa
Axial strain at failure	0.90 %
Mode of failure	Splitting
Deformation in bolt	Slight
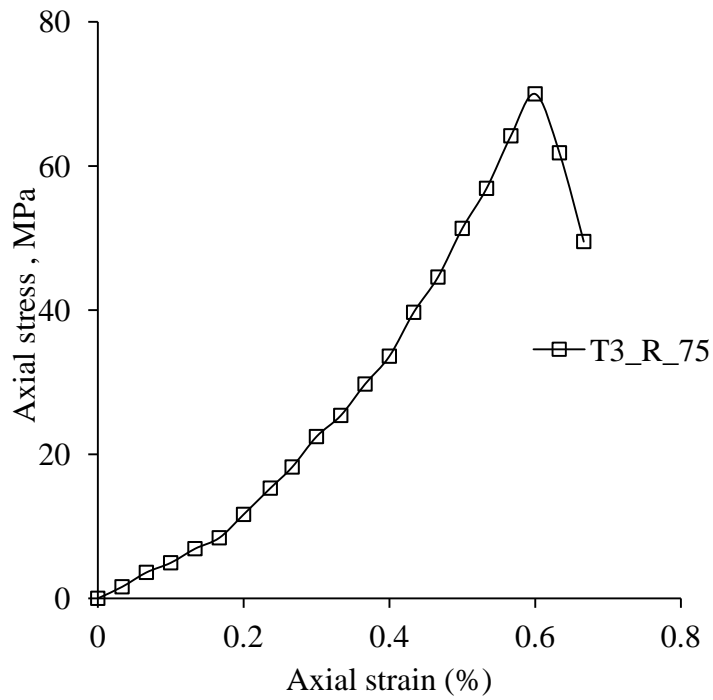
Fig.A-I.27 Axial stress vs axial strain plot of reinforced jointed synthetic rock

(T3) at θ = 75°

Observations

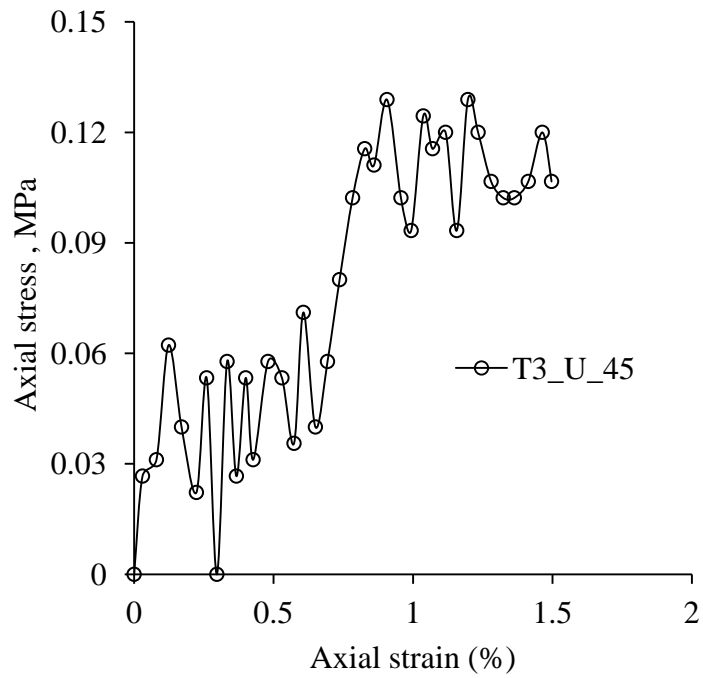|	
Peak stress	70.00 MPa
Axial strain at failure	0.60 %
Mode of failure	Splitting
Deformation in bolt	No
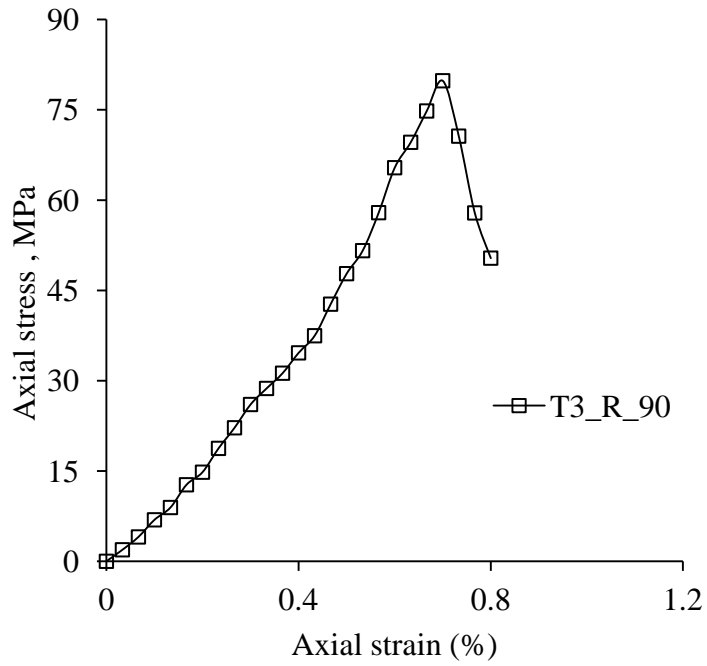
Fig.A-I.28 Axial stress vs axial strain plot of reinforced jointed synthetic rock

(T3) at $\theta = 90°$

Observations

|	
Peak stress	79.82 MPa
Axial strain at failure	0.70 %
Mode of failure	Splitting
Deformation in bolt	No

APPENDIX II

DEVIATOR STRESS VS AXIAL STRAIN PLOTS OF INTACT, UNREINFORCED JOINTED AND REINFORCED JOINTED NATURAL ROCK AT DIFFERENT CONFINING STRESS LEVELS
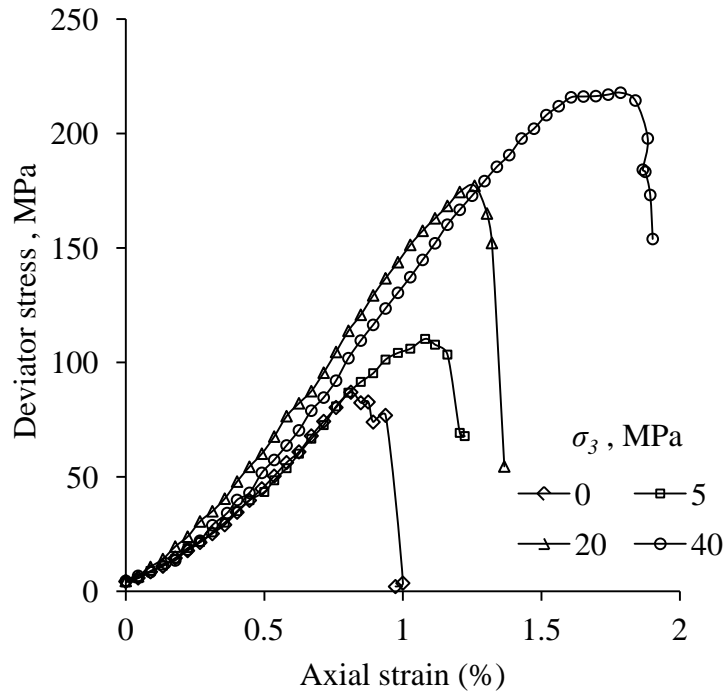
Fig.A-II.1 Deviator stress vs axial strain plots of intact rock at different confining

stress levels

σ_3 , MPa	Observations		
	σ_d, MPa	ϵ, %	Failure mode
0.0	87.00	0.813	Sliding
5.0	110.31	1.08	Splitting
20.0	177.19	1.259	Splitting
40.0	217.86	1.786	Splitting + Shearing
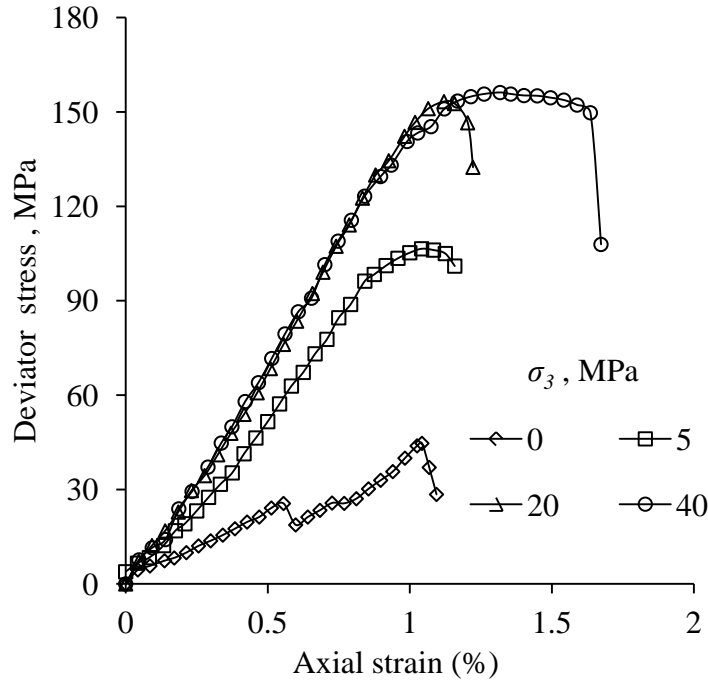
Fig.A-II.2 Deviator stress vs axial strain plots of unreinforced jointed rock (θ = 0°-10°) at different confining stress levels

σ_3 , MPa	Observations		
	σ_d, MPa	ϵ, %	**Failure mode**
0.0	44.69	1.043	Splitting
5.0	106.52	1.042	Splitting
20.0	153.29	1.120	Splitting
40.0	156.18	1.318	Splitting + Shearing
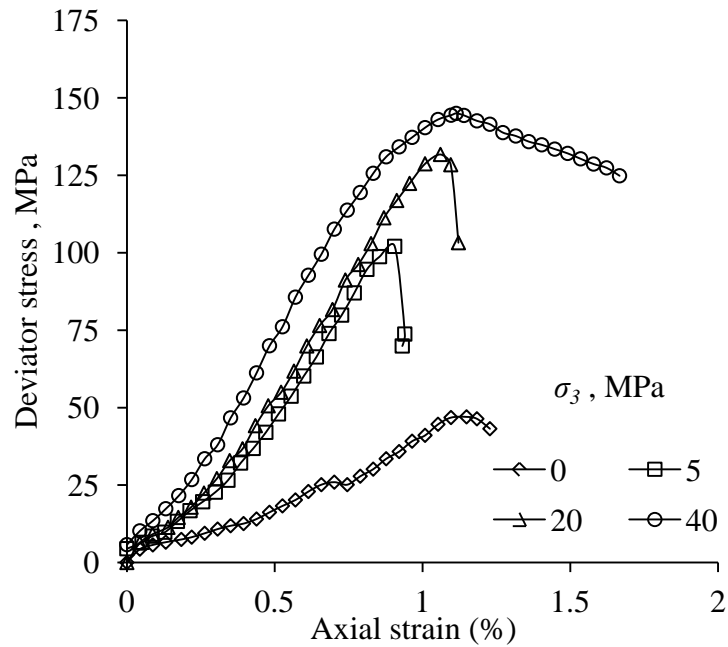
Fig.A-II.3 Deviator stress vs axial strain plots of unreinforced jointed rock (θ = 10°-20°) at different confining stress levels

σ_3 , MPa	Observations		
	σ_d, MPa	ϵ, %	Failure mode
0.0	47.01	1.149	Splitting
5.0	102.05	0.906	Splitting
20.0	131.71	1.061	Splitting
40.0	144.96	1.114	Splitting + Shearing

Fig.A-II.4 Deviator stress vs axial strain plots of unreinforced jointed rock (θ = 20°-30°) at different confining stress levels

σ_3 , MPa	Observations		
	σ_d, MPa	ϵ, %	Failure mode
0.0	32.02	0.883	Splitting
5.0	54.05	0.585	Splitting
20.0	65.55	1.545	Splitting + Shearing
40.0	89.12	0.927	Splitting

Fig.A-II.5 Deviator stress vs axial strain plots of unreinforced jointed rock (θ = 30°-40°) at different confining stress levels

σ_3 , MPa	Observations		
	σ_d, MPa	ϵ, %	Failure mode
0.0	6.55	0.094	Sliding
5.0	44.58	0.525	Splitting + Shearing
20.0	46.94	0.619	Splitting
40.0	95.69	1.139	Splitting

Fig.A-II.6 Deviator stress vs axial strain plots of unreinforced jointed rock (θ = 40°-50°) at different confining stress levels

σ_3 , MPa	Observations		
	σ_d, MPa	ϵ, %	Failure mode
0.0	1.22	0.98	Sliding
5.0	46.94	2.917	Splitting + Shearing
20.0	53.98	0.667	Splitting
40.0	74.24	1.008	Splitting + Shearing

Fig.A-II.7 Deviator stress vs axial strain plots of unreinforced jointed rock (θ = 50°-60°) at different confining stress levels

σ_3 , MPa	Observations		
	σ_d, MPa	ϵ, %	Failure mode
0.0	1.08	1.770	Sliding
5.0	20.67	0.216	Splitting + Shearing
20.0	28.66	2.328	Sliding + Splitting
40.0	26.68	2.328	Splitting
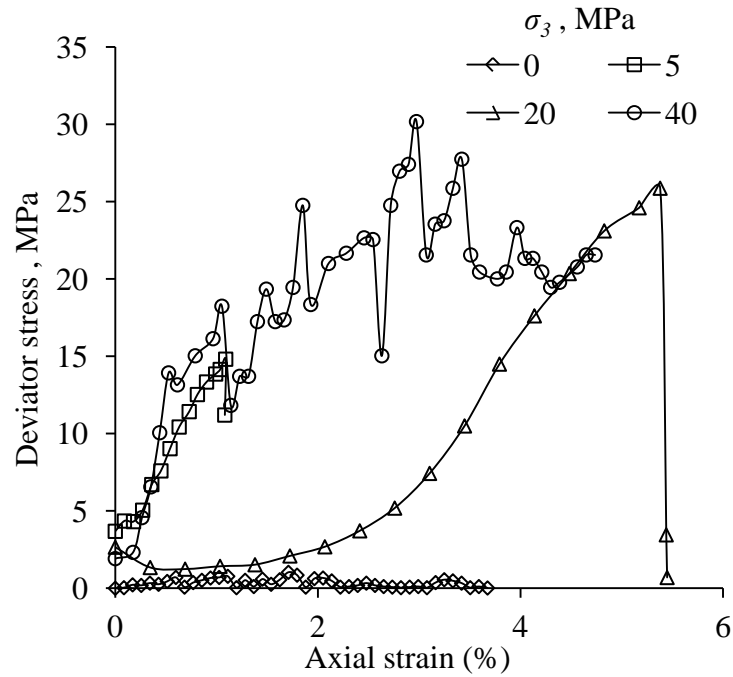
Fig.A-II.8 Deviator stress vs axial strain plots of unreinforced jointed rock (θ = 60°-70°) at different confining stress levels

σ_3 , MPa	Observations		
	σ_d, MPa	ϵ, %	Failure mode
0.0	1.03	1.709	Sliding
5.0	14.81	1.090	Sliding + Splitting
20.0	25.87	5.379	Sliding + Splitting
40.0	30.18	2.974	Splitting + Shearing
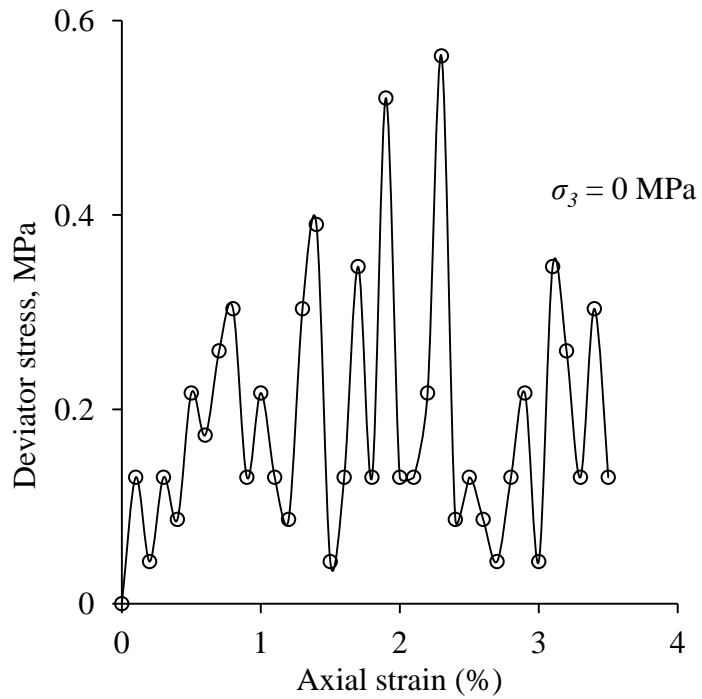
Fig.A-II.9 Deviator stress vs axial strain plots of unreinforced jointed rock (θ = 70°-80°)

Observations

$\sigma_3 = 0.0$ MPa   Peak stress (deviator) = 0.56 MPa

Axial strain at failure = 1.917 %

Failure mode = Sliding

Fig.A-II.10 Deviator stress vs axial strain plots of unreinforced jointed rock (θ = 80°-90°)

Observations

σ_3 = 0.0 MPa   Peak stress (deviator) = 21.52 MPa

Axial strain at failure = 0.383 %

Failure mode = Splitting
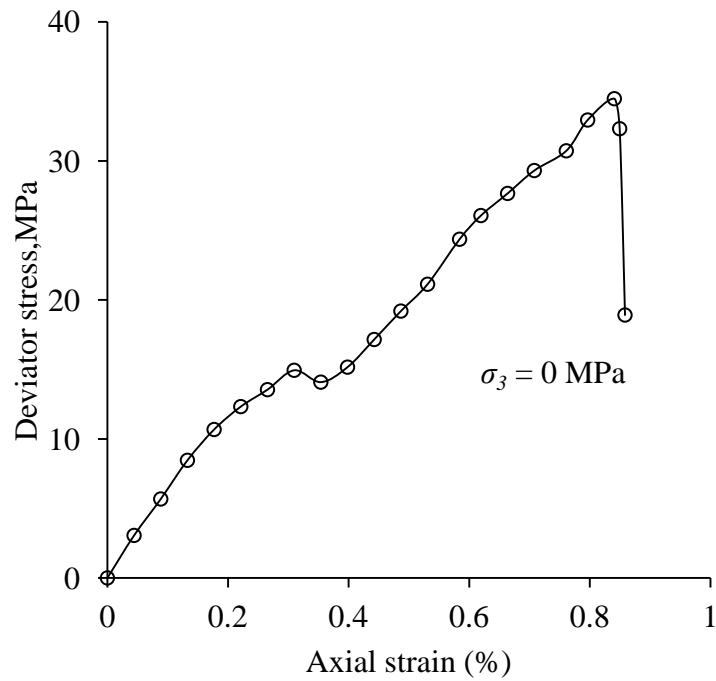
Fig.A-II.11 Deviator stress vs axial strain plots of reinforced jointed rock (θ = 20°-30°)

Observations

σ_3 = 0.0 MPa   Peak stress (deviator) = 34.47 MPa

Axial strain at failure = 0.841 %

Failure mode = Splitting

Deformation in bolt = Slight
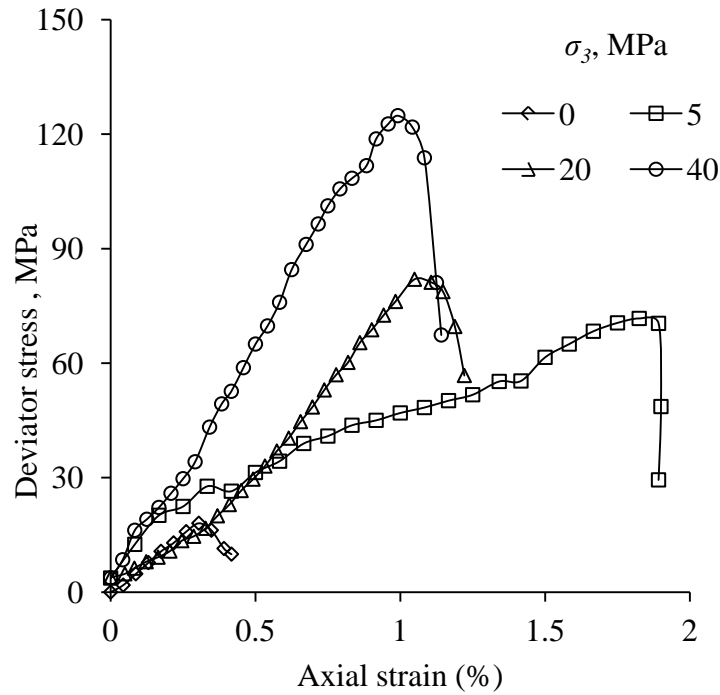
Fig.A-II.12 Deviator stress vs axial strain plots of reinforced jointed rock ($\theta =$ 30°-40°) at different confining stress levels
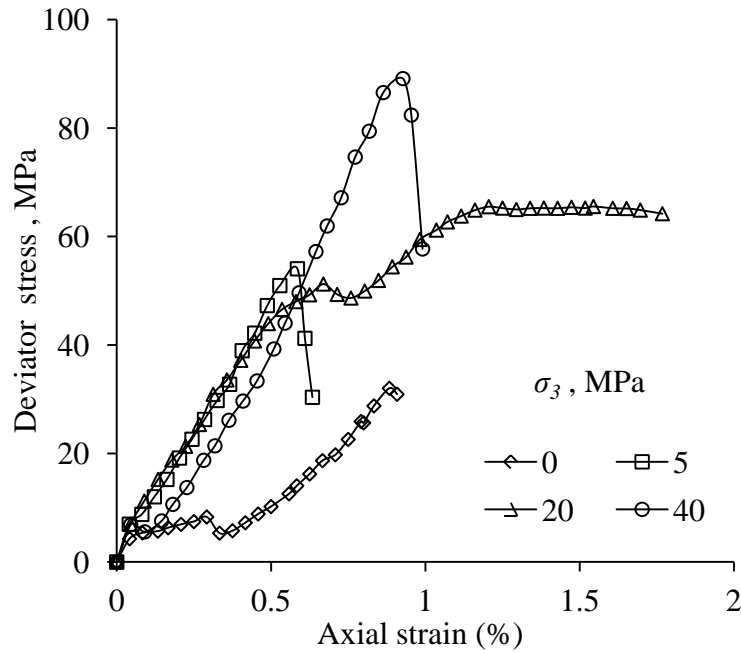
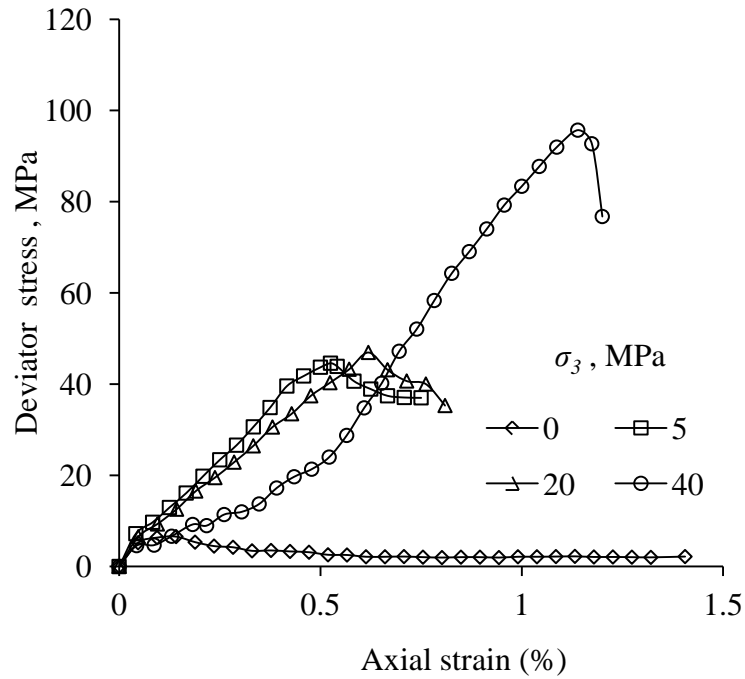| σ_3 , MPa	Observations			
	σ_d, MPa	ϵ, %	Failure mode	Deformation in bolt
0.0	18.05	0.304	Splitting	Slight
5.0	71.70	1.825	Splitting	Slight
20.0	81.97	1.049	Splitting	Slight
40.0	124.83	0.992	Splitting	Slight
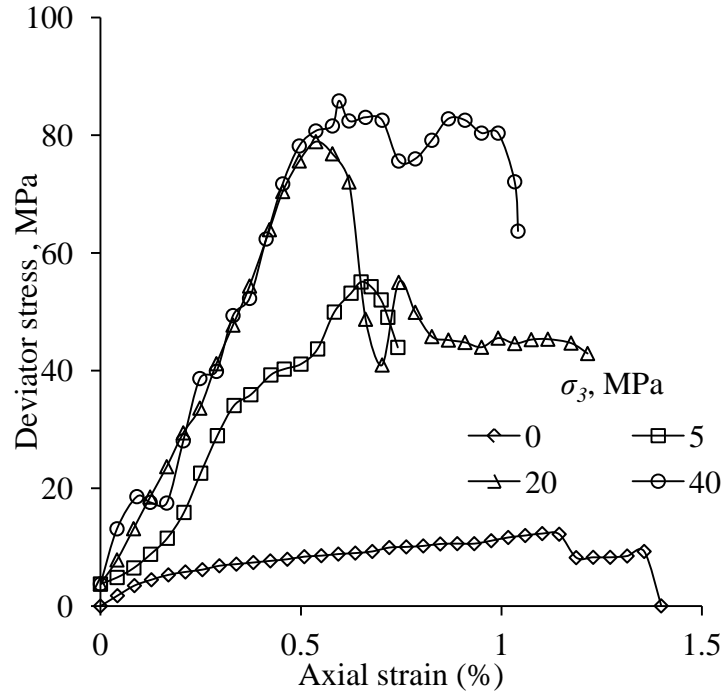
Fig.A-II.13 Deviator stress vs axial strain plots of reinforced jointed rock ($\theta =$ 40°-50°) at different confining stress levels

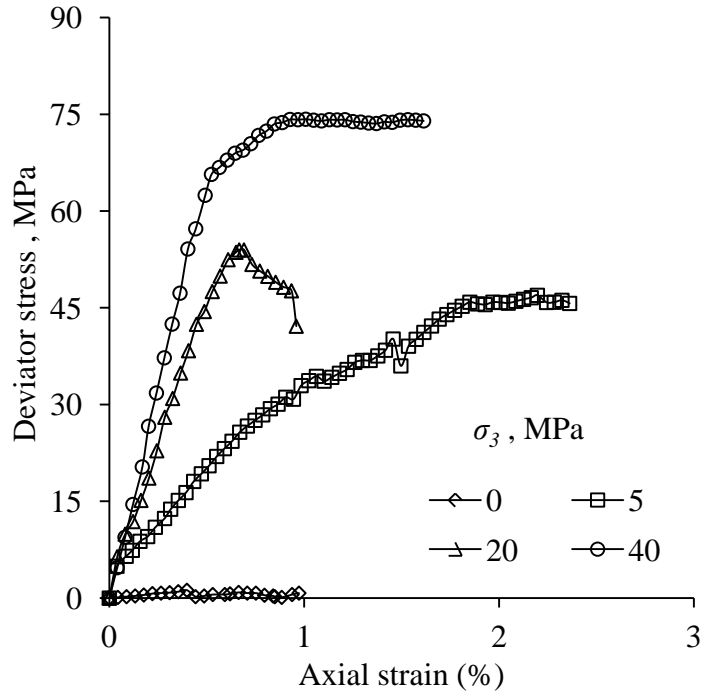| σ_3 , MPa	Observations			
	σ_d, MPa	ϵ, %	Failure mode	Deformation in bolt
0.0	12.32	1.102	Splitting + Shearing	Bolt completely sheared
5.0	55.08	0.650	Splitting	Significant
20.0	79.82	0.537	Splitting + Shearing	Significant
40.0	85.84	0.595	Splitting + Shearing	Significant
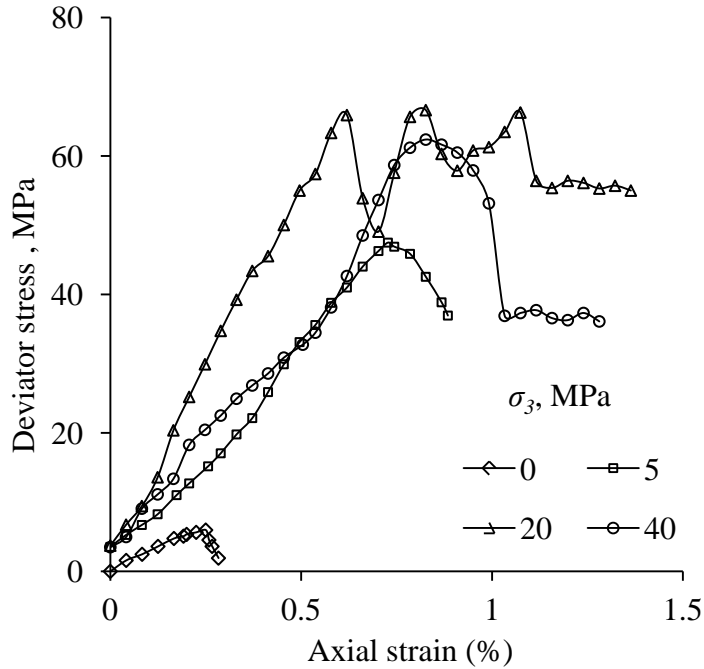
Fig.A-II.14 Deviator stress vs axial strain plots of reinforced jointed rock ($\theta =$ 50°-60°) at different confining stress levels

σ_3 , MPa	Observations			
	σ_d, MPa	ϵ, %	**Failure mode**	**Deformation in bolt**
0.0	5.97	0.250	Splitting	Significant
5.0	47.49	0.727	Splitting	Significant
20.0	66.63	0.826	Splitting + Shearing	Significant
40.0	62.38	0.826	Splitting + Shearing	Significant
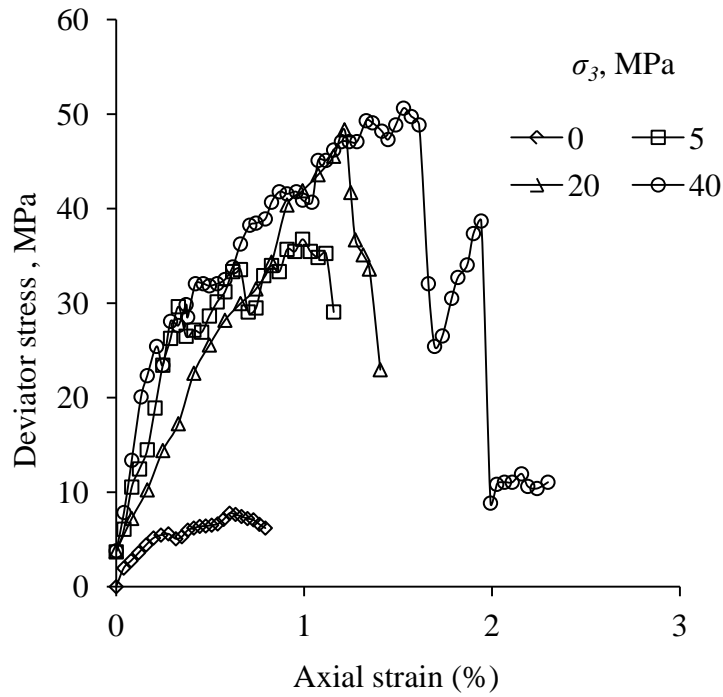
Fig.A-II.15 Deviator stress vs axial strain plots of reinforced jointed rock (θ = 60°-70°) at different confining stress levels
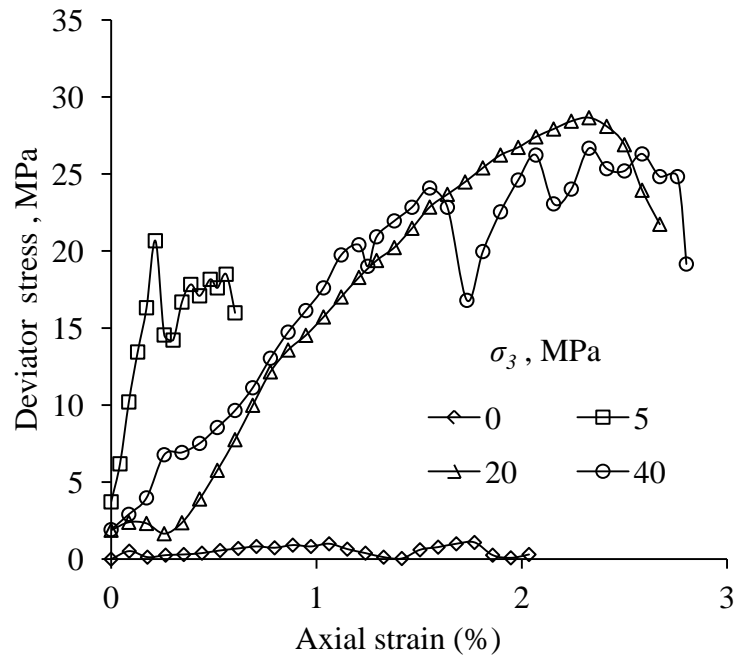
σ_3 , MPa	Observations			
	σ_d, MPa	ϵ, %	Failure mode	Deformation in bolt
0.0	7.78	0.603	Splitting + Shearing	Significant
5.0	36.76	0.992	Splitting + Shearing	Bolt completely sheared
20.0	48.34	1.215	Splitting	Bolt completely sheared
40.0	50.62	1.529	Splitting + Shearing	Bolt completely sheared
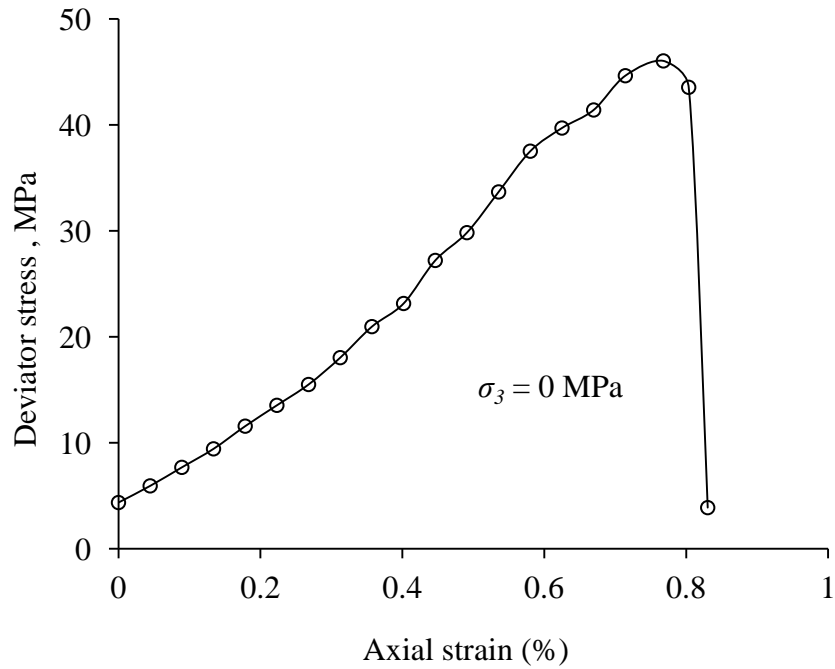
Fig.A-II.16 Deviator stress vs axial strain plots of reinforced jointed rock (θ = 70°-80°)

Observations

σ_3 = 0.0 MPa   Peak stress (deviator) = 46.05 MPa

Axial strain at failure = 0.768 %

Failure mode = Splitting

Deformation in bolt = Slight
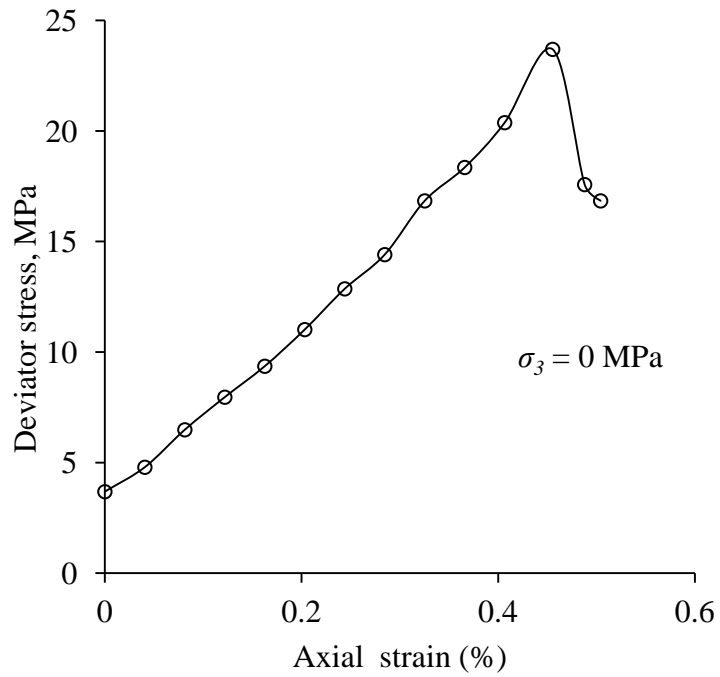
Fig.A-II.17 Deviator stress vs axial strain plots of reinforced jointed rock (θ = 80°-90°)
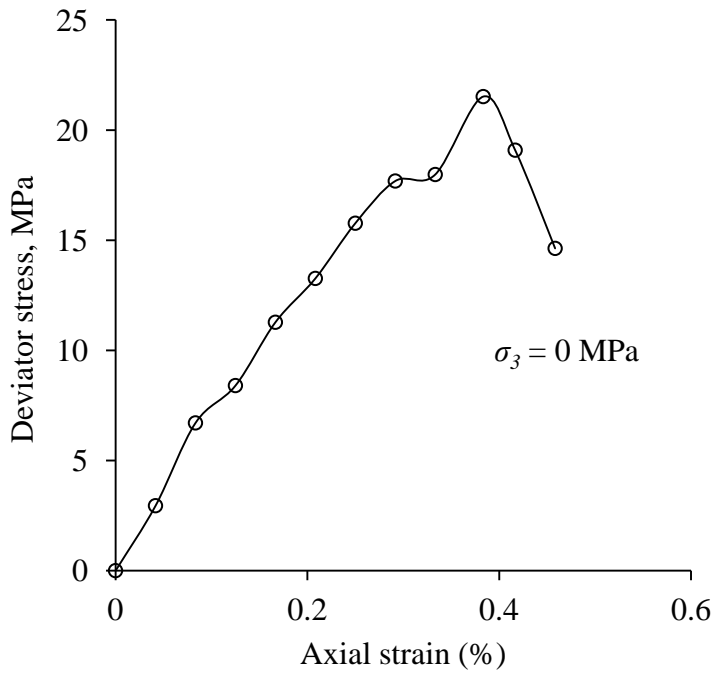
Observations

$\sigma_3 = 0.0$ MPa   Peak stress (deviator) = 23.69 MPa

Axial strain at failure = 0.455 %

Failure mode = Splitting

Deformation in bolt = Slight

INDIAN INSTITUTE OF TECHNOLOGY ROORKEE
ROORKEE

CANDIDATE'S DECLARATION

I hereby certify that the work which is being presented in the thesis entitled "**STRENGTH BEHAVIOUR OF JOINTED ROCKS REINFORCED WITH PASSIVE BOLTS**" in partial fulfilment of the requirements for the award of the Degree of Doctor of Philosophy and submitted in the Department of Civil Engineering of the Indian Institute of Technology Roorkee is an authentic record of my own work carried out during a period from December, 2009 to February, 2015 under the supervision of **Dr. Mahendra Singh**, Professor, Department of Civil Engineering.

The matter presented in the thesis has not been submitted by me for the award of any other degree of this or any other Institute.

(LOK PRIYA SRIVASTAVA)

This is to certify that the above statement made by the candidate is correct to the best of my knowledge.

(MAHENDRA SINGH)
Supervisor

Dated:

Chapter 1

INTRODUCTION

1.1 GENERAL

Rock masses encountered in the field comprise of blocks of intact rock separated by discontinuities like joints, foliations, bedding planes and faults. Theses discontinuities create planes of weaknesses in the rock mass. Generally, failure occurs due to sliding along these discontinuities (Fig.1.1a). If sliding along theses discontinuities could be prevented the rock mass would become stronger and stiffer. Hence, reinforcement techniques are used for strengthening the rock mass and preventing the failure along discontinuities. One of the most popular reinforcement techniques is rock bolting. The rock bolting has been widely used in rock engineering applications since 19th century and has become the most reliable and convenient technique for strengthening and stabilizing the rock structures. The bolts increase the stiffness of the rock mass and convert it into a relatively rigid mass. They increase the stiffness by providing additional resistance against failure on the joint plane (Fig.1.1b). The design of rock bolts depends upon various factors; mainly engineering properties of intact rock and rock mass. For designing the rock-bolt-support system, it is necessary that the strength behaviour of the rock mass, without and with reinforcement is understood clearly. Assessment of engineering behaviour of reinforced rock through laboratory studies is tedious because it requires special facilities like equipments, materials, drilling and grouting techniques. Very few studies are available in literature, which focused on the laboratory testing of rock bolt reinforced rock (Bjurström, 1974; Dight, 1982; Ludvig, 1983; Ferrero, 1995; Ferrero et al., 1997; Grasselli et al., 1999; McHugh and Signer, 1999; Grasselli, 2005; Sakurai, 2010; Jalalifar and Aziz, 2010). An attempt has been made in the present study to assess the engineering behaviour of reinforced rock/rock mass through laboratory physical model tests.
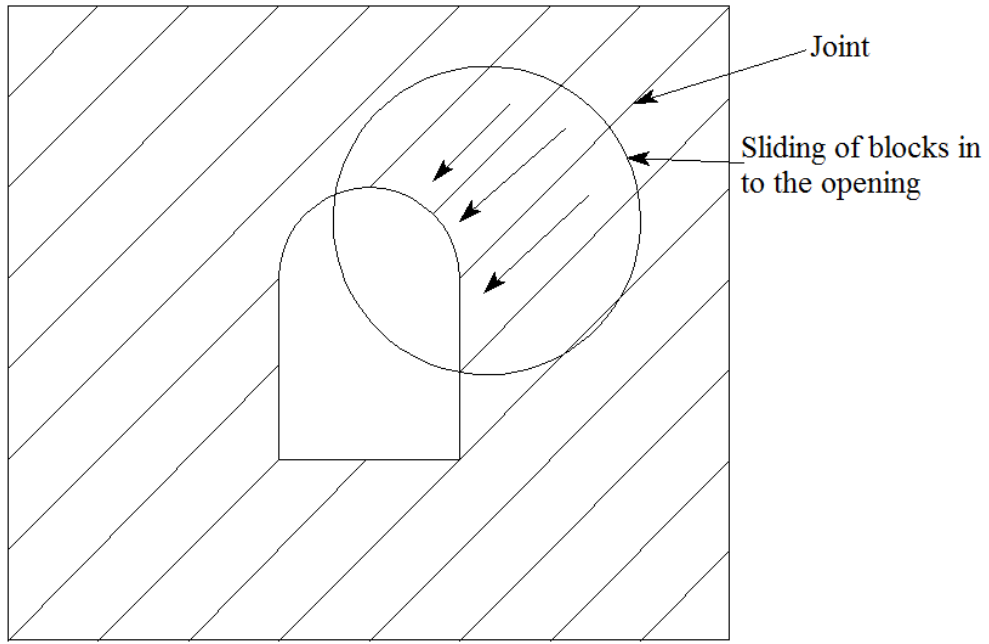
Fig.1.1a Failure though joints in an undergrounding opening
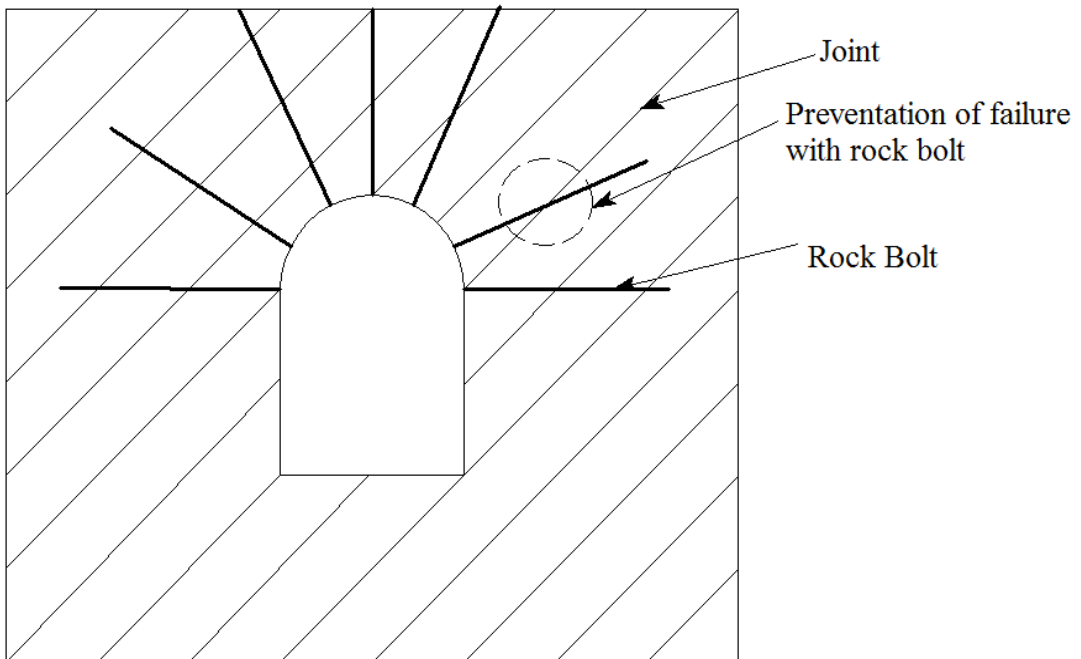
Fig.1.1b Preventation of failure through joint by rock bolts in an underground opening

1.2 SCOPE OF THE THESIS

The main objective of the present research works is to improve the understanding of engineering behaviour of jointed rock reinforced with passive rock bolts. To meet the objective, an experimental study was planned on the specimens of natural and synthetic rocks without and with bolts. The experimental study was divided into the three parts. In the first part of study, direct shear tests were conducted on the specimens of blocky mass without and with bolts. The size of the blocky mass specimen was 750 mm x 750mm x 900 mm (height). The mass was prepared by piling concrete blocks of size 150 mm x 150 mm x 150 mm each. The mass consists of three orthogonal joints sets with joint spacing of 150 mm. To reinforce the mass, three different configurations of bolts were used. The direst shear tests were conducted at normal stress levels varying from 0 to 2 MPa. The purpose of direct shear tests has been

i.   To examine the shear strength behavior of unreinforced and reinforced blocky mass under different normal stress levels,
ii. To examine the parameters which influence the shear strength of unreinforced and reinforced blocky mass, and
iii. To examine the contribution of bolts towards shear strength enhancement.

The outcome of this part can be used in the situations where analysis is done σ, τ space like rock slopes. In the second part of the study, uniaxial compression tests have been conducted on the specimens of synthetic rocks without and with bolts. High strength concretes blocks of size 150 mm x150 mm x 300 mm were used as specimens. Jointed specimens consisted of one smooth joint. The joint orientation was varied between 0° to 90°. To reinforce the rock, two bolts of 6 mm diameter were used and were grouted with cement mortar. Uniaxial compression tests were conducted in displacement-controlled mode and load, deformation and failure modes were recorded. The aim of this part has been

i.   To examine the behaviour of unreinforced and reinforced jointed rock under uniaxial compression,
ii. To study the effect of bolt on strength and modulus of the jointed rock,
iii. To study the effect of bolt on anisotropic behaviour of the jointed rock,

iv.   To study the relationship between strength and modulus of intact, unreinforced and reinforced jointed rocks.

The outcome of this study can be used to assess the uniaxial compressive strength of reinforced rocks, which is required as an input parameter in strength criterion. In third part of the work, triaxial tests were conducted on the specimens of natural jointed rocks. The NX size specimens having joint orientation varying from 0° to 90° were retrieved and were tested without and with bolt. To reinforce the jointed rock, 4 mm diameter grouted steel bar was used. The triaxial tests were conducted at confining pressure ranging between 0 to 40 MPa. The main objectives of this part are

i.   To investigate the behaviour of unreinforced and reinforced rock under different confining pressures,

ii.   To examine the effect of the bolt on failure modes of jointed rock,

iii.   To examine the effect of bolt on shear strength parameters (c and ϕ and),

iv.   To examine the contribution of bolt towards strength enhancement,

v.   To examine the effect of bolt on the anisotropic behaviour of jointed rock under confinement,

vi.   To suggest failure criterion for reinforced rock.

The outcome of this can be used in the situations were analysis is done in $\sigma_1 - \sigma_3$ space.

1.3 ORGANISATION OF THE THESIS

The thesis has been organised in eight chapters. The description of each chapter is listed below.

Chapter 1 Introduction

This chapter deals with the basic concepts and necessity of rock bolts to reinforce the rock masses. The major objective, scope, and organisation of thesis are discussed briefly.

Chapter 2 Literature Review

In this chapter, the review of literature related to intact rocks, jointed rocks and rock bolt reinforced rocks is presented in detail. Parameters that influence the engineering behaviour of rock are discussed. The parameters that govern the design of rock bolt in the field situation are also discussed. The criteria proposed for assessment of strength of intact rocks and jointed rocks are also presented in this chapter.

Chapter 3 Experimental Study

The details of the experiments performed are discussed in this chapter. Selection of model material, preparation of specimens, installation of bolts, equipment used and testing procedure are discussed in detail.

Chapter 4 Results and Discussions

The observations taken during tests and results obtained from tests are summarized in the chapter. The discussion made on observations and results are also presented in this chapter. The result for direct shear tests on blocky mass, uniaxial compression tests on synthetic rocks and triaxial tests on natural rocks are discussed separately. Observations on failure modes, strength and deformational behaviour of unreinforced and reinforced rock are discussed in detail. Effect of bolt on the behaviour of blocky mass and jointed rock is also summarized.

Chapter 5 Shear Strength Behaviour of Blocky Mass

The results of direct shear tests conducted on large sized specimens of blocky mass unreinforced and reinforced are analysed in this chapter. The parameters that influence the shear strength of reinforced rock are discussed in detail. Comments are made on the reasons for enhancement of shear strength due to bolts. An attempt has been made to find out the correlation which can be used in the field for assessing the shear strength of reinforced mass.

Chapter 6 Behaviour of natural and synthetic jointed rocks under uniaxial compression

The results of uniaxial compression tests conducted on natural and synthetic rocks are analysed and presented in this chapter. The effect of bolt on the strength and deformation behaviour of jointed rocks is discussed in detail. The parameters that influence the strength and deformation behaviour of bolt-reinforced jointed rock are

also discussed. Attempt has been made to find out correlations between strength and modulus of intact, unreinforced jointed and reinforced jointed rock.

Chapter 7 Triaxial Strength of Reinforced Jointed Rocks

        The results of triaxial compression tests conducted on specimens of natural rock are analysed and presented in this chapter. The effect of passive bolt, confining pressure and joint orientation on the behaviour of jointed rocks are discussed. The applicability of failure criteria in vogue for reinforced rock has also been investigated. Modifications have been suggested to strength criterion for its use for reinforced rocks.

Chapter 8 Summary and Conclusions

        The summery of observations and conclusions obtained in the present research work are presented in this chapter. Scope of future work is also listed in this chapter. In the last references used in the work are listed.

LITERATURE REVIEW

2.1 GENERAL

The design of support system for rock structures is an important and challenging task in geotechnical engineering. The support systems used in practice are mainly of two types, namely primary supports and secondary supports. Primary supports like rock bolts are installed immediately after the excavation and act as an integral part of the rock structure. The secondary or permanent support includes shotcrete and concrete liners, which provide additional stiffness and smooth surface to the rock structures.

A rock bolt (Fig.2.1) consists of a bar or tube made of steel or any other material. One end of this is anchored or plane and the other end consists of a faceplate and nut-washer system. Based on the requirement it may be grouted or ungrouted.
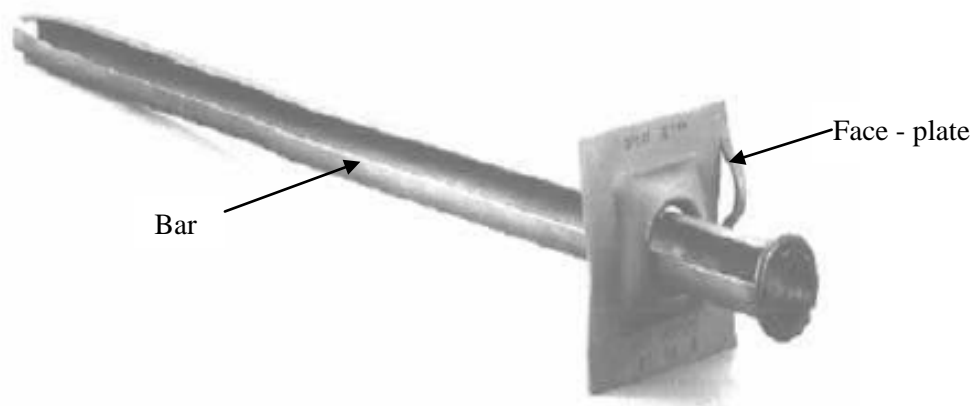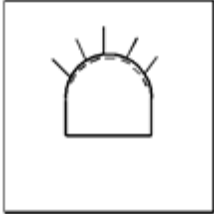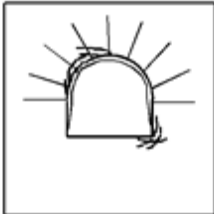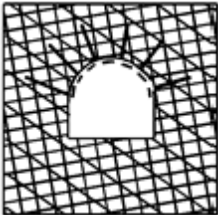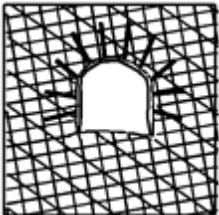
Fig.2.1 A typical rock bolt (Singh and Goel, 2006)

The typical applications of rock bolt in different field conditions are presented in Table. 2.1. Based on application, the bolts are classified into two categories, pre-tensioned point-anchored or active bolts, and untensioned full column grouted bolts (Grasselli, 2005; Singh and Goel, 2006). Pre-tensioned point anchored bolts (active bolts) have a mechanical anchor at one end and a faceplate with nut at the other end (Fig. 2.2a). These are always tensioned after their installation. The tensioned rock bolts provide the additional resistance in rock mass by the pretension forces. These may be either grouted or ungrouted. Untensioned full-column grouted bolts (Passive bolts) consist of a steel bar, which is grouted throughout its length into the rock mass (Fig. 2.2b). No pretension force is applied to this type of bolt. The other end of the bolt, exposed to the atmosphere, consists of a face plate tightened by nut washer system. The active bolts are used where supports are required immediately after the excavations (Grasselli, 2005), whereas passive bolts are used, where the rock mass deforms with time. The passive bolts become effective after a significant movement in the rock mass. Therefore, for effective performance, the passive bolts should be installed in the rock mass before significant movement has taken place. The present study deals with passive bolts only. The engineering behaviour of a rock reinforced with bolts is a complex phenomenon and needs understanding of behaviour of intact as well as jointed unreinforced rocks. The discussion about the behaviour of intact, unreinforced jointed, reinforced jointed mass is presented in this chapter.
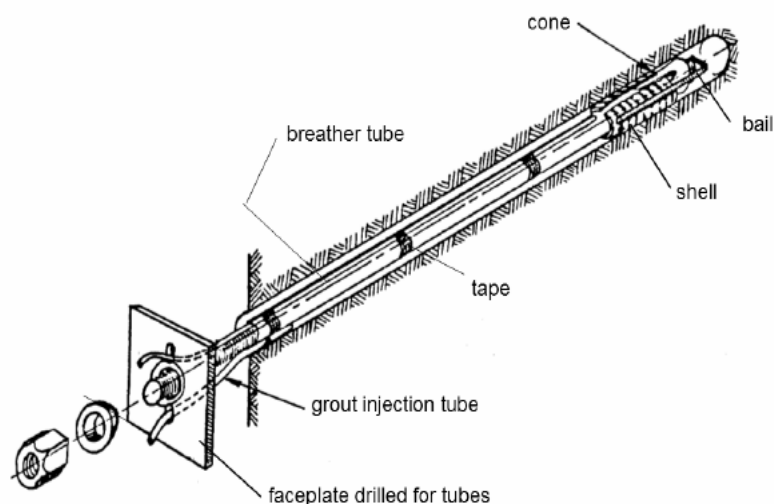
Fig.2.2a Components of a pre-tensioned point- anchored rock bolt with provision for grouting (Active bolts)

Table 2.1 Typical rock bolt applications in different field conditions
(Hoek, 2007)

	Low stress levels	High stress levels
Massive rock	Massive rock subjected to low in-situ stress levels. No permanent support. Light support may be required for construction safety.	Massive rock subjected to high in-situ stress levels. Pattern rock bolts or dowels with mesh or shortcrete to inhibit fracturing and to keep broken rock in place.
Jointed rocks	Massive rock with relatively few discontinuities subjected to low in-situ stress condition. 'Spot' bolts located to prevent failure of individual blocks and wedges. Bolts must be tensioned.	Massive rock with relatively few discontinuities subjected to high in-situ stress condition. Heavy bolts or dowels, inclined to cross rock structure, with mesh or steel fibre reinforced shotcrete on roof and sidewalls.
Heavily jointed rock	Heavily jointed rock subjected to low in-situ stress conditions. Light pattern bolts with mess and/or shotcrete will control ravelling of near surface rock pieces.	Heavily jointed rock subjected to low in-situ stress conditions. Heavy rock bolt or dowel pattern with steel fibre reinforced shotcrete. In extreme cases, steel sets with sliding joints may be required. Invert struts or concrete floor slabs may be required to control floor heave.
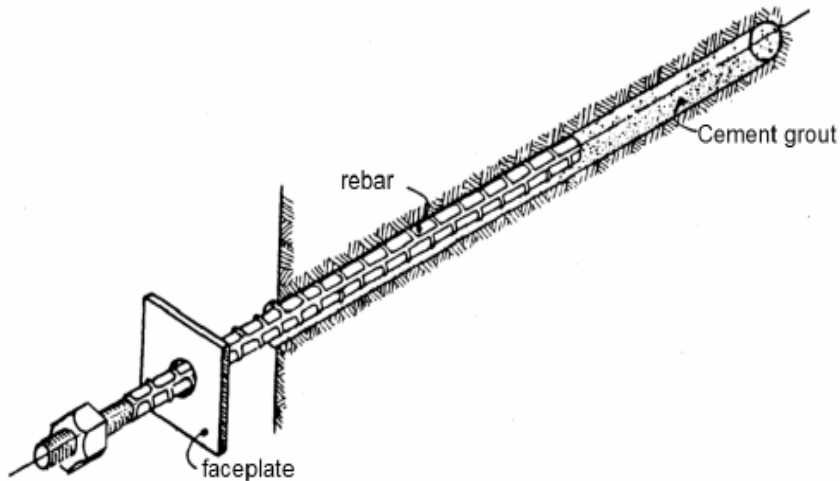
Fig.2.2b Components of untensioned full column grouted bolts (Passive bolts)

2.2 NECESSITY OF ROCK BOLTING

Rock bolts are in use in civil and mining engineering projects since 19th century. The main objective of rock bolting is to strengthen the rock mass. The rock mass itself a complex structure. In the field, the rock mass consists of intact material separated by the discontinuities (joints, bedding plane joints, foliation surfaces, shear zones, or faults). In most of the applications, the strength of the intact material between the discontinuities is higher as compared to expected stresses (US Army corps of Engineers, 1980). The discontinuities substantially influence the deformation in rock mass and create planes of low strength in the rock mass and progressive failure in mass occurs along these planes which results in collapse of rock structure. The mass may become quite stronger, if failure along these planes is prevented (US Army corps of Engineers, 1980). To counter failure along the discontinuities the rock bolts are used. Bolts enhance the self-supporting ability of the rock mass. Also the installation of the bolts restricts the deformation in the mass.

There are numerous factors which influence the engineering behaviour of rock bolt reinforced mass. Some of these are properties of surrounding intact material and strength, deformability, frequency and orientation of discontinuities (mainly joints) present in the rock mass. To have a complete understanding of behaviour of reinforced rock, understanding the behavior of intact rock and joints becomes

10

indispensible. A brief discussion about the behavior of intact and jointed rock has been presented in the next sections.

2.3 ENGINEERING BEHAVIOUR OF INTACT ROCKS

Intact rock refers to the solid material with no hair or small cracks. The engineering properties of intact rock depend upon the mineralogical composition and method of formation in the field. The properties can be assessed by laboratory tests i.e. uniaxial compression, point load index, triaxial, ultrasonic wave velocity tests and many more. The behaviour of intact rocks is discussed below.

2.3.1 Classification of Intact Rocks

Several classifications have been proposed by various investigators to classify intact rock based on engineering and physical properties (Coates, 1964; Hansagi, 1965; Deere and Miller, 1966; Stapledon, 1968; Geological society, 1970; Franklin et al., 1971; Bieniawski, 1973, 1975, 1978; ISRM, 1978, 1981). Deere and Millar (1966) classified the intact rock based on its uniaxial compressive strength (σ_{ci}) and tangent modulus (E_{t50}) at 50% failure stress. They plotted the tangent modulus (E_{t50}) against the uniaxial compressive strength (σ_{ci}) on log-log scale (Fig.2.3). The Deere-Miller classification consists of two lettered symbol, the first letter denotes the ranges of compressive strength and the second denotes the modulus ratio ($M_{ri} = E_{t50} / \sigma_{ci}$). The values of ranges of uniaxial compressive strength and modulus ratio for various classes are given in Table 2.2a and Table 2.2b.

Based on the uniaxial compressive strength and point load index, Bieniawski (1975) classified the intact rock into five categories i.e. very high strength, high strength, medium strength, low strength and very low strength (Table 2.3).

International Society of Rock Mechanics (ISRM, 1978), classified the intact rocks into seven categories based on their values uniaxial compressive strength. The detailed description of classification is presented in Table 2.4a. ISRM (1981) modified its previous classification system and divided the intact rocks into the five categories (Table 2.4b). The classification is similar to the classification suggested by Bieniawski (1975).
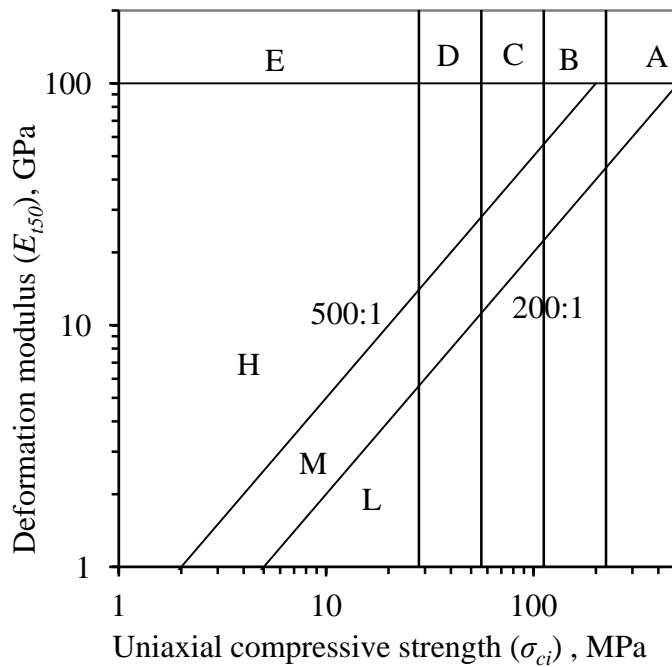
Fig. 2.3 Engineering classification of intact rocks (after Deere and Miller, 1966)

Table 2.2a Strength classification by Deere and Millar (1966)

Class	σ_{ci} , MPa	Description
A	> 224	Very high strength
B	112-224	High strength
C	56-112	Medium strength
D	28-56	Low strength
E	< 28	Very low strength

Table 2.2b Modulus ratio classification by Deere and Millar (1966)

Class	M_{ri}	Description
H	> 500	High modulus ratio
M	200-500	Medium modulus ratio
L	< 200	Low modulus ratio

Table 2.3 Strength classification of intact rock, Bieniawski (1975)

Description	σ_{ci} , MPa	Point load index (MPa)
Very high strength	> 200	>8
High strength	100-200	4-8
Medium strength	50-100	2-4
Low strength	25-50	1-2
Very low strength	< 25	< 1

Table 2.4a Strength classification of intact rock, ISRM (1978)

Grade	σ_{ci} , MPa	Description	Field Identification
R0	0.25 - 1	Extremely low strength	Intended by thumbnail.
R1	1 - 5	Very low strength	Crumbles under firm blows with point of geological hammer; can be peeled by a pocket knife.
R2	5 - 25	Low strength	Can be peeled by a pocket knife with difficulty, shallow identifications made by firm blow with point of geological hammer.
R3	25-50	Medium strength	Cannot be scraped or peeled with a pocket knife; specimen can be fractured with single firm blow of geological hammer.
R4	50-100	High strength	Specimen requires more than one blow of geological hammer to fracture it.
R5	100-250	Very high strength	Specimen requires many blows of geological hammer to fracture it.
R6	250	Extremely high strength	Specimen can only be chipped with geological hammer.

Table 2.4b Strength classification of intact rock, ISRM (1981)

Description	σ_{ci} , MPa
Very high strength	> 200
High strength	60-200
Medium strength	20-60
Low strength	6-20
Very low strength	< 6

2.3.2 Strength Behaviour of Intact Rocks

The uniaxial compressive strength (UCS), σ_{ci} and tangent modulus (E_{t50}) values of intact rocks can be directly estimated by conducting the laboratory uniaxial compressive strength tests on the rock specimens. The UCS can also be estimated by using indirect approaches like point load index test and Schmidt hammer test. The deformation modulus can be estimated indirectly by conducting Schmidt hammer test and ultrasonic wave velocity test. The ranges of properties of some intact rocks are listed in Table 2.5.

Table 2.5 Ranges of properties of some intact rocks (Ramamurthy, 2010)

Rock type	Dry density, kN/m^3	Compressive strength (σ_{ci}), MPa	Tensile strength, MPa	Modulus, MPa x 10^3	Poisson's ratio
Basalt	28-29.5	100-350	10-30	28-80	0.19
Diabase	-	140-240	-	70-100	0.25
Diorite	27-30.5	150-300	12-30	4-10	-
Dolerite	-	227-319	12-26	60-90	0.15-0.29
Dolomite	25-28.7	30-500	15-25	25-80	0.29
Gneiss	28-30	50-250	5-20	24-80	0.1-0.40
Granite	26-29	100-340	7-25	2-75	0.1-0.39
Limestone	22-26	30-250	5-25	3-82	0.08-0.39
Marble	26-27	50-250	7-20	3-44	-
Phyllite	26.9-27.9	79-102	15-19	7.5-14.5	0.33
Quartzite	26-27	150-320	10-30	16-94	0.11-0.25
Sandstone	20-26	20-300	4-25	0.6-68	0.1-0.40
Schist	26.3-28.8	29-190	9-29	6-57	0.1-0.25
Shale	20-24	5-100	2-10	2.5-44	0.1-0.19
Siltstone	24.4-26	25-50	3-6	26-62	0.27
Slate	26-27	100-200	2-5	0.6	-
Coal	-	10-39	-	2.4-5.3	0.33-0.42

In the field, the rock is subjected to polyaxial or triaxial stress conditions. The strength behaviour of intact rocks under triaxial or polyaxial conditions can be obtained by conducting the polyaxial or triaxial compression tests on the intact rock specimens. The polyaxial strength (or major principal stress, σ_1 at failure) is expressed as

$$\sigma_1 = f\left(\sigma_2, \sigma_3\right) \tag{2.1}$$

where σ_2 is the intermediate principal stress and σ_3 is the minor principal stress at failure. For triaxial condition, $\sigma_2 = \sigma_3$, hence equation 2.1 becomes

$$\sigma_1 = f\left(\sigma_3\right) \tag{2.2}$$

Several strength criteria have been proposed by various researchers to estimate the strength of intact rock in triaxial conditions (Mohr- Coulomb, 1773; Bieniawski and Yudhbir, 1974; Hoek and Brown, 1980; Rao, 1984; Johnston, 1985; Ramamurthy, 1993 and 2001; Singh and Singh, 2005; Singh et al., 2011).

According to the Mohr- Coulomb failure criterion (1773), the triaxial strength of an intact rock is expressed as a linear function of σ_3 as

$$\sigma_1 = \frac{2\,c_i\,\cos\phi}{(1-\sin\phi_i)} + \frac{(1+\sin\phi_i)}{(1-\sin\phi_i)}\,\sigma_3 \tag{2.3}$$

where c_i and ϕ_i are the criterion parameter known as cohesion and angle of internal friction of the intact material respectively. This criterion is linear and widely used in the rock engineering applications.

Actual strength behaviour of the rocks is not linear and strength varies in non-linear manner with confining pressure. To account for non-linearity in strength behaviour, Bieniawski (1974) and Yudhbir et al. (1983) proposed the following strength criterion for intact rock based on the curve fitting of more than 700 tests results:

$$\frac{\sigma_1}{\sigma_{ci}} = 1 + b\left(\frac{\sigma_3}{\sigma_{ci}}\right)^{0.65} \tag{2.4}$$

where σ_{ci} is the uniaxial compressive strength of intact rock and b is an unknown parameter.

Hoek and Brown (1980) proposed the following failure criterion for intact rocks

$$\sigma_1 = \sigma_3 + \sigma_{ci} \left(m_i \frac{\sigma_3}{\sigma_{ci}} + 1 \right)^{0.5} \tag{2.5}$$

where σ_{ci} and m_i are the criterion parameters. The values of these parameters are determined by the statistical analysis of the results obtained from the triaxial tests on the intact rock specimens.

Rao (1984) suggested the following strength criterion for isotropic intact rocks

$$\frac{\sigma_1 - \sigma_3}{\sigma_3} = B \left(\frac{\sigma_c}{\sigma_3} \right)^{\alpha} \tag{2.6}$$

where σ_1 and σ_3 are major and minor principal stresses respectively, σ_c is the uniaxial compressive strength, α and B are the non dimensionless parameters. For all rocks α is constant and almost equal to 0.8. Parameter B depends on rock quality and type and for each rock group the maximum value of B lies between 1.8 and 3.0. The criterion can also be applicable in case of anisotropic and jointed rocks.

Johnston (1985) conducted tests on the rock and soil specimens and proposed the following criterion for intact rocks;

$$\sigma'_{1n} = \left(\frac{M}{B} \sigma'_{3n} + 1 \right)^B \tag{2.7}$$

where σ'_{1n} and σ'_{3n} are the normalized effective principal stresses at failure. The normalized effective principal stresses were obtained by dividing the effective principle stresss (σ'_1 and σ'_3) by the unconfined compressive strength of material (σ_{ci}). B and M are the intact material constants. The parameter, B is independent of material type and is a function of uniaxial compressive strength (σ_{ci}). It also describes the nonlinearity of failure envelope and is expressed as

$$B = 1 - 0.0172 \left(\log \sigma_{ci} \right)^2 \tag{2.8}$$

The parameter M describes the slope of the failure envelope at $\sigma'_{3n} = 0$, and depends upon the material type and uniaxial compressive strength. The parameter M is expressed as

$$M = 2.065 + 0.276 \, (\log \sigma_{ci})^2 \tag{2.9}$$

Ramamurthy (1993, 1994, and 2001) included the effect of tensile strength in the criterion proposed by Rao (1983) and proposed a non-linear criterion for isotropic intact rock expressed as

$$\frac{(\sigma'_1 - \sigma'_3)}{(\sigma'_3 + \sigma'_t)} = B_i \left(\frac{\sigma_{ci}}{(\sigma'_3 + \sigma'_t)} \right)^{\alpha_i} \tag{2.10}$$

where σ'_1 and σ'_3 are the effective principal stresses; σ_{ci} is the uniaxial compressive strength; σ_t is the tensile strength of the material; B_i and α_i are the strength parameters, which remains practically constant over the entire range of confining pressures. Ramamurthy (1994) suggested that in absence of triaxial data, the values of strength parameters may be taken as

$$\alpha_i = 2/3 \quad \text{and} \quad B_i = 1.1 \, to 1.3 \, \times \left(\frac{\sigma_{ci}}{\sigma_t} \right)^{1/3} \tag{2.11}$$

Triaxial strength (σ_1) of rock increases with increase in confining stress (σ_3). At low confining stress levels, the failure is brittle and rate of increase of σ_1 is high. At high confining stress levels, the rate of increase in σ_1 is lower and the failure is ductile. At sufficiently high confining stress, the plot of $\sigma_1 - \sigma_3$ with σ_3 becomes almost horizontal. This state of confining stress is termed as critical state. The critical state concept (Barton, 1976) envisages that "*the critical state is the condition under which Mohr envelope of peak shear strength approaches a line of zero gradient. This condition represents the maximum possible shear strength of the rock. For each rock, there will be a critical effective confining pressure above which the shear strength cannot be made to increase*". Singh and Singh (2004, 2005), Singh and Rao (2005) and Singh et al. (2011) employed critical state concept for rocks to correctly define the shape of the non-linear strength criterion for intact rocks. It is emphasised that Mohr-Coulomb criterion parameters c–ϕ which are used widely in geotechnical practice could be used with confidence to get non-linear strength behaviour of intact rock.

Singh and Singh (2004, 2005) used the following non-linear equation (Fig.2.4) to define the strength criterion for intact rocks

$$y = Ax^2 + Bx + C \qquad \text{and } A \neq 0 \qquad\qquad (2.12)$$

where A, B and C are the constants. Substituting y = deviator stress at failure = $\sigma_1 - \sigma_3$ and x = confining stress at failure = $\sigma_3 \leq \sigma_{ci}$, the equation 2.12 becomes,

$$(\sigma_1 - \sigma_3) = A\sigma_3{}^2 + B\sigma_3 + C \qquad\qquad (2.13)$$

where σ_1 and σ_3 = major and minor principal stresses at failure; σ_{ci} = uniaxial compressive strength (UCS) of the intact rock.
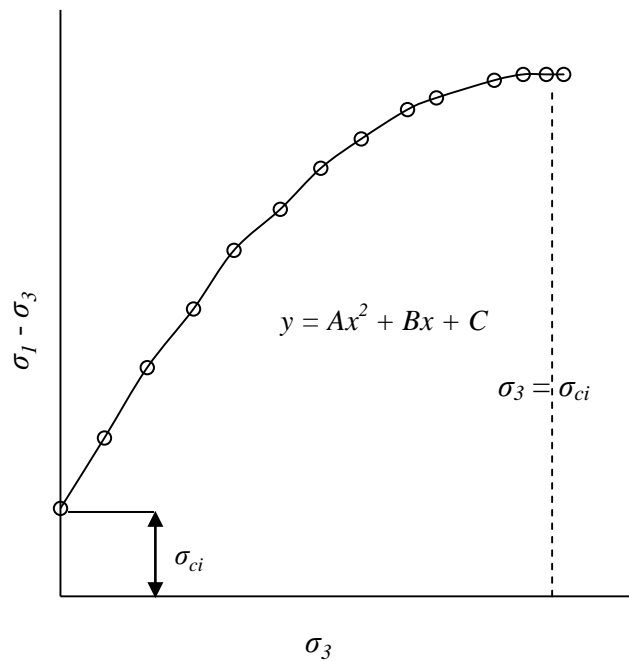
Fig.2.4 Strength criterion (Singh and Singh, 2005)

For unconfined condition, $\sigma_3 = 0$ and $\sigma_1 = \sigma_{ci}$, the equation 2.13 reduces to

$$\sigma_{ci} = C \qquad\qquad (2.14)$$

Putting the value of C in equation 2.13, the equation 2.13 becomes

$$(\sigma_1 - \sigma_3) = A\sigma_3{}^2 + B\sigma_3 + \sigma_{ci} \qquad\qquad \text{for } 0 \quad \sigma_3 \leq \sigma_{ci}$$
$$(2.15)$$

18

Singh and Singh (2005) suggested that at critical state $\phi \rightarrow 0$ and $\sigma_3 \approx \sigma_{ci}$. Differentiating equation 2.15 with respect to σ_3,

$$\frac{\partial(\sigma_1 - \sigma_3)}{\partial(\sigma_3)} = 2A\sigma_3 + B \tag{2.16}$$

At critical state, the gradient of failure envelope becomes constant. Putting boundary condition in equation 2.16

$$\frac{\partial(\sigma_1 - \sigma_3)}{\partial(\sigma_3)} = 0;$$

$$\Rightarrow 2A\sigma_{ci} + B = 0$$
$$B = -2A\sigma_{ci} \tag{2.17}$$

The equation 2.15 now written as

$$(\sigma_1 - \sigma_3) = A\sigma_3{}^2 - 2A\sigma_{ci}\sigma_3 + \sigma_{ci} \qquad \text{for} \quad \leq 0 \qquad \sigma_3 \quad \leq \quad \sigma_{ci}$$
(2.18)

The value of criterion parameter A can be obtained by fitting experimental triaxial data into the equation 2.18. However, in the absence of triaxial data the value of A can be obtained as

$$A \approx -3.97\,(\sigma_{ci})^{-1.10} \qquad ; \qquad \sigma_{ci} \quad = \quad 7 \quad - \quad 500 \quad \text{MPa}$$
(2.19)

Singh et al. (2011) modified the Mohr-Coulomb criterion by introducing the required deviation in the linear form of the criterion (Fig.2.5). Mohr-Coulomb criterion in the linear form can be written as

$$(\sigma_1 - \sigma_3) = \frac{2c_i \cos\phi_i}{(1 - \sin\phi_i)} + \frac{2\sin\phi_i}{(1 - \sin\phi_i)}\sigma_3 \tag{2.20}$$

where c_i and ϕ_i are the strength parameters of intact rock. The actual behaviour of rock is non-linear. To incorporate the effect of non-linearity a second-degree term $A'\sigma_3{}^2$ has been deducted from the right hand side of the equation 2.20. The equation 2.20 now can be written as

$$(\sigma_1 - \sigma_3) = \frac{2c_{i0}cos\phi_{i0}}{(1-sin\phi_{i0})} + \frac{2sin\phi_{i0}}{(1-sin\phi_{i0})}\sigma_3 - A'\sigma_3^2 \tag{2.21}$$

where c_{i0} and ϕ_{i0} are the Mohr-coulomb shear strength parameters obtained by conducting triaxial strength tests on rock specimens at low confining pressure ($\sigma_3 \rightarrow 0$). Using critical state concept the parameters A' can be obtained. At critical state, the gradient of non-linear curve (Fig.2.5) should approaches to 0 and σ_3 becomes the critical confining pressure (σ_{crti}). Differentiating equation 2.21 with respect to σ_3, and putting the boundary condition
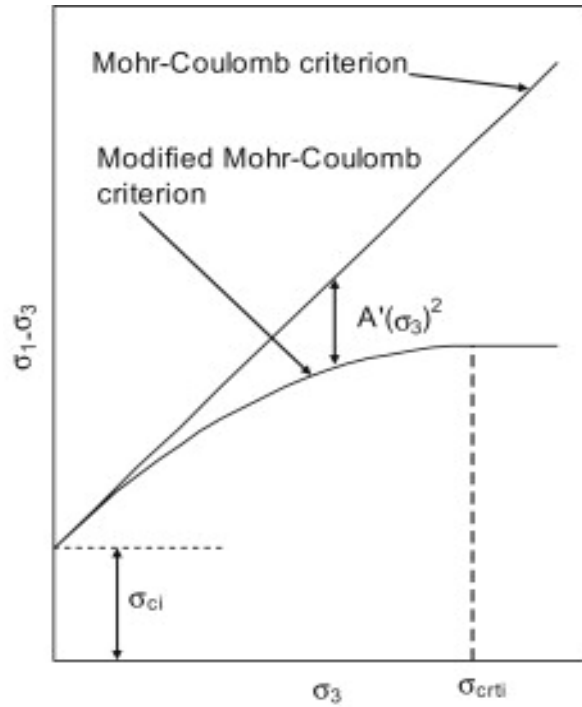
Fig.2.5 Modified Mohr-Coulomb criterion (Singh et al., 2011)

$$\frac{\partial(\sigma_1-\sigma_3)}{\partial(\sigma_3)} = \frac{2sin\phi_{i0}}{(1-sin\phi_{i0})} - 2A'\sigma_{crti} = 0$$

$$\Rightarrow A' = \frac{sin\phi_{i0}}{\sigma_{crti}(1-sin\phi_{i0})} \tag{2.22}$$

The modified Mohr-Coulomb criterion now may be written as

$$(\sigma_1 - \sigma_3) = \sigma_{ci} + \frac{2\,sin\phi_{i0}}{1-sin\phi_{i0}}\sigma_3 - \frac{1}{\sigma_{crti}}\frac{sin\phi_{i0}}{1-sin\phi_{i0}}\sigma_3{}^2 \quad for\ 0 \le \sigma_3 \le \sigma_{crti} \tag{2.23}$$

where $\quad \sigma_{ci} = \frac{2c_{i0}\,cos\phi_{i0}}{1-sin\phi_{i0}}$ \hfill (2.24)

20

σ_{ci} is the uniaxial compressive strength of intact rock and σ_{crti} is the critical confining pressure. The above criterion is applicable only up to critical state ($\sigma_3 = \sigma_{crti}$). After critical state the deviator stress at failure ($\sigma_1 - \sigma_3$) becomes constant. For $\sigma_3 \geq \sigma_{crti}$ the equation 2.23 can be written as

$$(\sigma_1 - \sigma_3)_{max} = \sigma_{ci} + \frac{2\,sin\phi_{i0}}{1-sin\phi_{i0}}\sigma_{crti} \qquad\qquad\qquad \text{for } \sigma_3 \geq \sigma_{crti}$$

(2.25)

Based on the back analysis of more than 1100 triaxial data, Singh et al. (2011) suggested that the value of critical confining pressure (σ_{crti}) may be taken nearly equal to the uniaxial compressive strength of intact rock (σ_{ci}).

2.4 EFFECT OF JOINTS (DISCONTINUITY)

A joint can be defined as "A break of geological origin in the continuity of a body of rock along which there has been no visible displacement" (ISRM, 1978). A group of parallel joints is termed as joint sets. A joint can affect the engineering behaviour of mass by its roughness (Patton, 1966; Ladanyi and Archambault, 1970; Jaeger, 1971; Barton, 1973, 1974, 1976; Chappell, 1975; Barton and Chaubey, 1977; Haberfield and Johnston, 1994; Indraratna et al., 1998, 1999; Indraratna and Haque, 2000, Misra, 1997, 1999, 2002; Pearce, 2001; Seidel and Haberfield, 2002a, 2002b; Grasselli, 2001, 2006; Gu et al., 2003, 2005; Cai et al.,2007; Zandarin et al., 2013), intensity (Goldstein et al., 1966; Hayashi, 1966; Lama, 1974; Priest and Hudson, 1976; Arora, 1987; Priest, 1993; Kulatilke et al., 2001), and orientation (Jaeger, 1960; Brown, 1970a, b; Ladanyi and Archambault, 1972; Jaeger and Cook, 1979; Arora, 1987; Singh, 1997). Strength and deformational behaviour of a joint is disused below.

2.4.1 Strength Behaviour of Joints

A joint has negligible tensile strength. However, a joint has shear strength which in general smaller than the surrounding intact rock material. The shear strength models of joint are discussed below.

2.4.1.1 Mohr- Coulomb Model

Shear strength model described by Mohr-Coulomb is the simplest model. This criterion is expressed as

$$\tau_f = c_j + \sigma'_n \mathrm{Tan} \phi_j \tag{2.26}$$

where τ_f= shear strength of joint; c_j=cohesion of joint; ϕ_j= angle of internal friction of joint; σ'_n= effective normal stress on the joint. Mohr- Coulomb model gives a liner relationship between the shear strength at failure and normal stress acting on joint plane. This criterion has global acceptability and can be used in all field situations like slopes, foundations and underground openings.

2.4.1.2 Patton (1966) bilinear model

Generally, joints contain rough profile. They consist of small asperities and undulations, hence dilation due to roughness affects the strength behaviour. Patton (1966) proposed a bilinear model to account for the effect of dilation on the Mohr-Coulomb model (Fig.2.6), which is as follows:

$$\tau_f = \sigma'_n \mathrm{Tan}\,(\phi_b + i) \qquad \text{for } \sigma'_n \leq \sigma'_o \tag{2.27a}$$

$$\text{and} \quad \tau_f = c_a + \sigma'_n \mathrm{Tan}\,\phi_r \qquad \text{for } \sigma'_n \geq \sigma'_o \tag{2.27b}$$

where ϕ_b= basic friction angle for an apparently smooth surface of the rock material; i = effective roughness angle; σ'_o = Transition stress where failure mode changes from sliding to shearing of asperities; c_a= apparent cohesion derived from asperities; ϕ_r= residual friction angle of the rock material forming the asperities.
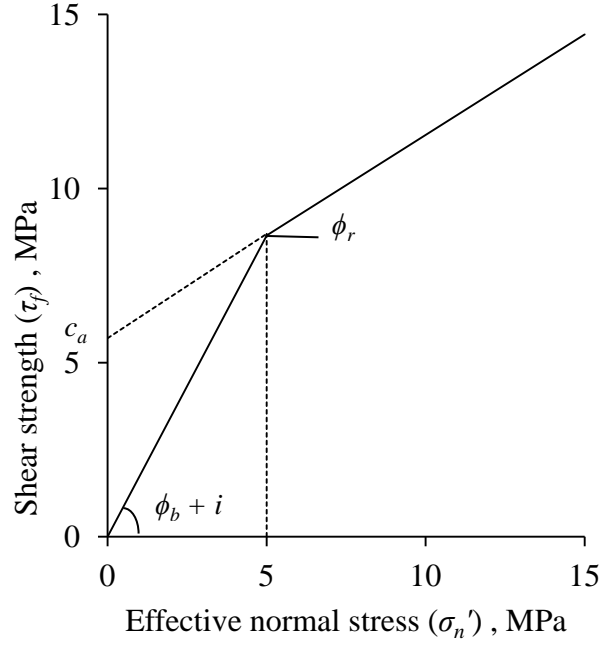
Fig. 2.6 Patton (1966) bilinear model

2.4.1.3 Ladanyi and Archambault (1970) model

Ladanyi and Archambault (1970) proposed a non-liner model based on conservation of energy concept. The equation is as follows:

$$\tau_p = \frac{\sigma_n(1-a_s)(\tilde{v}+tan\phi_\mu)+\tau_{rock}a_s}{1-(1-a_s)(\tilde{v}\,tan\phi_\mu)} \tag{2.28}$$

where τ_p = peak shear stress; $a_s = A_s/A$ =sheared area ratio; A = area of total joint surface; A_s = area of sheared surface; σ_n = mean of applied normal stress; $\tilde{v}$ = dilatency rate; ϕ_μ = friction angle of sliding surface; τ_{rock} = shear strength of intact rock

2.4.1.4 Jaeger (1971) model

Jaeger (1971) proposed the following shear strength model to provide a curved transition between the straight lines of the Patton model

$$\tau_f = c_a(1 - e^{-d\sigma'_n}) + \sigma'_n \text{Tan}[\phi_j] \tag{2.29}$$

Where d is an experimentally determined empirical parameter, which controls the shape of the transition curve.

2.4.1.5 Barton model (Barton, 1976; Barton and Choubey, 1977; Barton and Bandis, 1990)

Barton and Choubey (1977) suggested the following model to obtain the shear strength τ_f of a joint subjected to a given normal stress σ'_n

$$\tau_f = \sigma'_n \text{Tan}[\text{ JRC log}[\frac{\text{JCS}}{\sigma'_n}] + \phi_r] \qquad (2.30)$$

where JRC = joint roughness coefficient (geometrical component); JCS = joint wall compressive strength (asperity failure component); ϕ_r = residual friction angle of the joint. Barton and Choubey (1977) suggested that the residual friction angle (ϕ_r) can be calculated as

$$\phi_r = (\phi_b - 20°) + 20 \left(\frac{r}{R}\right) \qquad (2.31)$$

where ϕ_b = basic friction angle ; r = Schmidt rebound on wet joint surfaces ; R = Schmidt rebound on dry unweathered sawn surfaces.

The joint roughness coefficient (JRC) is a number that represent the roughness of joint surface. It can be estimated by comparing the appearance of a discontinuity surface with standard profiles published by Barton and Choubey (1977). Figure 2.7 shows the standard roughness profiles of joints suggested by Barton and Choubey (1977). Barton and Bandis (1982) presented a chart for estimation of JRC according to amplitude of asperities and the length of joint profile (Fig. 2.8).

The joint wall compressive strength (JCS) is the measure of uniaxial compressive strength of joint surfaces. It can be estimated by following equation (Barton and Choubey, 1977):

$$JCS = 10^{(0.00088\,R\,\gamma+1.01)}\ MPa \qquad (2.32)$$

where γ = dry density of rock (kN/m^3) and R = rebound number.

Figure 2.9 shows the correlation chart between the JCS and the Schmidt hammer rebound number. Using this chart, the JCS can be estimated.

2.4.2 Deformational Behaviour of Joints

The deformation behaviour of a joint can be characterized by its normal stiffness k_n and shear stiffness k_s. The normal and shear stiffness can be obtained by conducting direct shear tests on the joint surface. Normal stiffnesses (k_n) is defined as the normal stress (σ_n) required for unit normal displacement (u_n) (Fig.2.10a). Similar to normal stiffness, the shear stiffness (k_s) is defined as shear stress (τ) required for unit shear displacement (u_s) (Fig.2.10b). The following equations can be used

$$k_n = \frac{\Delta\sigma_n}{\Delta u_n} \quad\quad\quad (2.33a)$$

$$k_s = \frac{\Delta\tau}{\Delta u_s} \quad\quad\quad (2.33b)$$

where Δ is the increment.
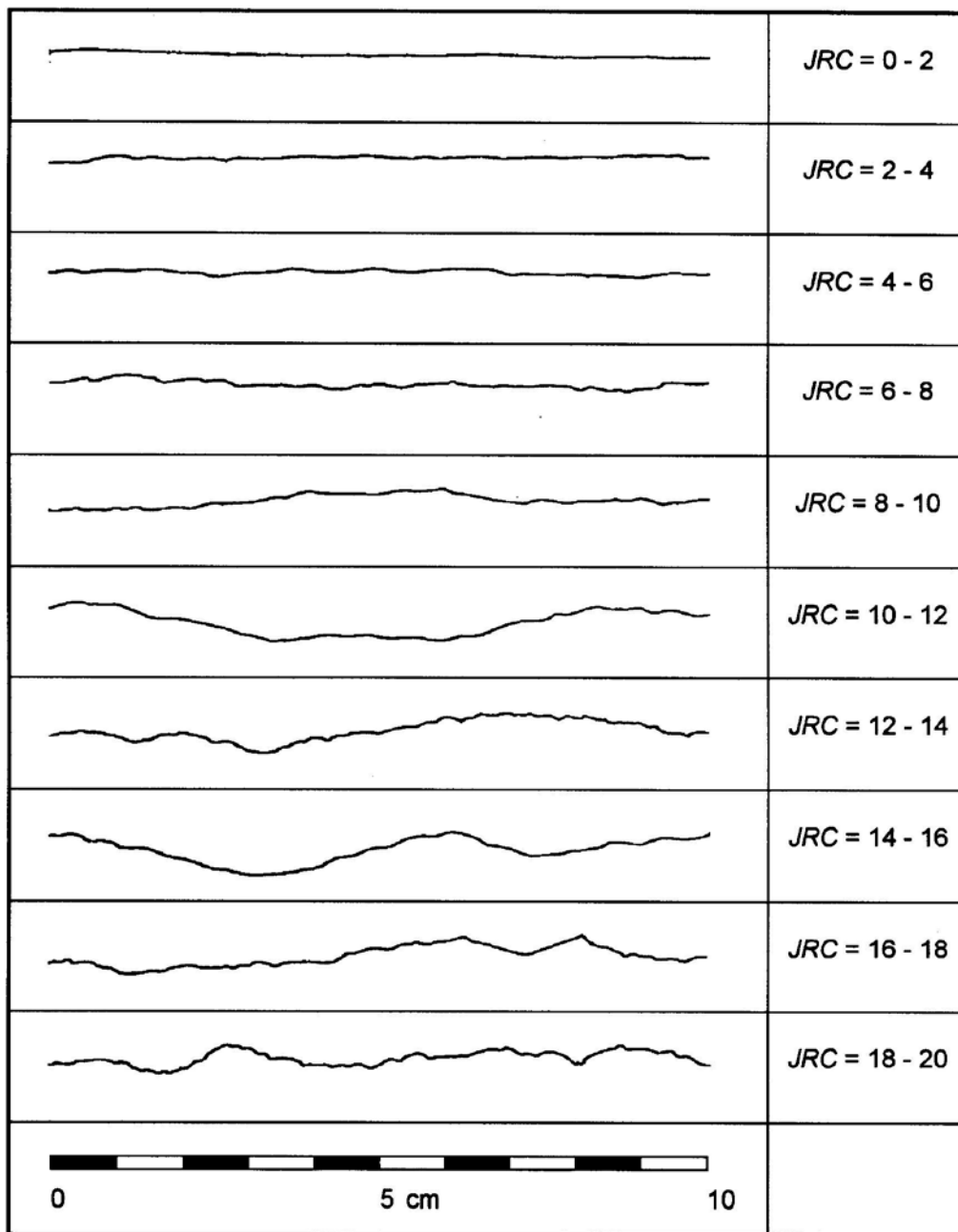
Fig. 2.7 Roughness profiles and corresponding JRC values (After, Barton and Choubey, 1977)
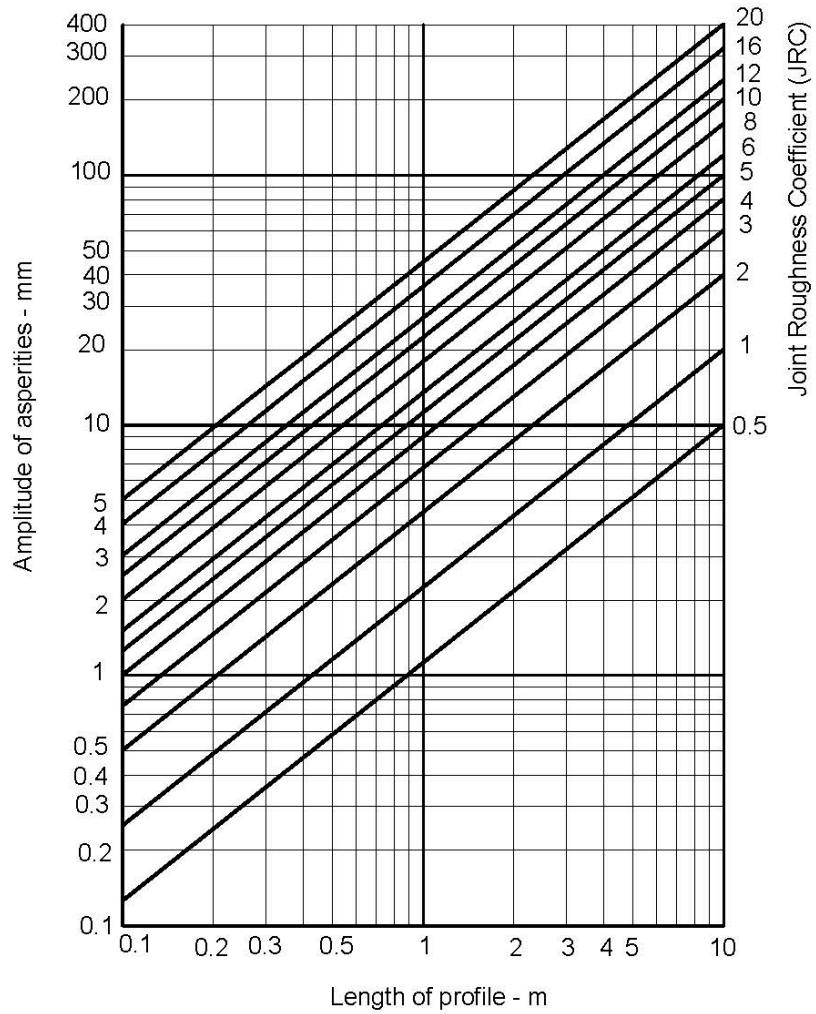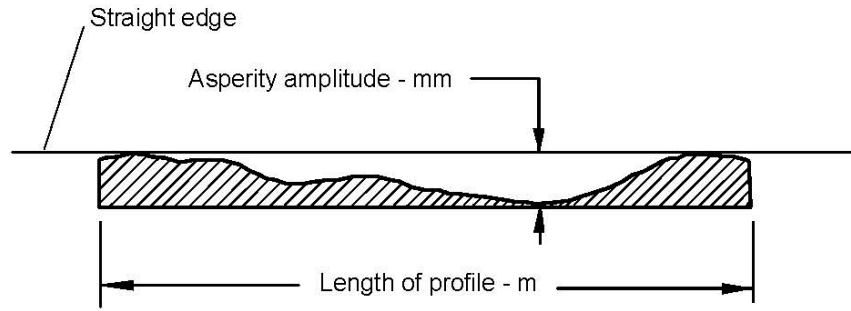
Fig. 2.8 Alternative method for estimating JRC from measurements of surface roughness amplitude from a straight-line edge (Barton and Bandis, 1982)
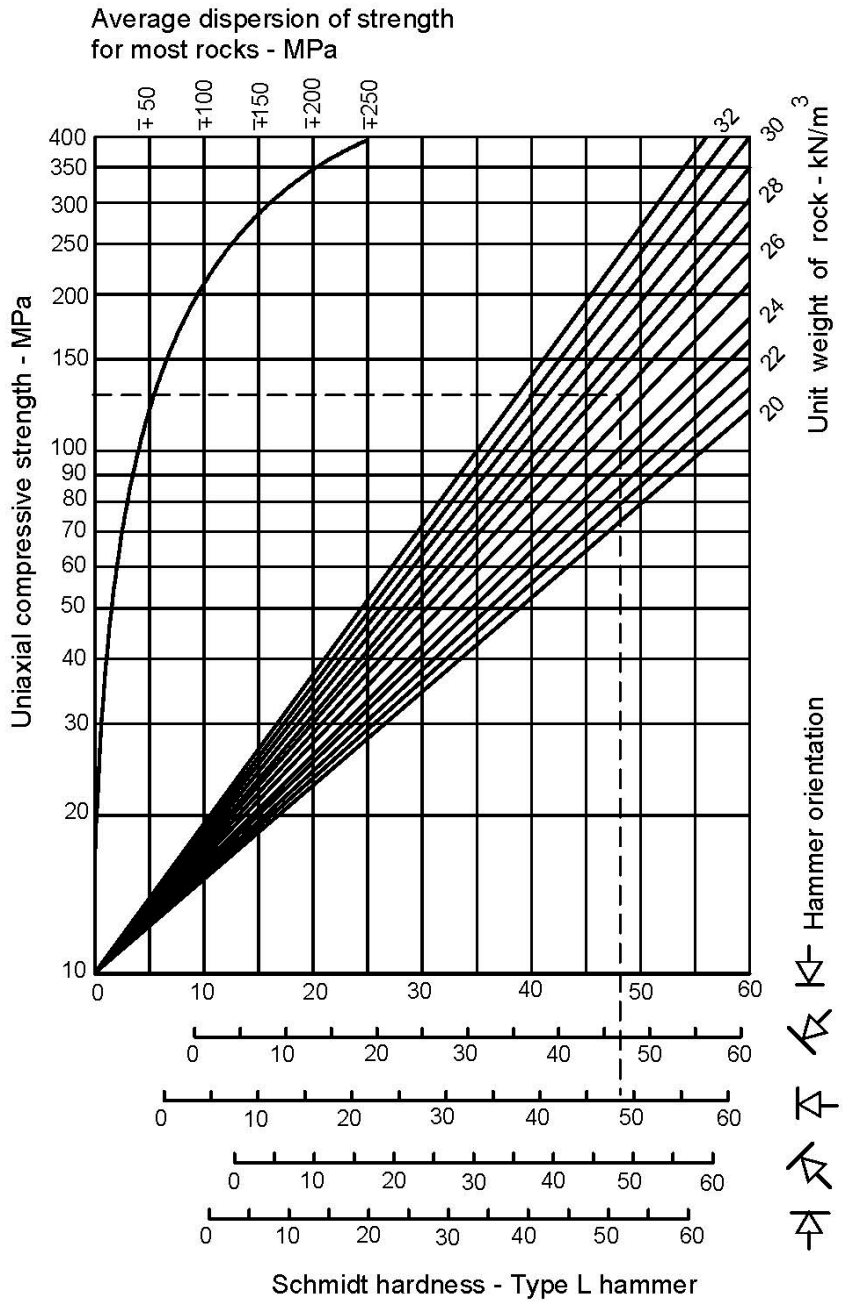
Fig. 2.9 Estimation of JCS from Schmidt Hammer rebound number (Deere and Miller, 1966)
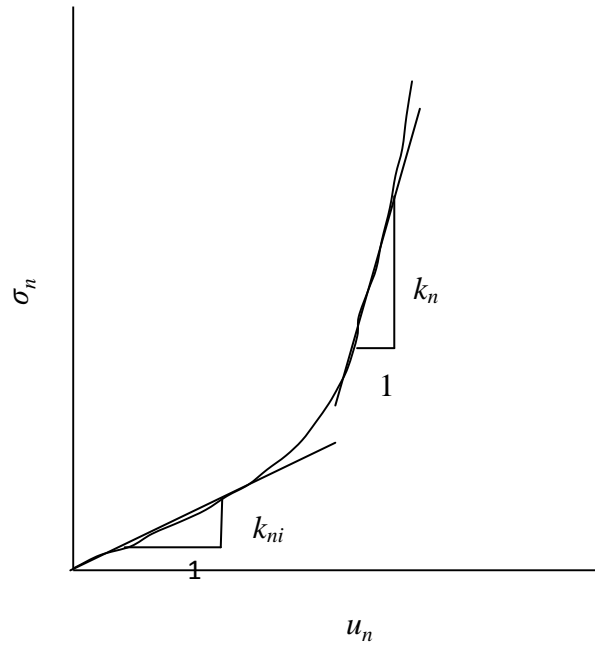
Fig. 2.10a Normal stress (σ_n) vs normal displacement (u_n) plot (Zhang, 2005)
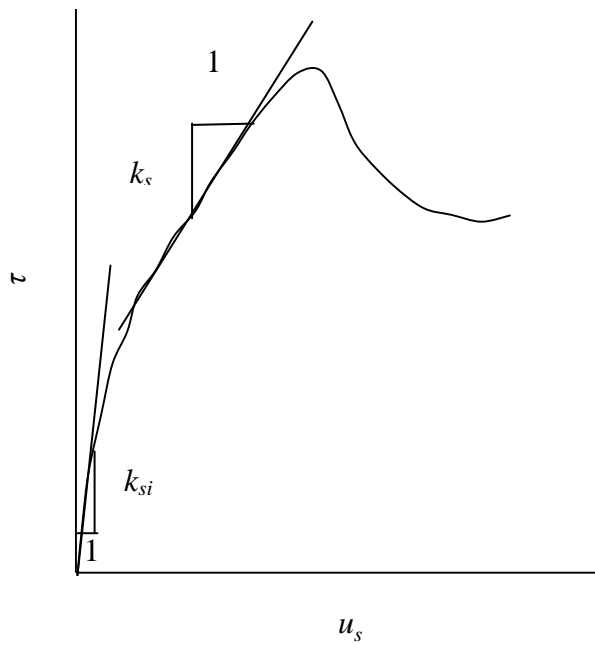
Fig. 2.10b Shear stress (τ) vs shear displacement (u_s) plot (Zhang, 2005)

Barton (1972) suggested that the stiffnesses k_n and k_s can be estimated by following equations respectively.

$$k_n = \frac{E_i E_m}{L(E_i - E_m)}$$ (2.34a)

$$k_s = \frac{G_i G_m}{L(G_i - G_m)}$$ (2.34b)

where E_i = intact rock modulus; E_m = rock mass modulus; L = mean joint spacing; G_i = intact rock shear modulus; G_m = rock mass shear modulus.

2.5 ENGINEERING BEHAVIOUR OF JOINTED ROCKS AND ROCK MASSES

If a rock consists of a single or multiple joints, it is termed as jointed rock. A large mass comprising of intact rock blocks separated by discontinuities is termed as rock mass. During failure, the blocks may slide along the discontinuities, rotate, shear or split. The failure surface may pass partly through the pre-existing joints and partly through intact rock blocks. The failure mechanism is therefore complex, which makes assessment of strength and deformational behavior of a rock mass a challenging task. Attempts have been made during past to study the engineering behaviour of jointed rock and rock masses through physical model tests.

. Laboratory studies were conducted on jointed specimens comprising single or multiple joints (Yazi, 1984; Arora, 1987; Roy, 1993; Kulatilake et al., 2001) and jointed mass specimens (Goldstein et al., 1966; Hayashi, 1966; Brown, 1970a; Brown and Trollope, 1970; Ladanyi and Archambault, 1972; Einstein and Hirschfeld, 1973; Lama 1974; Singh, 1997; Kulatilake et al., 1997, 1999 and Agrawal, 2005). These studies indicated that the strength behaviour of jointed rock/mass depends upon factors like properties of intact material, orientation of joint and failure modes. Further it is emphasized that the properties of rock mass are scale dependent (Pratt et al., 1972; Bieniawski, 1968; Bieniawski and Van Heerden, 1975; Daemen, 1981; Barton and Bandis, 1980; Barton, 1981; Bandis et al., 1981; Hoek, 1983).

In field, the assessment of engineering behaviour of rock mass is generally done through classification techniques and as consequence, classification techniques

have been employed as design process. Some of the classification systems are discussed in brief in the following section.

2.5.1 Classification of Rock masses

Several rock mass classification systems have been proposed in the to classify the mass (Terzaghi, 1946; Deere's Rock Quality Designation (RQD) (Deere, 1964); RSR Concept (Wickham et al., 1972); Rock Mass Rating (RMR) system (Bieniawski, 1973, 1976, 1989); *Q*-System (Barton et al., 1974; Barton, 1976; Barton, 2002, 2012, 2013); Geological Strength Index (GSI) system (Hoek, 1994; Hoek et al., 1995; Hoek and Brown, 1997). In most of the classification system, a numeric value has been assigned to rock mass for quantitative assessment of rock mass quality.

Terzaghi (1946) was probably the first person, who divided rock mass into the several classes and suggested methodology to assess rock load for each class. Classification systems have thus been used not only for deciding rock mass into different system rather as design methodology for underground structures.

Deere (1964, 1989) and Deere and Deere (1988) provides a quantitative estimate of rock mass quality from drill core logs. This quantitative estimate of rock mass quality is termed as "Rock Quality Designation index (*RQD*)".RQD is defined as the "percentage of intact core pieces longer than 100 mm (4 inches) in the total length of core". The classification of rock mass based on *RQD* is presented in Table 2.6.

Table 2.6 Classification of rock mass based on *RQD* (Deere, 1964)

RQD (%)	Rock quality
0-25	Very poor
25-50	Poor
50-75	Fair
75-90	Good
90-100	Excellent

Palmstrom (1982) suggested that in the absence of core recovery the *RQD* may be estimated from the following equation

$$RQD = 115 - 3.3J_v \tag{2.35}$$

where J_v volumetric joint count (sum of the number of joints per unit length for all joint).

Wickham et al. (1972) developed a quantitative method "Rock structure rating (*RSR*)" for describing the quality of rock mass. In this system, three parameters *A*, *B,* and *C* are used. A numeric value has been assigned for each parameter. Based on these three parameters the Rock structure rating (*RSR*) can be calculated as

$$RSR = A + B + C \tag{2.36}$$

The maximum value of *RSR* is 100. The RSR reflects the quality of the rock mass with respect to its need of support. The parameters *A*, *B* and *C* account for geology, geometry and water inflow in the rock mass respectively.

Bieniawski (1973, 1993, and 1989) proposed a geomechanics classification popularly known as *RMR* system. In this system, six parameters, which can be measured from a borehole data or in the field, are used. The parameters are

   i.   Uniaxial compressive strength of intact material

  ii.   Rock Quality Designation (*RQD*)

 iii.   Spacing of discontinuities

 iv.   Condition of discontinuities

  v.   Groundwater conditions

 vi.   Orientation of discontinuities

For each parameter, a rating has been assigned. The sum of all ratings for all the parameters is grouped into five categories, very good, good, fair, poor, and very poor (Table 2.7). The classification system also provides the guideline for selection of support system in case of tunnels.

Table 2.7 Classification of rock mass based on *RMR* (Bieniawski, 1989)

Rating	Class number	Description
100-81	I	Very good rock
80-61	II	Good rock
60-41	III	Fair rock
40-21	IV	Poor rock
< 21	V	Very poor rock

Barton, Lien, and Lunde (1974) analysed case histories of 212 tunnel and developed a classification system for rock masses. This classification system is popularly known as *Q* system. In this system, six parameters i.e. *RQD*, Number of joints sets, joint roughness, degree of alternation or filling, water inflow and stress conditions are used. For each parameter, a numeric value is assigned. The rock mass quality index, *Q* is expressed as

$$Q = \left(\frac{RQD}{J_n}\right) \left(\frac{J_r}{J_a}\right) \left(\frac{J_w}{SRF}\right) \tag{2.37}$$

where *RQD* = Rock Quality Designation; J_n = Joint set number; J_r = Joint roughness; number; J_a = Joint alteration number; J_w = Joint water reduction factor; *SRF* = Stress reduction factor to consider in situ stresses. The first term (RQD/J_n) in the equation 2.37 represents the block size in the rock mass. Second term ((J_r/J_a) represents the characteristics of joint while third term (J_w/SRF) represents the state of stress in the rock mass. Barton (2002) modifies his earlier *Q*. The modified *Q* system is presented in Table 2.8.

Ramamurthy and Arora (1994), Ramamurthy (2001, 2004) presented classification of jointed rock based on its strength and modulus. For this purpose Deere –Miller (1966) classification chart was used (Fig.2.11). In this classification, Ramamurthy and Arora (1994) divide the strength of rock into six classes and the modulus ratio into five different classes. The classification proposed by Ramamurthy and Arora (1994) is given in Tables 2.9a and 2.9b.

33

Table 2.8 Classification of rock mass based on *Q* (Barton, 2002)

Q	Classification
0.001-.01	Exceptionally poor
0.01-0.1	Extremely poor
0.1-1.0	Very poor
1-4	Poor
4-10	Fair
10-40	Good
40-100	Very good
100-400	Extremely good
400-1000	Exceptionally good
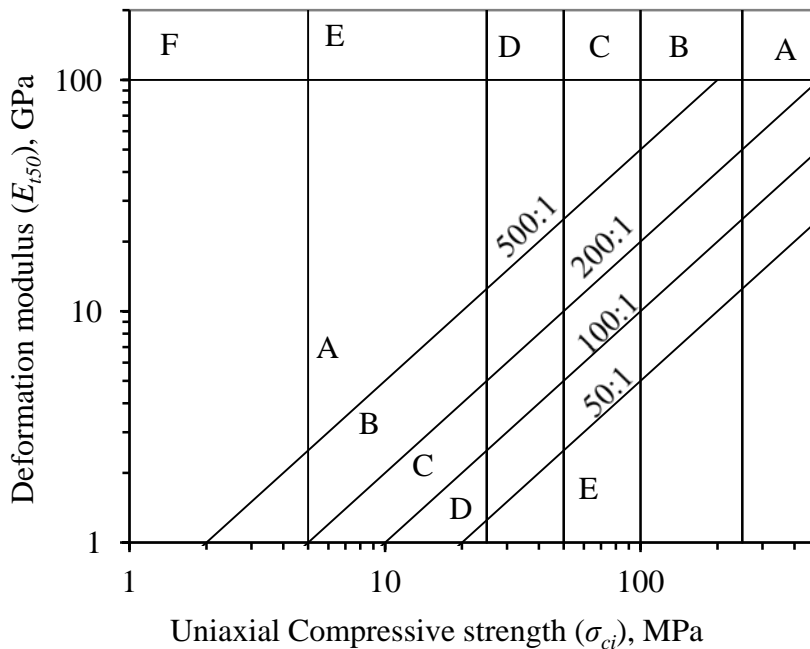
Fig. 2.11 Modification to Deere- Miller chart (1966) for classification of jointed rocks (Ramamurthy and Arora; 1994, Ramamurthy, 2001and 2004)

**Table 2.9a Strength classification of intact and jointed rock
(Ramamurthy and Arora, 1994)**
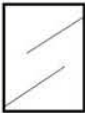
Class	σ_{ci} , MPa	Description
A	> 250	Very high strength
B	100-250	High strength
C	50-100	Moderate strength
D	25-50	Medium strength
E	5-25	Low strength
F	< 5	Very low strength

**Table 2.9b Modulus classification of intact and jointed rock (Ramamurthy and
Arora, 1994)**

Class	M_{ri}	Description
A	> 500	Very high modulus ratio
B	200-500	High modulus ratio
C	100-200	Medium modulus ratio
D	50-100	Low modulus ratio
E	< 50	Very low modulus ratio

Hoek (1994) and Hoek, Kaiser and Bawden (1995) developed the Geological
strength Index system (*GSI*) which provides the classification of rock masses based
on its geological characteristics. In this system, a numeric value is assigned to the
rock mass. The classification system is tabulated in Table 2.10. Based on the
interlocking and joint conditions (very good, good, fair, poor, and very poor) the
blocky mass is classified into six categories intact or massive, blocky, very blocky,
blocky/disturbed, disintegrated, and laminated.

Table 2.10 Characterisation of blocky rock masses on the basis of interlocking and joint Conditions (Hoek, 1994)

GEOLOGICAL STRENGTH INDEX FOR JOINTED ROCKS (Hoek and Marinos, 2000) From the lithology, structure and surface conditions of the discontinuities, estimate the average value of GSI. Do not try to be too precise. Quoting a range from 33 to 37 is more realistic than stating that GSI = 35. Note that the table does not apply to structurally controlled failures. Where weak planar structural planes are present in an unfavourable orientation with respect to the excavation face, these will dominate the rock mass behaviour. The shear strength of surfaces in rocks that are prone to deterioration as a result of changes in moisture content will be reduced is water is present. When working with rocks in the fair to very poor categories, a shift to the right may be made for wet conditions. Water pressure is dealt with by effective stress analysis.	SURFACE CONDITIONS	VERY GOOD Very rough, fresh unweathered surfaces	GOOD Rough, slightly weathered, iron stained surfaces	FAIR Smooth, moderately weathered and altered surfaces	POOR Slickensided, highly weathered surfaces with compact coatings or fillings or angular fragments	VERY POOR Slickensided, highly weathered surfaces with soft clay coatings or fillings
STRUCTURE		DECREASING SURFACE QUALITY ⟹				
INTACT OR MASSIVE - intact rock specimens or massive in situ rock with few widely spaced discontinuities	DECREASING INTERLOCKING OF ROCK PIECES	90 80			N/A	N/A
BLOCKY - well interlocked un-disturbed rock mass consisting of cubical blocks formed by three intersecting discontinuity sets			70 60			
VERY BLOCKY- interlocked, partially disturbed mass with multi-faceted angular blocks formed by 4 or more joint sets				50		
BLOCKY/DISTURBED/SEAMY - folded with angular blocks formed by many intersecting discontinuity sets. Persistence of bedding planes or schistosity				40	30	
DISINTEGRATED - poorly inter-locked, heavily broken rock mass with mixture of angular and rounded rock pieces					20	
LAMINATED/SHEARED - Lack of blockiness due to close spacing of weak schistosity or shear planes		N/A	N/A			10

2.5.2 Behaviour of jointed rocks

The strength and deformation behaviour of jointed rock is highly anisotropic. Laboratory studies conducted by Yaji, 1984; Arora, 1987; Roy, 1993 and Singh 1997 on the specimens of plaster of Paris, sandstone, granite and blocks specimens of sand – lime bricks indicate that the factor which most influence the strength and modulus of jointed rocks are

   i.   Joint frequency (number of joint per metre length)
  ii.   Critical joint orientation (β with respect to major principal stress direction) and
 iii.   Joint strength along critical joint.

To incorporate the effect of these factors, Ramamurthy (1993), Ramamurthy, and Arora (1994) introduce a joint factor J_f given by

$$J_f = \frac{J_n}{n.r} \qquad\qquad (2.38)$$

where J_n = Joint frequency i.e. number of joints per meter; n = inclination parameter depending upon the orientation of joint (β) and r = joint strength parameter dependent upon joint condition. β is the orientation of joint with respect to loading direction. The inclination factor (n) indicates the anisotropic behaviour of jointed rocks. The values of n for different joint orientations (β) are presented in Table 2.11.

Table 2.11 Values of n for different joint orientations ($\beta°$)

$\beta°$	Type of anisotropy	
	U-shaped	**Shoulder shaped**
0	0.82	0.85
10	0.46	0.60
20	0.11	0.20
30	0.05	0.06
40	0.09	0.12
50	0.30	0.45
60	0.46	0.80
70	0.64	0.90
80	0.82	0.95
90	0.95	0.98

Ramamurthy and Arora (1994) and Ramamurthy (2001) suggested the following relationship based on joint factor concept to assess the uniaxial compressive strength (σ_{cj}) and modulus (E_j) of jointed rocks

$$\sigma_{cj} = \sigma_{ci} exp\left(-0.008\, J_f\right) \tag{2.39}$$

$$E_j = E_i exp\left(-0.015\, J_f\right) \tag{2.40}$$

where σ_{ci} and E_i is the uniaxial compressive strength and modulus of intact rock.

Ramamurthy (2001) proposed a criterion for jointed rocks under confined state, which is given by following equation:

$$\frac{\sigma_1' - \sigma_3'}{\sigma_3'} = B_j \left(\frac{\sigma_{cj}}{\sigma_3'}\right)^{\alpha_j} \tag{2.41}$$

where $\sigma_1{}'$ and $\sigma_3{}'$ are major and minor principal stresses respectively and σ_{cj} is the uniaxial compressive strength of intact rock. α_j and B_j are the strength parameters for jointed rock and given by

$$\frac{\alpha_j}{\alpha_i} = \left(\frac{\sigma_{cj}}{\sigma_{ci}}\right)^{0.5} \tag{2.42a}$$

$$\frac{B_j}{B_i} = 0.13 \exp\left[2.04\, \frac{\alpha_j}{\alpha_i}\right] \tag{2.42b}$$

where α_i and B_i are the strength parameters of intact rock obtained from triaxial tests.

Based on the concept of critical state, Singh and Singh (2012) proposed a criterion for jointed rock, expressed as

$$(\sigma_1 - \sigma_3) = \sigma_{cj} + \frac{2\, sin\phi_{j0}}{1 - sin\phi_{j0}}\sigma_3 - \frac{1}{\sigma_{crtj}}\frac{sin\phi_{j0}}{1 - sin\phi_{j0}}\sigma_3{}^2 \quad for\ 0 \leq \sigma_3 \leq \sigma_{crtj} \tag{2.43}$$

where c_{j0} and ϕ_{j0} is the MC shear strength parameters of the anisotropic jointed rock at low confining pressure ($\sigma_3 \rightarrow 0$), σ_{crtj} is the critical confining pressure of jointed rock σ_{cj} is the anisotropic UCS of the jointed rock in the direction of major principal stress. The intact and jointed rocks parameters were correlated with other through following expression:

$$\frac{B_j}{2} = \left(1 + \frac{B_i}{2} - SRF\right)\frac{\sigma_{ci}}{\sigma_{crtj}} \tag{2.44a}$$

$$B_j = \frac{2\sin\phi_{j0}}{1-\sin\phi_{j0}} \tag{2.44b}$$

$$B_i = \frac{2\sin\phi_{i0}}{1-\sin\phi_{i0}} \tag{2.44c}$$

$$SRF = stregth\ reduction\ factor = \frac{\sigma_{cj}}{\sigma_{ci}} \tag{2.44d}$$

Hoek and brown (1997) and Hoek et al. (2002) proposed a failure criterion for jointed rock mass which is given by

$$\sigma'_1 = \sigma'_3 + \sigma_{ci}\left(m_b\frac{\sigma'_3}{\sigma_{ci}} + s\right)^a \tag{2.45}$$

where σ'_1 and σ'_3 are the maximum and minimum effective stresses at failure respectively, m_b is the value of the Hoek-Brown constant for the rock mass, s and a are constants which depend upon the characteristics of the rock mass, and σ_{ci} is the uniaxial compressive strength of the intact rock pieces. The values of constant are as follows

$$m_b = m_i exp\left(\frac{GSI-100}{28-14D}\right) \tag{2.46a}$$

$$s = exp\left(\frac{GSI-100}{9-3D}\right) \tag{2.46b}$$

$$a = \frac{1}{2} + \frac{1}{6}\left(e^{-GSI/15} - e^{-20/3}\right) \tag{2.46c}$$

where D is the disturbance factor which depends upon degree of disturbance due blast damage and stress relaxation.

2.5.3 Empirical correlations for Strength and Modulus of Rock masses

The strength of rock mass in the field can be assessed using several classification approaches. The empirical correlations for assessing the rock mass strength are presented in Table 2.12a. The rock mass strength can also be assessed by computing strength reduction factor, which is a function of modulus reduction factor (Singh and Rao, 2005) as given below

$$\frac{\sigma_{cj}}{\sigma_{ci}} = \left[\frac{E_j}{E_i}\right]^n \qquad\qquad\qquad\qquad (2.47\text{a})$$

or $\qquad$ SRF = (MRF)^n $\qquad\qquad\qquad\qquad\qquad\qquad$ (2.47b)

where, SRF = Strength Reduction Factor = σ_{cj}/σ_{ci}; MRF = Modulus Reduction Factor = E_j/E_i; σ_{cj} and σ_{ci} = UCS of jointed and intact rock respectively; E_j and E_i = modulus values of jointed and intact rock respectively; n = constant depends on failure mode of jointed rock.

The modulus of rock mass can be determined by conducting the deformability tests in the field. The commonly used deformability tests are plate jacking test, plate loading test, flat jack test, pressure chamber test and Goodman jack tests (Singh, 2010, 2011; Singh et al., 2010). Suitability of these tests depends upon the characteristics of rock mass (Palmstrom and Singh, 2001; Singh 2009). In absence of field tests, the classification approaches may be used to assess the modulus values. Empirical correlations suggested by various researchers are presented in Table 2.12b.

For complex field condition, numerical approaches provide best solutions for stress-strain behaviour of the mass in the field. Significant contributions have been made by several researchers in this field (Dhawan et al., 1991; Bhasin et al., 1996, 2002; Bhasin and Hog, 1997, 1998; Varadarajan et al., 2001; Sridevi and Sitharam, 2000, 2003; Madhvi Latha and Sitharam, 2004; Sitharam et al., 2001, 2005; Verma and Singh, 2010; Sazid and Singh, 2013, Barton, 2013).

Table 2.12a Deformation modulus of rock mass (E_m)

Correlations relating E_m with RQD	
Coon and Merritt (1970)	$\frac{E_m}{E_i} = 0.0231 RQD - 1.32$
Gardner (1987)	$E_{m=} \alpha_E \, E_i$ $\alpha_E = 0.0231 \, RQD - 1.32 \geq 0.15$ where α_E is the reduction factor, which accounts for frequency of discontinuities by *RQD*.
Kayabasi et al. (2003)	$E_m = 0.1423 \left[\frac{E_m \, (1-0.01RQD)}{WD} \right]^{1.1747}$ where *WD* is the weathering degree of discontinuity.
Zhang and Einstein (2004)	$\frac{E_m}{E_i} = 10^{0.0186RQD - 1.91}$
Correlations relating E_m with RMR	
Bieniawski (1978)	$E_m = 2RMR - 100$ GPa
Serafim and Pereirra (1983)	$E_{mass} = 10^{(RMR-10)/40}$ GPa
Gokceoglu et al. (2003)	$E_m = 0.0736 \, e^{0.0755RMR}$ GPa
Ramamurthy (2001)	$E_m = E_i exp\left(\frac{RMR-100}{17.4} \right)$
Correlations relating E_m with GSI	
Hoek and Brown (1997)	$E_m = \sqrt{\frac{\sigma_{ci}}{100}} \, 10^{(GSI-10)/40}$ GPa where σ_{ci} = unconfined compressive strength of intact rock less than 100 MPa.
Gokceoglu et al. (2003)	$E_m = 0.1451 \, e^{0.0654GSI}$ GPa
Hoek (2004)	$E_m = 0.33 \, e^{0.064 \, GSI}$ GPa
Hoek and Diederichs (2006)	$E_m = E_i \left(0.02 + \frac{1-D/2}{1+exp((60+15D-GSI)/11))} \right)$ where *D* is the damage factor
Correlations relating deformation modulus E_m with Q	
Barton et al. (1980)	$E_m = 25 \log_e Q$
Barton (2002)	$E_{mass} = 10Q_c^{1/3}$ $Q_c = Q\left(\frac{\sigma_{ci}}{100} \right)$ where σ_{ci} is the intact rock strength in MPa.
Correlations relating E_m with joint factor (J_f)	
Ramamurthy (1993) and Ramamurthy and Arora (1994)	$E_m = E_i exp\left(-0.0115 J_f \right)$
Singh et al. (2002)	$E_{mass} = E_i exp\left(-0.020 J_f \right)$ Splitting / shearing failure $E_{mass} = E_i exp\left(-0.035 J_f \right)$ Sliding mode of failure $E_{mass} = E_i exp\left(-0.040 J_f \right)$ Rotational failure

E_m and E_i is the deformation modulus of the rock mass and the intact rock respectively. *RQD* = rock quality designation; *RMR* = Rock mass rating; *Q* = Tunnel quality index; *GSI* = Geological strength index; J_f = joint factor

Table 2.12b Uniaxial compressive Strength of rock mass

Correlations relating σ_{cm} with RQD	
Zhang (2010)	$\frac{\sigma_{cm}}{\sigma_{ci}} = 10^{(0.013RQD-1.34)}$
Correlations relating σ_{cm} with RMR	
Yudhbir et al. (1983)	$\frac{\sigma_{cm}}{\sigma_{ci}} = exp\left(\frac{7.65\,(RMR-100)}{100}\right)$
Laubscher (1984), Singh and Goel (1999)	$\frac{\sigma_{cm}}{\sigma_{ci}} = \frac{RMR-Rating\ or\ \sigma_{ci}}{106}$
Trueman (1988) and Asef et al. (2000)	$\frac{\sigma_{cm}}{\sigma_{ci}} = 0.5\,exp(0.06\,RMR)$ MPa
Kalamaras and Bieniawski (1993)	$\frac{\sigma_{cm}}{\sigma_{ci}} = exp\left(\frac{RMR-100}{24}\right)$
Ramamurthy (1993, 2001)	$\frac{\sigma_{cm}}{\sigma_{ci}} = exp\left(\frac{RMR-100}{25}\right)$
Sheorey (1997)	$\frac{\sigma_{cm}}{\sigma_{ci}} = exp\left(\frac{RMR-100}{20}\right)$
Aydan and Dalgic (1998)	$\frac{\sigma_{cm}}{\sigma_{ci}} = \frac{RMR}{RMR+6(100-RMR)}$
Correlations relating σ_{cm} with GSI	
Hoek (1994) and Hoek et al. (1995)	$\frac{\sigma_{cm}}{\sigma_{ci}} = exp\left(\frac{GSI-100}{18}\right)$
Hoek (2004)	$\frac{\sigma_{cm}}{\sigma_{ci}} = 0.036exp\left(\frac{GSI}{30}\right)$
Correlations relating σ_{cm} with Q	
Grimstad and Bhasin (1996), Singh and Goel (1999)	$\sigma_{cm} = 7\gamma\,f_c\,Q^{1/3}$ where $f_c = \sigma_{ci}\,/\,100$ for $Q > 10$ and $\sigma_{ci} > 100$ MPa, otherwise $f_c = 1$ γ = Unit weight of the rock mass in g/cm^3
Barton (2002)	$\sigma_{cm} = 5\gamma\,\left(\frac{Q\,\sigma_{ci}}{100}\right)^{1/3}$MPa γ = Unit weight of the rock mass in g/cm^3
Correlations relating σ_{cm} with J_f	
Singh, Rao, and Ramamurthy (2002)	$\frac{\sigma_{cm}}{\sigma_{ci}} = exp(-0.0123J_f)$ for splitting failure $\frac{\sigma_{cm}}{\sigma_{ci}} = exp(-0.011J_f)$ for shearing failure $\frac{\sigma_{cm}}{\sigma_{ci}} = exp(-0.0118J_f)$ for sliding failure $\frac{\sigma_{cm}}{\sigma_{ci}} = exp(-0.025J_f)$ for rotational failure

σ_{cm} =uniaxial compressive strength of rock mass and σ_{ci}= uniaxial compressive strength of intact rock.

2.6 REINFORCEMENT OF ROCK MASS THROUGH ROCK BOLTS IN FIELD CONDITIONS

In field, the design of support system is mainly governed by the characteristics of the rock mass like strength, deformation modulus, and stiffness (Daemen and Fairhurst, 1970, 1972; Daemen, 1975). These characteristics lead to optimization of support system for a particular type of rock (Daemen, 1975). Field studies and numerical modelling conducted by the researchers (Barton and Bakhtar, 1984; Sharma and Pande, 1988; Shen and Barton, 1997; Singh and Singh, 1997; Singh et al, 1989, 1996) suggested that the efficient design of rock bolt support system depends upon the compatible properties of the bolt and the mass. The diameter, length and tensile strength of the bolt is generally governed by the characteristics of mass, dimension of rock structures and in-situ stresses.

For designing rock bolt empirical approaches or classification system are used. Hoek and Moy (1993) suggested empirical relationship to determine the length (L) and spacing (S) of rock bolts in an underground opening as follows:

(i) Length of the bolt

$$\text{Roof: Rock bolts,} \quad L = 2 + 0.15\,B \tag{2.48a}$$

$$\text{Cables,} \quad L = 0.4\,B \tag{2.48b}$$

$$\text{Walls: Rock bolts,} \quad L = 2 + 0.15\,H \tag{2.48a}$$

$$\text{Cables,} \quad L = 0.35\,B \tag{2.48b}$$

(ii) Spacing of bolt

$$S < L/2 \text{ for uniform rock reinforcement} \tag{2.49a}$$

$$S = (T/P)^{1/2} \text{ for square grid of bolts or cables, in m} \tag{2.49b}$$

where L = length of bolt in m; S = spacing of bolt in m; H = Height of underground opening in m; B = span width of underground opening in m; T = working load per bolt or cable in ton and P = support pressure in ton.

Based on *Q* system, Barton et al. (1974, 1980) suggested the following expressions for calculation of rock bolt length (*L*)

$$L = 2 + \frac{0.5\,B}{ESR} \qquad \text{for roof} \qquad\qquad (2.50a)$$

$$L = 2 + \frac{0.5\,H}{ESR} \qquad \text{for wall} \qquad\qquad (2.50b)$$

where *ESR* is the excavation support ratio. For different category of excavation, the value of ESR is presented in Table 2.13.

Table 2.13 Value of ESR (Barton et al., 1974)

Excavation category		*ESR*
A	Temporary mine openings	3-5
B	Permanent mine openings, water tunnels for hydro power (excluding high pressure penstocks), pilot tunnels, drifts and headings for large excavations	1.6
C	Storage rooms, water treatment plants, minor road and railway tunnels, surge chambers, access tunnels	1.3
D	Power stations, major road and railway tunnels, civil defence chambers, portal intersections	1.0
E	Underground nuclear power stations, railway stations, sports and public facilities, factories	0.8

2.7 STUDIES CONDUCTED ON REINFORCED JOINTED ROCK

Bjurström (1974) conducted laboratory and field shear tests on bolted rock joint to study the force-deformation characteristics under the application of shear load. Granite specimens with natural and artificial joints were prepared for shear tests. For conducting laboratory shear tests, Bjurström (1974) used a shear machine having maximum loading capacity of 2.5 MN. The cross section of the rock specimens was 25 cm x 40 cm and each specimen consisted of one smooth joint. Bolts were installed at different angles with respect to joint surface (Fig.2.12a). Deformed steel bars having diameter of 16 mm or 25 mm were used as bolts. The ultimate tensile strength of bolt was 600 MPa. The bolt was grouted with cement-sand mortar of ratio 1:1. More than 110 shear tests were conducted on the unreinforced and reinforced specimens. The tests were performed at constant normal pressure and with constant

shear velocity of 0.15 mm/ min. To compare the laboratory results, field shear tests were conducted using 25 mm diameter steel bolts embedded in two granite blocks of size 4 x 4 x 2 m. The blocks were rested on a natural, undisturbed and rough surfaces. Bolts were installed at angle $\alpha = 30°$ and $60°$ as shown in Fig.2.12b.
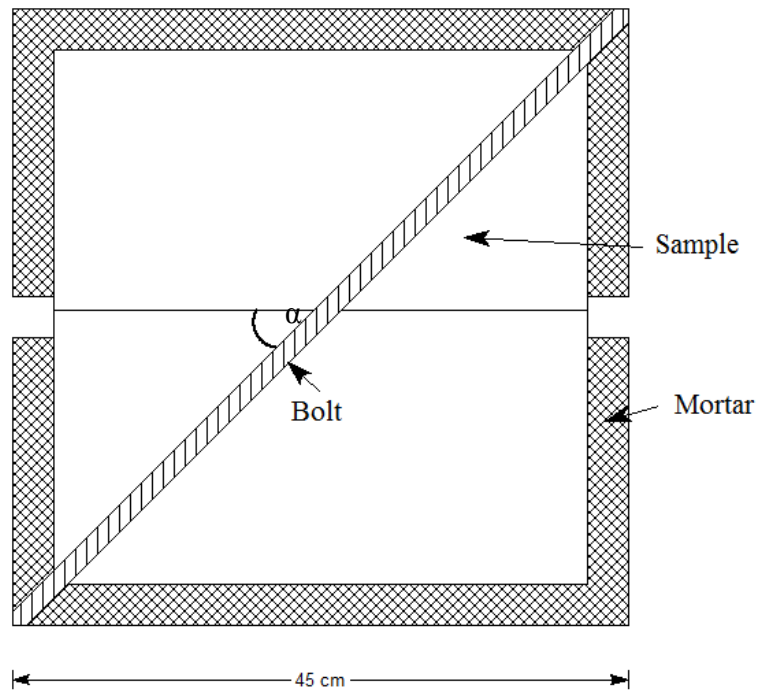
Fig.2.12a Cross section of specimen tested in laboratory (Bjurström, 1974)
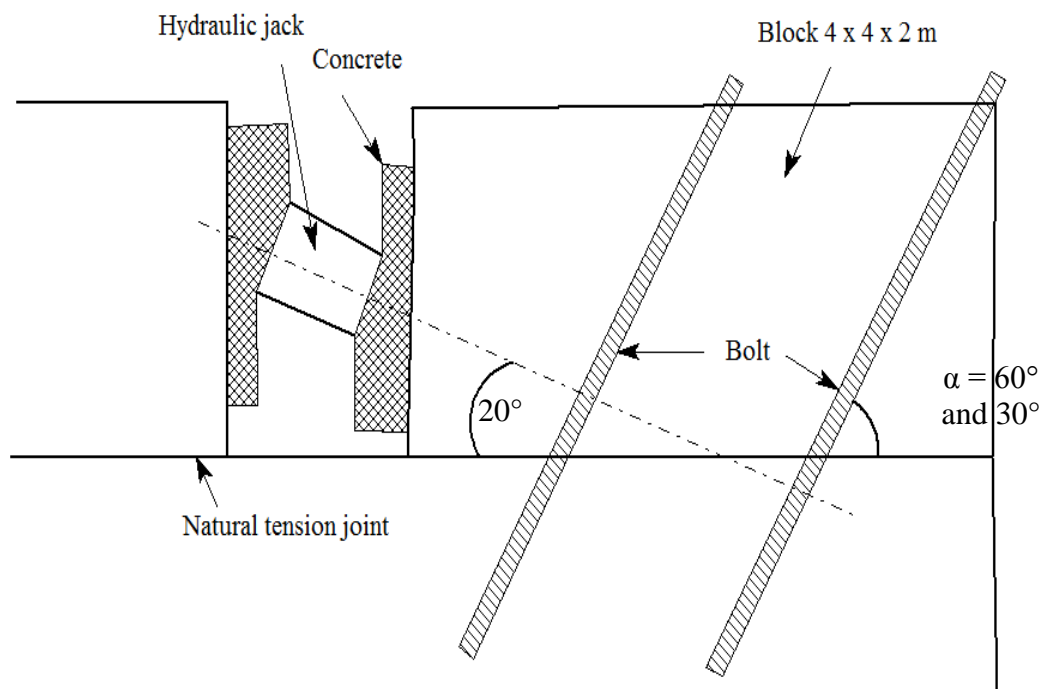
Fig.2.12b Setup of field shear test (Bjurström, 1974)

From the results of the laboratory and field shear tests, Bjurström (1974) suggested that the shear resistance of reinforced joint increases due to following reasons:

i.   An increased normal pressure due to bolt with addition to original normal pressure on joint surface,

ii. Development of tensile forces in bolts, and

iii. Dowel effect of the bolt.

Bjurström (1974) further suggested that the "tensile force in the bolts due to shear displacement acts in two ways:- (i) The component tangential to the joint surface gives a direct contribution to shear resistance, and (ii) The component normal to the surface will increase the normal pressure and contract the dilation of the joint and thus increases the friction strength of the joint." From the study following conclusions were drawn:

i.   Strength of grouted bolts depends upon factors like strength of rock material, size, strength of bolt, its inclination from joint surface and roughness of joint.

ii. Bolt increases the stiffness of joints.

iii. Normal pressure on joint plays an important role to strengthen of bolted joint.

Haas (1976, 1981) conducted laboratory shear tests on different types of bolts and anchors embedded in blocks of limestone and shale. Following conclusions were drawn from the study:

- As compared to unreinforced jointed rock, the shear stress of reinforced rock was increased.

- Inclined bolts added more contribution to shear strength of jointed rock as compared with perpendicular bolts.

- Dilation contributed in the shear stiffness of bolted joint.

- Fully grouted bolts are stiffer than the point anchored bolts.

Azuar (1977) tested resin-grouted bolts embedded in concrete and concluded that perpendicular bolts contributed more in shear strength of jointed rock as compared to inclined one and dilation increased the strength of bolted joint.

Hibino and Motjima (1981) conducted shear tests on the pre-tensioned grouted bolts (fully bonded and point anchored) embedded in concrete. The outcome of the study was:

- Shear resistance of fully grouted bolts was greater as compared point anchored bolts.
- The inclination of bolts did not have any influence on shear resistance.
- Pre-tensioning of bolts influenced the final shear displacements but did not contribute to the shear strength.

Dight (1982) carried out shear tests on un-tensioned fully grouted bolts with smooth and rough joints in the rock blocks of gypsum and basalt. It was concluded that the bolts installed at an angle with respect the joints exhibited higher stiffness as compared to the bolts installed in the direction perpendicular to the joints. It was also observed that the effect of normal stress on the bolted joint was insignificant, whereas dilation had same influence on inclined bolts. In addition, deformability of surrounding rock was observed to be an influencing parameter with regard to bolt-deformation.

Egger and Fernandez (1983) studied shear strength of bolts installed in concrete blocks and observed that shear strength was maximum for the bolts installed at an angle ranges from 30° to 60° with the joint surface, whereas the bolts installed in the direction perpendicular to the joint surface exhibited minimum shear strength.

Ludvig (1983) performed shear tests on swellex bolts, massive steel bolts, massive and tube bolts of fibreglass in a large shear rig same as used by Bjurström (1974). The rig consists of two steel boxes of size 450 mm x 600 mm x 300 mm. Different types of materials like concrete, granite, slate, and gneiss were used for making jointed rock. The maximum size of sample block was 420 x 320 x 560 mm. Different bolts were tested in different media having inclination α = 45° and 90° respect to joint surface (Fig.2.13). Following observations and conclusions are made:

i. Shear strength of the jointed rock blocks reinforced with bolt strongly depends upon the rock material.

ii. Bolts' properties and type also influenced the shear strength.

iii. Inclination between bolt and joint surface is an important factor, which governs the strength of bolted joints.
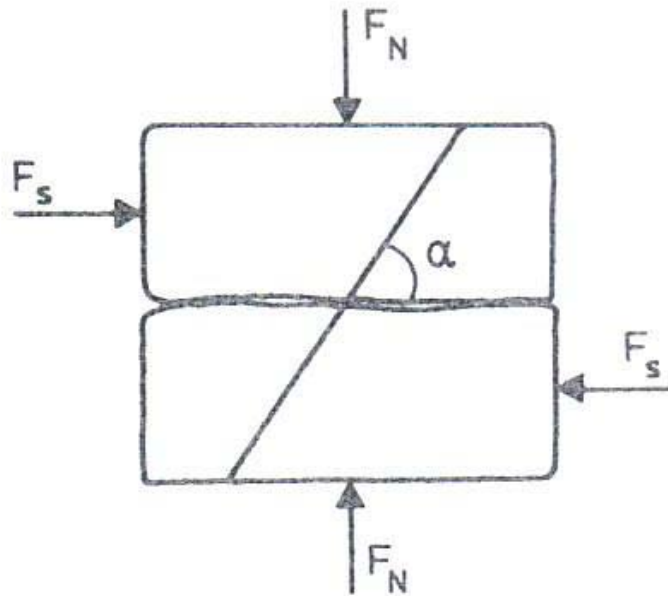
Fig. 2.13 Sketch of experimental setup (Ludvig, 1983)

Schubert (1984) conducted shear tests on bolted concrete and limestone blocks and suggested that the strength and deformability of the surrounding rock are important factors. The study concluded that bolts embedded in harder rock exhibited higher stiffness than in the softer rock. He further added that soft steel improved the deformability of the bolted system in soft rock.

Spang and Egger (1990) conducted laboratory and field studies to study the behaviour of fully bonded rock bolts. The laboratory shear tests were conducted on blocks of sizes 15 cm x 15 cm x 13 cm and 22 cm x 20 cm x 15 cm using conventional shear tests apparatus (Fig.2.14a). They used steel bolts of 8 mm and 10mm diameter in laboratory tests. Field tests were conducted using 40 mm diameter

bolts on the foundation rock at a dam site (Fig.2.14b). The diameter of borehole for installation of bolt was twice the bolt's diameter. The bolts were grouted with cement mortar. Parameters like normal stress, diameter and inclination of bolt, and steel quality were varied in the tests.

Based on the results of laboratory tests, Spang and Egger (1990) suggested that the shear resistance of grouted bolts depends upon a series of parameters. These parameters are properties of bolt, inclination between joint and bolt, strength of surrounding material, angle of friction along joint and dilatancy.
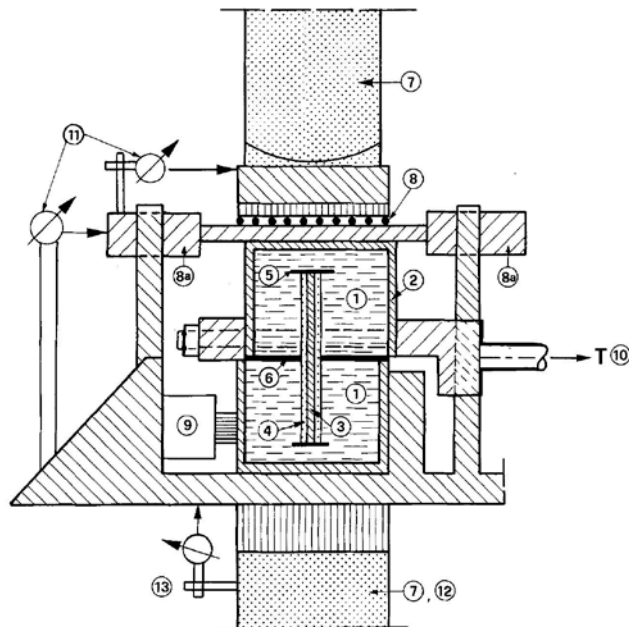
1- Parallelepipedic blocks; 2- Shear box; 3- Bolt; 4- cement mortar; 5- Face plate; 6- Shaer surface; 7- Vertical jack for applying normal stress; 8- Guided cam which prevent the rotation of upper and lower halve of shear box; 9- Horizontal jack; 10- Monitoring unit for shear load; 11- Dial gauges for recording horizontal shear displacement; 12- Monitoring unit for normal load; 13- Dial gauges for recording horizontal shear displacement.

Fig.2.14a Schematic layout of the laboratory shear tests (after Spang and Egger, 1990)
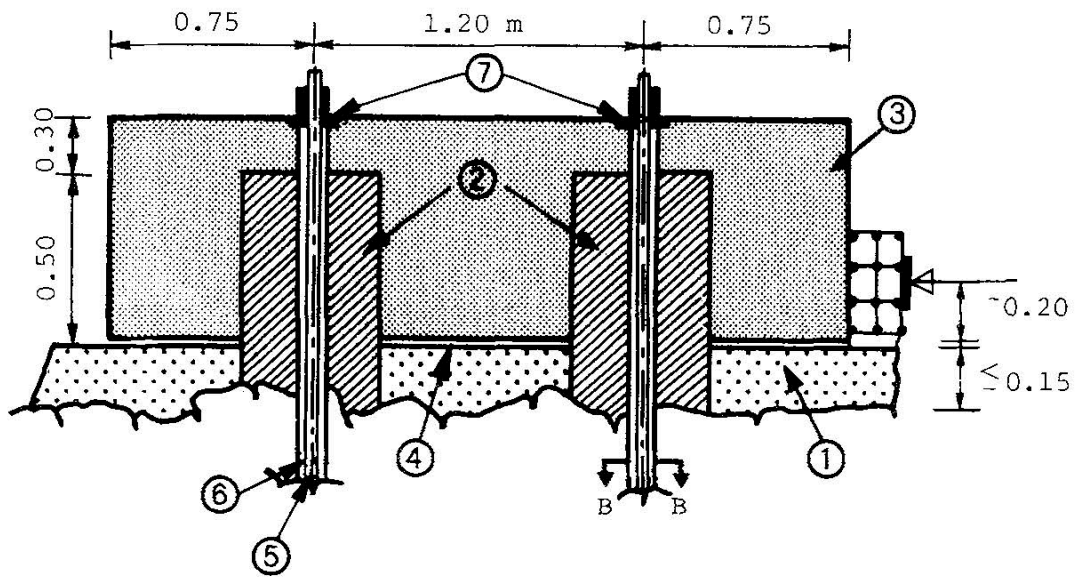
1- Dam foundation; 2- Special concrete blocks in which the bolt are embedded; 3- Large concrete blocks, 4-Shear plane; 5- Rock bolt; 6- Grout; 7- Face plate

Fig.2.14b Schematic layout of the field shear tests (after Spang and Egger, 1990)

The results of field tests were compared with the results of laboratory tests and they observed that the maximum contribution of the bolt (T_o) to the total shear strength of the joint is a function of various parameters, expressed as:

$$T_o = T_u \left[1.55 + 0.011 \, \sigma_c^{1.07} \, sin^2[\beta + i] \, \sigma_c^{-0.14} \, (0.85 + 0.45 \, tan\phi) \right] \qquad (2.51)$$

where T_u = ultimate axial bolt load; β = angle between the bolt and joint surface; i = angle of dilatancy; ϕ= angle of friction along the shear plane, and σ_c= compressive strength of the host rock. They further concluded that the high friction joint (rough joint) gives more contribution to shear strength as compared to frictionless joint. Inclined bolts have higher resistance to shear as compared to perpendicular one.

The study of Egger and Zabuski (1991) concluded that the bolts provide additional resistance to the joints against shear failure and hence this provision increases stiffness of the joints. They further stated that the uniaxial compressive strength of material surrounding the bolt plays an important role against shear failure.

Ferrero (1995) evaluated the shear strength of rock joints reinforced by steel dowels through laboratory experiments and numerical modelling. He used two types of rock materials, i.e., granite and concrete (to make weak rock). The specimens were composed of two prismatic blocks of size 300 mm x 300 mm x 400 (height). Different types of steel and tube bolt were used for shear tests. The bolt was installed perpendicular to the joint (Fig.2.15). The surfaces of the joint were plane and perfectly smooth. In some tests, pre-stressing was applied to the bolts. Ferrero (1995) observed that the shear resistance is proportional to square of the bar diameter for a given testing conditions. However, shear displacement is proportional to the bar diameter. Maximum shear resistance of reinforced joint was found with most ductile steel reinforcement. Higher shear stress in the bars developed for stronger and stiffer rock materials. It led to lower global resistance of the reinforced joint. Maximum resistance to shear was observed for the combination of ductile rock bolt and weak rock specimen. An important conclusion about the effect of pretension was made as he mentioned, "pretension only influences the stress-strain behaviour of the reinforced joint and not the final resistance of the system". The tube reinforcement showed lower resistance as compared to the other tested reinforcement types. Based on the result, the author concluded that the reinforcement contributed to shear strength by two combined effects.

i.   The normal stress acting on the joint surface induces tensile stress in the bar, and

ii. The bar resistance to shear and to tensile stress.
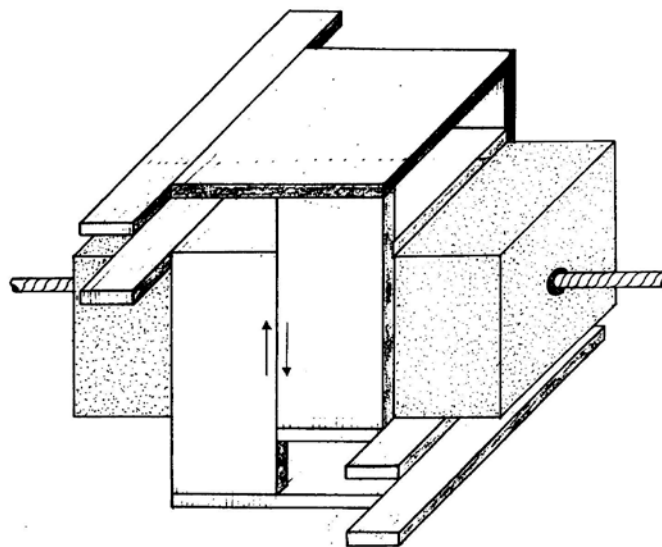
Fig.2.15 Laboratory test device (Ferrero, 1995)

Pellet and Egger (1996) studied shear strength of bolts installed in model materials and revealed that the bolts installed perpendicular to a joint plane allowed the greatest displacement along the joint before failure, but that displacement at failure decreased rapidly as the angle between the bolt and joint plane decreased. In addition, harder rock led to bolt failure at smaller displacements.

Ferrero et al. (1997) carried out experimental and analytical study to investigate the behaviour of rock bolt reinforced joint. Shear tests were performed using concrete blocks reinforced by single and multiple steel bolts. The size of concrete block was 60 cm x 60 cm x 100 cm (height). The uniaxial compressive strength of concrete was 39.2 MPa. The bolts (tensile strength 620/690 MPa) were installed perpendicular to shearing direction (Fig.2.16). The diameter of bolt and drill hole was 16 mm and 32 respectively. The bolts were grouted with cement mortar having uniaxial compressive strength of 55 MPa. Ferrero et al. (1997) observed that the resistance of joint reinforced with several bolts was greater as compared to joint reinforced with single bolt. This indicates that the group action of bolts plays an important role for strengthening the rock and there is complex interaction between blocks and bolts. The stiffness of multiple bolt structure is greater as compared to single one. It was also concluded that increase in spacing between bolts decreases the peak displacement. Further Ferrero et al. (1997) suggested that "overall system resistance increases almost proportionately to the number of bars. When bolts are largely spaced, the interaction between bars are reduced and peak displacement gradually decreases."

Using concrete as a model material, Goris et al. (1996) studied shear strength of bolts installed through joints (rough and smooth) and concluded that strength of reinforced joint was influenced by factors like joint profile, and grout material. They further suggested that shear stress induced the tensile stress in the bolt and increased the normal force on joint resulting in the increased shear strength.
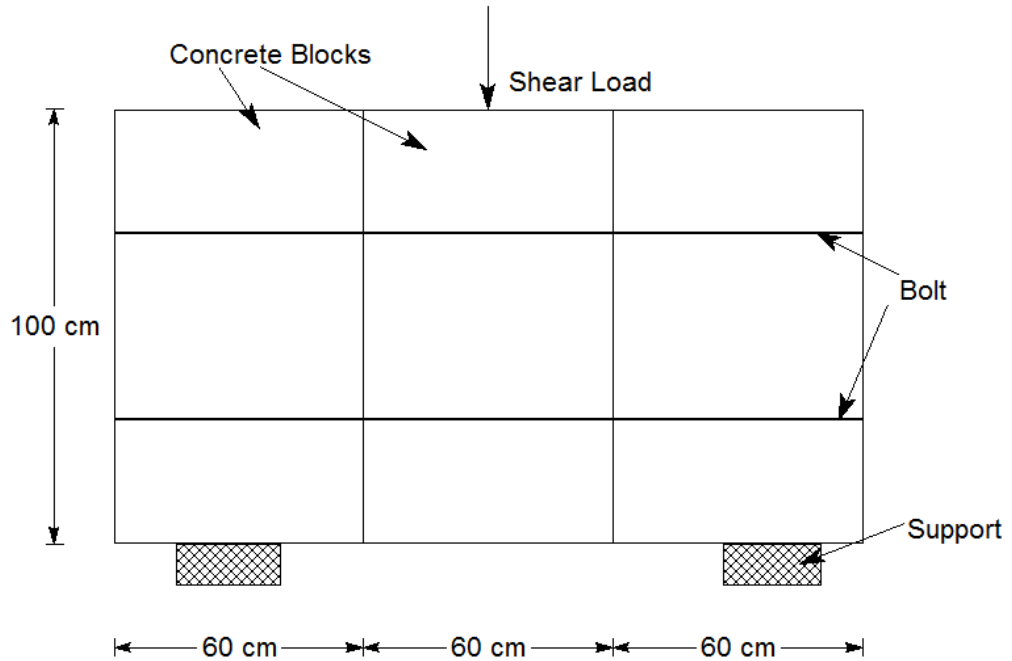
Fig. 2.16 Experimental setup (Ferrero, 1997)

McHugh and Signer (1999) conducted laboratory shear tests on rock bolts installed in high strength concrete blocks. The concrete blocks consisted of fine sand-cement mix having uniaxial compressive strength of 85.5 MPa. The bolt was 58.4 cm long having 22 mm diameter. Polyester resin was used as grout having unconfined compressive strength of 69 MPa. The shear tests were conducted using a shear machine of capacity 1334 kN (Fig.2.17). From the laboratory results following conclusions were drawn:

  i. Axial loading has little effect on a joint's resistance to shear.
 ii. Hardness of surrounding rocks contributes in shear loading.
iii. Pre-tensioning of the bolts effectively minimizes separation of the joint faces during shear displacement. Unlike fully grouted bolts in mine installations, the nut and plate anchors at the ends of the test bolts ensured that grout failure would not be a factor in load and displacement profiles. Separation of the shearing faces and plastic failure of grout would tend to propagate bending forces to greater distances along the bolt.
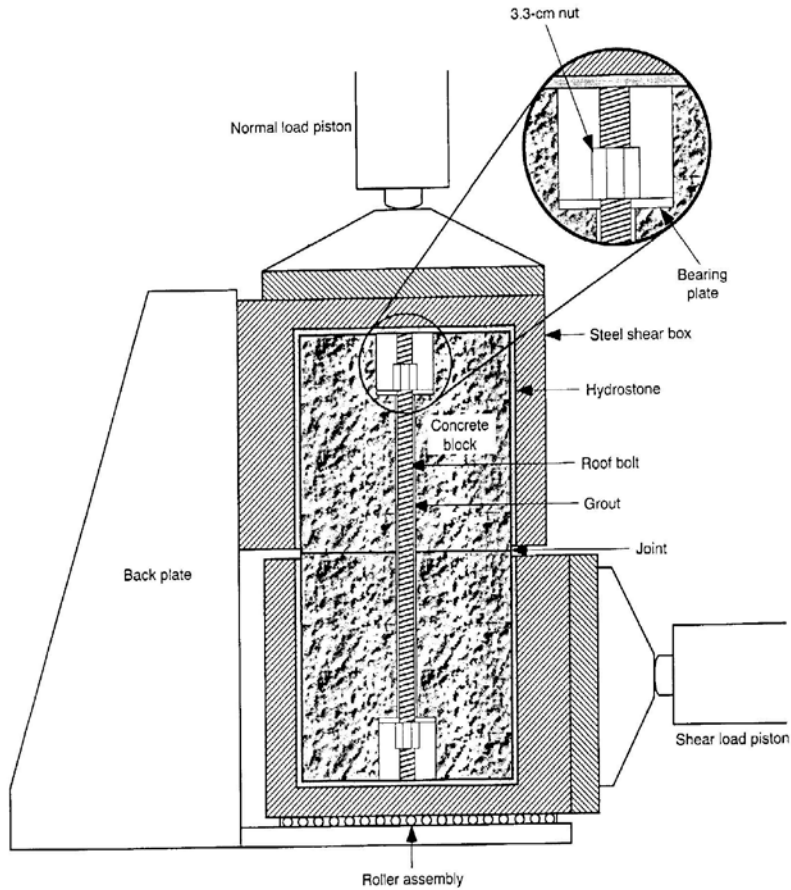
Fig.2.17 Shear box assembly (McHugh and Signer, 1999)

Grasselli et al. (1999) conducted the double shear tests on the bolted joints. Large-scale laboratory tests were performed with fully grouted solid bars and hollow tubes (Fig.2.18). Concrete was used as model material. They observed that the plastic hinge was formed at the interface of joint and bolt. The development of plastic hinge led to greater displacement. They further suggested a numerical relationship for estimating the bolt contribution to shear strength, T^* as following:

$$T^* = \frac{T_v - 2.N.\tan \phi_i}{2.F_{max}} \qquad (2.52)$$

where T_v = vertical force applied; N = confinement force; ϕ_i = friction angle of the block surface, and F_{max} = ultimate tensile load of the bolt.
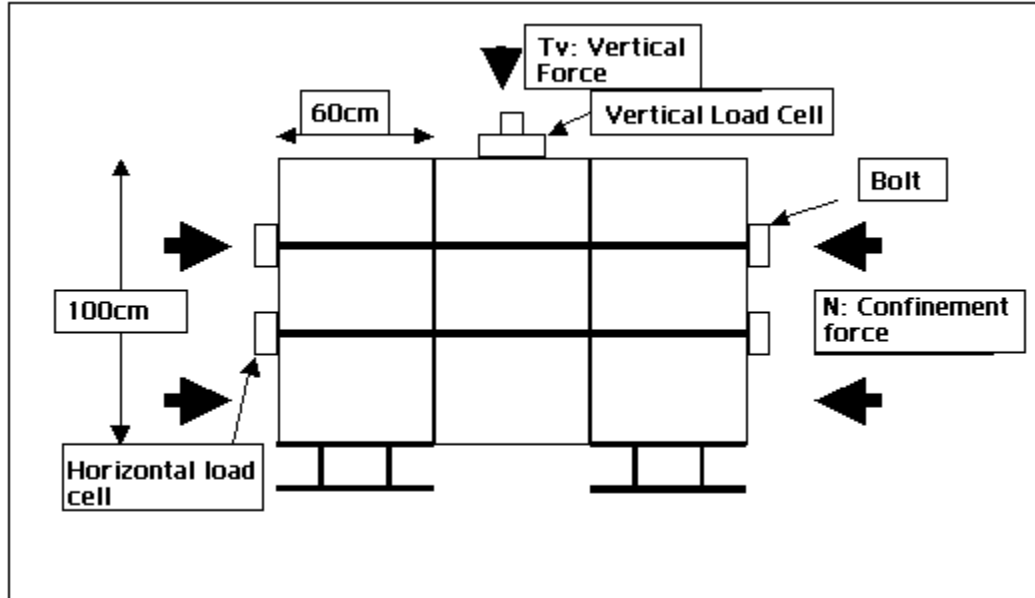
Fig.2.18 Experimental set up (Grasselli et al., 1999)

Similar to his previous work of Grasselli et al, 1999, Grasselli (2005) carried out experimental investigation and numerical modelling to understand the mechanical responses of steel bars and frictional Swellex bolts. Grasselli (2005) conducted large shear tests on the bolted joints. He used three large concrete blocks of size 100 cm x 60 cm x 60 cm each (Fig.2.19). The assembled block consisted of two macroscopically smooth joints. The joints were stitched by installing rock bolts at an angle with the joints. Based on the observations of his experimental work, he modified the expression represented by Eq. 2.32 to the new expression as following:

$$T^* = \frac{T_v - 2.N.\tan\phi_i}{2.n.F_{max}}$$
(2.53)

where T^* = dimensionless bolt contribution to shear strength; N = force that acts normally to the joint; ϕ_i =frictional angle of the smooth joint; n = number of bolt sections on each joint.
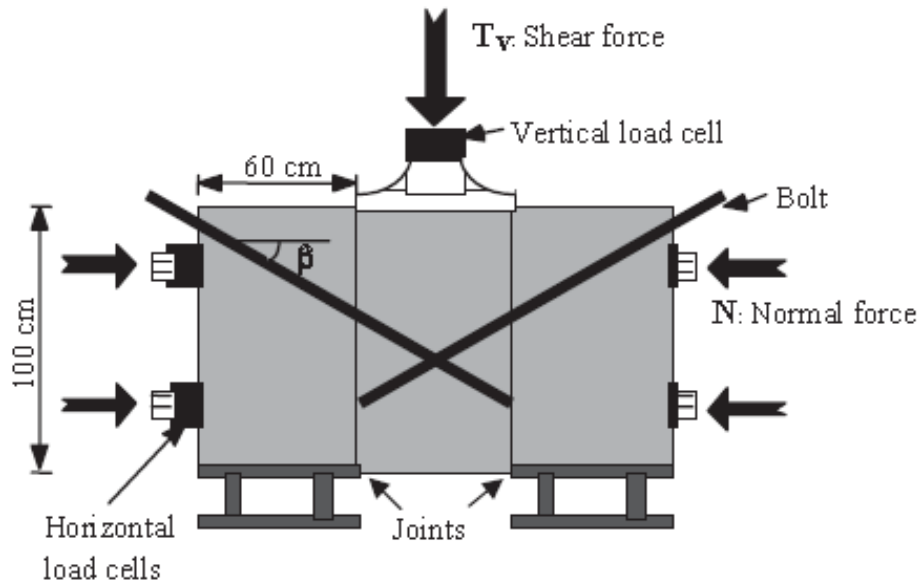
Fig.2.19 Experimental set-up adopted for the shear tests on double bolted joints (Grasselli, 2005)

A comparison of typical behaviour of two different types of reinforcement (full steel bolt and hollow bolt) is presented in Fig.2.20. Grasselli (2005) suggested that the regardless of the type, each plot has three different parts. Each part exhibits different mechanical reaction of the reinforcement. The first part indicates the linear behaviour in which large shear load at smaller shear displacement was observed. Mobilisation of shear resistance through steel bolt was grater for swellex bolt. Second part of the plots indicates a non-linear behaviour, which corresponds to the yielding of the materials. In steel bolts, a great displacement is associated with the formation of plastic hinges. In the swellex bolt, the plastic yielding begins at the joint plane and consequently, when the deformation progresses, the swellex flatten out over a progressively longer free length. The third part of the plot indicates a nearly unconstrained plastic deformation of the bolt, until its failure. However, the failure mechanisms are different, depending on the bolt type and on the angle joint/bolt. Grasselli (2005) further stated that the resistance mobilised by the bolts is proportional to the contact area of steel. The main findings of work carried out by (2005) are

i.   Strength of reinforced rock strongly depends upon the type of bolts either solid or hollow. Solid steel bolts add more resistance in joints compared to hollow bolts.

ii.   Solid bolts exhibit higher shear resistance due to development of plastic hinges at the interface between joint and bolt.
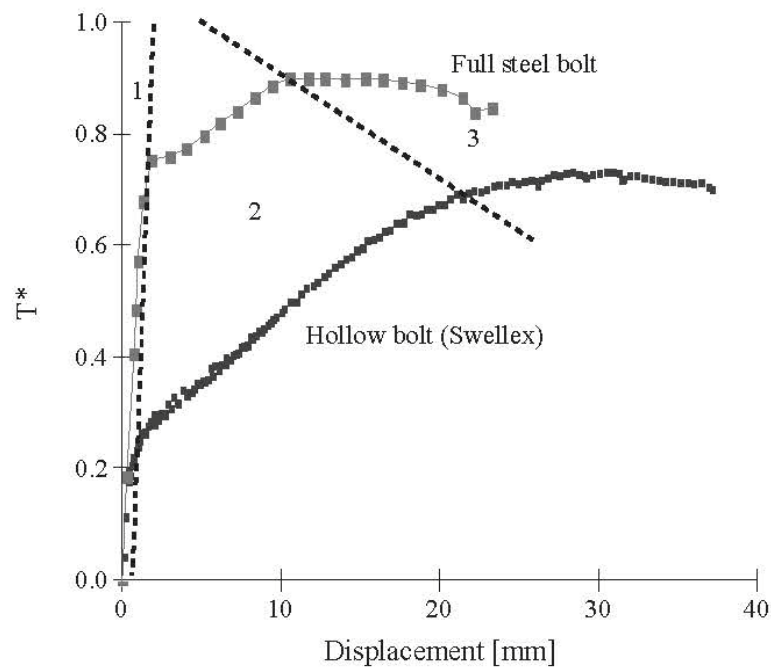
Fig. 2.20   Comparison between the typical mechanical behaviour of steel bolts (20 mm diameter) and Swellex dowels, both positioned perpendicular to the joint (Grasselli, 2005)

Aziz et al. (2004) conducted double shear testing on fully grouted and tensioned bolts. The bolt was embedded in three-piece concrete blocks having cross section of 150 mm x 150 mm. The used concrete blocks were of three different lengths, i.e., 150 mm, 300 mm and 150 mm. The concrete of two uniaxial compressive strength values (40 MPa and 20 MPa) were used for construction of the blocks. Bolts of 1400 mm length were installed in concrete blocks with resin grouts. The shear tests were conducted at three different pretension forces i.e., 20 kN, 50 kN, 80 kN respectively. Results from the tests indicated that the strength of surrounding rock and pretension of bolts are important factor and govern the strength of bolted rock joints.

Jalalifar and Aziz carried out the double shear tests on bolted joints with different block strength (20 , 40 and 100 MPa) and different pretension forces (0, 5, 10 ,20, 50, 80 kN). They strongly recommended that the medium and pretensioning have substantial effect on shear strength of bolted joints. Increased pretension forces caused increase in failure stresses.

Sakurai (2010) investigated the reinforcement effect of rock bolts on the different types of model material through physical model tests in laboratory. He conducted uniaxial compression tests on the different model materials. The size of each specimen was 100 mm × 100 mm × 200 mm (height). Uniaxial compression tests were performed on unreinforced and reinforced specimens. Based on the results, he suggested that the rock bolts are extremely effective in hard rock. In case of reinforced jointed specimens, the mechanical properties depend upon the strength of rock material and orientation between joint and bolts.

2.8 CONCLUDING REMARKS

For improving strength properties of jointed rocks, the bolting is widely used for reinforcing the mass (Ferrero et al. 1997). Rock bolts not only enhance the strength of the mass through structural action, but also by imposing restriction on the rotation and sliding of the blocks. Assessing the shear strength of such reinforced mass is an important but difficult task, and in many cases experience dictates the design. Based on the literature available on reinforced joint, it is understood that the behavior of reinforced joint is substantially different from the unreinforced joint due to presence of bolt. The behaviour of reinforced jointed rock is governed by the following factors

  i.   Engineering properties of parent intact rock
 ii.   Numbers of joints crossing the bolts
iii.   Joint condition
 iv.   Inclination between bolt and joint
  v.   Mechanical properties of bolts (tensile strength, young modulus etc)
 vi.   Type of bolt (Solid or hollow etc) and material of bolt
vii.   Diameter and length of bolt
viii.   Strength of grout used

A number of studies are available in literature on the effect of bolts on the engineering behaviour of rock joints (Bjurström 1974; Haas 1976, 1981; Hibino and Motjima 1981; Dight 1982; Ludvig 1983; Schubert 1984; Egger and Zabuski 1991; Roberts 1995; Pellet and Egger 1996; McHugh and Signer 1999; Grasselli et al. 1999; Grasselli 2005; Sakurai 2010). The majority of these studies has only considered single joints, and do not truly capture the behaviour of joints within a large mass. In addition, the studies mainly focused on the yielding of bolts rather than the interaction between the bolt and the intact blocks during shearing. Ferrero et al. (1997) emphasized that the assessment of enhancement in the engineering properties of a rock mass is very difficult since it involves complex failure mechanisms, the interaction between different materials and the characteristics of joints. In addition the complexities of interactions between a large numbers of blocks add to the difficulties. Therefore, to improve the understanding of engineering behaviour of reinforced mass there is need to study the behaviour of rock bolt reinforced mass.

Several strength criteria are in vogue for assessing the strength response of jointed rocks subject to given confining pressure (Hoek and Brown, 1980; Ramamurthy, 2001; Singh and Singh, 2012). However, for reinforced rock no such criterion is available. Therefore for reinforced rock a strength criterion is required which should be able to predict the strength of reinforced jointed rock under varying confining stress levels.

EXPERIMENTAL STUDY

3.1 GENERAL

The main objective of present research work is to investigate the strength behaviour of blocky mass/jointed rock without and with reinforcement. To achieve the objective, an experimental study has been conducted on the specimens of unreinforced and bolt-reinforced specimens. Passive rock bolts were used as reinforcement. The experimental study comprises of the following parts

i.   Direct shear tests on blocky rock mass specimens of size 750 mm x 750mm x 900 mm (height).

ii. Uniaxial compression tests on synthetic rock (concrete) specimens of size 150 mm x150 mm x 300 mm (height).

iii. Triaxial compression tests on specimens of a natural rock (cylindrical specimens of NX size).

This section describes the detailed methodology used for experimental study. The detailed schematic plan of experimental work is given in Fig.3.1.

3.2 DIRECT SHEAR TESTS ON BLOCKY MASS SPECIMENS

3.2.1 Methodology

Direct shear tests were conducted on large size specimens of a blocky mass without and with reinforcement by subjecting them to shear load along a joint surface. To obtain scale free behaviour of blocky mass, it is necessary for the specimen to have an adequate number of elemental blocks in each direction. Studies conducted by Walker (1971) and Lama (1974) have indicated that if the size of the specimen is about five times the size of the elemental block, the strength behaviour can be treated as scale free. Therefore, it was decided to have at least five elemental blocks in each

direction of the specimen. In addition, the blocks were drilled and bolts were installed, which could make the elemental block weak. The elemental blocks should therefore be as large as possible, so that the drilling would not affect the overall strength of the elemental block. These essential requirements warrant that large size blocky mass specimens be prepared and tested.

Direct shear tests on blocky mass specimens

Model material (Concrete)

Elemental block size: 150 mm x 150 mm x 150

Blocky mass size: 750 mm x 750 mm x 900 mm (height)

Unreinforced mass

Reinforced mass

(Grouted bolts, diameter 6 mm)

σ_n (MPa)   0.0   0 .5   1 .0   2 .0

Configurations of specimens

R3   R5   R9

σ_n (MPa)   0.0   0 .5   1   2
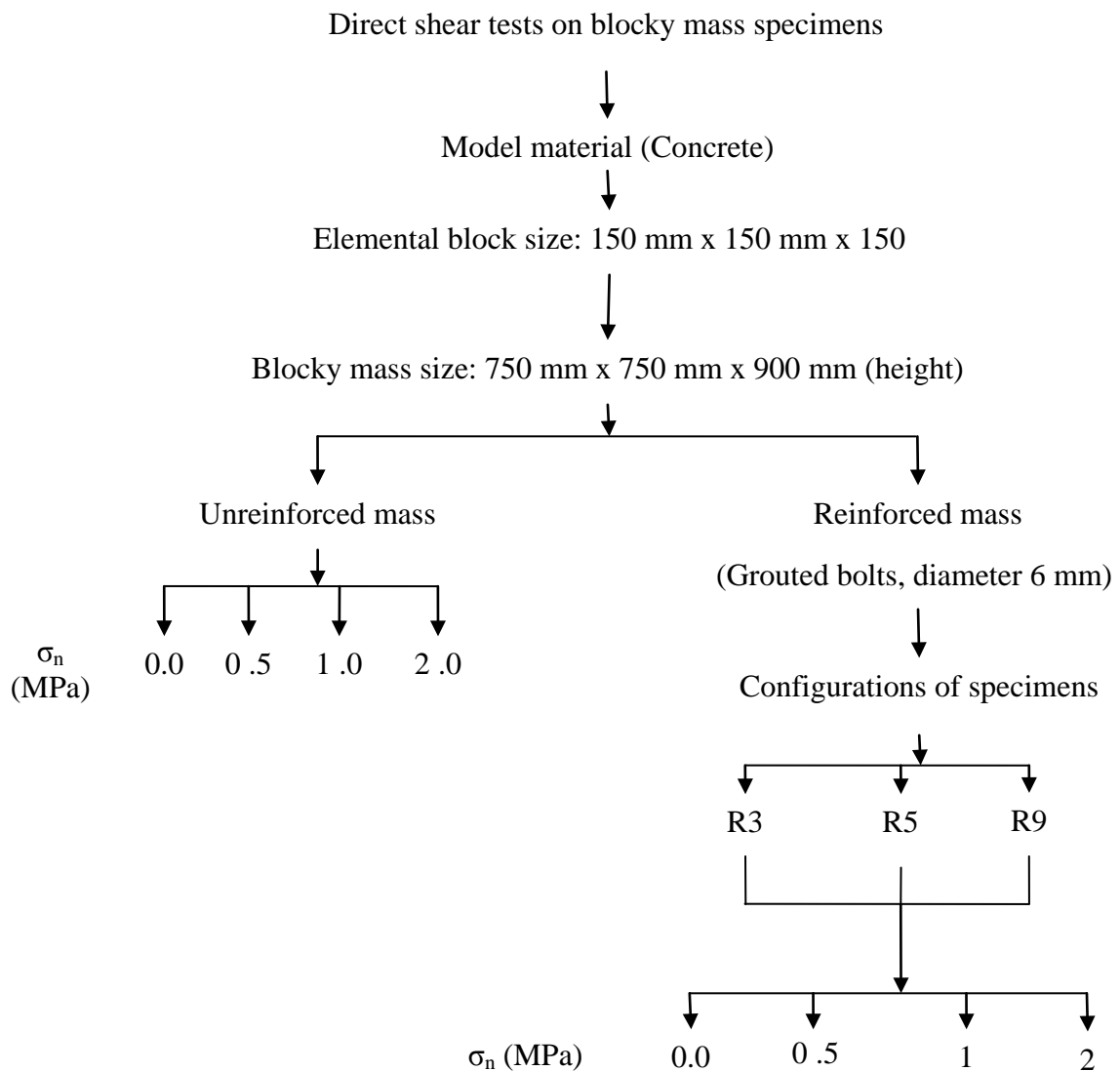
Fig. 3.1a Experimental plan: Direct shear tests on blocky mass specimens

Uniaxial compression tests

Synthetic Rock
(Concrete)

Natural Rock
(Gneiss)

Prismatic Specimens
Size 150 mm x 150 mm x 300
mm (height)

Cylindrical Specimens
NX size (diameter 54 mm)

Unreinforced

Reinforced
(2 Grouted bolts of 6 mm

Unreinforced

Reinforced
(1 Grouted bolt of 4 mm

Joint orientation

θ°   0   15   30   45   60   75   90

Joint orientation

θ°   0-10   10-20   20-30   30-40   50-60   60-70   70-80   80-90
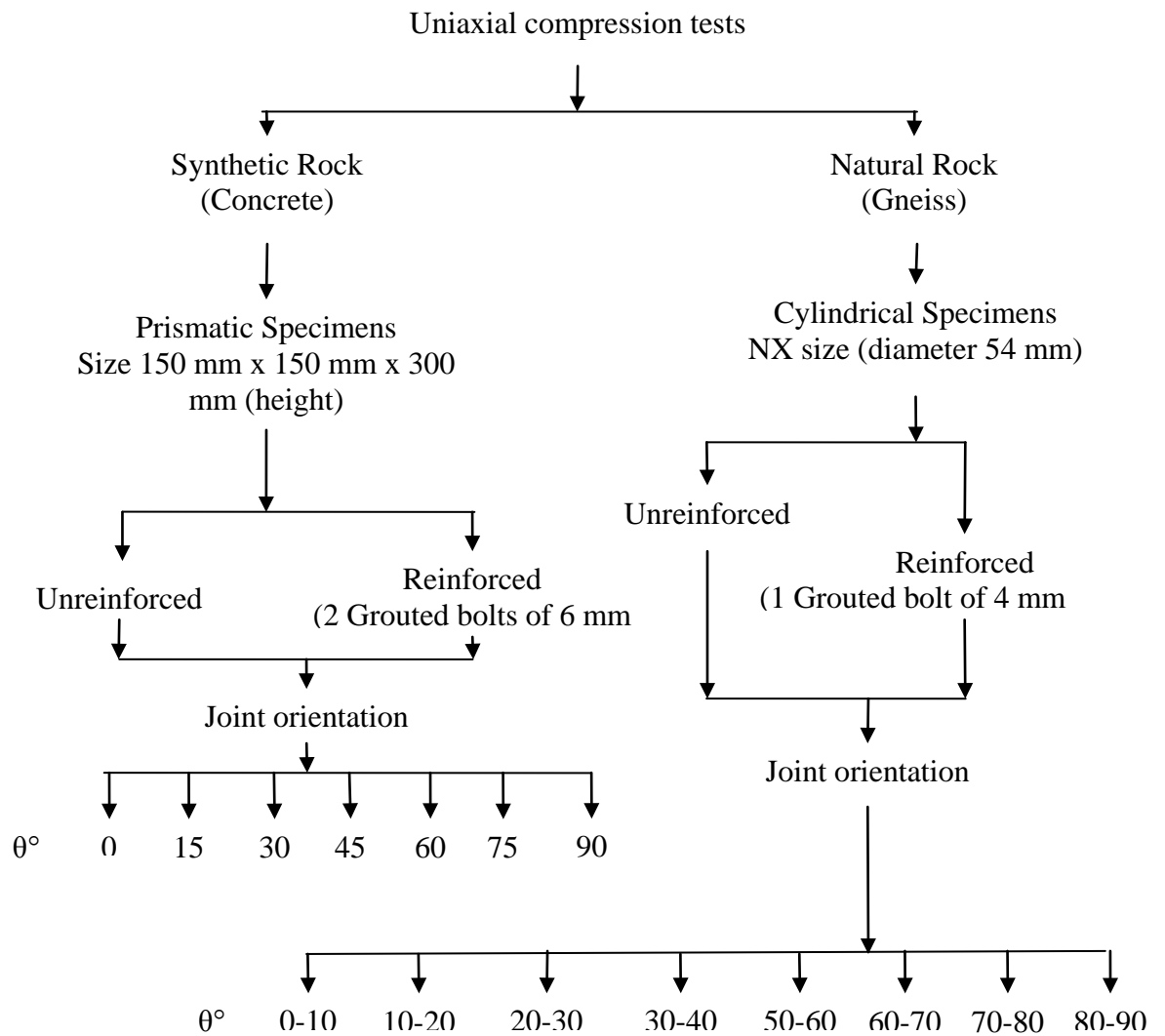
Fig. 3.1b Experimental plan: Uniaxial compression tests on jointed rocks

Triaxil compression tests

Natural Rock
(Gneiss)

Cylindrical Specimens
NX size (diameter 54 mm)

Unreinforced

Reinforced
(1Grouted bolt of 4 mm diameter)

Joint orientation

| $\theta°$ | 0-10 | 10-20 | 20-30 | 30-40 | 50-60 | 60-70 |

σ_3 (MPa)   0   5   20   40
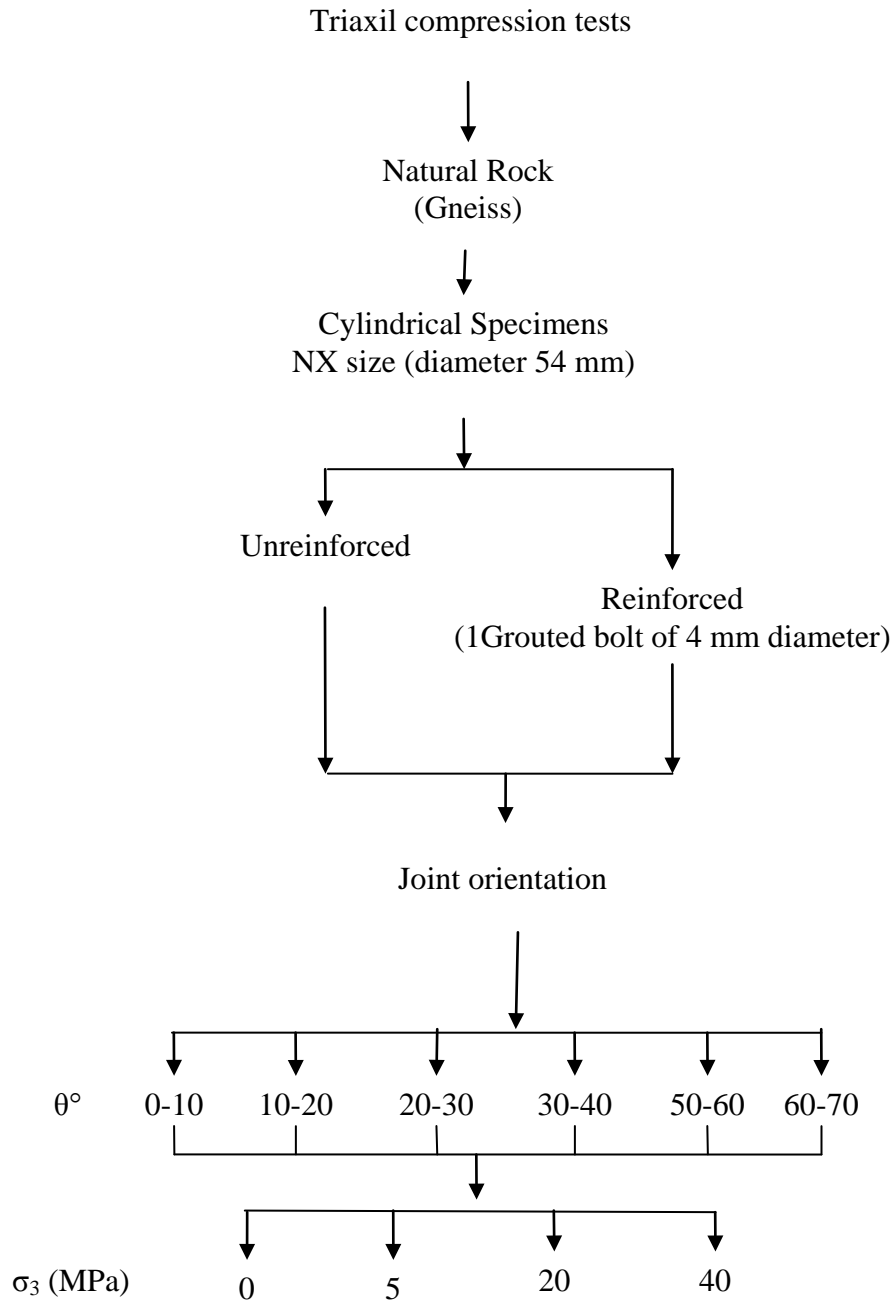
Fig. 3.1c Experimental plan: Triaxial compression tests on jointed Rocks

3.2.2 Equipment Used

For testing large blocky mass, a specially designed and fabricated large direct shear tests apparatus was used (Fig.3.2). The size of shear box in the apparatus is 750 mm x 750 mm x 1000 mm (height). The maximum normal and shear load capacities of the apparatus are 1500 kN and 2000 kN respectively. The apparatus consists of the following parts/section

 i.   A rectangular loading frame which consists of four different rectangular sections,
 ii.   A large shear box of size 750 mm x 750 mm x 1000 mm,
 iii.   Shear and normal loading actuators,
 iv.   Load cell to measure normal and shear load,
 v.   Pull out frame,
 vi.   A platform of size 1000 mm x 1000 mm,
 vii.   A jack to push shear box back after testing,
 viii.   Shear box control panel,
 ix.   Computerized display and control unit.

3.2.2.1 Loading frame

The shear test machine consists of four different sections made of steel. These four sections make a rectangular frame in which the main features of the apparatus have been mounted. The brief description of these sections is given below.

Base Section

Base of the machine consists of heavy steel plate made of four I sections @ 350 mm centre-to-centre spacing. The total width of the base is 3860 mm. The base plate has an assembly of guide rollers in which large shear box has been placed. The guide rollers move in the horizontal direction along the width of the base. Outside the base section a steel platform is attached which has been used for resting the shear box for filling and empty operations.

Fig.3.2 Servo-controlled large direct shear test machine

Columns

The machine has two heavy columns of height approximately 3500 mm. Left column consists of shear actuator to apply shear load on the specimens. The shear actuator has a capacity of 2000 kN. The actuator moves in horizontal direction and maximum travel displacement is 200 mm. A load cell of capacity 5000 kN has been attached to the right column for measuring the shear resistance during testing.

Top Section

Top section of the machine comprises of four I-sections similar to the base. The normal loading actuator of capacity 1500 kN is mounted on it. The base of this actuator consists of a square plate for applying the normal load on the specimens in the shear box.

3.2.2.2 Large shear box

The inner dimensions of large shear box are 750 mm x 750mm x1000 mm. The box consists of two half each of size 750 mm x 750mm x 500 mm (Fig.3.3). Upper half has four rollers which are placed on its sides. Relative displacement occurs between two halves of shear box along theses rollers during shearing. Lower half of shear box is also placed on a set of rollers (termed as guide rollers). During shearing, the lower half moves on these rollers and the upper halve remains stationary. Lower half of the shear box consists of four hydraulic rams placed on its sides. Using theses rams, the shear box can be pulled out from main-frame for filling and un-filling of specimens.

Fig. 3.3 Large shear box of size 750 mm x 750 mm x 1000 mm

3.2.2.3 Shear and normal loading actuators

A shear actuator of capacity 2000 kN has been attached on the left column of the loading frame (Fig.3.4a). The actuator moves in horizontal direction with a maximum displacement of 200 mm. The main function of shear actuator is to apply shear load on the specimen during the test. The normal loading actuator of capacity 1500 kN has been attached to the top section of loading frame (Fig.3.4b). It applies normal load on the specimen through a rectangular steel plate attached to the bottom of actuator. Both shear and normal loading actuators apply load at an accuracy of 0.001% of the total capacity. Sensors attached to theses actuators record the shear and normal load during the test. The movement of these actuators can be controlled through a control unit.

| (a) Shear load actuator | (b) Normal load actuator |

Fig. 3.4 Loading units of direct shear apparatus

3.2.2.4 Pull out frame

A long travel hydraulic ram is attached to the base of the machine to pull/back the shear box for loading of specimens (Fig.3.5a). Pull out frame consists of a rectangular platform in which the shear box has been placed for loading and unloading of specimens or material. Pull out assembly is attached to the shear box with a key. During the test, the entire assembly is separated from the machine.

3.2.2.5 Platform

A platform (Fig.3.5b) of size 1000 mm x 1000 mm has been placed outside the loading frame for resting of shear box during filling and un-filling operations. It is made of steel and having bearing capacity more than 200 tones. After test, the shear box is pulled out from the main frame and is kept on this platform.

3.2.2.6 Jack

A jack (Fig.3.5c) of capacity 2000 kN is used to push back the lower half of the shear box after the test, because during shearing process the lower half of the box gets some displacement. It is made of hard steel and has a maximum travel of 200 mm.

3.2.2.7 Shear box control panel

A control panel has been attached to the left column to control the movement of shear box. This control panel consists of following controls:

(a) Switch for On-OFF the main pump,
(b) Control button for lifting and lowering the shear box,
(c) Control button for pulling and push back the shear box,
(d) Control button for jack.

(a) Pull out frame	**(b) Platform**

(c) Jack	**(d) Computerized control unit**

Fig. 3.5 Additional components of machine

3.2.2.8 Computerized display and control unit

An electronic control unit with a computer (Fig.3.5d) is attached to the machine for controlling the various operations during test. This unit controls the movement of shear and normal loading actuator and adjusts the desire normal/shear load on the specimen at the start of the test. Various sensors of machine like LVDTs connect with this unit for proper operation. Four LVDTs are used to measure the vertical displacement while two LVDTs are used to measure the horizontal displacement. A computer has also been joined with this unit. The computer has specific software, which has the following special features:

(a) It displays the position of normal and shear loading actuator,

(b) Controls the mode of operation i.e. displacement control or load control,

(c) Applies the constant normal load (CNL) or Constant normal stress (CNS) condition on the specimens

(d) Adjusts the normal load and applies it in steps,

(e) Records the time, shear load, horizontal and vertical displacement during the test,

(f) Displays the shear load vs horizontal displacement and horizontal displacement vs vertical displacement plot.

3.2.3 Model Material

It is very difficult to retrieve a large number of intact blocks of natural rock with the desired shape and properties and test them in the laboratory. Therefore, model materials are commonly used to simulate rock in laboratory physical model tests. In the present study, concrete was used as a model material to simulate the intact rock. The constituents of model material are listed in Table 3.1.The physical and engineering properties of the model material were obtained by conducting tests on cylindrical cores extracted from concrete block specimens.

Table 3.1 Constituents of model material

Material	Ratio (by weight)
Cement	1
Sand	1.57
Coarse aggregate	2.91
Water	0.48

3.2.4 Casting of Concrete Blocks

Cubical concrete blocks of 150 mm x 150 mm x 150 mm were cast using steel moulds (Fig.3.6a). The blocks were cured in water and air for 28 and 7 days respectively (Fig.3.6b). For conducting one shear test, about 150 numbers of concrete blocks were required.

Fig. 3.6a Casting of concrete blocks

Fig. 3.6b Prepared concrete blocks of size 150 mm x 150 mm x 150 mm

3.2.5   Unreinforced and reinforced blocky mass

Four different configurations of blocky mass were tested in the study. The configurations of the unreinforced and reinforced blocky mass are shown in Fig.3.7. The blocky unreinforced mass (U) specimens were prepared by piling elemental cubical blocks of concrete. The size of prepared specimens was 750 mm x 750mm x 900 mm (height). The formed jointed mass consists of three orthogonal joint sets having joint spacing of 150 mm. For preparing the mass specimens, the shear box was pulled out of the loading frame and the concrete blocks were piled inside the shear box (Fig.3.8). Care was taken to ensure that the joint surface was aligned along the shearing plane.

Six mm diameter steel bars were used as bolts to reinforce the blocky mass. For installing the bolts, a 10 mm diameter cylindrical void was left in the respective blocks while casting them. For this purpose a 10 mm diameter steel rod was inserted into the mould, and then concrete was poured into the mould. The rod was removed after 24 hours; blocks were cured in water for 28 days. This way a cylindrical hole was formed in the block which was used for installing the bolts. The bolts were installed perpendicular to the shearing direction, and were grouted with cement mortar to produce a proper bonding between the bolt and the surrounding concrete (Fig.3.9). The grout was allowed to cure for seven days.

The bolts were tightened by a nut and washer system at the top and bottom, however, no pre-tensioning was applied. Three configurations of bolts were used as shown in Fig.3.7b. In the first case (R3), three bolts were installed in the middle columns of blocks with a centre-to-centre spacing of 300 mm. In the second case (R5), five bolts were installed in the mass; one at the centre and the others in the four outermost corners of the mass. The centre-to-centre spacing for the staggered pattern was 300 mm. In the third case (R9), nine bolts were installed in square grid pattern with a centre-to-centre spacing of 300 mm. Figure 3.10 shows the some prepared reinforced blocky mass.
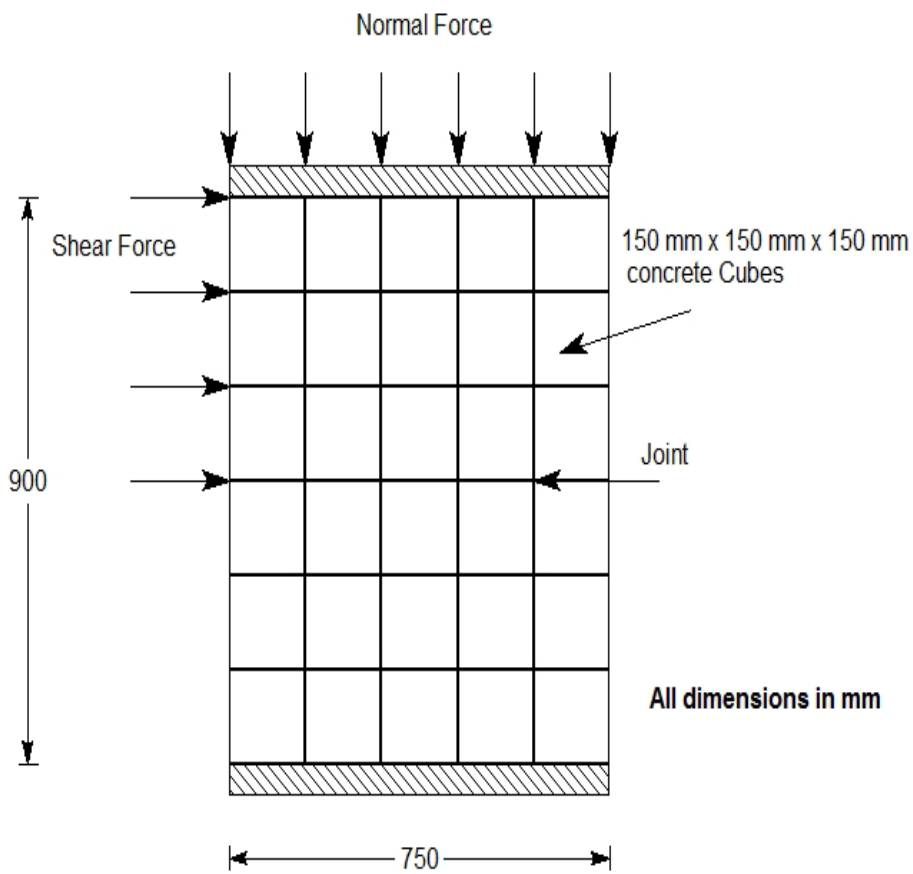
(a) Elevation of blocky mass

Fig. 3.7 Configurations of unreinforced and reinforced specimens
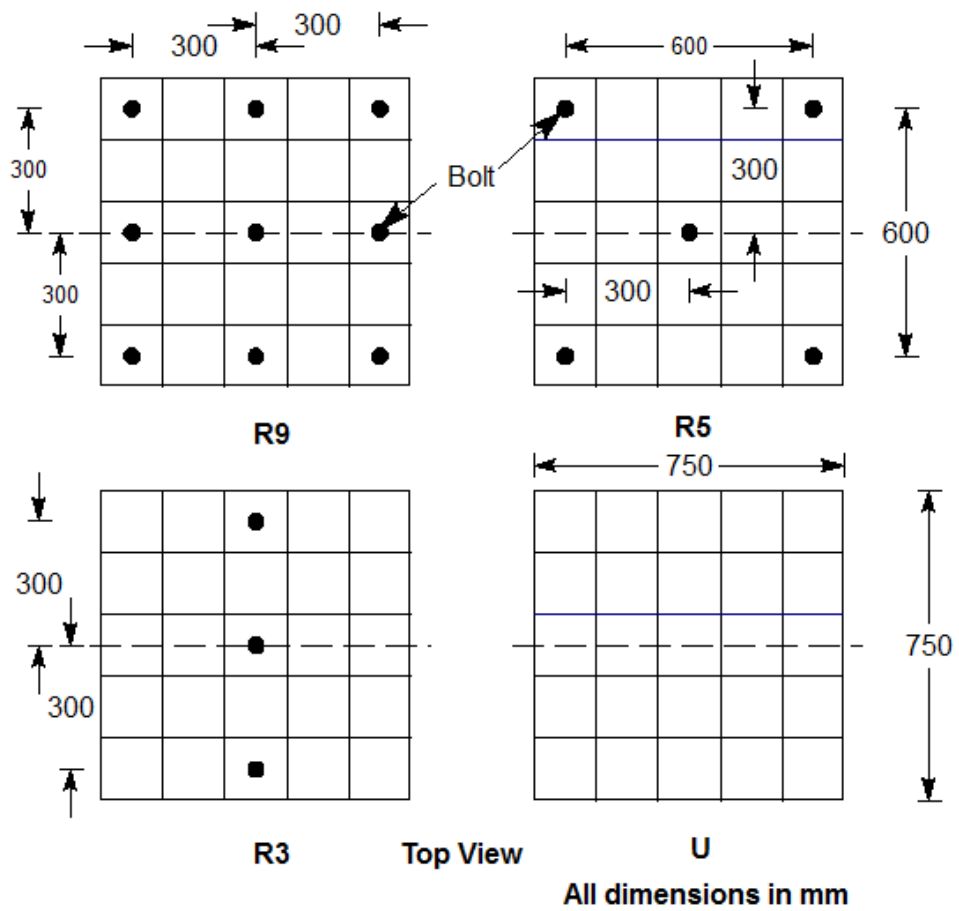
(b) Plan of unreinforced and reinforced specimens

Fig. 3.7 Configurations of unreinforced and reinforced specimens

Fig. 3.8 Filling of shear box with 150 mm^3 concrete blocks

Fig. 3.9 Grouting of bolts

Fig. 3.10 Reinforced specimen in shear box

3.2.6 Preparation of Specimens and Set-up of Machine

For preparing a specimen in the shear box, the box assembly was moved out from the main loading frame through the pull out ram. The box rested on the platform outside the frame. At this stage, the concrete blocks were piled in the box. This way a blocky mass specimen was prepared, which consisted of three joint sets. One of the joint planes was horizontal and aligned along shearing plane. After filling the box, it was moved back into the loading frame at its original position. A small normal stress of 0.01 MPa was applied through the rectangular steel plate attached to the bottom of the normal loading actuator. Two LVDTs were placed on the lower halve of the shear box in horizontal direction for measuring horizontal displacements. Four LVDTs were placed on the rectangular plate for recording vertical displacements. The rollers of the upper half of box are so adjusted to have gap of 5 mm between two halves of the box. At this stage, the shear pins were removed. The complete setup of machine during test is shown in Fig.3.11.

75

3.2.7 Test Procedure

The tests were conducted at different normal stress levels ranging between 0 to 2 MPa (0.0, 0.5, 1.0, and 2.0 MPa). The tests were conducted in displacement-controlled mode. The shearing rate was kept at 1.25 mm per minute. For each test, shear load, vertical displacement and horizontal shear displacement were recorded. For each configuration, four tests were performed, one at each normal stress level. The shearing was continued until the shear load dropped substantially after reaching its peak value. The peak shear stress is indicative of the shear strength of the mass. In cases of reinforced mass, the test was stopped shortly after the peak since the dilation was substantially high, and there was a possibility of tilting the upper half of the shear box that could damage the machine. After the test was over, the shear box was pulled out of the loading frame and the blocks were taken out for inspection.

Fig 3.11 Complete setup of apparatus during test

3.3   UNIAXIAL COMPRESSION TESTS ON SYNTHETIC ROCK

3.3.1 Methodology

Uniaxial tests have been performed on the specimens of size 150 mm x 150 mm x 300 mm (height). The joint orientation of the prepared specimens was varied with respect to bolt direction to study the effect of inclination between bolts and joint on the strength behaviour of jointed rocks.

3.3.2   Model Material

Two different grades of concrete (referred to T2 and T3) have been used to simulate the intact rock material. The constituents of these grades are given in Table 3.2. Cylindrical specimens of NX size were extracted from the blocks of concrete, and tested, to find out the physical and engineering properties of intact materials.

Table 3.2 Constituents of synthetic rock

Material	Ratio (by weight)	
	T2	T3
Cement	1	1
Coarse Sand	1.27	0.75
Coarse aggregate	2.33	1.74
Silica Fume	0.1	0.1
Water	0.36	0.25
Superplastizer (Glenium 51)	0.175	0.30

3.3.3   Casting of Concrete Blocks

The specimens were prepared by casting concrete through steel moulds, which were especially designed for the study (Fig.3.12). For preparing jointed specimens, a thin steel plate was placed in mould to separate the two halves of the specimen. The prepared specimens carried one smooth joint having orientation 0° to 90° with the base of the specimen. The specimens were cured in water and air for 28 and 7 days respectively. For preparing reinforced specimens, two plastic pipes of 10 mm diameter were placed at a proper place in the mould before casting. The pipes were

removed after 24 hours of casting. This way, two holes were prepared, which were used for installation of bolts. Two steel bars of diameter 6 mm were installed in the specimens perpendicular to loading direction and grouted. Figure 3.13 shows pictures of some of the prepared specimens.

3.3.4 Equipment Used

All the tests on the synthetic rock were performed using the high capacity compression-testing machine (Fig.3.14). The axial loading capacity of the machine is 2000 kN. This machine consists of two simple units

I. Loading unit, and
II. Pumping unit and data accusation system

3.3.4.1 Loading unit

The loading unit consists of a loading frame, which is made of steel. The base carries a fine finished hydraulic ram and the lower platen. The top plate has the spherical seating to take care of any irregularity of the specimen surface or slight misplacement of the specimen from the central position.
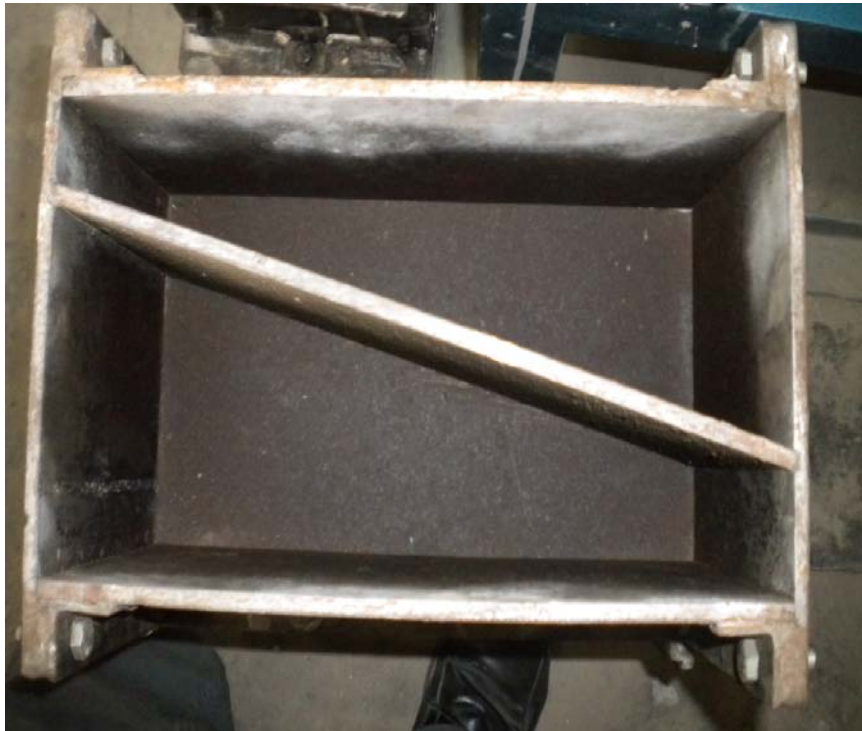
Fig. 3.12 Special steel mould for casting of jointed specimens

Fig. 3.13 Prepared reinforced specimens of synthetic rock

Fig. 3.14 Compression testing machine

3.4.4.2   Pumping unit and data accusation system

Pumping unit is attached on the right hand side of the loading unit. It is a multi plunger pump submersed in the tank and is powered by a 1.5 kW electric motor. Power pack gives non-pulsating flow to the hydraulic ram. A data accusation system with a computer is attached to the machine, which records the load, and displacement.

3.4.5   Experimental Setup and Test Procedure

Schematic diagram of configuration of jointed specimens is given in Fig.3.15. The uniaxial tests were performed in displacement-controlled mode with a displacement rate of 0.002 mm/sec. For testing, the specimen was placed on the lower platen of the machine having a steel plate with surface area greater than the specimen's surface area (Fig. 3.16). At the top of specimen, another steel plate was placed. Teflon sheets were used between specimen and steel plates for minimised friction. The load was applied to the specimen through steel plate. The loading rate was adjusted manually with lever provided with the pumping unit. For each test axial load and axial displacement was recorded through computer and data logger attached with the machine. Total 34 numbers of specimens were tested.

3.4   UNIAXIAL AND TRIAXIAL TESTs ON NATURAL ROCK

3.4.1 Methodology

Uniaxial compression tests and triaxial compression tests have been performed on the specimens of natural rocks with joint without and with bolt. Natural rock cores (Fig.3.17) of NX size were retrieved from a project site in Garhwal region of the Indian Himalayas. The rock exposed at the site is Gneiss.

3.4.2 Preparation of Specimens

The cores of natural rocks were cut into small pieces to make the specimens of intact, unreinforced jointed and reinforced jointed (Fig.3.18). The height to diameter ratio of the prepared specimens was about 2. Lapping was done to make the end surfaces of the specimens smooth and perpendicular to the vertical axis.
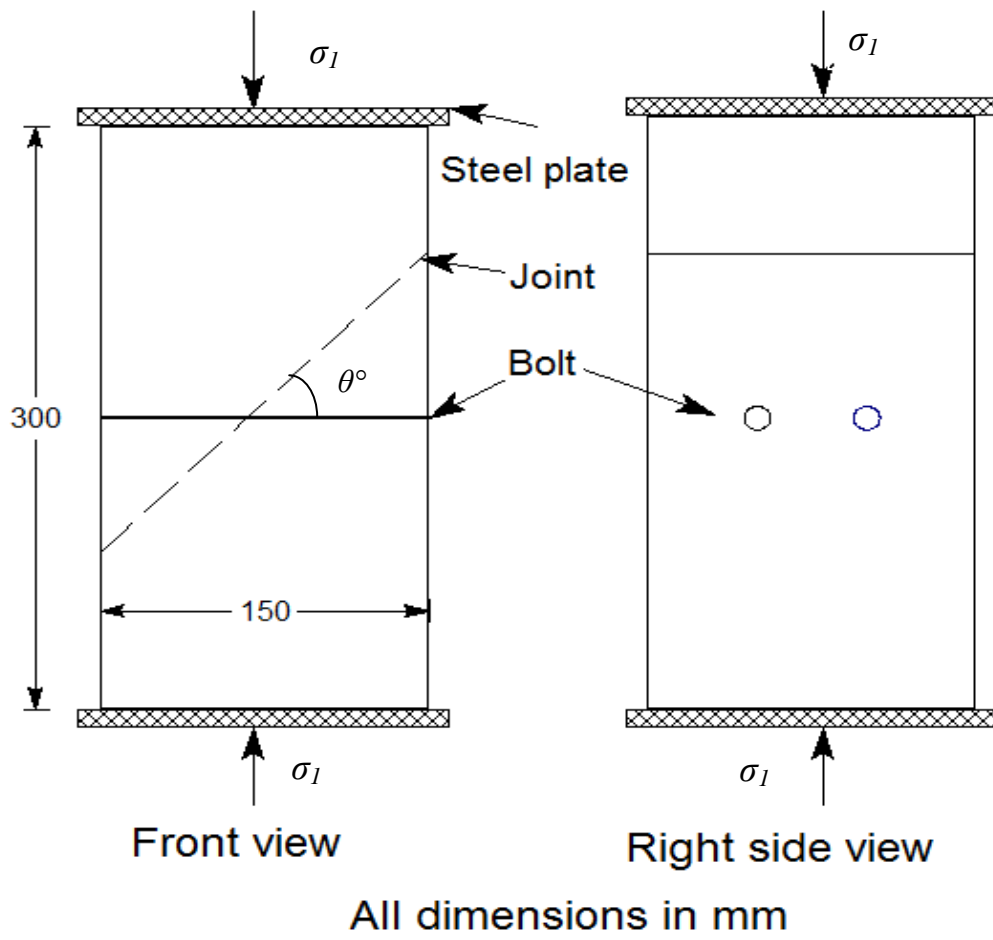
Fig.3.15 Joint and bolt configuration in concrete specimens

Fig. 3.16 Testing of specimens under uniaxial compression

Fig.3.17 Natural rock cores obtained from the site

Fig. 3.18 Cutting operation of core to prepare specimens

3.4.3 Configuration of Specimens

The jointed specimens have joint orientation (θ) vary from 0° to 90° with respect to the base of the specimens from the horizontal axis. For preparing reinforced specimens, a 6 mm diameter hole was drilled through specimens and 4 mm diameter bolt was installed and grouted. Figure 3.19 shows the photographs of prepared specimens.

Fig. 3.19a Prepared specimens of intact natural rock

Fig. 3.19b Prepared specimens of jointed natural rock
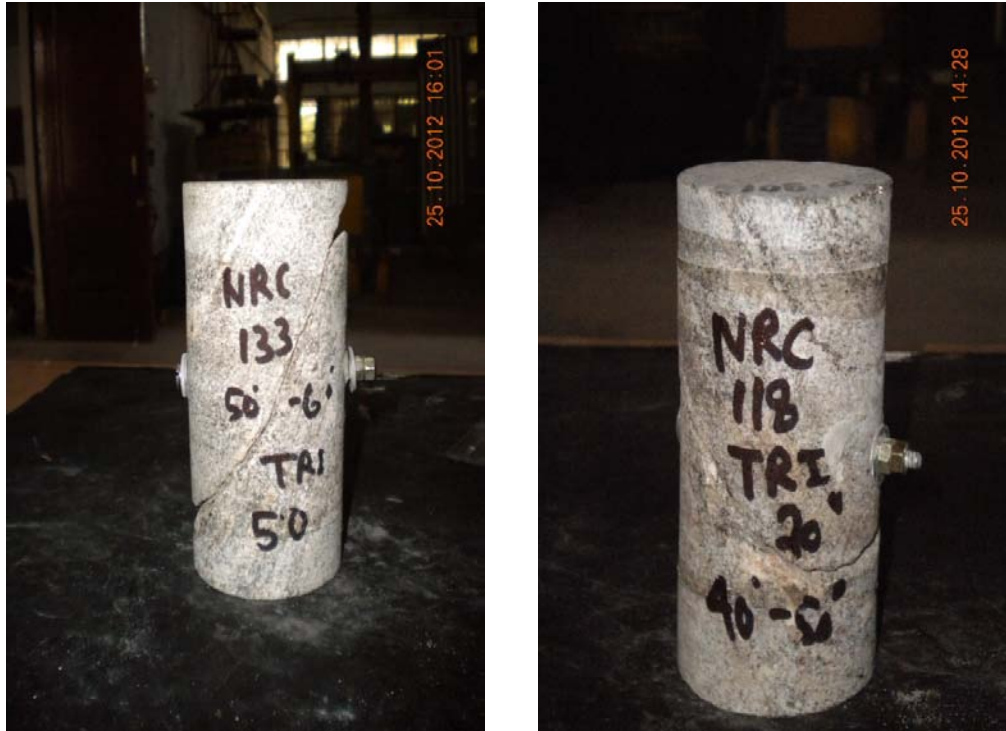
Fig. 3.19c Prepared specimens of natural reinforced rock

3.4.4 Equipment Used

A servo controlled triaxial machine was used (Fig.3.20) for conducting triaxial tests. The maximum axial loading capacity of machine is 2000 kN. The machine has a high-pressure triaxial cell which accommodates standard specimen size. The machine consists of the following parts

   i.   Loading unit with actuator,

  ii.   Triaxial cell,

 iii.   High pressure controller,

 iv.   Control panel,

  v.   Electronic control unit and data acquisition system.

3.4.4.1 Loading unit with actuator

Loading unit, which accommodates the triaxial cell, is a welded structure having stiffness of 230MN/m. The unit comprises of a base plate, top plate, and side plates. All the plates are welded in the loading unit to form a very stable and stiff structure. The lower base plate carries hydraulic actuator and the top plate carries two

hydraulic jacks for lifting and lowering the triaxial chamber, a load cell of capacity 2000 kN and a hydraulic ram. The minimum clearance between the upper and bottom plate is 1125 mm (as the bottom plates move during the test).

The actuator is a linear motion device, which loads the specimen based on the command signal either in stress control mode or in strain control mode. The unit has a bottom cap attached to the lower base plate of the loading unit. This unit is fitted with precision servo valve. It is a two-stage high response valve, which keeps the system in line with the control signal. The actuator has a capacity of 2000 kN and stroke length is 75 mm. The operating pressure of the actuator is 20 MPa.

Fig. 3.20 Servo-controlled static / dynamic triaxial machine

3.4.4.2   Triaxial cell

A triaxial cell is fitted with the loading unit. It is a high-pressure triaxial cell and accommodates standard samples of EX, AX, BX and NX sizes. The cell is made of steel and can sustain pressure up to 100 MPa. The cell has a circular base for fitting the specimen. Initially the base is separated from the triaxial cell. This base has four

take off points for confining pressure, back- pressure, top drainage and pore pressure. Base is permanently attached to the ram of the loading unit. At the time of testing base is joined to the triaxial chamber through bolts.

3.4.4.3 High-pressure controller

It is an intensifier, which converts low pressure from the main pumping unit to the required pressure in the triaxial cell. It can develop pressure up to 100 MPa and has a volume displacement of nearly 300 cc. The unit is based on close loop principle. Feedback of the set pressure is taken from the high-pressure sensor, which is fixed on the line of lateral pressure port. Power pack has been used for creating confining pressure.

3.4.4.4 Control panel

Control panel controls the various functions of the machine. It is attached to left side of the loading unit. It has following attachments

  i. ON –OFF starter for the main pump,
  ii. Control for filling and emptying the triaxial cell,
 iii. Lifting and lowering the triaxial cell for fixing the specimens,
 iv. Emergency switch for switching off the complete system in case of emergency.

3.4.4.5 Electronic control unit

The unit consists of electronic control unit and data acquisition system. It controls all the operations of the machine during the testing. It is connected to the main machine through various sensors. A computer attached to this acts as a display unit and records the data during the test. The main functions of this unit are to

  i. Control the movement of actuator during test,
  ii. Apply desired confining pressure to the cell,
 iii. Control the test mode i.e. load control or displacement control. It also sets the loading rate,
 iv. Record the load, displacement and time and other parameters during the test.

3.4.5 Experimental Setup and Testing Procedure

The schematic diagram of configuration of test specimen is given in Fig.3.21. The triaxial tests have been performed on the specimens having joint orientation (θ) vary from 0°-70°. The details of numbers of specimens tested are given in Table 3.3. Rubber membrane was used around the specimens to restrict flow of oil in to the specimens. The membrane-enclosed specimen was fitted in to triaxial cell with the help of spacer and pedestal. By using the control panel button the cell is lowered down and bolts are tightened. Bolts joined the upper and lower portion of the machine. After this, oil is filled into the cell, and entrapped air is removed with the help of air release value. Now the machine is ready for use. With the help of electronic control unit, the desired confining pressure is applied to the specimens. Figure 3.22 shows the fixing of specimen in the triaxial chamber. The specimens were tested under unconfined and confined condition at confining pressure of 0, 5, 20, and 40MPa respectively. All the tests were performed in displacement-controlled mode and displacement rate was kept as 0.002 mm/sec. For each test, axial load and axial displacement were recorded.

Table 3.3 Number of specimens tested

$\theta°$	Number of specimens							
	$\sigma_3 = 0$ MPa		$\sigma_3 = 5$ MPa		$\sigma_3 = 20$ MPa		$\sigma_3 = 40$ MPa	
	U	R	U	R	U	R	U	R
Intact	34	-	1	-	1	-	1	-
0-10	1	-	1	-	1	-	1	-
10-20	1	-	1	-	1	-	1	-
20-30	1	-	1	-	1	-	1	-
30-40	1	1	1	1	1	1	1	1
40-50	1	1	1	1	1	1	1	1
50-60	1	1	1	1	1	1	1	1
60-70	1	1	1	1	1	1	1	1
70-80	1	1	-	-	-	-	-	-
80-90	1	1	-	-	-	-	-	-

.
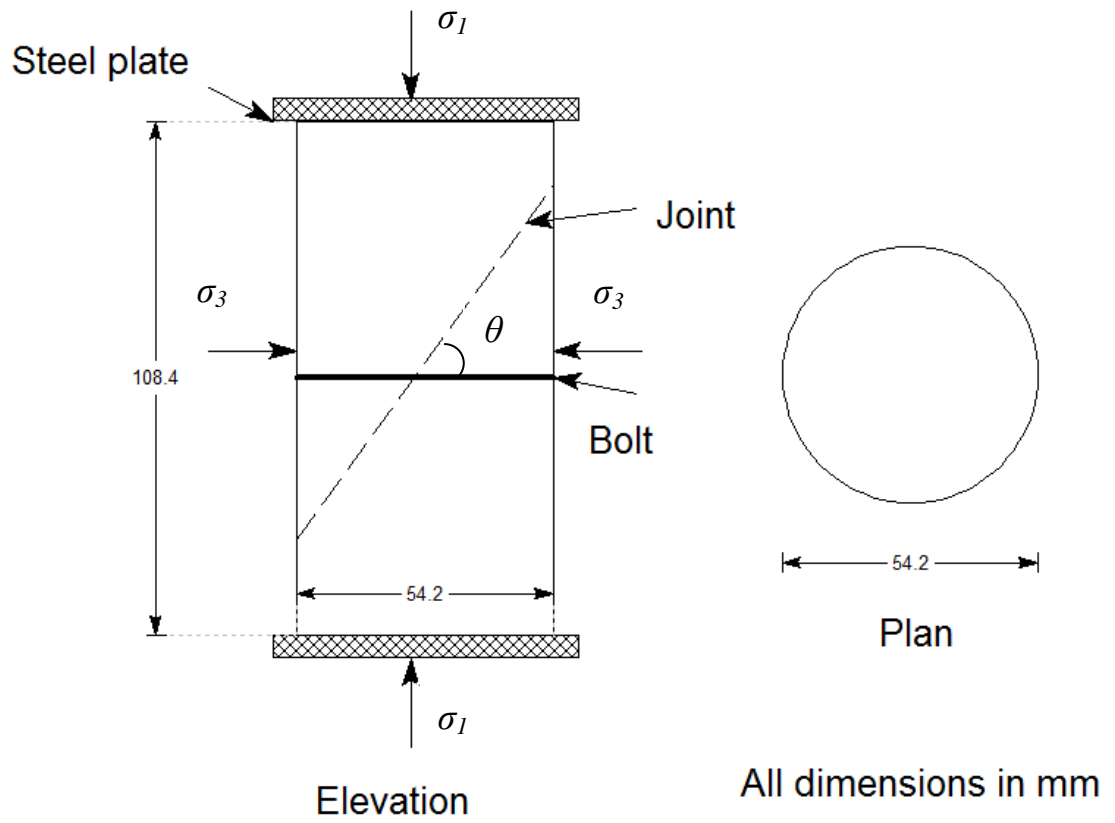
Fig. 3.21 Schematic diagram of configuration of test specimen

Fig.3.22 Fixing of specimen in triaxial cell

3.5   CONCULDING REMARKS

An experimental programme was planned and executed to investigate the behaviour unreinforced and reinforced rocks. Three different types of tests were conducted. Large Sized direct shear tests were conducted on the unreinforced and reinforced blocky mass of size 750 mm x 750 mm x 900 mm at normal stress varying from 0 to 2 MPa. Specially designed large size direct shear apparatus was used for this purpose. Elemental concrete blocks of size 150 mm x 150 mm x 150 mm were used to prepare the blocky mass. The specimens thus formed comprised of three orthogonal joint sets. To reinforce the blocky mass six mm diameter steel bars were used. The bolts were installed perpendicular to shearing direction and were grouted with cement mortar to produce a proper bonding between the bolt and the surrounding rock. Three different configurations of reinforcement were used. For each test, shear load, horizontal shear displacement and vertical displacement were recorded.

Uniaxial compression tests were conducted on prismatic specimens of synthetic rocks. Two different grades of concrete (referred to T2 and T3) were used as model material. The size of the specimens was 150 mm x 150 mm x 300 mm (height). The prepared specimens carried one joint having orientation 0° to 90° with the base of the specimen. Two steel bars of diameter 6 mm were installed in the specimens perpendicular to loading direction and were grouted. The tests were performed in displacement-controlled mode and for each test axial load and axial displacement was recorded.

Triaxial compression tests were performed on the specimens of natural jointed rocks without and with bolts. Natural rock cores of NX size were retrieved from a project site in Garhwal region of the Indian Himalayas. The height to diameter ratio of prepared specimens was about 2. The joint orientation (θ) varied from 0° to 90° from base of the specimens from. For bolted specimens a 6 mm diameter hole was drilled and 4 mm diameter bolt was installed and grouted. The specimens were tested at confining pressure of 0, 5, 20, and 40 MPa respectively. The tests were performed in displacement-controlled mode and displacement rate was kept as 0.002 mm/sec. For each test axial load and axial displacement was recorded.

<div align="right">**Chapter 4**</div>

RESULTS AND DISCUSSIONS

4.1 GENERAL

This chapter deals with detailed discussions on the results obtained from the experimental investigations. Physical model tests were conducted on the specimens of unreinforced and reinforced jointed blocky mass / jointed rock. The chapter consists of three different sections i.e. direct shear testing of blocky mass, uniaxial compression testing on synthetic rocks, and triaxial compression testing of natural rock specimens. In each section, the properties of the model materials used, the observation made during the tests, stress vs strain behaviour, and failure modes observed have been discussed.

4.2. PROPERTIES OF BOLT

Structural steel bars (Tata tiscon SD – Grade Fe 500) have been used as rock bolts. The bar were cut into small pieces to make the bolts. The bolts were threaded at both the ends. The ultimate tensile strength of bolt is 550 MPa. The typical stress vs strain plot of the material is plotted in Fig.4.1. The chemical and mechanical properties of the bolt are listed in Table 4.1.

Table 4.1 Chemical and Mechanical property of bolt

Chemical Properties	
Percent Carbon (Max)	0.25
Percent Sulphur (Max)	0.035
Percent Phosphorous (Max)	0.035
Mechanical Properties	
Yield stress, MPa	523
Ultimate tensile strength, MPa	550
Percent Elongation	16
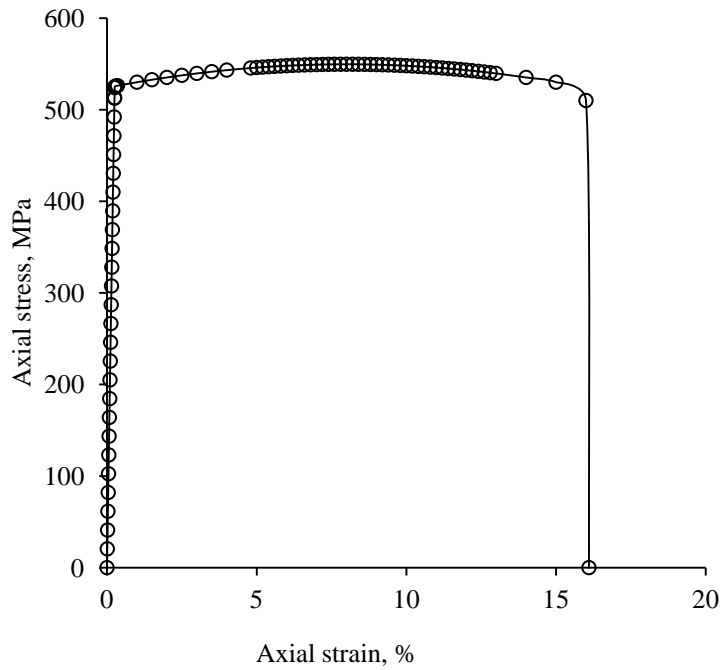
Fig.4.1 Stress vs strain plot of steel bolt

4.3 PROPERTIES OF GROUT

The grout consists of cement, sand, and water having ratio 2:2:1 by weight. Cylindrical specimens of grout were prepared, and laboratory tests were conducted to find out the physical and engineering properties. The triaxial tests were conducted at confining pressure equal to 0, 2.5, 5 and 10 MPa respectively (Fig.4.2). The properties of the grout are listed in Table 4.2.

Table 4.2 Physical and engineering properties of Grout

Property	Value
Uniaxial compressive strength, σ_{ci} MPa	17
Tangent modulus, E_{t50} MPa	4000
Cohesion, c_i , MPa	4.5
Friction angle, ϕ_i °	34
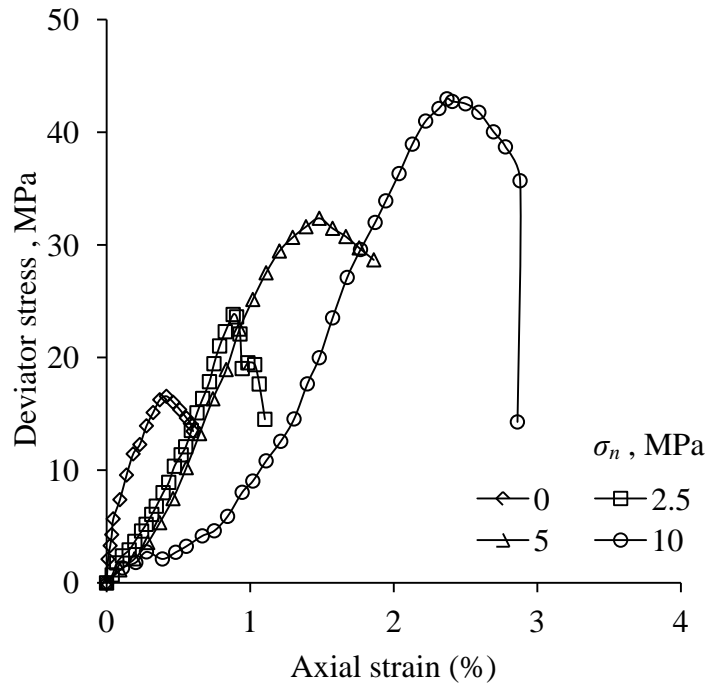
Fig.4.2 Deviator stress vs axial strain plots of grout material

4.4 LARGE SIZED DIRECT SHEAR TESTS ON BLOCKY MASS SPECIMENS

Direct shear tests have been performed on large sized specimens of unreinforced and reinforced blocky mass with normal stress varying from 0 to 2 MPa. The details are discussed below.

4.4.1 Intact Model Material Properties

Concrete was used as a model material to simulate the intact rock. The physical and engineering properties of the model material were obtained by conducting tests on cylindrical cores extracted from concrete block specimens. To obtain the shear strength parameters, triaxial tests were performed at 0, 2.5, 5, and 10 MPa confining pressure respectively. The axial stress (deviator) vs axial strain plots of triaxial tests are given in Fig. 4.3. The uniaxial compressive strength of the model material is 42.38 MPa. Figure 4.4 shows the Mohr circles at failure and failure envelope of the model material. The physical and engineering properties of the model material are listed in Table 4.3. On Deere-Miller (1966) classification chart, the model material is classified as DL i.e. having low strength and low modulus ratio (Fig.4.5).
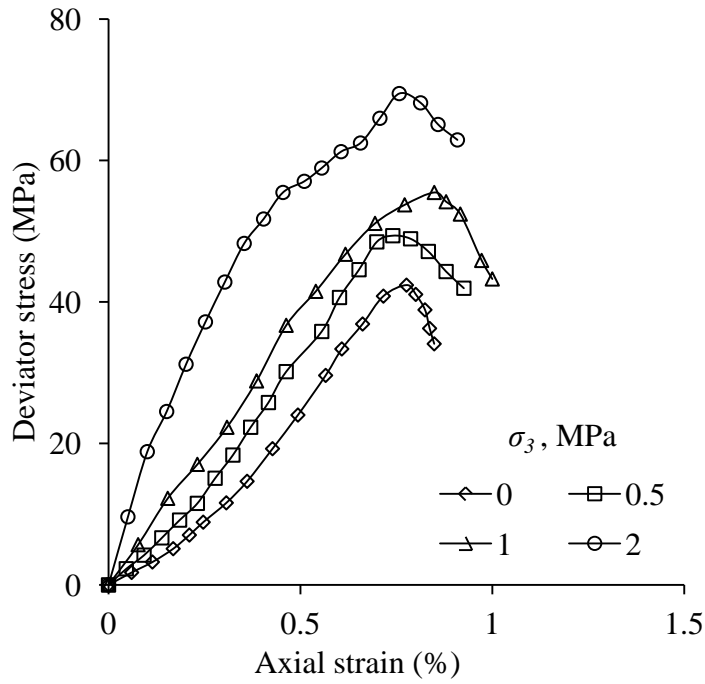
Fig. 4.3 Deviator stress vs axial strain plots for concrete cores

Table 4.3 Physical and engineering properties of the intact model material

Serial No.	Property	Value
1	Unit weight (γ)	24 kN/m^3
2	Uniaxial compressive strength, σ_{ci}	42.38 MPa
3	Tangent modulus at 50% of failure stress, E_{t50}	7220 MPa
4	Brazilian tensile strength	3 MPa
4	Cohesion of intact material, c_i	11 MPa
5	Friction angle of intact material , ϕ_i	35°
6	Cohesion along joint, c_j	0.008 MPa
7	Friction along joint, ϕ_j	34°
8	Deere Millar (1966) classification	DL
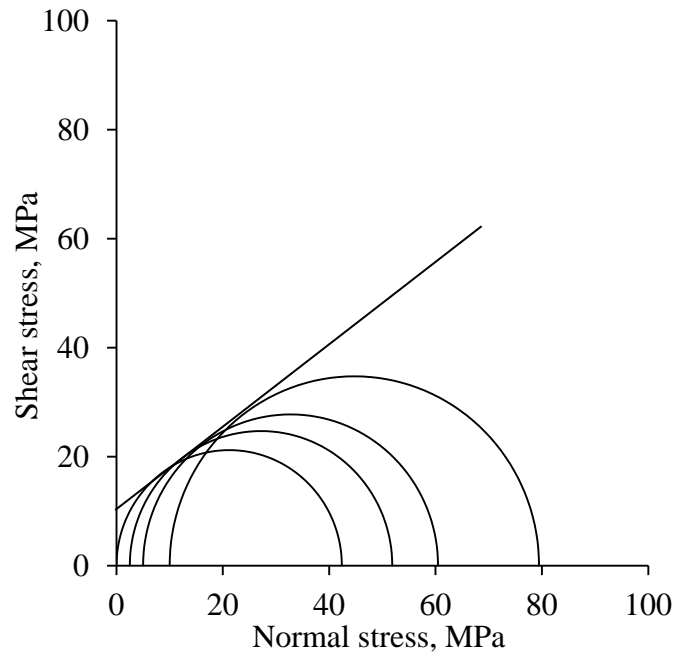
Fig.4.4 Mohr circles plot for model material
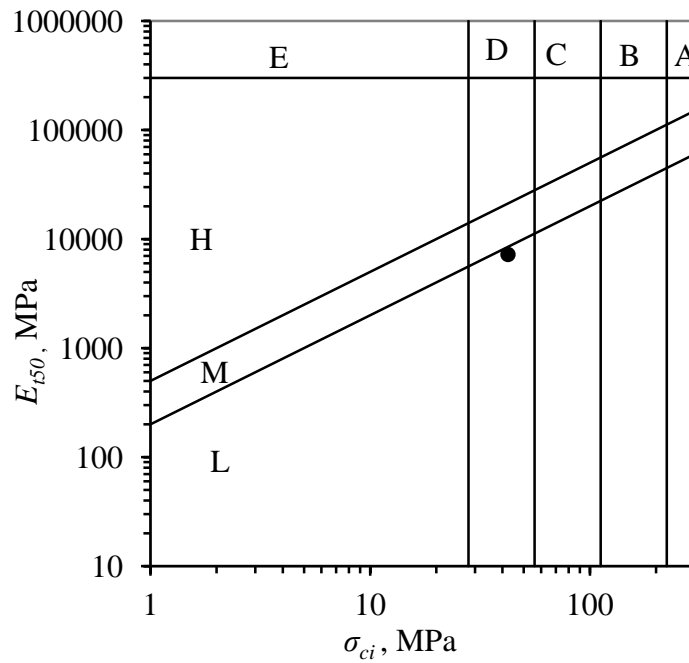
Fig.4.5 Deere-Miller classification of the model material

4.4.2 Observations during Direct Shear Testing of Blocky Mass

Four different configurations of blocky mass were tested. Observations were made on shear load, horizontal shear displacement, and vertical displacement during the shearing process. The specimen was sheared gradually until peak shear stress was reached. In case of unreinforced specimens, the shearing was continued until the shear stress dropped substantially with respect to peak shear stress. In cases of reinforced mass, the test was stopped shortly after the peak since the dilation was substantially high, and there was a possibility of tilting the upper half of the shear box that could damage the machine. The summery of observations taken during the tests are summarized and discussed below.

4.4.2.1 Unreinforced blocky mass (U)

σ_n = 0.0 MPa

Shear stress increases with horizontal shear displacement up to a value of 0.048 MPa (Fig. 4.6-1a). A sudden drop is followed with further increase in shear displacement, the shear stress again increases and reaches the peak followed by gradual recession and approaches an asymptotic value of 0.041 MPa. Stick-slip pattern is observed due to edge-to-edge contact failure. Sliding of the blocks in the mass has been observed. The peak shear stress in this case was 0.048 MPa which was observed at horizontal displacement of 25.5 mm. The vertical displacement was also found to be increasing with horizontal displacement, which became constant after about 26 mm of horizontal displacement (Fig. 4.6-1b).
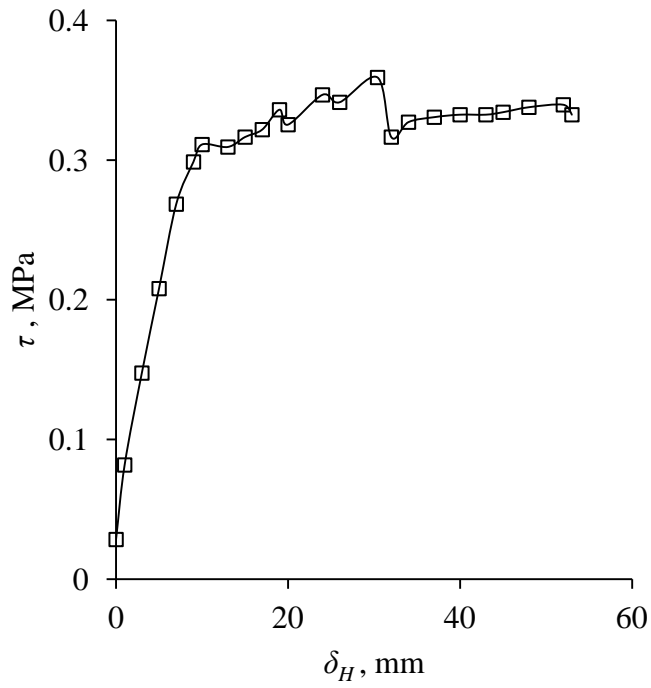
σ_n = 0.5 MPa

Shear stress increases with horizontal displacement up to a displacement of about 32 mm, suddenly drops, and then remains almost constant (Fig. 4.6-2a). Sliding of intact blocks was observed. Peak shear stress of 0.36 MPa was observed at a horizontal displacement of 30.4 mm. The vertical displacement increases in a zigzag manner with horizontal shear displacement (Fig. 4.6-2b).
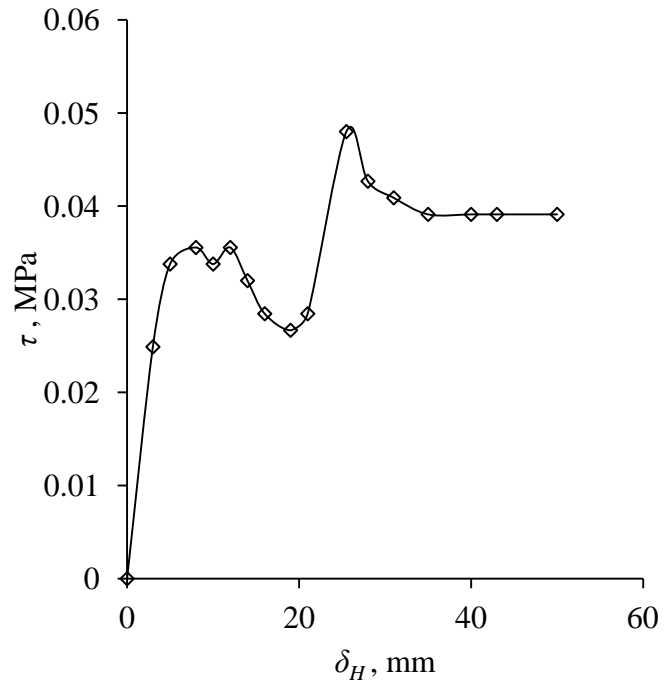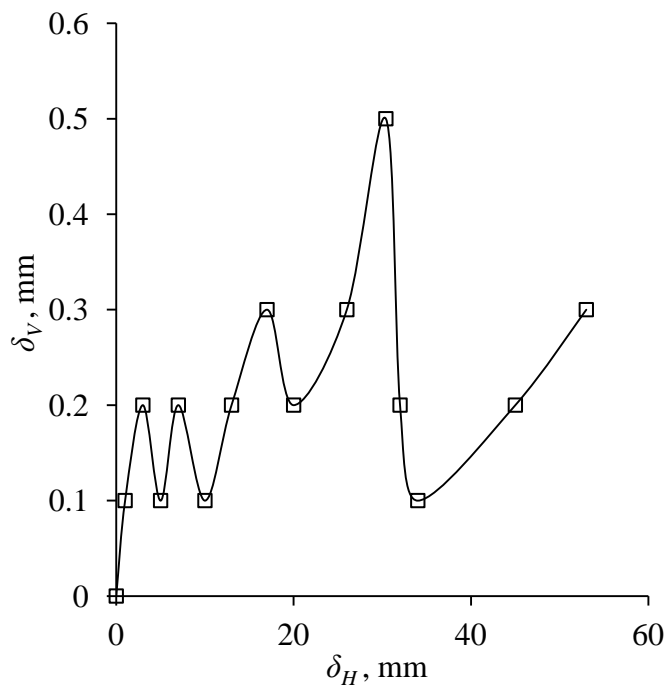
Fig.4.6-1a Shear stress (τ) vs horizontal shear displacement (δ_H) plot for unreinforced mass at σ_n = 0.0 MPa
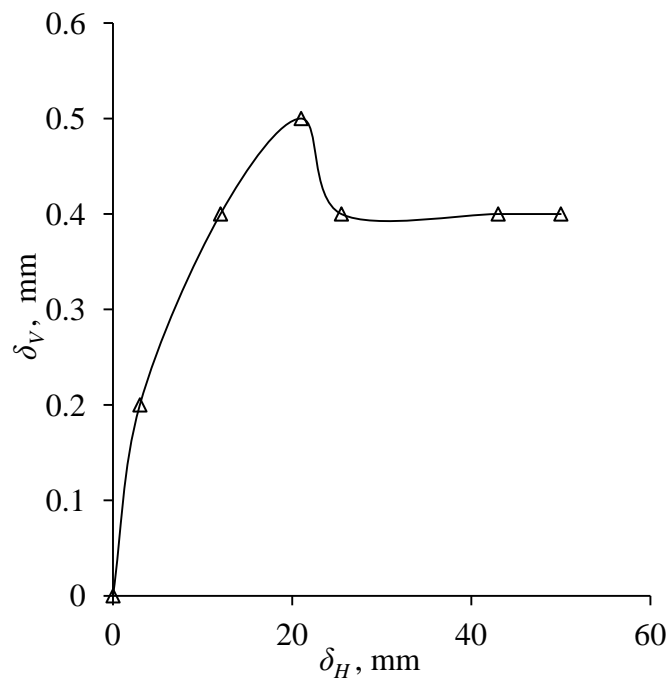
Fig.4.6-1b Vertical displacement (δ_V) vs horizontal shear displacement (δ_H) plot for unreinforced mass at σ_n = 0.0 MPa
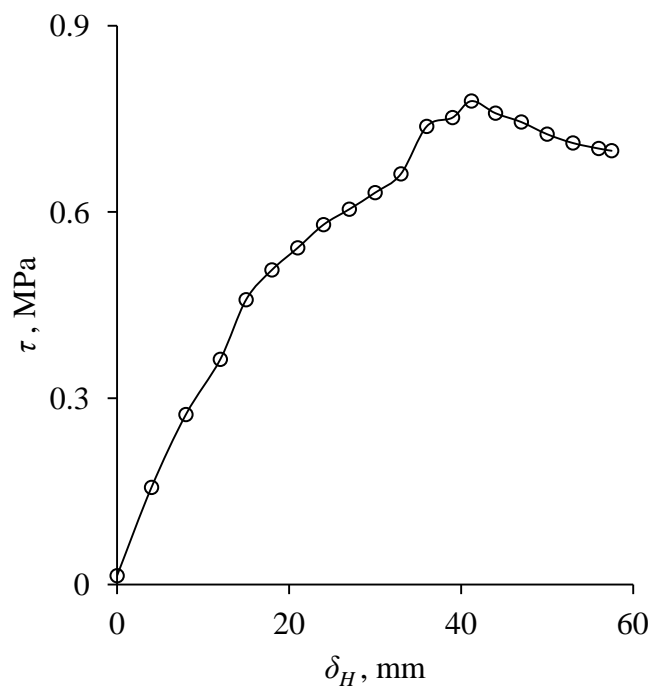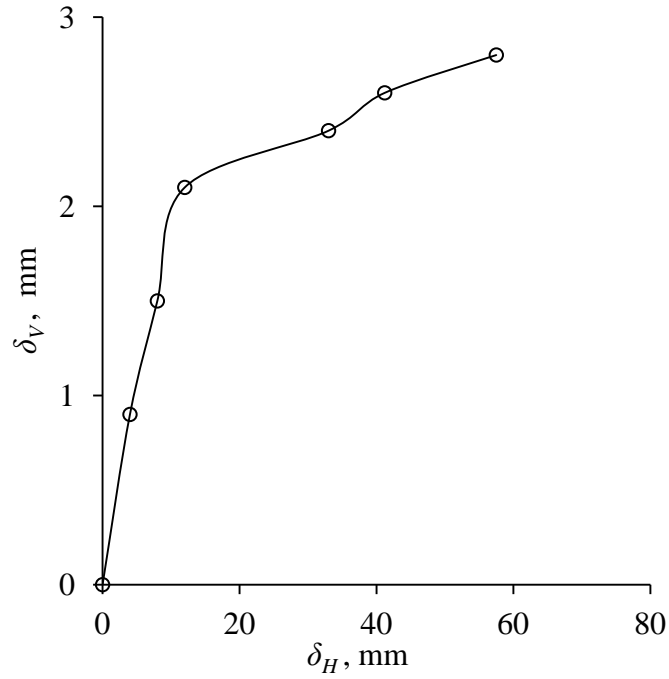
99

Fig.4.6-2a Shear stress (τ) vs horizontal shear displacement (δ_H) plot for unreinforced mass at σ_n = 0.5 MPa

Fig.4.6-2b Vertical displacement (δ_V) vs horizontal shear displacement (δ_H) plot for unreinforced mass at σ_n = 0.5 MPa

σ_n = 1.0 MPa

A relatively well-defined peak value has been observed in this case. Stick-slip nature is suppressed due to relatively higher normal stress. Shear stress increases with horizontal shear displacement showing relatively smoother plot (Fig.4.6-3a). Peak shear stress of 0.779 MPa was observed at a horizontal displacement of 41.2 mm. Edges of some blocks were found to have been damaged. Fracturing of some intact blocks was observed. Sliding of intact blocks through joint plane was observed. Vertical displacement increases rapidly upto 12 mm of horizontal displacement and after this, the vertical displacement increases gradually (Fig. 4.6-3b).
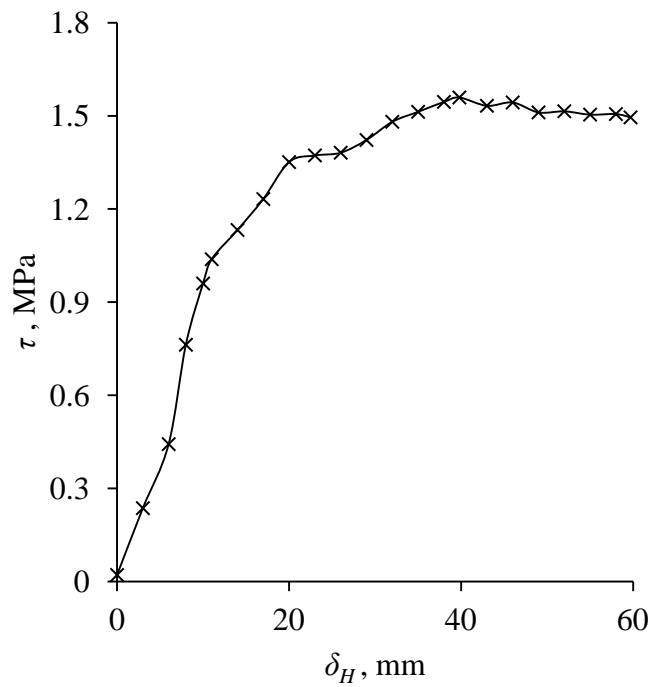
σ_n = 2.0 MPa

Better compacting of joints occurs due to high normal stress. About 30 percent of intact blocks observed damage. Some blocks observed splitting due to high concentration of stresses. Peak shear stress of 1.559 MPa was observed at a horizontal displacement of 39.8 mm (Fig. 4.4a). Rotation and sliding of blocks increases the vertical displacement rapidly upto 10 mm of horizontal displacement and after this, the vertical displacement increases gradually (Fig. 4.4b).
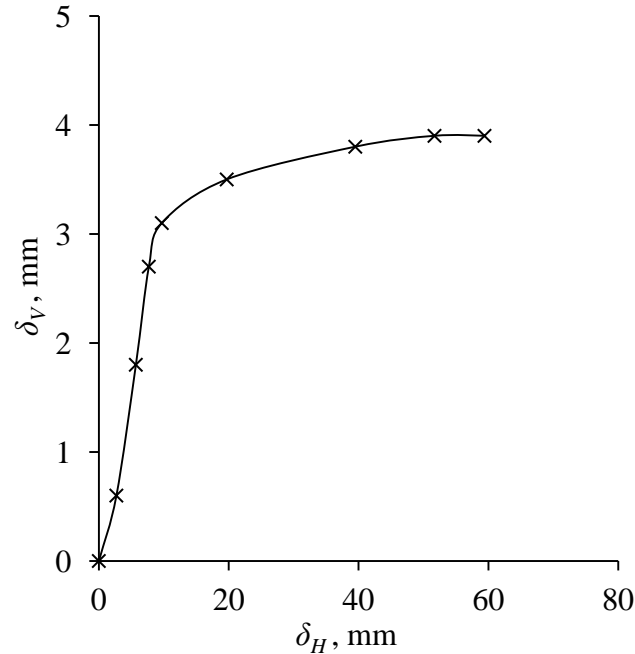

Fig.4.6-3a Shear stress (τ) vs horizontal shear displacement (δ_H) plot for unreinforced mass at σ_n = 1.0 MPa

Fig.4.6-3b Vertical displacement (δ_V) vs horizontal shear displacement (δ_H) plot for unreinforced mass at σ_n = 1.0 MPa

Fig.4.6-4a Shear stress (τ) vs horizontal shear displacement (δ_H) plot for unreinforced mass at σ_n = 2.0 MPa

Fig.4.6-4b Vertical displacement (δ_V) vs horizontal shear displacement (δ_H) plot for unreinforced mass at σ_n = 2.0 MPa

4.4.2.2 Reinforced blocky mass

In case of reinforced blocky mass, the shear stress vs the horizontal shear displacement plots exhibit two distinct segments. The first segament of the curve is relatively flat which shows the small mobilization of shear stress while the second segaments of the curve is steep which indicate the large shear stress mobilzation. However, in few cases theses two distinct segaments were not observed.

4.4.2.2.1 Reinforced mass with three rock bolts (R3)

σ_n= 0.0 MPa

Reinfocement imposes restriction on sliding of blocks through joint plane. Initially shear stress increases gradually, after about 8 mm of horizontal displacement, the shear stress increases rapidly and then drops after reaching peak value (Fig. 4.6-5a). Slight damage of blocks was observed around the reinforcement. Bolts were observed to have been deformed due to shearing. Peak shear stress of 0.169 MPa was observed at a horizontal displacement of 10.9 mm. Vertical displacement begins after 6 mm of horizontal displacement and increases with horizontal displacement upto the point at which peak stress has been observed (Fig. 4.6-5b).
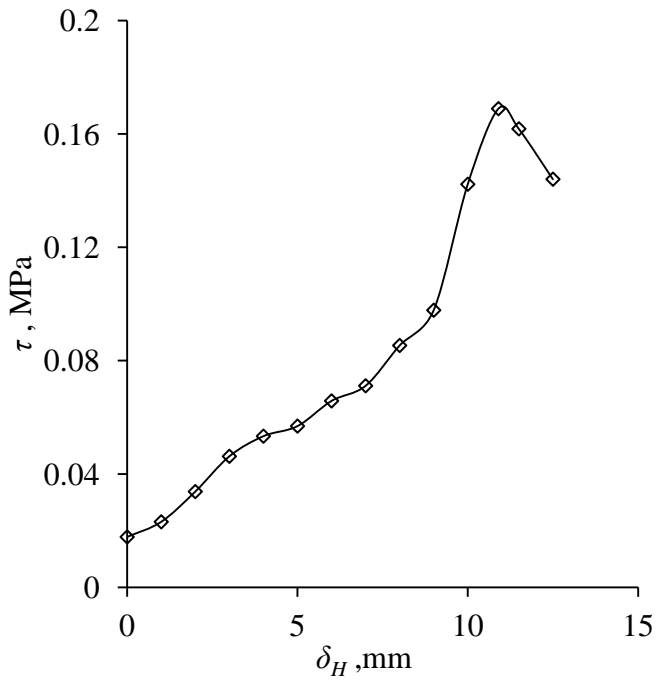
Fig.4.6-5a Shear stress (τ) vs horizontal shear displacement (δ_H) plot for reinforced mass with 3 bolts at σ_n = 0.0 MPa
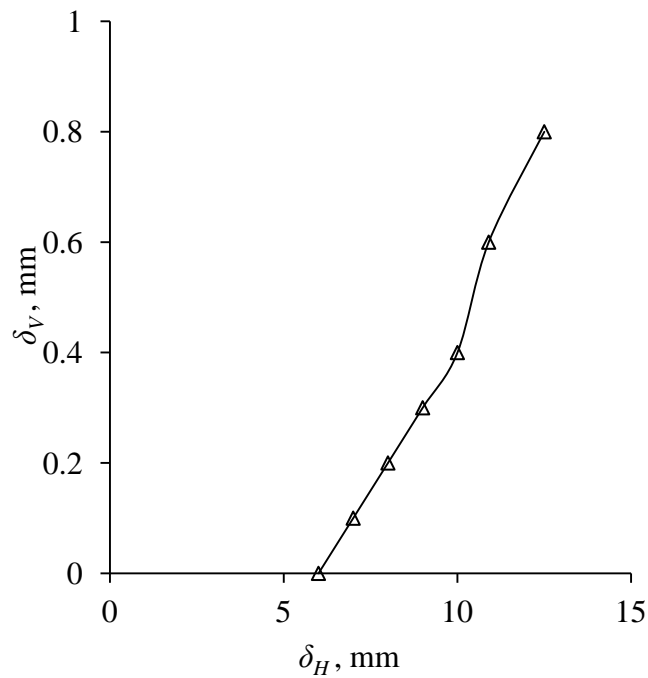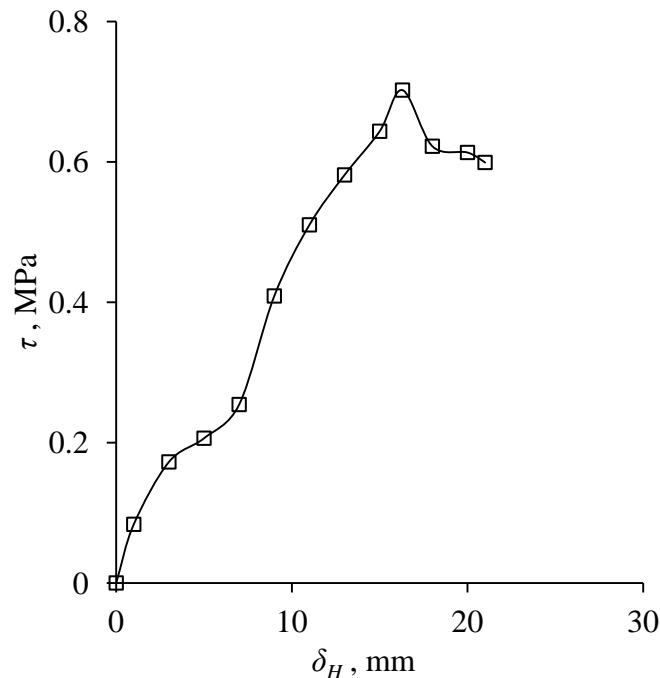

Fig.4.6-5b Vertical displacement (δ_V) vs horizontal shear displacement (δ_H) plot for reinforced mass with 3 bolts at σ_n = 0.0 MPa
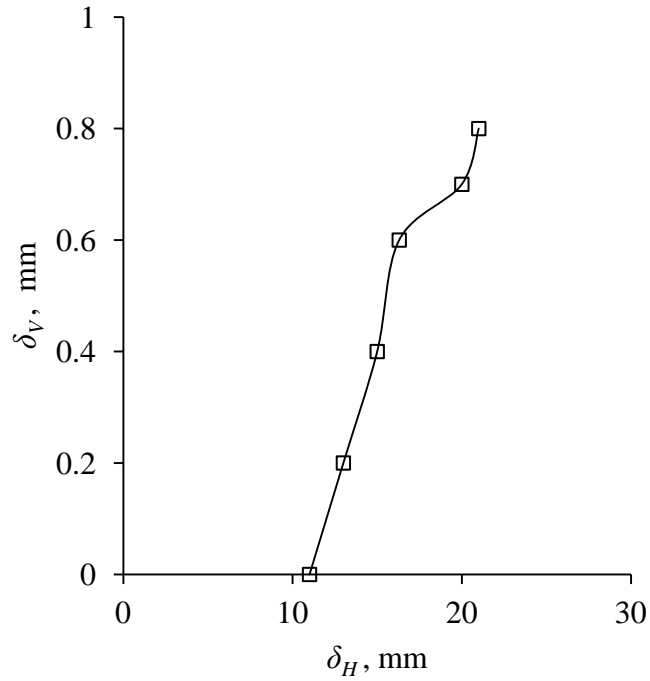
σ_n= 0.5 MPa

$\sigma_n= 0.5\ MPa$

The shear stress increased gradually up to about 7 mm horizontal displacement, afterwards the rate of increase in shear stress was fast up to peak stress (Fig. 4.6-6a). Peak shear stress of 0.702 MPa was observed at a horizontal displacement of 16.3 mm. A drop in shear stress was observed after the peak stress. Some damage was observed in the rock blocks. Bolts were deformed due to shearing. Vertical displacement starts after 6 mm of horizontal displacement and increases with horizontal displacement until end of the test (Fig. 4.6-6b).
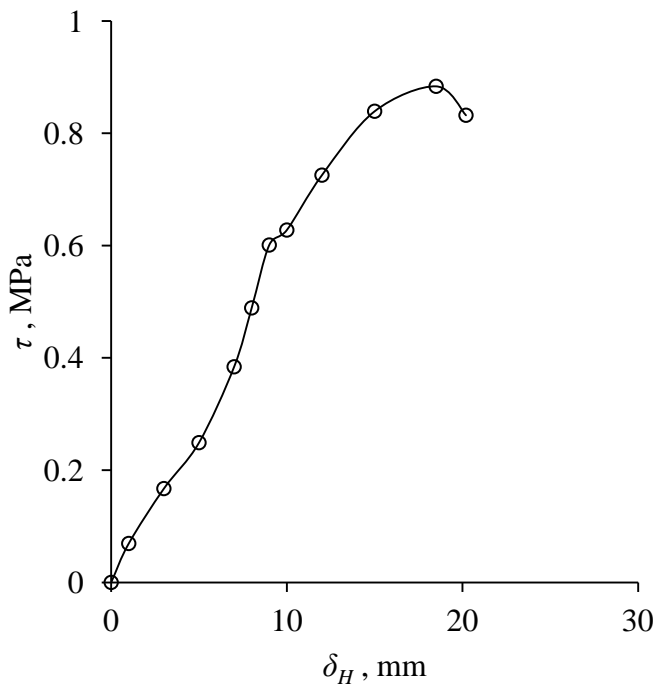
$\sigma_n = 1.0\ MPa$

The shear stress increases gradually with horizontal displacement and reaches its peak value of 0.884 MPa at 18.5 mm of horizontal displacement (Fig. 4.6-7a). The flat portion of curve diminishes in this case. More than 10 percent of rock blocks in the mass showed signs of damage at edges. Deformation in bolts was also observed in this case. Vertical displacement increases with horizontal displacement until end of the test (Fig. 4.6-7b).
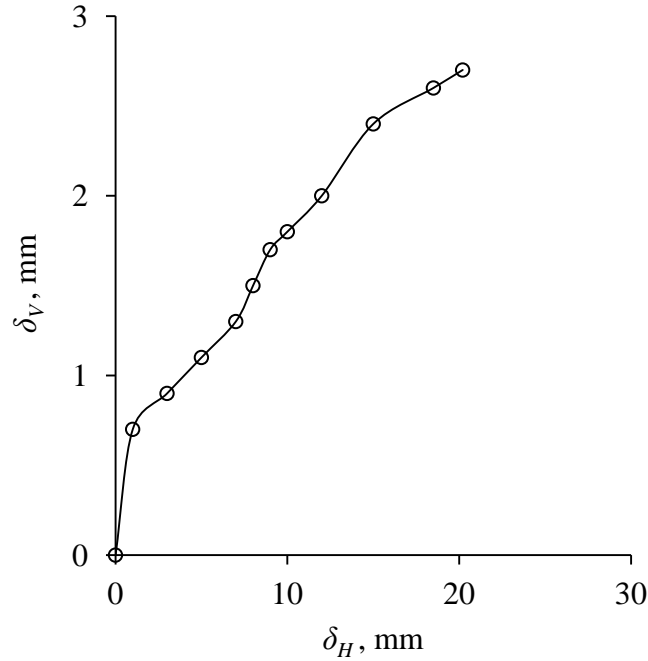

Fig.4.6-6a Shear stress (τ) vs horizontal shear displacement (δ_H) plot for reinforced mass with 3 bolts at $\sigma_n = 0.5$ MPa

Fig.4.6-6b Vertical displacement (δ_V) vs horizontal shear displacement (δ_H) plot for reinforced mass with 3 bolts at σ_n = 0.5 MPa

Fig.4.6-7a Shear stress (τ) vs horizontal shear displacement (δ_H) plot for reinforced mass with 3 bolts at σ_n = 1.0 MPa

Fig.4.6-7b Vertical displacement (δ_V) vs horizontal shear displacement (δ_H) plot for reinforced mass with 3 bolts at σ_n = 1.0 MPa
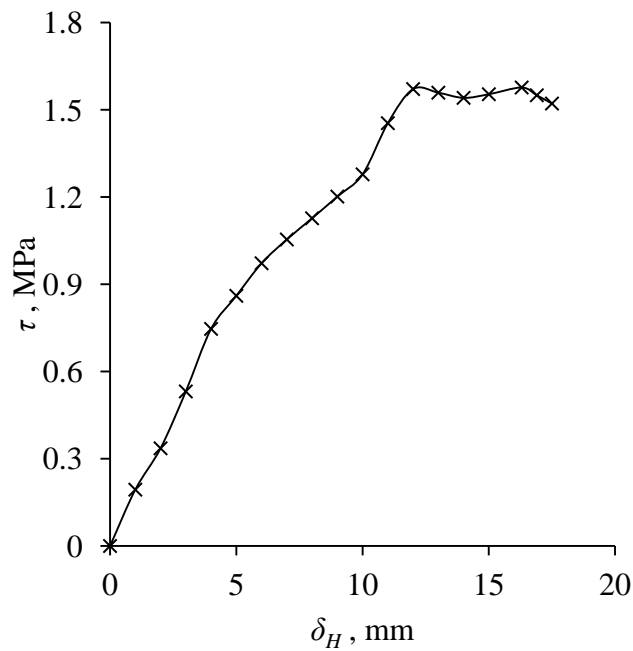
σ_n = 2.0 MPa

Shear stress increases with increasing horizontal displacement without showing distinct flat portion (Fig. 4.6-8a). The peak shear stress in present case is only slightly higher than that observed for unreinforced mass for same normal stress. Peak shear stress of 1.577 MPa was observed at a horizontal displacement of 16.3 mm. More than 40 percent of the rock blocks in the mass showed damage in the form of small shearing at corners or splitting due to high normal stress and reinforcement. Deformation in bolts was also observed. During shearing, the vertical displacement increased with increase in horizontal displacement (Fig. 4.6-8b).

**4.4.2.2.2 Reinforced mass with five rock bolts (R5)**

σ_n= 0.0 MPa

Shear stress mobilization is low up to a horizontal displacement of about 6 mm. After this, the shear stress increases rapidly and reaches its peak value of 0.802 MPa at horizontal displacement of 9.4 mm (Fig. 4.6-9a). Small cracks were observed in some of the blocks. Deformation in bolts was also observed. Vertical displacement

starts after about 6.5 mm of horizontal displacement and increases very rapidly with horizontal displacement until the end of the test (Fig. 4.7-9b).
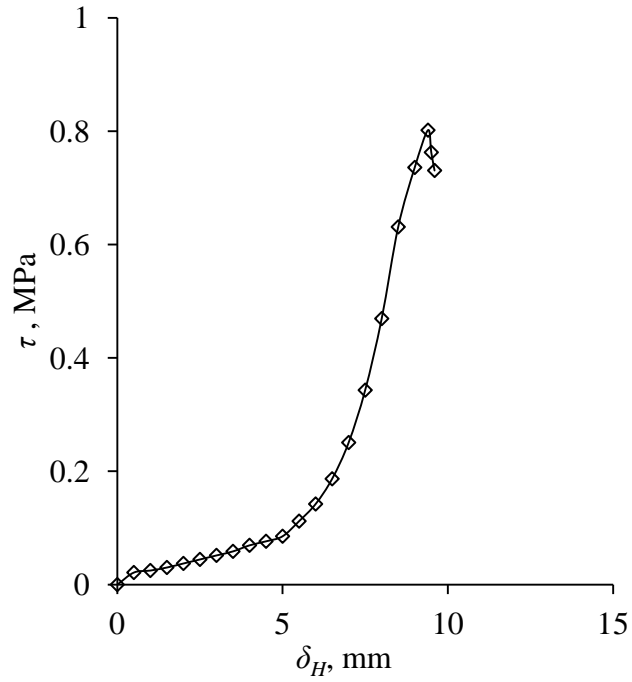

Fig.4.6-8a Shear stress (τ) vs horizontal shear displacement (δ_H) curve for reinforced mass with 3 bolts at σ_n = 2.0 MPa
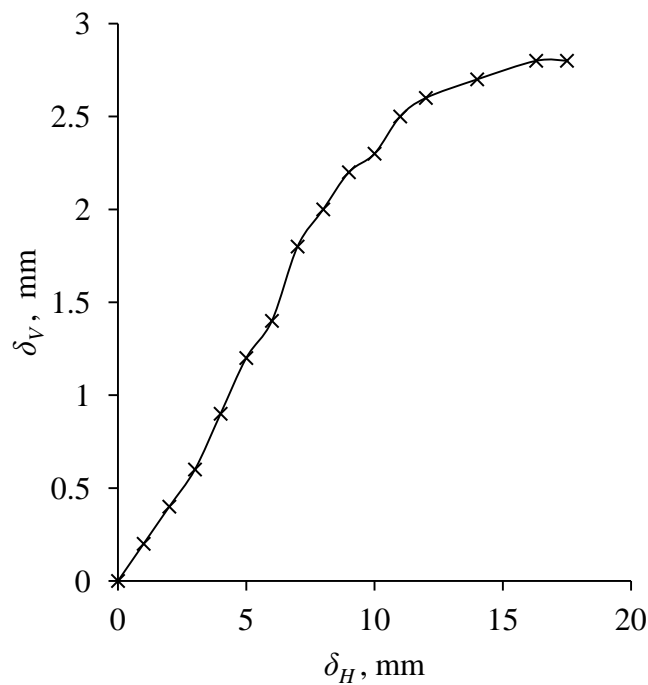
Fig.4.6-8b Vertical displacement (δ_V) vs horizontal shear displacement (δ_H) curve for reinforced mass with 3 bolts at σ_n = 2.0 MPa

Fig.4.6-9a Shear stress (τ) vs horizontal shear displacement (δ_H) plot for reinforced mass with 5 bolts at $\sigma_n = 0.0$ MPa

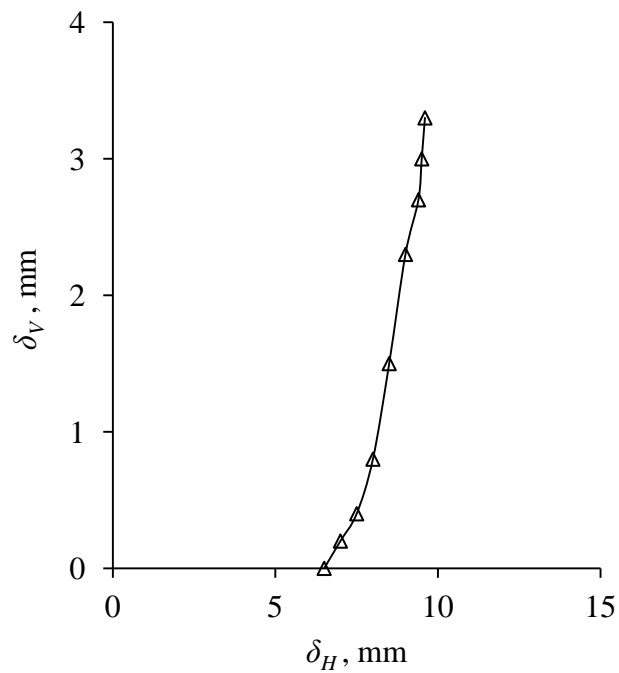**Fig.4.6-9b Vertical displacement (δ_V) vs horizontal shear displacement (δ_H) plot for reinforced mass with 5 bolts at $\sigma_n = 0.0$ MPa**

σ_n = 0.5 MPa

The first flatter part of the shear stress vs displacement curve is observed up to about 10 mm of displacement. Beyond this, the shear stress mobilisation is fast due to interaction of bolts with blocks. Peak stress of 1.095 MPa was observed at a horizontal displacement of 12.5 mm (Fig. 4.6-10a). Deformation in bolts was observed due to shearing. Vertical displacement increased gradually with horizontal displacement till end of the test (Fig. 4.6-10b).

σ_n = 1.0 MPa

The first part of the shear tress vs displacement curve extended up to 11 mm. The second part of the curve continues up to 14.8 mm at peak. The peak stress of 1.335 MPa was observed at a horizontal shear displacement of 14.8 mm (Fig. 4.6-11a). After test, inspection of mass indicates damage to more than about 20% of blocks. Deformation in bolts was observed. Vertical displacement was also found to increase with horizontal displacement (Fig. 4.6-11b).

Fig.4.6-10a Shear stress (τ) vs horizontal shear displacement (δ_H) plot for reinforced mass with 5 bolts at $\sigma_n = 0.5$ MPa
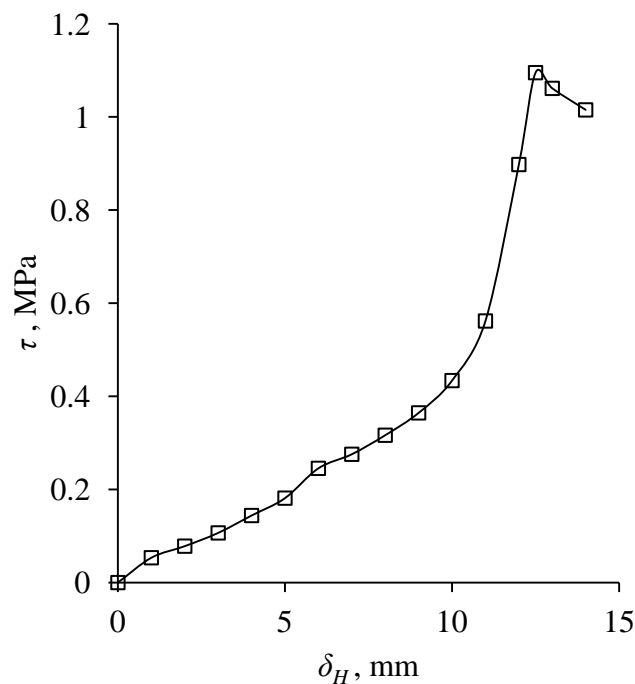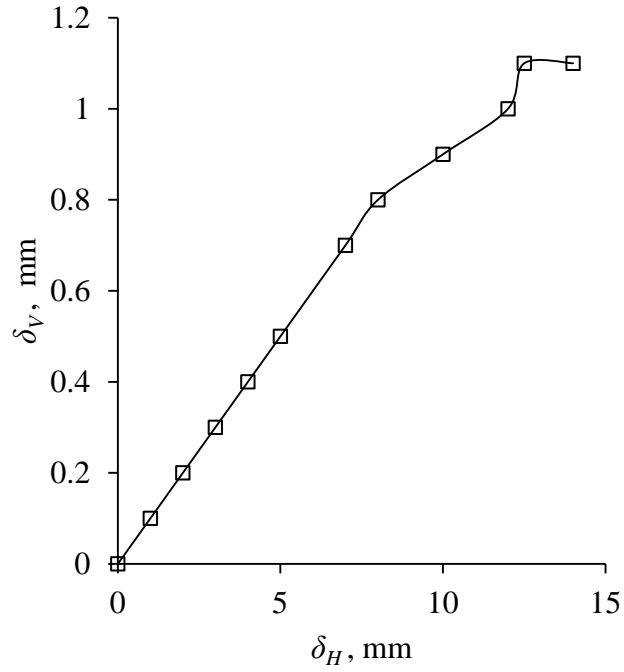
Fig.4.6-10b Vertical displacement (δ_V) vs horizontal shear displacement (δ_H) plot for reinforced mass with 5 bolts at σ_n = 0.5 MPa
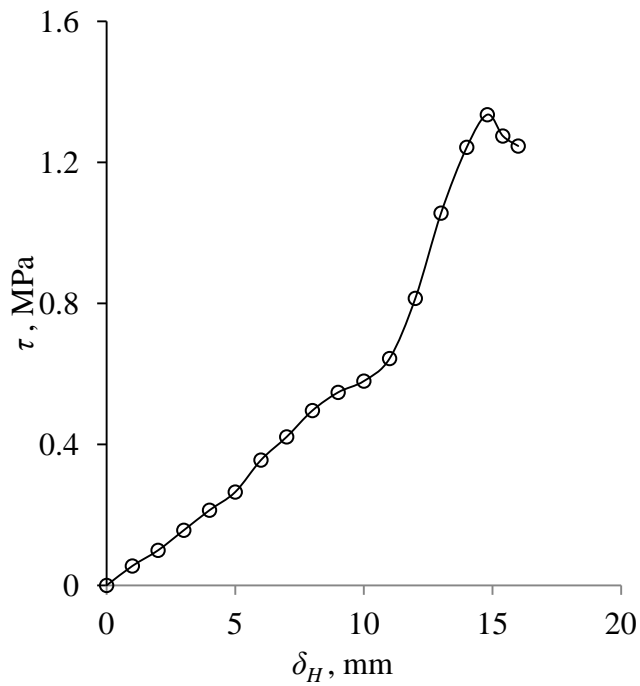
Fig.4.6-11a Shear stress (τ) vs horizontal shear displacement (δ_H) plot for reinforced mass with 5 bolts at σ_n = 1.0 MPa

Fig.4.6-11b Vertical displacement (δ_V) vs horizontal shear displacement (δ_H) plot for reinforced mass with 5 bolts at $\sigma_n = 1.0$ MPa

$\sigma_n = 2.0$ MPa

The two segments of the shear stress vs displacement curve tend to merge with each other in this case (Fig. 4.6-12a). Peak shear stress of 1.911 MPa was observed at a horizontal displacement of 14.7 mm. More than 40 percent of blocks exhibit damage due to high stress concentration in the mass. Bolts were found to have been deformed. Vertical displacement was found to increase with horizontal displacement (Fig.4.6-12b).

4.4.2.2.3 Reinforced mass with nine rock bolts (R9)

$\sigma_n = 0.0$ MPa

Initial part of the shear stress vs displacement curve continues up to a displacement of 7.5 mm. Beyond this displacement a well-defined peak has been observed. Peak shear stress of 1.093 MPa was observed at a horizontal displacement of 19 mm (Fig. 4.6-13a). Deformation in bolts was observed. The vertical displacement increases gradually with horizontal displacement until end of the test (Fig. 4.6-13b).
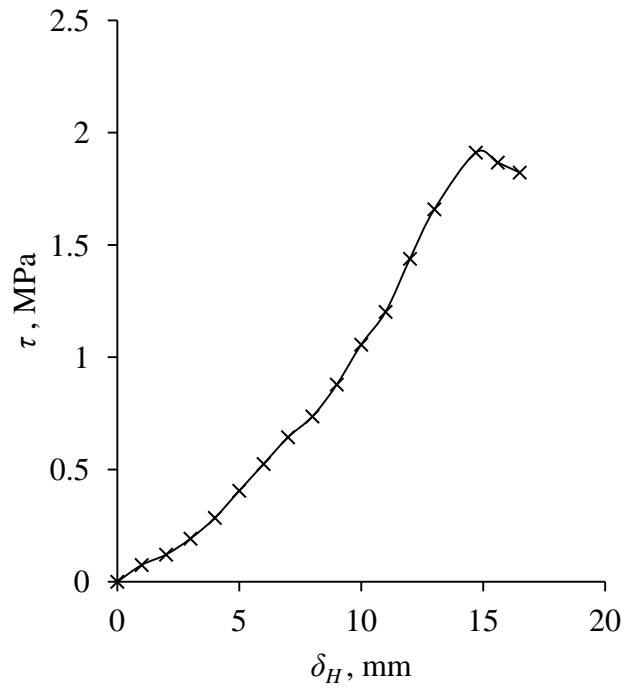
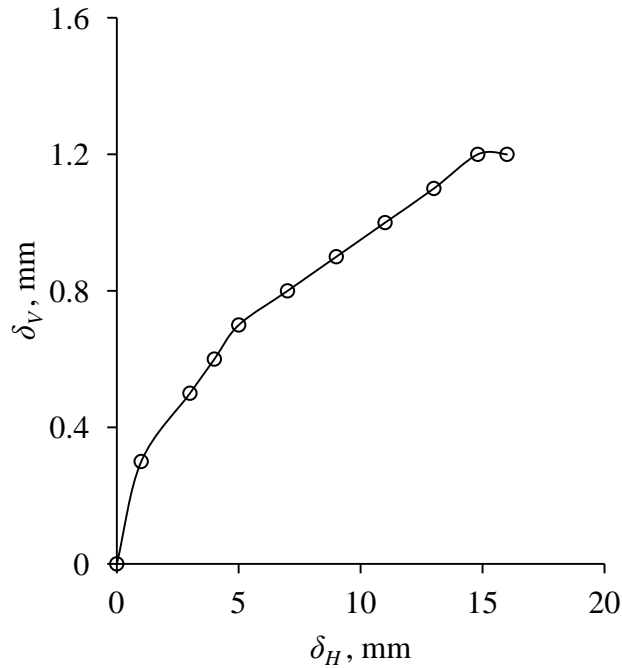**Fig.4.6-12a Shear stress (τ) vs horizontal shear displacement (δ_H) plot for reinforced mass with 5 bolts at $\sigma_n = 2.0$ MPa**
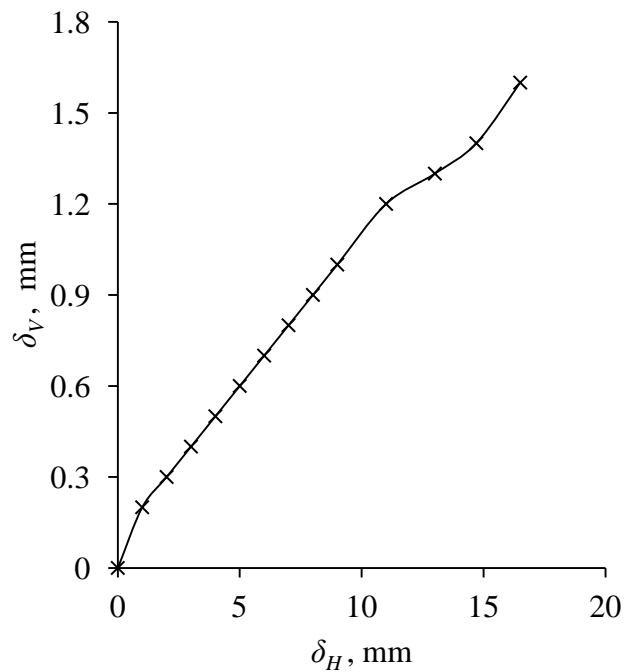
Fig.4.6-12b Vertical displacement (δ_V) vs horizontal shear displacement (δ_H) plot for reinforced mass with 5 bolts at $\sigma_n = 2.0$ MPa
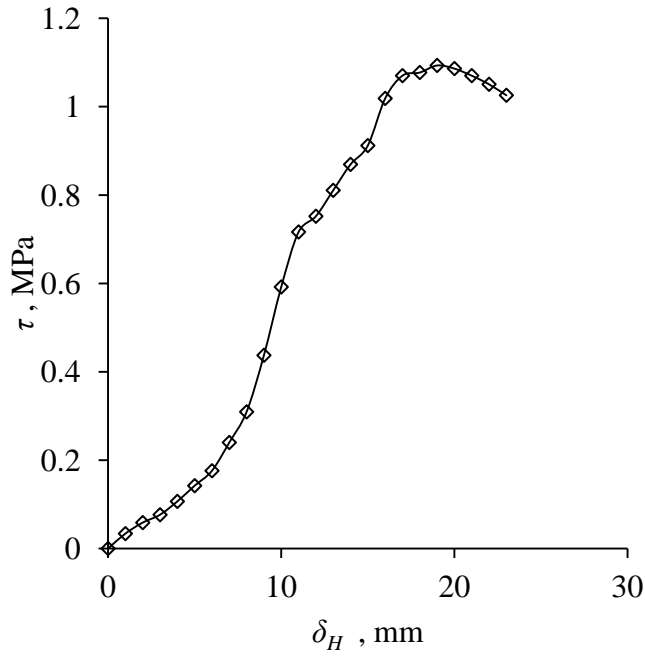
Fig.4.6-13a Shear stress (τ) vs horizontal shear displacement (δ_H) plot for reinforced mass with 9 bolts at $\sigma_n = 0.0$ MPa

Fig.4.6-13b Vertical displacement (δ_V) vs horizontal shear displacement (δ_H) plot for reinforced mass with 9 bolts at $\sigma_n = 0.0$ MPa

σ_n = 0.5 MPa

The first segment of the shear stress vs displacement curve continues up to about 14 mm of displacement followed by second part and well-defined peak (Fig. 4.6-14a). Peak shear stress of 1.371 MPa was observed at a horizontal deformation of 19 mm. Twenty percent of blocks in the mass exhibit signs of damage due to high shearing stress. Due to shearing, the deformation in bolts was observed. Vertical displacement was found to increase with horizontal displacement (Fig. 4.6-14b).

σ_n = 1.0 MPa

The first flat segment of shear stress vs displacement curve continues up to about 9 mm of shear displacement, followed by curve showing steep gradient (Fig. 4.6-15a). However, there seems to be local failure and again the curve of low gradient was observed. The stress was again mobilized through bolts, and at 33.5 mm of shear displacement, peak stress of 1.579 MPa was observed. Bolts were deformed due to shearing. About 40 percent of blocks in the mass were damaged or fractured. Vertical displacement was also found to increase with horizontal displacement till the end of the test (Fig. 4.6-15b).

σ_n = 2.0 MPa

The initial flat segment of shear stress vs displacement curve extends up to about 25 mm of displacement. Peak shear stress 2.347 MPa was observed at a horizontal displacement of 32.9 mm (Fig. 4.6-16a). Deformation in bolt was observed. More than 60 percent blocks exhibit heavy damage. Cracks or edge failure was observed in another 30 percent block in the mass. Vertical displacement increased with horizontal displacement and relatively flat curve of vertical displacement vs horizontal displacement was observed (Fig. 4.6-16b).
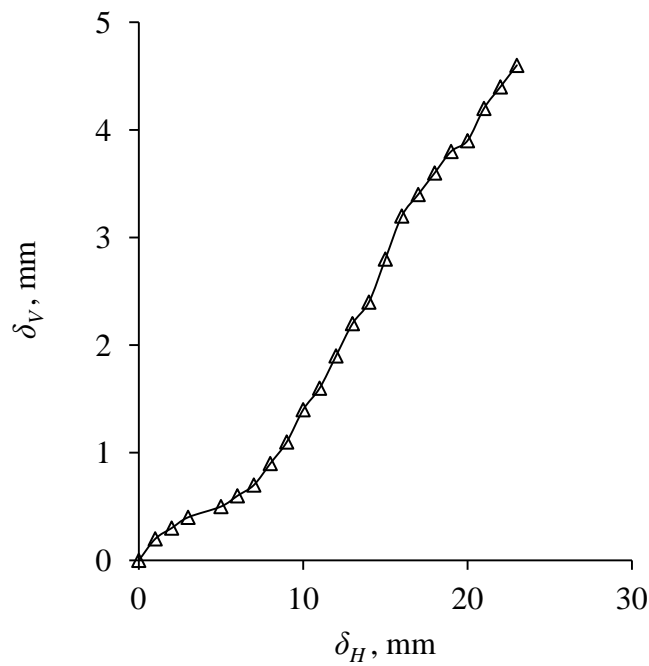
Fig.4.6-14a Shear stress (τ) vs horizontal shear displacement (δ_H) plot for reinforced mass with 9 bolts at σ_n = 0.5 MPa
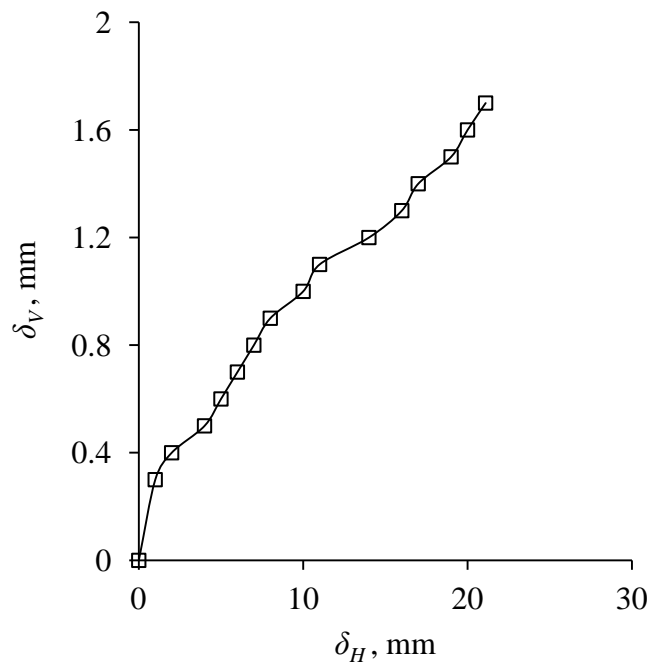
Fig.4.6-14b Vertical displacement (δ_V) vs horizontal shear displacement (δ_H) plot for reinforced mass with 9 bolts at σ_n = 0.5 MPa
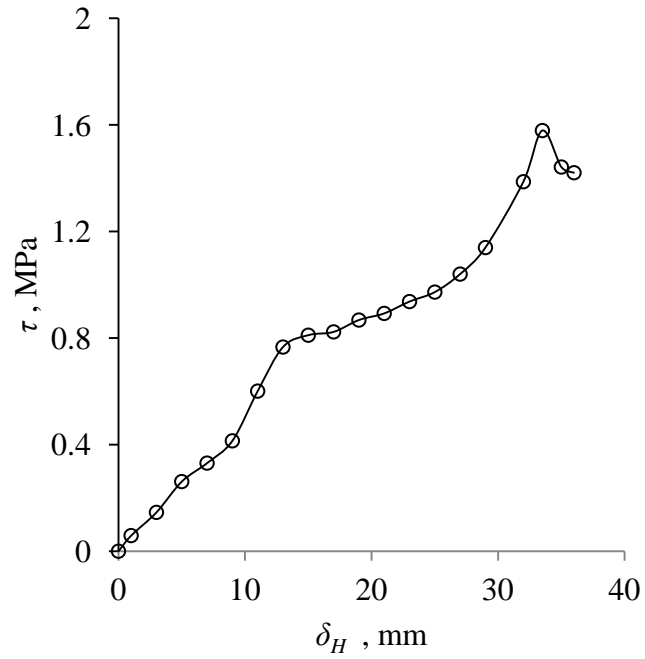
Fig.4.6-15a Shear stress (τ) vs horizontal shear displacement (δ_H) plot for reinforced mass with 9 bolts at $\sigma_n = 1.0$ MPa

Fig.4.6-15b Vertical displacement (δ_V) vs horizontal shear displacement (δ_H) plot for reinforced mass with 9 bolts at $\sigma_n = 1.0$ MPa
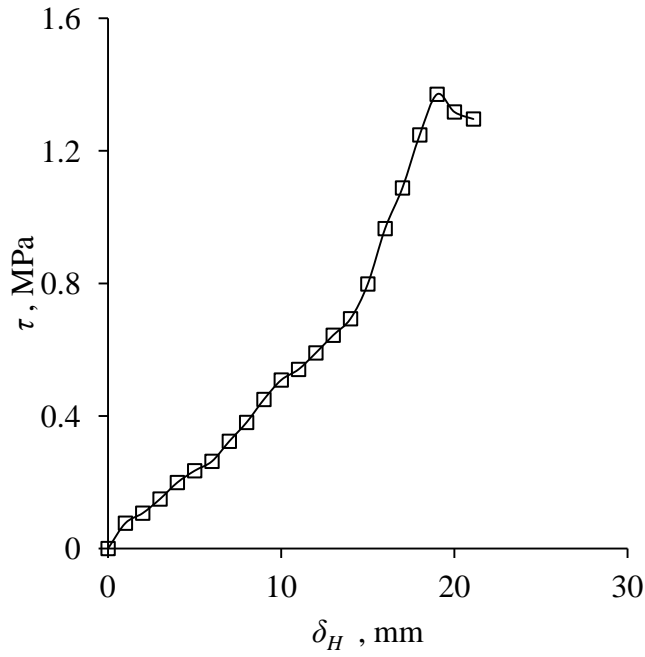
Fig.4.6-16a Shear stress (τ) vs horizontal shear displacement (δ_H) plot for reinforced mass with 9 bolts at σ_n = 2.0 MPa

Fig.4.6-16b Vertical displacement (δ_V) vs horizontal shear displacement (δ_H) plot for reinforced mass with 9 bolts at σ_n = 2.0 MPa
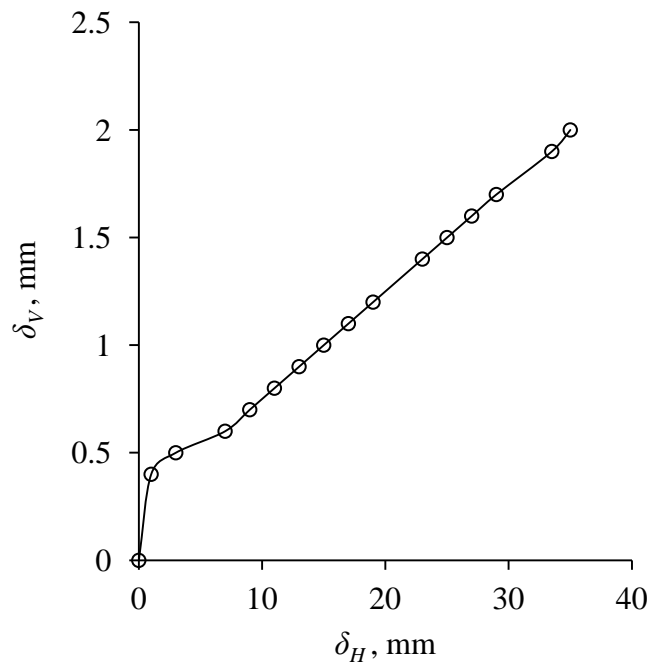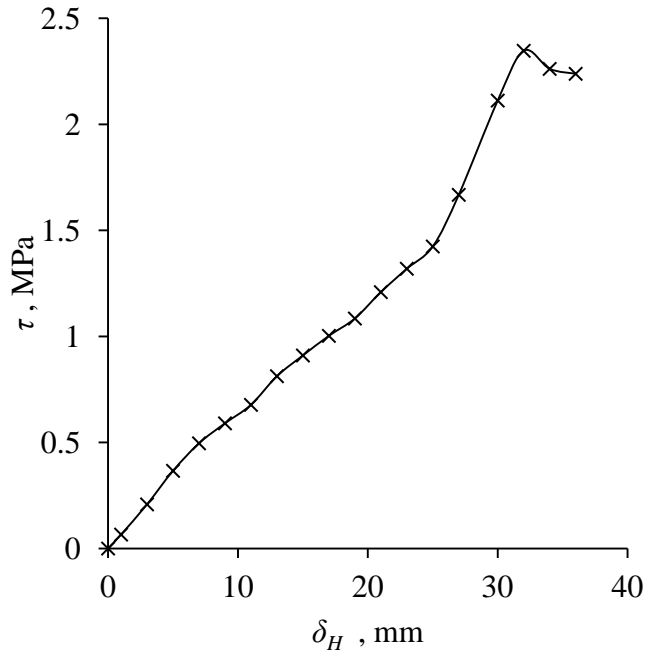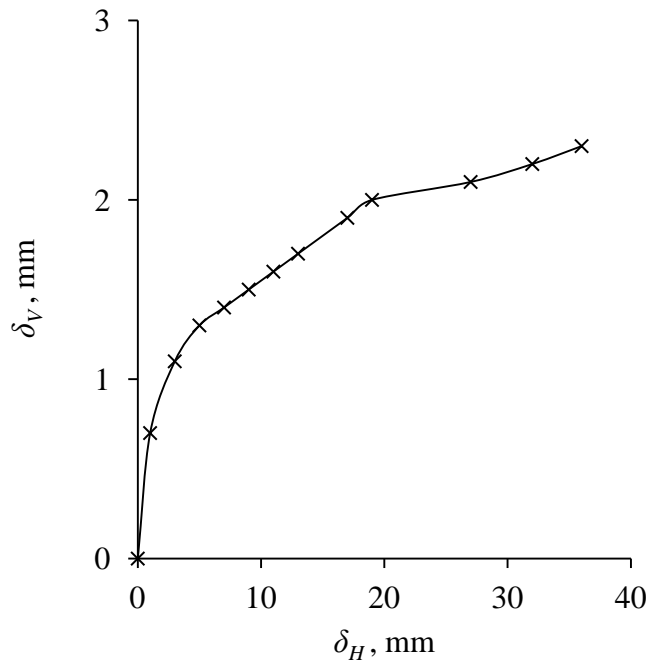
4.4.3 Summery of Observations

Sliding of blocks was observed in unreinforced mass whereas no sliding was observed in case of reinforced specimens. Installation of bolts prevents the sliding of blocks through joint plane in the mass. Bolts improve the interlocking in the joints and due to the development of tensile stress in the bolt, an additional normal stress is induced on the joint surface. Due to development of additional normal stress, the mass becomes stronger and stiffer.

The comparison of shear stress (τ) vs horizontal shear displacement (δ_H) plots for different configurations of blocky mass at different normal stress levels is presented in Fig.4.7. In general, the shear stress increases with increasing shear displacement and exhibits a clearly defined peak in the majority cases, except for unreinforced mass tested at low normal stresses (0 and 0.5 MPa). In case of reinforced blocky mass, the shear stress vs the horizontal shear displacement curves exhibit two distinct segments. The first segament is relatively flat which indicates the mobilization of shear stress due to the interaction of the blocks. Interaction between blocks gives rise to the development of tensile stress in the bolts at the end of this segment. The second part of the curve is steep which indicates the mobilization of shear stress through the bolts.

The values of shear strength (peak shear stress at failure, τ_{peak}) and corresponding horizontal shear displacements ($\delta_{H,\ peak}$) are shown in Table 4.4a and 4.4b respectively. The results indicated that the shear strength of reinforced mass enhances due to provision of bolts. The shear strength was also found to increase with increase in number of bolts at all levels of normal stresses investigated in this study. Further, an increase in the normal stress results in increase in the shear strength.

The observations on horizontal shear displacements corresponding to peak shear stress indicate that with increase in number of bolts, the horizontal shear displacement decreases, and reaches its minimum value when five bolts (R5) are used (Table 4.4b). When nine bolts (R9) are used, the horizontal shear displacement again increases.
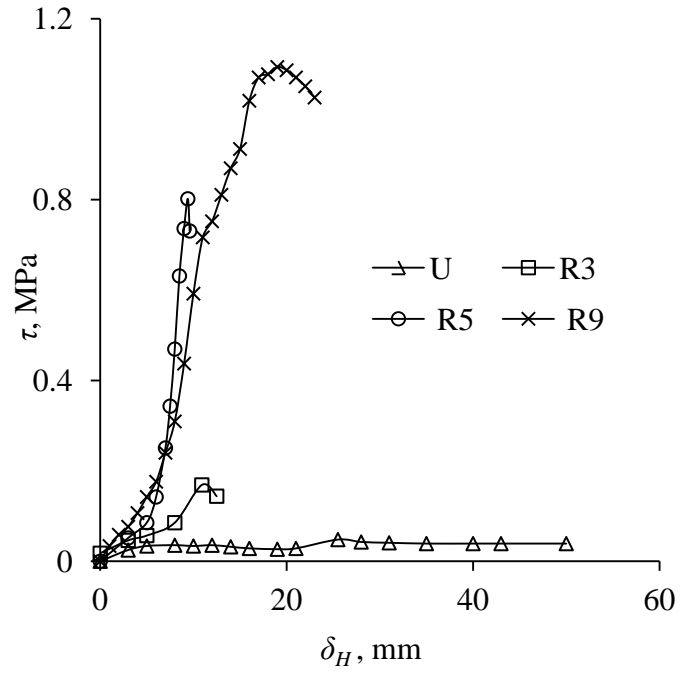
(a) $\sigma_n = 0.0$ MPa
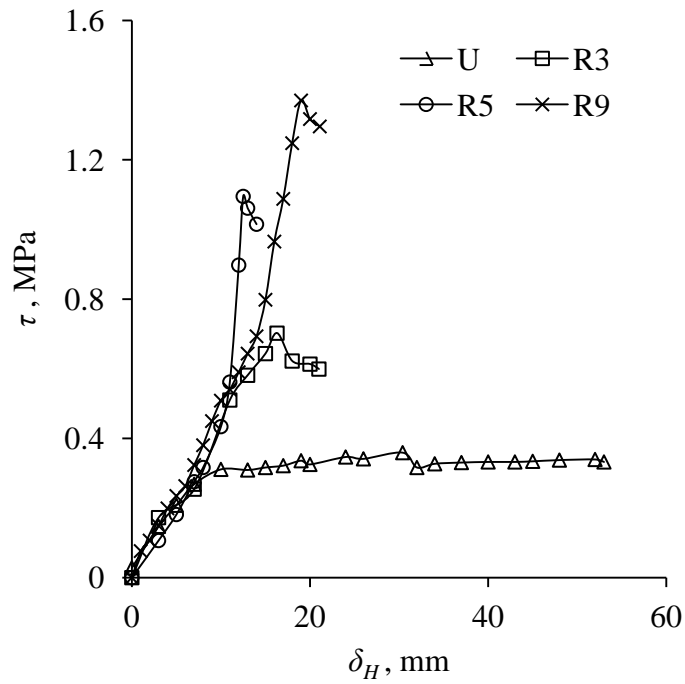
(b) $\sigma_n = 0.5$ MPa

Fig.4.7 Shear stress (τ) vs horizontal shear displacement (δ_H) plots at different normal stress levels for different configuration of blocky mass
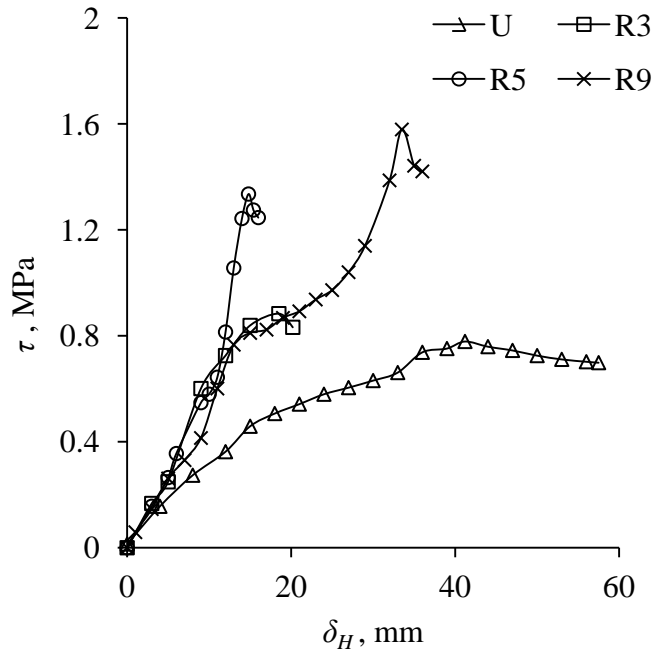
(c) σ_n = 1.0 MPa
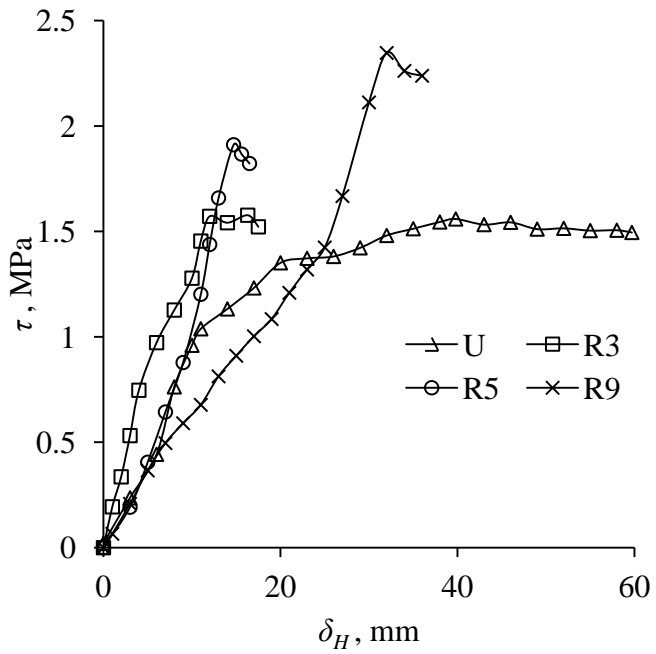
(d) σ_n = 2.0 MPa

Fig.4.7 Shear stress (τ) vs horizontal shear displacement (δ_H) plots at different normal stress levels for different configuration of blocky mass

Table 4.4a Shear strength (τ_f) at different normal stress levels

σ_n, MPa	τ_{peak}, MPa			
	U	R3	R5	R9
	$n = 0$	$n = 3$	$n = 5$	$n = 9$
0.0	0.048	0.169	0.802	1.093
0.5	0.359	0.702	1.095	1.371
1.0	0.779	0.884	1.335	1.579
2.0	1.559	1.577	1.911	2.347

n = numbers of bolts

Table 4.4b Values of $\delta_{H, peak}$ at different normal stress levels

σ_n, MPa	$\delta_{H, peak}$, mm			
	U	R3	R5	R9
	$n = 0$	$n = 3$	$n = 5$	$n = 9$
0.0	25.5	10.9	9.4	19
0.5	30.4	16.3	12.5	19
1.0	41.2	18.5	14.8	33.5
2.0	39.8	16.3	14.7	32.9

The comparison of vertical displacement (δ_v) vs the horizontal shear displacement (δ_H) curves for different configuration of mass at different normal stress levels are presented in Fig.4.8. The vertical displacement at peak shear stress ($\delta_{V, peak}$) is presented in Table 4.4c. For low normal stress levels (0 and 0.5 MPa), the $\delta_{V, peak}$ was minimum for unreinforced mass, and increased with number of bolts. At theses normal stress levels, the maximum $\delta_{V, peak}$ was observed for specimens with nine bolts (R9 case). However, at higher normal stress levels (1 to 2 MPa), this trend was not observed, and unreinforced specimens showed higher vertical displacement compared to reinforced specimens.

Table 4.4c Values of $\delta_{V, peak}$ at different normal stress levels

σ_n, MPa	$\delta_{V, peak}$, mm			
	U	R3	R5	R9
	$n = 0$	$n = 3$	$n = 5$	$n = 9$
0.0	0.4	0.6	2.7	3.8
0.5	0.5	0.6	1.1	1.5
1.0	2.6	2.6	1.2	1.9
2.0	3.8	2.8	1.4	2.2
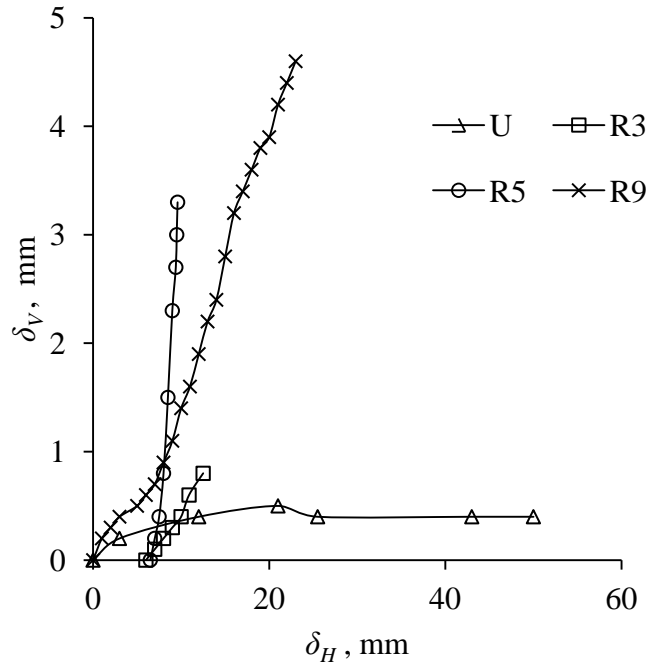
(a) σ_n = 0.0 MPa
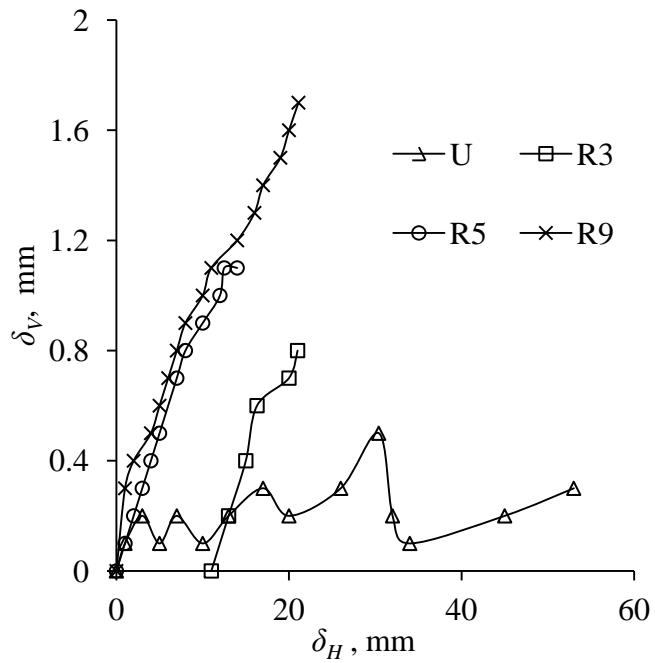
(b) σ_n = 0.5 MPa

Fig.4.8 Vertical displacement (δ_V) vs horizontal shear displacement (δ_H) plots at different normal stress levels for different configuration of blocky mass
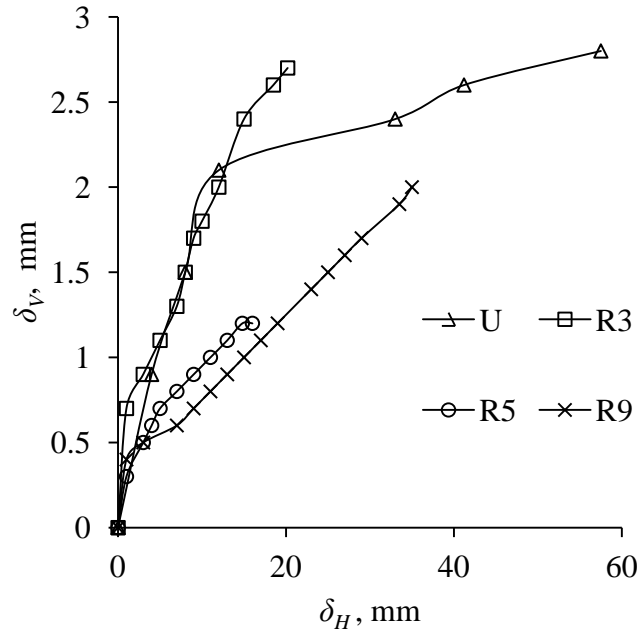
(c) σ_n = 1.0 MPa
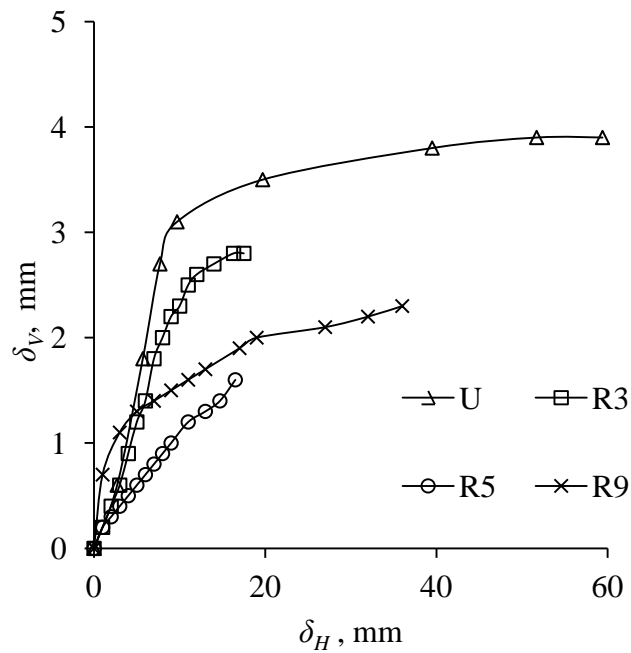
(d) σ_n = 2.0 MPa

Fig.4.8 Vertical displacement (δ_V) vs horizontal shear displacement (δ_H) plots at different normal stress levels for different configuration of blocky mass

124

4.5 UNIAXIAL COMPRESSION TESTS ON SYNTHETIC ROCK SPECIMENS

Uniaxial compression tests have been conducted on the prismatic specimens of synthetic rock specimens (referred to T2 and T3) of size 150 mm x 150 mm x 300 mm (height) without and with bolts. The joint orientation of specimens was varied from 0° to 90° from the horizontal axis (θ = 0°, 15°, 30°, 45°, 60°, 75° and 90°). The jointed specimens were reinforced with two passive bolts. The detailed description of results are summarized and presented below.

4.5.1 Intact Model Material

Cores were extracted from concrete blocks to obtain cylindrical specimens of NX size. These cylindrical specimens were subjected to routine tests i.e. UCS, triaxial and physical properties tests. The triaxial tests were performed at confining stress level of 0, 5, 10 and 20 MPa respectively. The deviator stress vs axial-strain plots of both types of synthetic rocks are plotted in Fig.4.9. Brittle behaviour was observed at low confining stress (σ_3 = 0 and 5 MPa) whereas ductile behaviour was observed at high confining stress (σ_3 = 10 and 20 MPa).
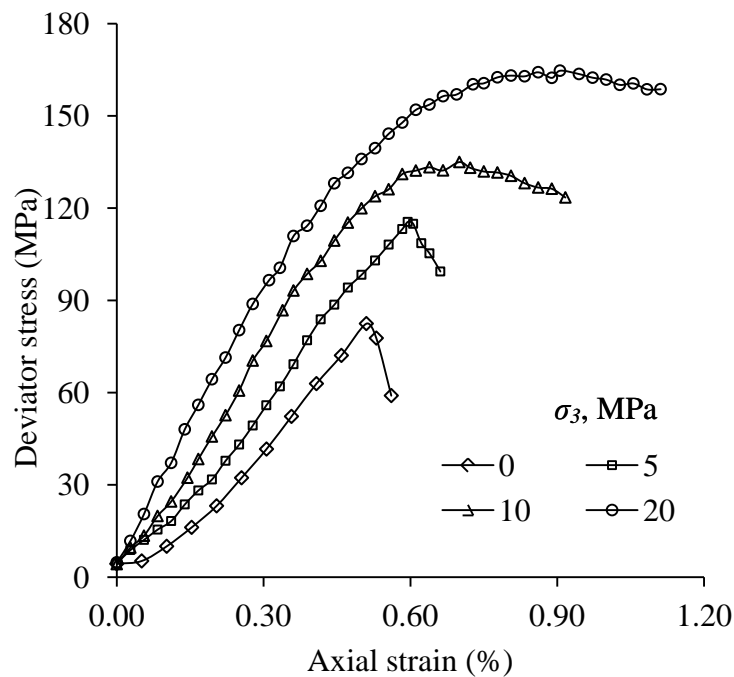
Fig.4.9a Deviator stress vs axial strain plots for T2 type of synthetic rock at different confining stress level

125
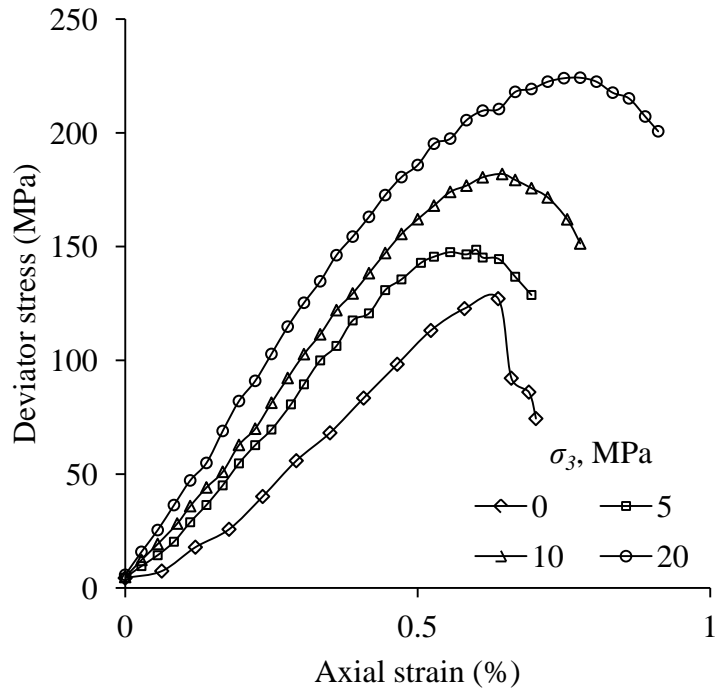
Fig.4.9b Deviator stress vs axial strain plots for T3 type of synthetic rock at different confining stress level

The Mohr circles at failure are presented in Fig.4.10. On Deere –Miller classification chart the T2 type of synthetic rock is classified as CM i.e. rock having medium strength and medium modular ratio while T3 type of synthetic rock is classified as BM i.e. rock having high strength and medium modular ratio (Fig.4.11). Joint shear strength parameters were obtained by conducting direct shear tests on the joint surface. The physical and engineering properties of the syntactic rocks are listed in Table 4.5.

Table 4.5 Physical and engineering properties of synthetic rocks

Property	Symbol	Value	
		T2	**T3**
Unit weight (KN/m^3)	γ	24.04	24.53
Uniaxial compressive strength , MPa	σ_{ci}	82.44	127.13
Tangent modulus ,GPa	E_{t50}	22.16	27.61
Cohesion , MPa	c_i	20.14	26.12
Friction angle	ϕ_i	42	45
Cohesion along joint	c_j	0.03	.06
Friction angle of joint	ϕ_j	35	43
Deere-Millar classification	-	CM	BM
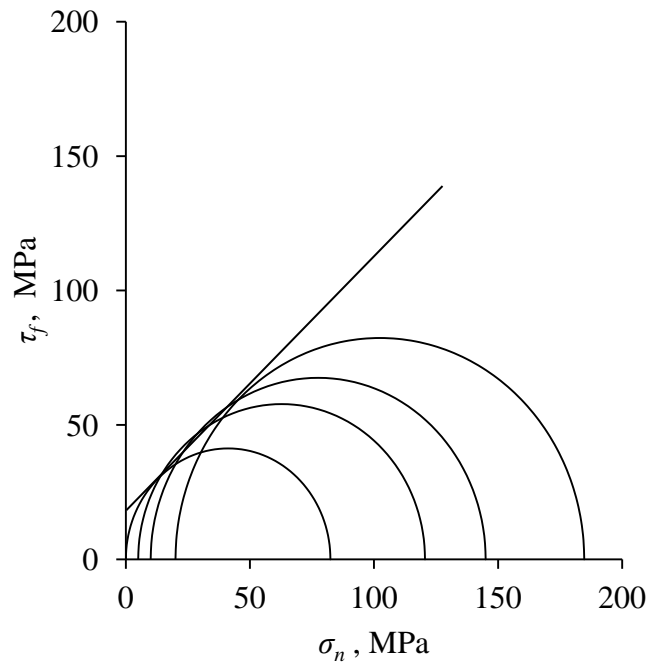
Fig.4.10a Mohr circles plot for T2 type of synthetic rock
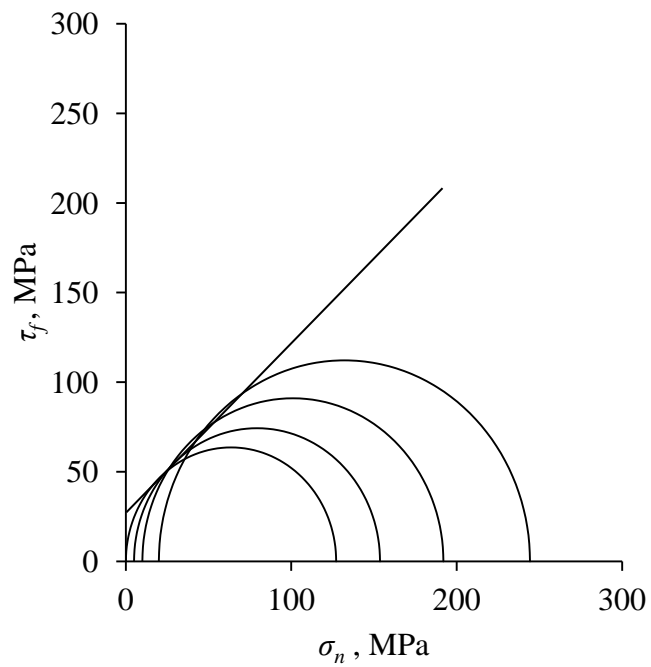
Fig.4.10b Mohr circles plot for T3 type of synthetic rock

127
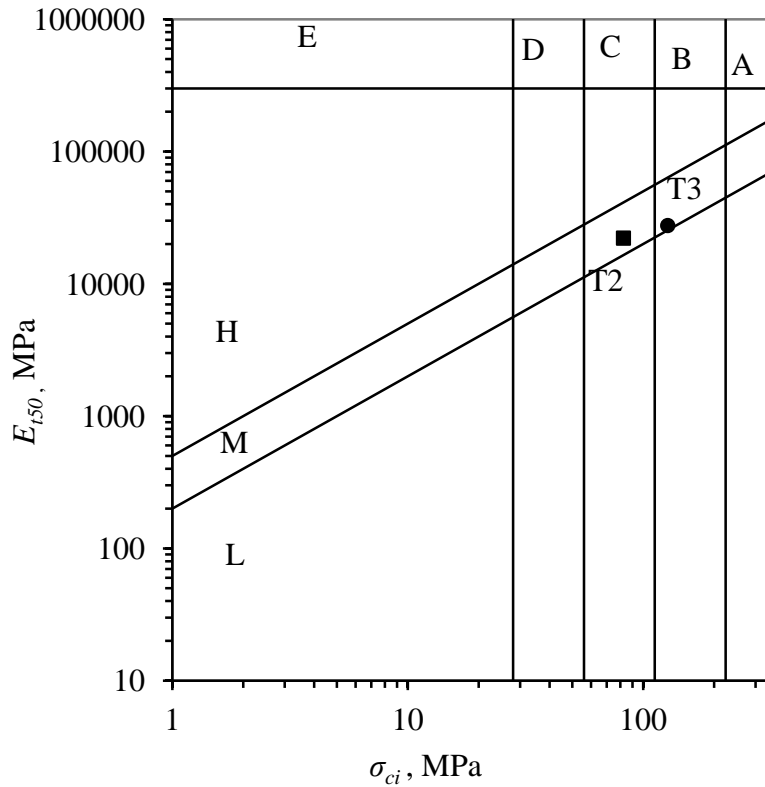
Fig.4.11 Deere-Miller classification of synthetic rocks

4.5.2 Observations Taken During Testing of Intact and Jointed Rock Specimens

Axial stress vs axial strain plot of intact (prismatic), unreinforced and reinforced synthetic rocks (T2 and T3) are presented in Appendix I. Some of these plots are presented in Fig.4.12. The details of observations taken during the testing are listed along with each plot. In most of the cases, a well-defined peak was observed in axial stress vs axial strain plot.
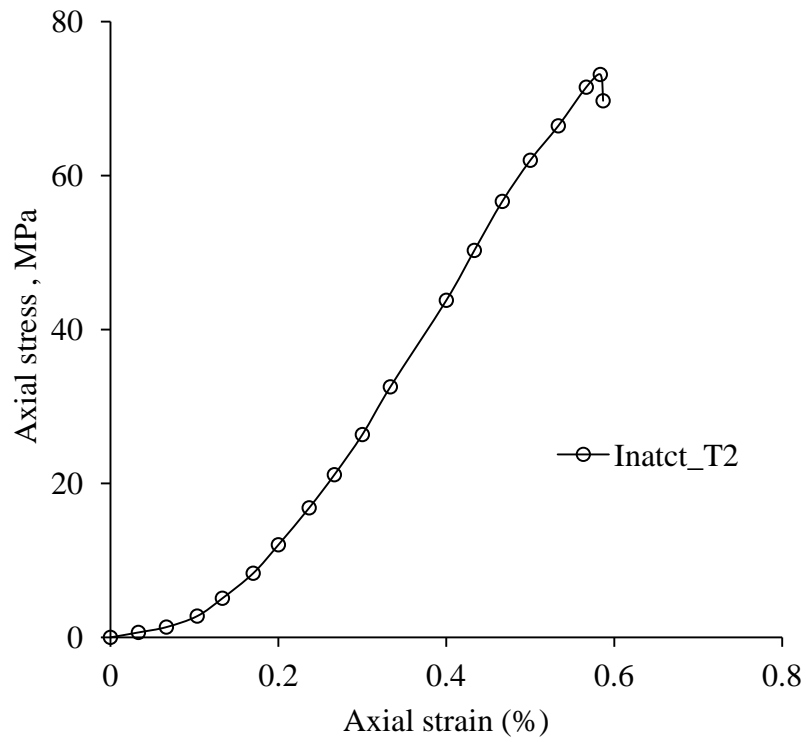
Fig.4.12a Axial stress vs axial strain plot of intact (prismatic section) synthetic rock (T2)

Observations

Peak stress	73.13 MPa
Axial strain at failure	0.583 %
Mode of failure	Splitting
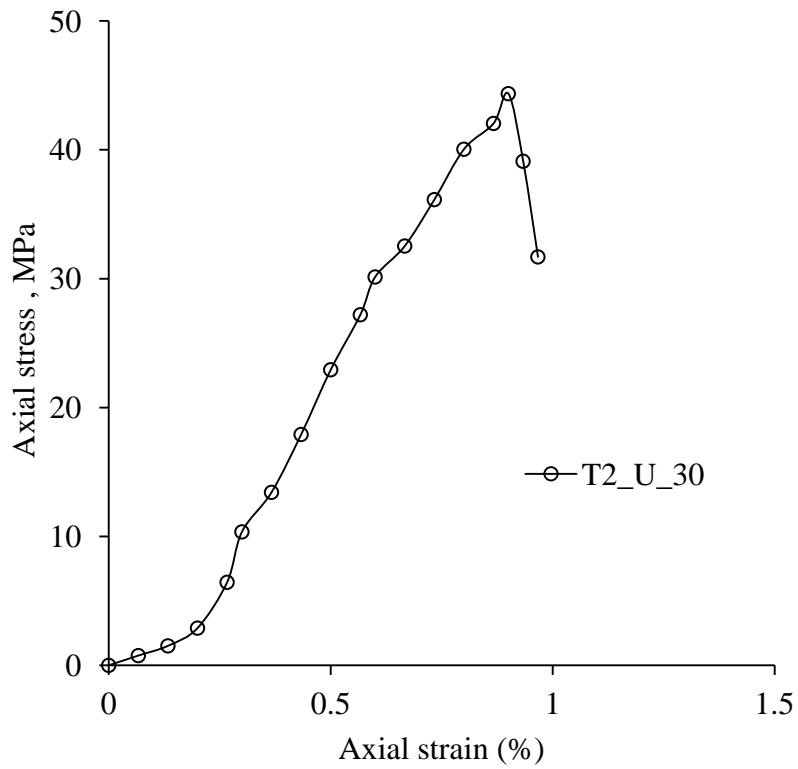
Fig.4.12b Axial stress vs axial strain plot of unreinforced jointed synthetic rock (T2) at $\theta = 30°$

Observations

Peak stress	44.36 MPa
Axial strain at failure	0.90 %
Mode of failure	Splitting
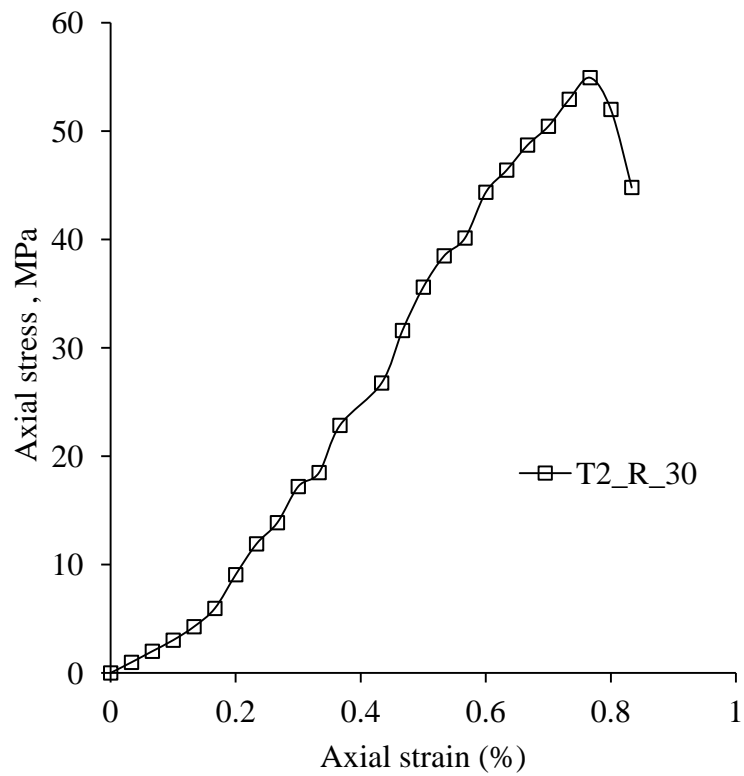
**Fig.4.12c Axial stress vs axial strain plot of reinforced jointed synthetic rock (T2)
at $\theta = 30°$**

Observations

Peak stress	54.93 MPa
Axial strain at failure	0.767 %
Mode of failure	Splitting
Deformation in bolt	No
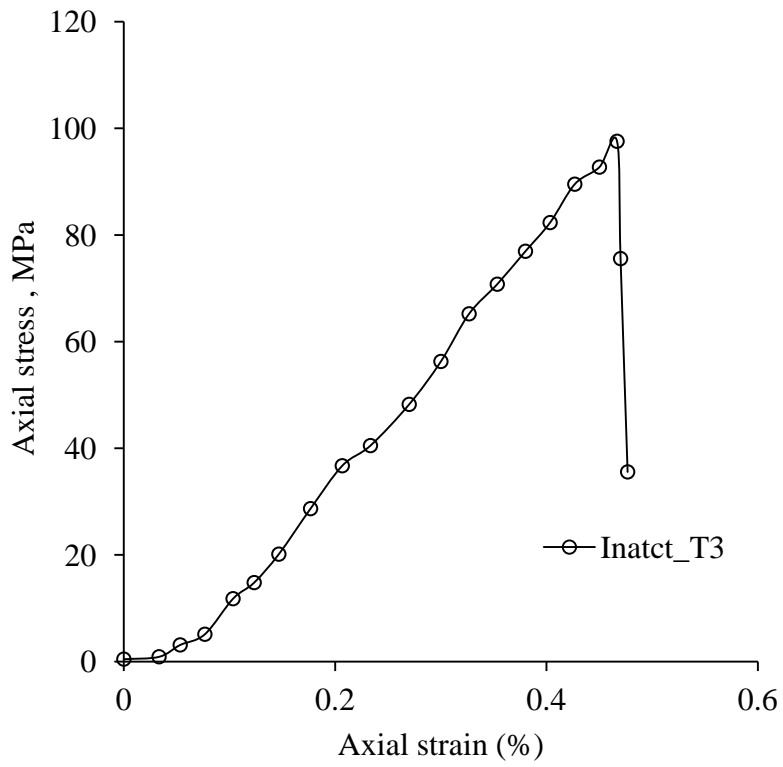
Fig.4.12d Axial stress vs axial strain plot of intact (prismatic) synthetic rock (T3)

Observations

Peak stress	97.56 MPa
Axial strain at failure	0.467 %
Mode of failure	Splitting
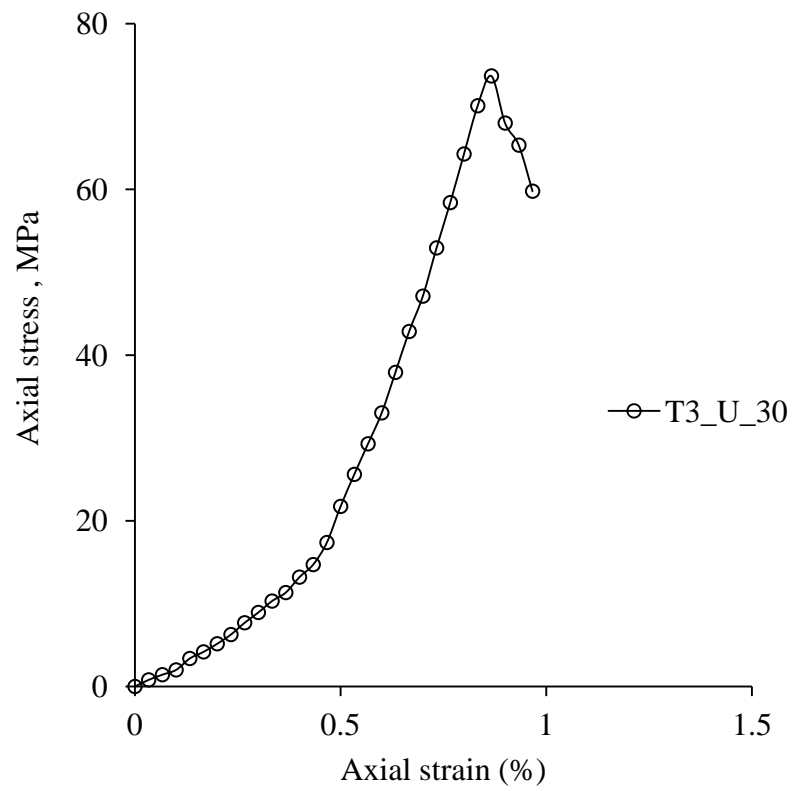
Fig.4.12e Axial stress vs axial strain plot of unreinforced jointed synthetic rock (T3) at $\theta = 30°$

Observations

Peak stress	73.69 MPa
Axial strain at failure	0.867 %
Mode of failure	Splitting
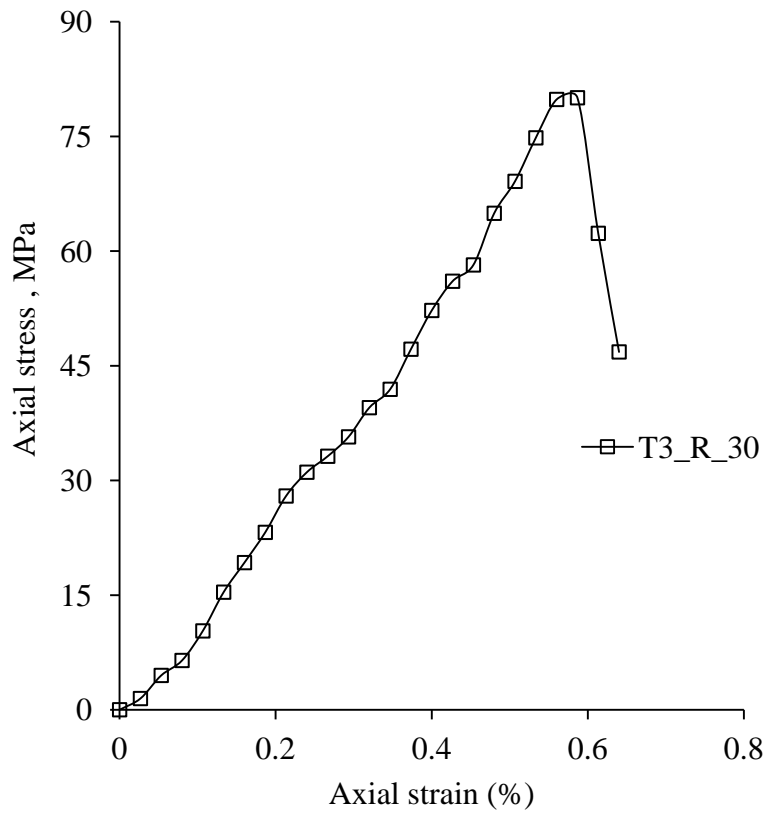
Fig.4.12f Axial stress vs axial strain plot of reinforced jointed synthetic rock (T3) at $\theta = 30°$

Observations

Peak stress	80.04 MPa
Axial strain at failure	0.587 %
Mode of failure	Splitting
Deformation in bolt	No

4.5.3 Discussion on observations taken during tests

4.5.3.1 Failure modes observed for intact, unreinforced and reinforced jointed specimens

The failure modes observed in case of synthetic rocks both T2 and T3 are listed in Table 4.6. Intact specimens of synthetic rocks (both T2 and T3) fail in brittle manner and vertical splitting was observed in the specimens (Fig 4.13). Majority of the unreinforced and reinforced jointed specimens of synthetic rocks failed due to splitting. Photographs of some failed unreinforced and reinforced jointed specimens are shown in Figs 4.14 and 4.15 respectively. The unreinforced jointed rock specimens exhibit splitting and sliding mode of failure while in case of reinforced specimens only splitting mode of failure was observed. At $\theta = 45°$ and 60° specimens of unreinforced jointed synthetic rocks (both T2 and T3) exhibit sliding mode of failure. At $\theta = 0°$, 15°, 30°, 75° and 90° the splitting failure mode was observed in unreinforced specimens.

Table 4.6 Failure modes observed in synthetic rocks

$\theta°$	Failure modes observed			
	T2		T3	
	U	R	U	R
Intact	SP	-	SP	-
0	SP	-	SP	-
15	SP	SP	SP	SP
30	SP	SP	SP	SP
45	SL	SP	SL	SP
60	SL	SP	SL	SP
75	SP	SP	SP	SP
90	SP	SP	SP	SP

U = unreinforced specimens; R = reinforced specimen; SP = Splitting; SL = Sliding

(a) Synthetic rock T2

(b) Synthetic rock T3

Fig.4.13 Failure in intact block due to vertical splitting

(a) $\theta = 0^\bullet$

(b) $\theta = 45^\bullet$

Fig.4.14 Failure in specimens of syntactic unreinforced jointed rock

(c) $\theta = 75^{\bullet}$

(d) $\theta = 90°$

Fig.4.14 Failure in specimens of syntactic unreinforced jointed rock

Fig.4.15 Failure in specimens of syntactic reinforced jointed rock

Reinforced jointed specimens of synthetic rocks both (T2 and T3) exhibit only splitting mode of failure at all joint orientations (θ =15° to 90°). At θ =45° and 60°, the installation of bolts altered the sliding failure mode of unreinforced specimens into splitting mode. Only at theses orientations, deformation in bolts was observed. Provision of bolts improves the interlocking in the joint and converts the jointed rock into a single stiffer body. For unreinforced jointed specimens, the cracks initiated from locations near joint surface, whereas in case of reinforced specimens, the cracks initiated from the locations where bolts were placed.

4.5.3.2 Strength and deformational behaviour

Comparison of axial stress vs axial strain plots of intact (prismatic), unreinforced (θ =30°) and reinforced (θ =30°) jointed specimens of synthetic rocks (both T2 and T3) is presented in Fig.4.16. Provision of reinforcement alters the stress vs strain behaviour of unreinforced jointed rock. The axial stress vs axial strain plot of reinforced rock lies between the axial stress vs axial strain plots of intact and unreinforced jointed rock for both types of synthetic rocks.
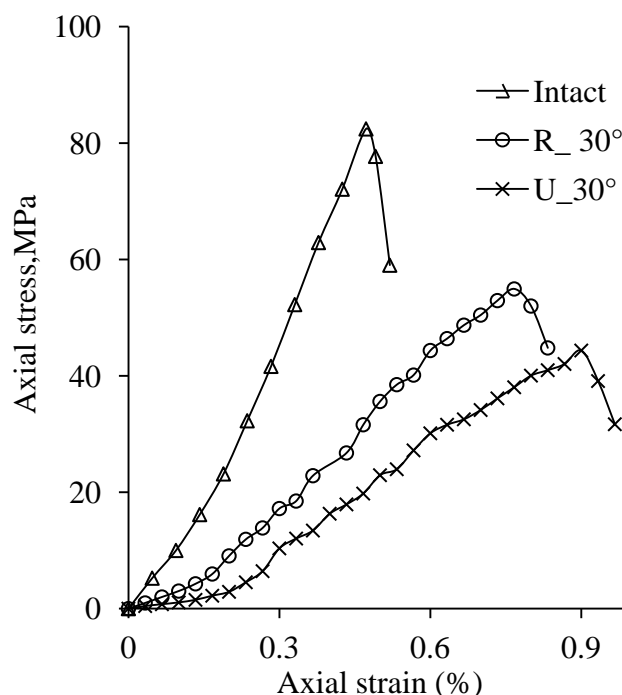
Fig.4.16a Comparisons of axial stress vs axial strain plots of intact, unreinforced and reinforced specimens of synthetic rock T2

140
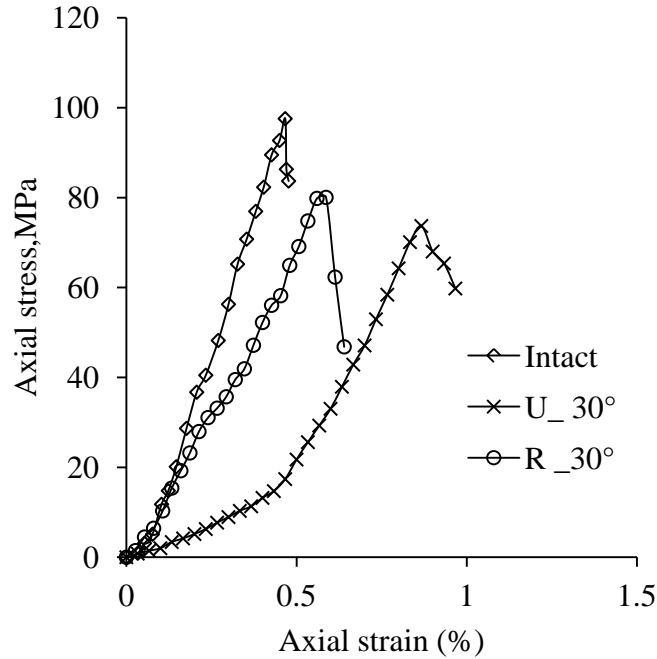
Fig.4.16b Comparisons of axial stress vs axial strain plots of intact, unreinforced and reinforced specimens of synthetic rock T3

The values of uniaxial compressive strength (σ_c) and tangent modulus (E_{t50}) of intact (prismatic), unreinforced and rock bolt-reinforced synthetic rock are presented in Table 4.7a. It is observed that for both type of synthetic rocks the strength and tangent modulus values of reinforced rock lie between the strength and tangent modulus of unreinforced rock and intact rock. The strength and modulus of reinforced rock is less than that for intact rock but more than that for unreinforced rock. The installation of bolts enhances the strength as well as modulus of unreinforced jointed rock due to interlocking produced by the bolts. Due to increased interlocking, the failure mode also gets altered. The sliding mode has been completely eliminated due to installation of bolts. Development of tensile stress in bolts induces additional normal stress on the joint surface, which enhances the engineering properties.

For unreinforced specimens, maximum strength is observed at $\theta = 0°$. As θ increases, the strength reduces and almost nil values are obtained at $\theta = 45°$ and 60°. Further increase in θ increases the strength upto $\theta = 90°$. In case of reinforced specimens, the strength decreases as the joint orientation increases from $\theta = 15°$ and becomes minimum at $\theta = 60°$. After $\theta = 60°$, the strength increases with θ.

For both T2 and T3 type of synthetic rocks, the modulus of unreinforced is maximum at $\theta = 0°$. As θ is varied, similar to strength behaviour almost nil values are obtained at $\theta = 45°$ and $60°$. The orientations $\theta = 45°$ and $60°$ are termed as critical orientations as they possess minimum value of strength and modulus as compared to other orientations. Provision of bolt improved the modulus of reinforced rock at all joint orientations. The modulus of reinforced rock is found to be minimum for critical orientations ($\theta = 45°$ and $60°$).

Table 4.7a Values of uniaxial compressive strength and modulus of deformation for T2 and T3 types of specimens

$\theta°$	T2		T3		T2		T3	
	σ_c , MPa		σ_c , MPa		E_{t50}, GPa		E_{t50}, GPa	
Intact	73.13		97.16		17.22		23.33	
0	59.82		86.00		13.63		20.0	
	U	R	U	R	U	R	U	R
15	52.62	55.02	74.76	75.64	8.88	10.50	13.00	13.68
30	44.36	54.93	73.69	80.04	5.88	8.62	16.00	17.77
45	0.19	9.57	0.13	12.57	0.025	1.23	0.1	3.80
60	0.10	4.97	0.18	10.31	0.008	0.35	0.05	1.70
75	40.93	43.14	67.11	70.00	7.5	13.47	13.95	18.42
90	45.96	50.40	77.96	79.82	6.15	6.81	15.70	16.00

The values of axial strain at failure (ε) obtained for intact (prismatic), unreinforced and reinforced synthetic rocks are presented in Table 4.7b. In general, provision of bolts reduces the failure strain of jointed synthetic rocks (both T2 and T3) except $\theta = 60°$. At $\theta = 60°$ the failure stain of reinforced specimen is found to be greater than the unreinforced specimens for both type of synthetic rocks. No good trend of variation of failure strain with joint orientation has been observed.

Table 4.7b Axial strain at failure (ε ,%)

θ°	T2		T3	
	σ_c , MPa		σ_c , MPa	
Intact	0.583		0.467	
0	0.867		0.650	
	U	R	U	R
15	0.70	0.633	0.800	0.680
30	0.90	0.767	0.867	0.587
45	1.093	1.073	1.197	0.60
60	1.087	1.550	0.680	0.90
75	0.867	0.60	0.667	0.60
90	1.067	0.90	0.767	0.70

4.6 TRIAXIAL COMPRESSION TESTS ON NATURALLY JOINTED ROCK

Triaxial compression tests were conducted on NX size specimens of jointed natural rock specimens without and with reinforcement. The triaxial tests were conducted at confining pressure of 0, 5, 20 and 40 MPa respectively. The joint orientation in the specimens was varied from 0° to 90°. The details of results obtained are summarized below.

4.6.1 Intact Rock Properties

Rock specimens were tested in the laboratory to find out the physical and engineering properties of the intact rock. The triaxial tests were performed at confining pressure of 0, 5, 20 and 40 MPa respectively. In general, the intact rock specimens failed in brittle manner, however some sign of ductility appeared in failure at 40 MPa. Vertical splitting has been observed in most of the cases investigated in this study (Fig.4.17). The axial stress (deviator) vs axial stress curves at different confining pressures are presented in Fig.4.18. The Mohr circles at failure for intact rock are presented in Fig.4.19. The values of shear strength parameters (c and ϕ) were obtained through best fitting linear equation. The engineering properties of the intact rock are listed in Table 4.8. On the Deere–Miller classification chart (Fig.4.20), the intact rock is classified as CL i.e. rock having medium strength and low modulus ratio.

Fig.4.17a Failure of intact rock under uniaxial compression

Fig.4.17b Failure of intact rock under triaxial compression
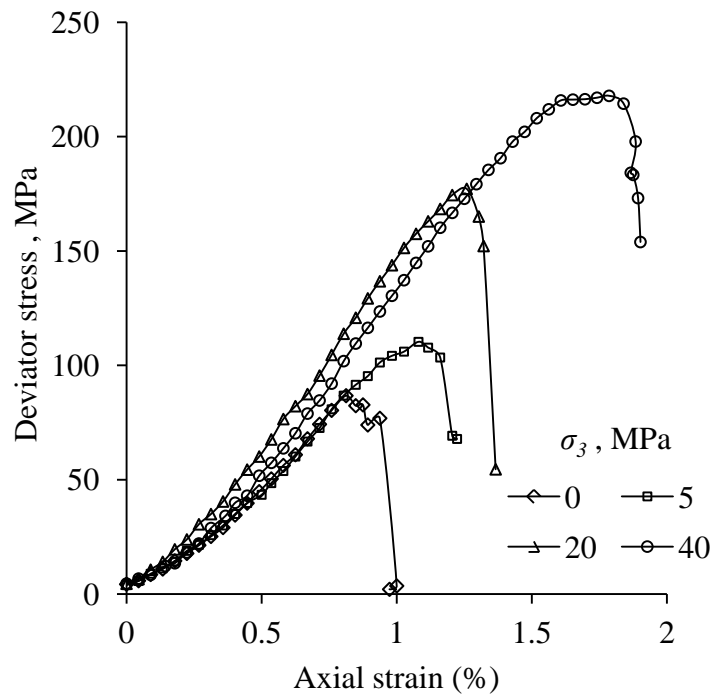
Fig.4.18 Deviator stress vs axial strain plots of intact rock at different confining stress levels

Observations

σ_3 , MPa	Peak stress (deviator) σ_d, MPa	Axial strain at failure (ϵ, %)	Failure mode
0.0	86.76	0.813	Splitting
5.0	110.31	1.08	Splitting
20.0	177.19	1.259	Splitting + Shearing
40.0	217.86	1.786	Splitting
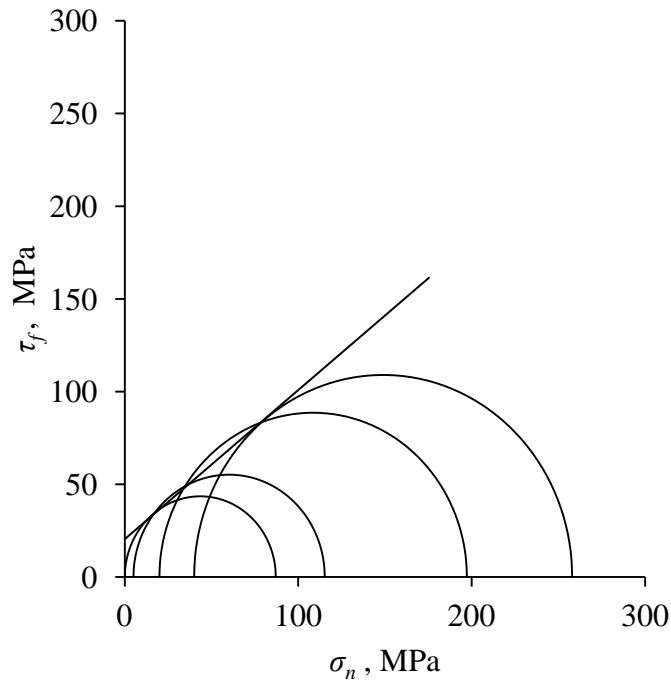
Fig.4.19 Mohr circles at failure for intact rock

Table 4.8 Engineering properties of intact rock

Property	Symbol	Value
Unit weight (KN/m^3)	γ	27
Uniaxial compressive strength, MPa	σ_{ci}	87
Tensile strength, MPa	σ_t	4.3
Tangent modulus, MPa	E_{t50}	12000
Cohesion, MPa	c_i	24
Friction angle, $\phi°$	ϕ_i	37
Deere Millar (1966) classification	-	CL

146
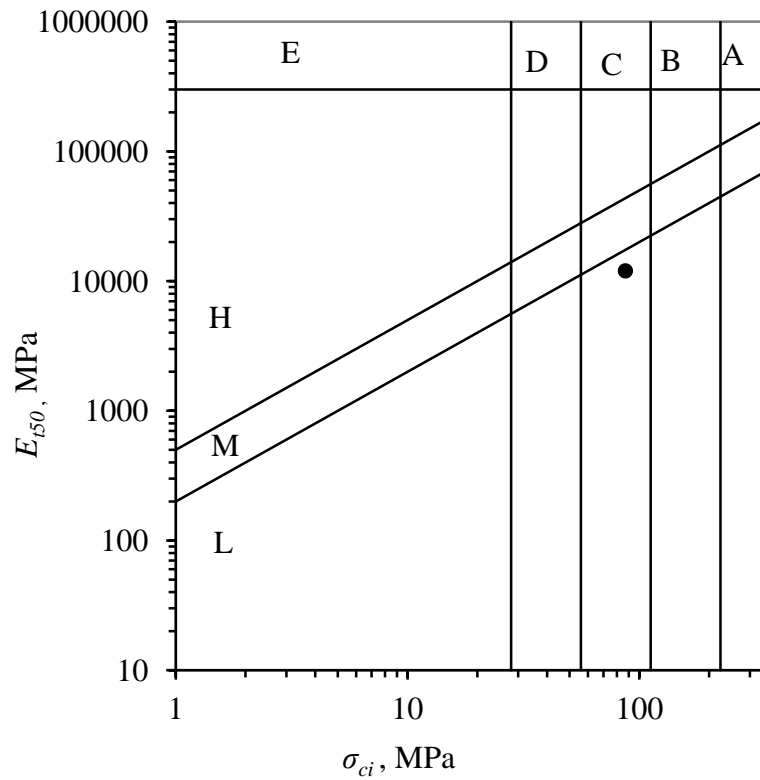
Fig. 4.20 Intact rock classification on Deere–Miller classification chart

4.6.2 Observations Taken During Testing of Jointed Rock Specimens

The photographs of some failed specimens of jointed rocks (both unreinforced and reinforced) are presented in Figs. 4.21. The details of observation taken during the testing of unreinforced and reinforced jointed rocks with axial stress vs axial strain plots at different normal stress levels are presented in Appendix II. Some of these are presented in Fig.4.22.
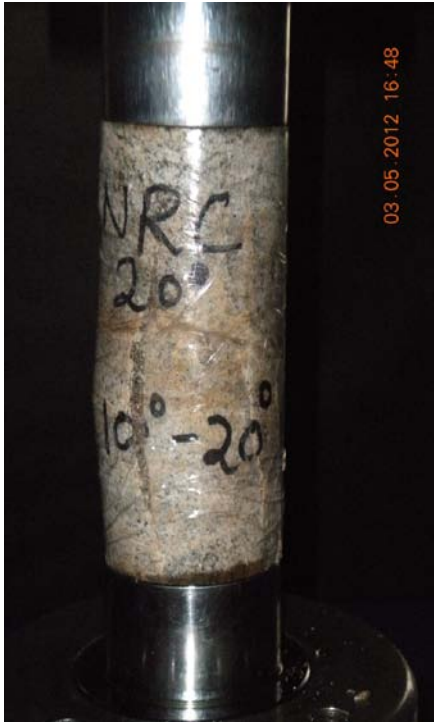
Fig. 4.21a Failure of unreinforced jointed rock under uniaxial compression

Fig.4.21b Failure of Reinforced jointed rock under uniaxial compression

Fig.4.21c Failure of jointed unreinforced rock under triaxial compression

Fig.4.21d Failure of jointed reinforced rock under triaxial compression

Fig.4.21e Failure of jointed reinforced rock under triaxial compression
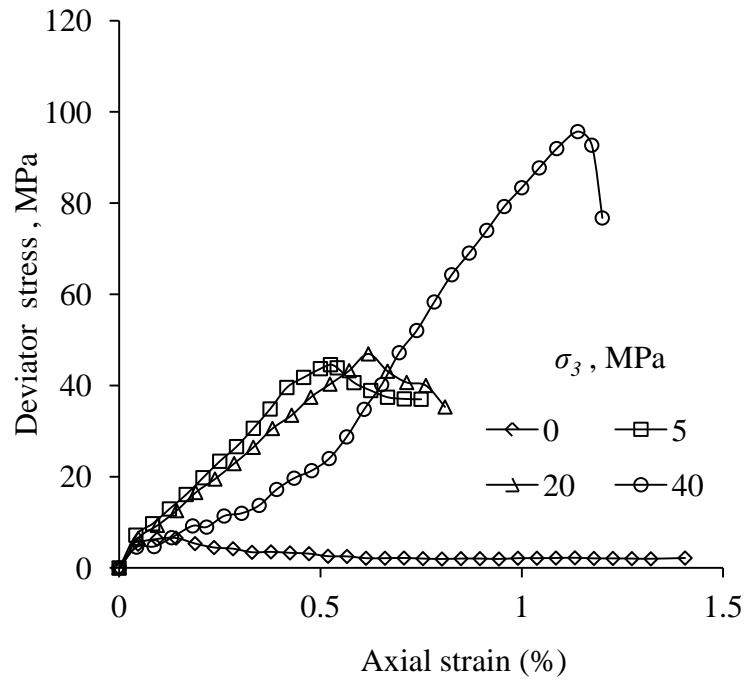
Fig.4.22a Deviator stress vs axial strain plots of unreinforced jointed rock (θ = 30°-40°) at different confining stress levels

Observations

σ_3 , MPa	σ_d, MPa	ϵ, %	Failure mode
0.0	6.55	0.094	Sliding
5.0	44.58	0.525	Splitting + Shearing
20.0	46.94	0.619	Splitting
40.0	95.69	1.139	Splitting
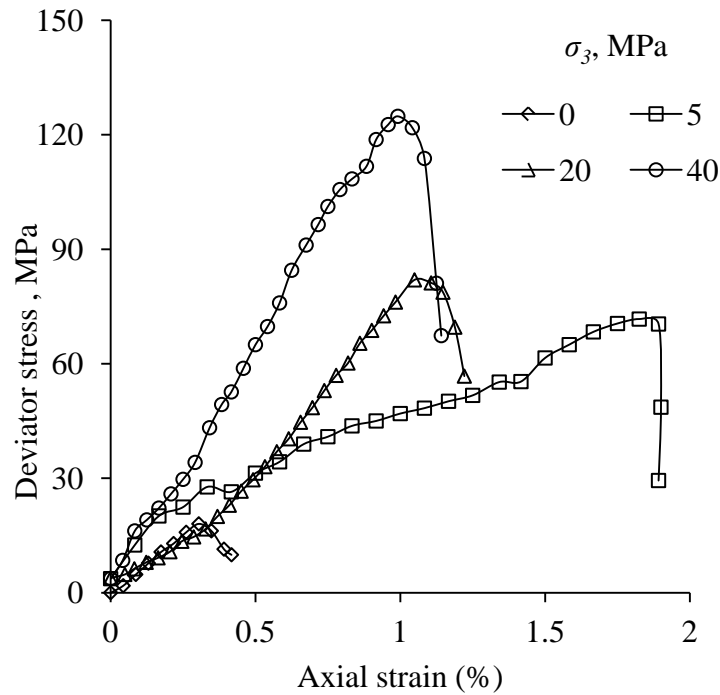
Fig.4.22b Deviator stress vs axial strain plots of reinforced jointed rock ($\theta = 30°$-40°) at different confining stress levels

Observations

σ_3 , MPa	σ_d, MPa	ϵ, %	Failure mode	Deformation in bolt
0.0	18.05	0.841	Splitting	Slight
5.0	71.70	1.825	Splitting	Slight
20.0	81.97	1.049	Splitting	Slight
40.0	124.83	0.992	Splitting	Slight

152

4.6.3 Discussion on the Observations Taken During the Tests

4.6.3.1 Failure modes observed

The summery of failure modes observed in case of unreinforced and reinforced jointed rocks is presented in Table 4.9. In case of unreinforced jointed specimens, sliding, shearing, and splitting or combination of these modes of failure were observed depending upon joint orientation. Reinforced jointed rocks exhibit splitting, shearing or combination of these two modes of failure. In most of the cases, the splitting mode of failure was dominant.

In unconfined condition ($\sigma_3 = 0$ MPa), unreinforced specimens failed due to sliding for joint orientation in the range of $\theta = 30°$ to $80°$. For unreinforced specimens having $\theta = 0°$ to $30°$ and $\theta = 80°$ to $90°$, splitting mode of failure was observed. Installation of bolt alters the sliding mode of failure at orientation between $\theta = 30°$ to $80°$. The restriction imposed by the bolt on relative displacement enhances interlocking and alters sliding modes into shearing and splitting modes of failure. For orientations $\theta < 30°$ and $\theta > 80°$, reinforced specimens exhibited splitting or combination of splitting and shearing modes of failure.

In triaxial condition ($\sigma_3 = 5$, 20 and 40 MPa), unreinforced jointed specimens exhibited splitting failure mode combined with shearing mode of failure or sliding mode of failure. In case of reinforced jointed specimens, splitting or splitting plus shearing mode of failure was observed. Not good trend of failure mode with joint orientation or confining pressure were observed.

4.6.3.2 Strength and deformation behaviour of unreinforced and reinforced specimens

Comparison of axial stress (deviator) vs axial strain plots of intact, unreinforced, and reinforced jointed rocks at all the confining stress levels are presented in Fig.4.23

Table 4.9 Failure modes observed at different confining stress levels

$\theta°$	Failure mode observed							
	σ_3 = 0 MPa		σ_3 = 5 MPa		σ_3 = 20 MPa		σ_3 = 40 MPa	
	U	R	U	R	U	R	U	R
Intact	SP		SP		SP		SP+SH	
0-10	SP	-	SP	-	SP	-	SP+SH	-
10-20	SP	-	SP	-	SP	-	SP+SH	-
20-30	SP	SP	SP	-	SP+SH	-	SP	-
30-40	SL	SP	SP+SH	SP	SP	SP	SP	SP
40-50	SL	SP+SH	SP+SH	SP	SP	SP+SH	SP+SH	SP+SH
50-60	SL	SP	SP+SH	SP	SL+SP	SP+SH	SP	SP+SH
60-70	SL	SP+SH	SL+SP	SP+SH	SL+SP	SP	SP+SH	SP+SH
70-80	SL	SP	-	-	-	-	-	-
80-90	SP	SP	-	-	-	-	-	-

SP = Splitting, SH = Shearing, SL= Sliding.
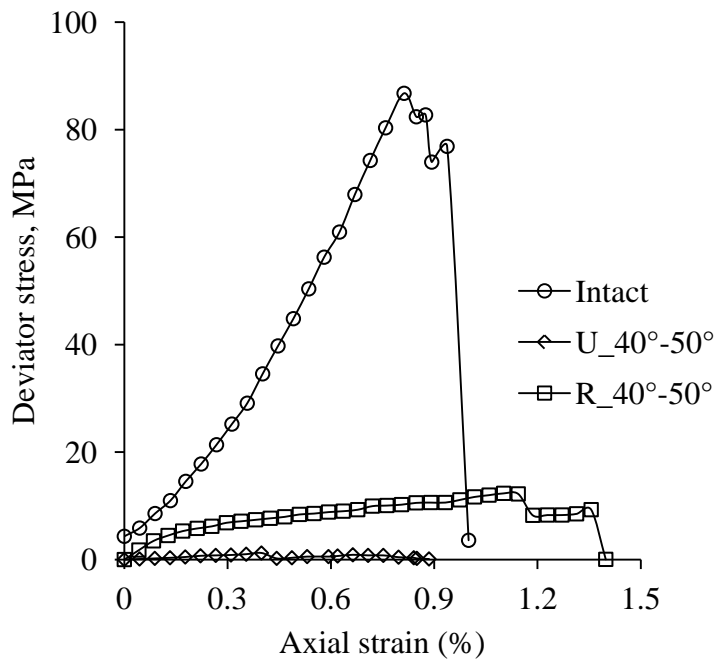
Fig.4.23a Comparisons of axial stress (deviator) vs axial strain plots of intact, unreinforced and reinforced jointed rocks at σ_3 = 0 MPa
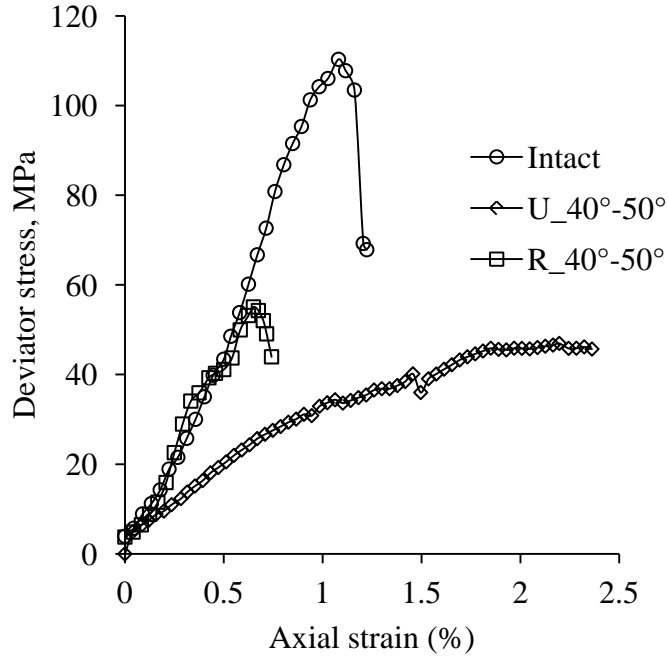
Fig.4.23b Comparisons of axial stress (deviator) vs axial strain plots of intact, unreinforced and reinforced jointed rocks at σ_3 = 5 MPa
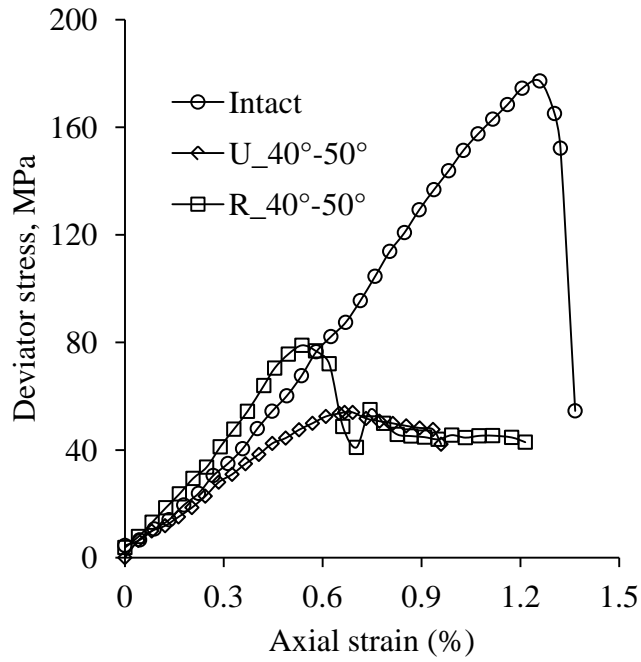
Fig.4.23c Comparisons of axial stress (deviator) vs axial strain plots of intact, unreinforced and reinforced jointed rocks at σ_3 = 20 MPa
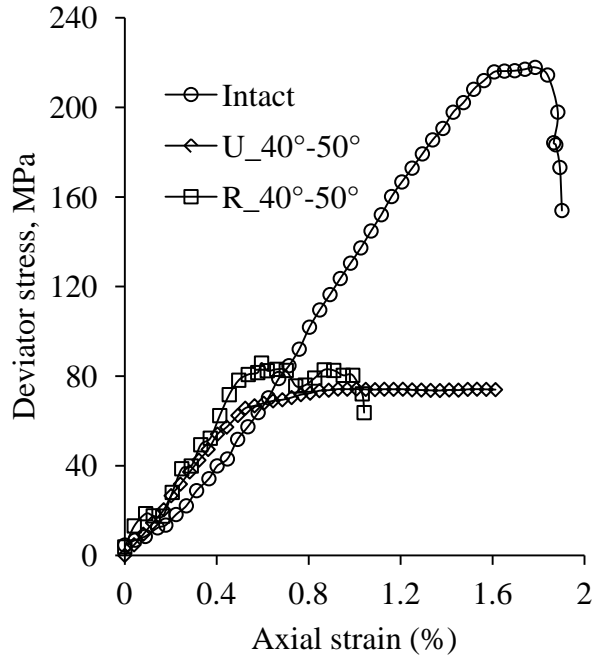
Fig.4.23d Comparisons of axial stress (deviator) vs axial strain plots of intact, unreinforced and reinforced jointed rocks at σ_3 = 40 MPa

Values of failure stress (σ_1) and axial strain (ε) at failure for all confining stress levels are listed in Table 4.10. The strength of reinforced jointed rock lies between the strengths of intact and unreinforced jointed rock. The results indicate that the strength of jointed unreinforced rock has been enhanced due to provision of bolt. Increase in confining stress, results in an increase in the strength. For $\theta = 0°$-$10°$, the strength of unreinforced jointed rock is found to be maximum, an increase in joint orientation results in general decrease in strength. For reinforced specimens similar trend was observed.

The values of tangent modulus (E_{t50}) obtained at 50% stress level (only for σ_3 = 0 case) are reported in Table 4.11. Similar to strength the modulus value of unreinforced jointed rock enhanced due to installation of bolts. The modulus of reinforced jointed rock lies between the modulus of intact and unreinforced jointed rock.

Table 4.10a Values of σ_1 at different confining pressure

$\theta°$	σ_3, MPa							
	$\sigma_3 = 0$ MPa		$\sigma_3 = 5$ MPa		$\sigma_3 = 20$ MPa		$\sigma_3 = 40$ MPa	
	U	R	U	R	U	R	U	R
Intact	87	-	115.31	-	197.19	-	257.86	-
0-10	44.69	-	111.52	-	173.29	-	196.18	-
10-20.	47.01	-	107.05	-	151.71	-	184.96	-
20-30	32.02	34.47	59.05	-	85.55	-	129.12	-
30-40	6.55	18.05	49.58	76.7	66.94	101.97	135.69	164.83
40-50	1.22	12.32	51.94	60.08	73.98	98.92	114.24	125.84
50-60	1.08	5.97	25.67	52.49	48.66	86.63	66.68	102.38
60-70	1.03	7.78	19.81	41.76	45.87	68.34	70.18	90.62
70-80	0.56	46.05	-	-	-	-	-	-
80-90	21.52	23.69	-	-	-	-	-	-

Table 4.10b Values of axial strain (ε %) at failure for different confining pressure

$\theta°$	Axial stain (%)							
	$\sigma_3 = 0$ MPa		$\sigma_3 = 5$ MPa		$\sigma_3 = 20$ MPa		$\sigma_3 = 40$ MPa	
	U	R	U	R	U	R	U	R
Intact	0.813		1.08		1.259		1.786	
0-10	1.043	-	1.042	-	1.120	-	1.318	-
10-20	1.149	-	0.906	-	1.061	-	1.114	-
20-30	0.883	0.841	0.585	-	1.545	-	0.927	-
30-40	0.094	0.841	0.525	1.825	0.619	1.049	1.139	0.992
40-50	0.398	1.102	2.197	0.65	0.667	0.537	1.008	0.595
50-60	1.770	0.250	0.216	0.727	2.328	0.826	2.328	0.826
60-70	1.709	0.603	1.090	0.992	5.379	1.215	2.974	1.529
70-80	1.917	0.768	-	-	-	-	-	-
80-90	0.383	0.455	-	-	-	-	-	-

Table 4.11 Values of E_{t50} for unreinforced (U) and reinforced (R) specimens of jointed rock

$\theta°$	E_{t50} , MPa	
	U	R
0-10	4920	-
10-20	5593	-
20-30	3798	4827
30-40	905	4487
40-50	322	744
50-60	-	1633
60-70	-	503
70-80	-	5770
80-90	4367	4382

4.7 CONCLUDING REMARKS

The results of physical model tests conducted on blocky mass/jointed rock have been summarized in this chapter. The chapter comprises of three different sections; first, large sized direct shear tests on the specimens of blocky masses, second, uniaxial compression tests on two different type of synthetic rock specimens and third triaxial tests on natural jointed rocks. The summery of observations are listed below.

A. Direct shear testing of blocky mass

i.   Sliding of blocks was observed in case of unreinforced blocky mass at all the normal stress levels. Provision of bolts restricted the sliding in the blocky mass and makes the mass stronger and stiffer.

ii. Bolts improve the interlocking of the joint in the mass and development of tensile stress in the bolt imposes additional normal stress on the joint surface in the blocky mass.

iii. In general, the shear stress increases with increasing shear displacement and exhibits a clearly defined peak in the majority of cases, except for unreinforced mass tested at low normal stresses (0 and 0.5 MPa).

iv. In case of reinforced blocky mass, the shear stress vs the horizontal shear displacement curves exhibit two distinct segments. The first part of the curve is relatively flat which indicates the mobilization of shear stress due to the interaction of the blocks. Interaction between blocks gives rise to the development of tensile stress in the bolts at the end of this segment. The second part of the curve is steep which indicates the mobilization of shear stress through the bolts.

v. At all the normal stress level, provision of bolts ehances the shear stregth of blocky mass. The incrsese in number of bolts increses the shear stregth of blocky mass. In all the cases, increase in the normal stress increases the peak shear stress at failure (shear strength).

vi. The horizontal shear displacement at peak stress becomes minimum when five bolts are used.

vii. For low normal stress levels (0 and 0.5 MPa), the maximum vertical displacement at peak shear stress was observed for specimens when nine bolts are used. At higher normal stress levels (1 to 2 MPa), unreinforced specimens showed higher vertical displacement compared to reinforced specimens.

B. Uniaxial compression tests on synthetic rocks

i. Unreinforced jointed rock specimens exhibit splitting/sliding mode of failure and reinforced jointed specimens exhibit only splitting mode of failure. In the majority of the cases, unreinforced and reinforced jointed specimens of synthetic rocks failed due to splitting. Sliding failure was observed in unreinforced jointed synthetic rocks (both T2 and T3) at $\theta = 45°$ and $60°$. The sliding mode of failure was eliminated due to installation of bolts. Intact specimens of synthetic rocks fail in brittle manner and vertical splitting was observed in the specimens.

ii. Provision of bolts improve the interlocking in the joint and converts the jointed rock into a single stiffer body. Development of tensile strength in the bolt imposes additional normal stress on jointed specimens.

iii. Reinforcement alters the stress vs strain behaviour of unreinforced jointed rock. The axial stress vs axial strain plot of reinforced rock lies between the axial stress vs axial strain plots of intact and unreinforced jointed rock for both types of synthetic rocks.

iv. The values of uniaxial compressive strength (σ_c) as well as tangent modulus (E_{t50}) of jointed synthetic rock enhanced due to provision of bolts. The strength and modulus of reinforced rock is less than that for intact rock but more than that for unreinforced rock. The orientations $\theta = 45°$ and $60°$ are termed as critically oriented joints because they possess minimum value of strength and modulus as compared to other orientations.

v. Provision of bolts reduces the failure strain of jointed synthetic rocks (both T2 and T3) except $\theta = 60°$.

C. Triaxial compression tests on natural rocks

i. Provision of bolt changes the failure modes of unreinforced jointed rock. Unreinforced specimens of natural rock exhibit splitting, sliding, shearing or combination of these modes while reinforced rock exhibit splitting and shearing or combination of these modes at all the confining stress levels. The failure modes observed depend on the joint orientation; and in the most of the cases, the splitting was dominant mode of failure.

ii. The bolt improves the interlocking in the jointed natural rocks. Development of tensile strength in the bolt imposes additional normal stress on jointed specimens of natural rock.

iii. The results indicate that the strength of jointed unreinforced rock is enhanced due to provision of bolt. Increase in confining stress, increases the strength for both unreinforced and reinforced jointed rocks. The strength of reinforced jointed rock lies between the strengths of intact and unreinforced jointed rock.

<div align="right">

Chapter 5

</div>

SHEAR STRENGTH BEHAVIOUR OF BLOCKY MASS

5.1 GENERAL

The results of large direct shear tests conducted on unreinforced and reinforced blocky mass specimens have been discussed in the previous chapter. Tests were conducted on the blocky mass specimens of size 750 mm x 750 mm x 900 mm at normal stress of 0, 0.5, 1.0, and 2.0 MPa respectively. Passive rock bolts were used to reinforce the mass. The outcome of this part is applicable in designing rock bolt reinforcement in situations like rock slopes where analysis is done σ, τ space and passive bolts are used. The results obtained from large direct shear tests have been analysed, summarized, and presented in this chapter.

5.2 FACTORS INFLUENCING THE BEHAVIOUR OF BLOCKY MASS

Results indicated that the shear strength of blocky mass has been enhanced by provision of bolts and is influenced by various factors i.e. normal stress, amount of reinforcement, spacing between joints and spacing between bolts.

5.2.1 Normal Stress

Normal stress is a factor significantly affecting the shear strength of the blocky mass. The shear stress (τ) vs horizontal shear displacement (δ_H) plots for different configurations of blocky mass at different normal stress levels are presented in Fig.5.1a, 5.1b, 5.1c and 5.1d respectively. The plots indicate that an increase in normal stress results in increase in shear strength for each configuration of the blocky mass. Increase in normal stress consolidates the joints and develops high frictional resistance in the joints of the blocky mass. Due to development of resistance in the joints, the peak shear stress enhances with an increase in the normal stress. This trend is observed for both unreinforced and reinforced blocky mass.
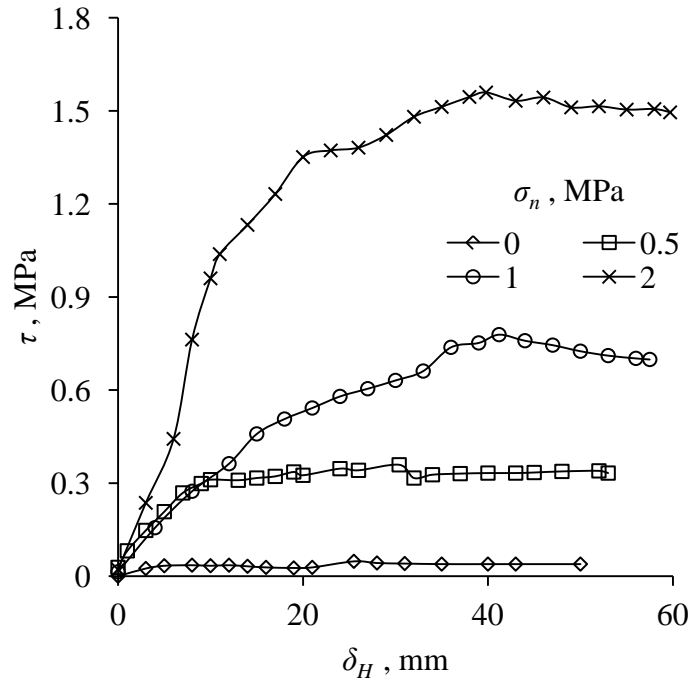
(a) Unreinforced mass (U)
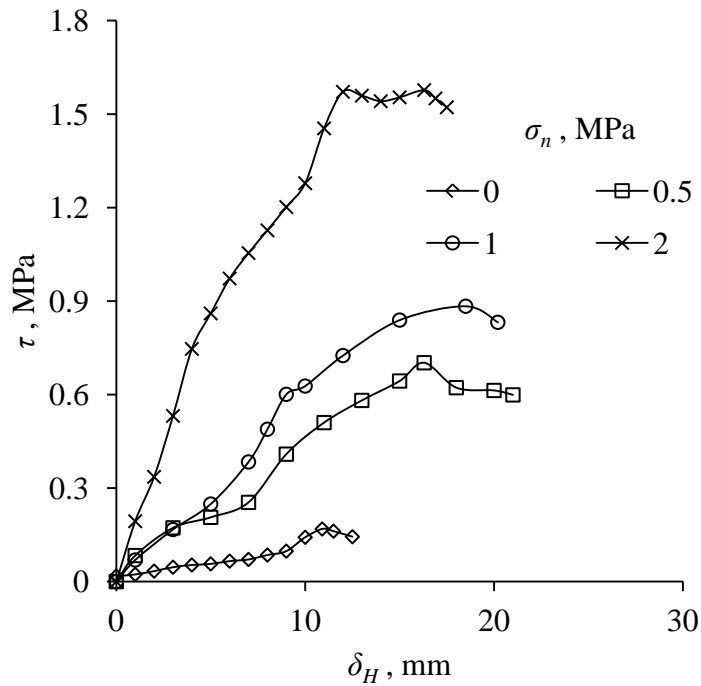
(b) Reinforced mass with 3 rock bolts (R3)

Fig.5.1 Shear stress (τ) vs horizontal shear displacement (δ_H) plots for different configurations of bolts at different normal stress levels
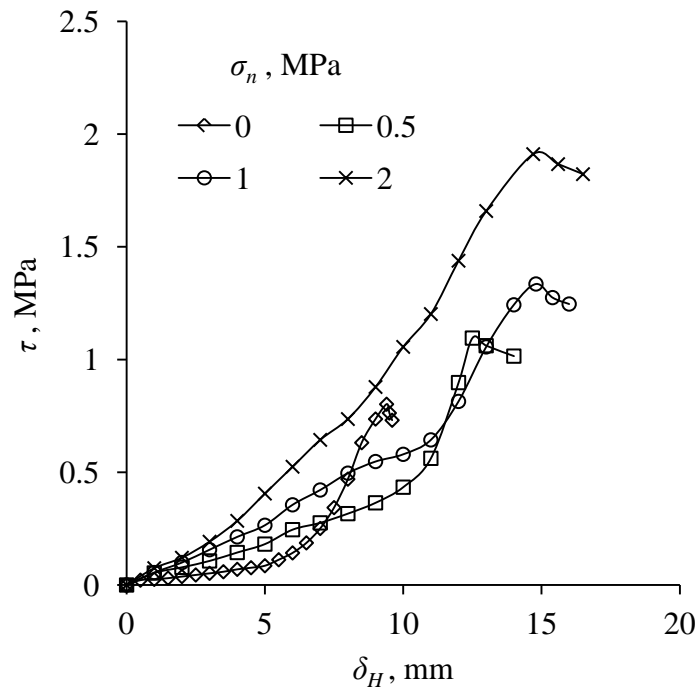
(c) Reinforced mass with 5 rock bolts (R5)
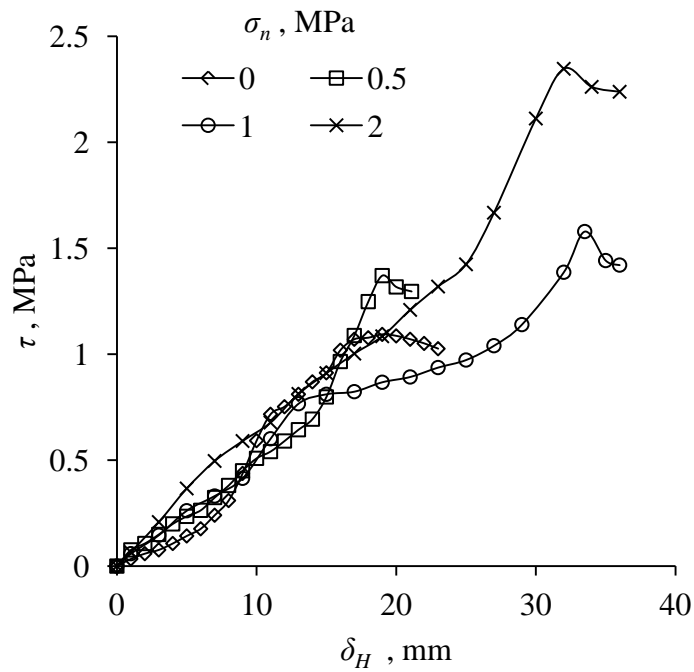
(d) Reinforced mass with 9 rock bolts (R9)

Fig.5.1 Shear stress (τ) vs horizontal shear displacement (δ_H) plots for different configurations of bolts at different normal stress levels

5.2.2 Amount of Reinforcement

The amount of reinforcement plays an important role in strengthening the rock mass. In reinforced mass, the tension developed in the bolts during shearing process induces additional normal stress on the joint surfaces. The induced additional normal stress on the shearing surface due to tension in the bolts will be directly proportional to the cross sectional area of the steel. The passive resistance offered by steel will also have a direct relationship with this area. The reinforcement amount is represented by the term percent area ratio, A_r given by

$$A_r = \frac{A_b}{A} \times 100 \ \% \tag{5.1}$$

where A_b= total cross section area of bolts, and A = area of mass on shearing plane. A_b depends on the number of bolts across the shearing plane and the diameter of the bolts.

5.2.3 Geometry of Blocky Mass and Configuration of Bolt Pattern

Relative values of block size and bolt spacing are important in governing engineering behaviour of reinforced blocky mass. These parameters have been incorporated through an equivalent block size (D_b) and equivalent spacing between bolts (S_b). Hoek (2007) suggested that, in order to develop an effective zone of compression between the bolts, the spacing of bolts should be less than three times of the average block size in the mass. If the block size is smaller and bolt spacing is large, the enhancement will be low. Whereas if the block size is large and bolts spacing is relatively small, the enhancement is expected to be high. To account for the importance of the relative dimensions of block and bolt spacing, a dimensionless number N (Spacing ratio) is defined as:

$$N = \frac{S_b}{D_b} \tag{5.2}$$

where $\quad S_b = equivalent \ bolt \ spacing = \sqrt{\dfrac{Area \ of \ shearing \ plane}{numbers \ of \ bolts}}$

$D_b = equivalent \ blcok \ size = \sqrt[3]{volume \ of \ representative \ block}$

The area of the shearing plane in present case is 562500 mm^2 and volume of representative block is 3375000 mm^3. The calculated values of A_r and N are given in Table 5.1.

Table 5.1 Calculated values of A_r and N

Case/Configuration	No of bolts	Ar (%)	S_b , mm	D_b , mm	N
U	0	0	0	150	-
R3	3	0.015	433	150	2.89
R5	5	0.025	335	150	2.24
R9	9	0.045	250	150	1.67

The shear strength (peak shear stress at failure, τ_{peak}) for each configuration of blocky mass is presented in Table 5.2. The variations of shear strength with normal stress, amount of reinforcement (A_r) and spacing ratio (N) are presented in Figs. 5.2a, 5.2b, and 5.2c respectively. Shear strength of blocky mass increases with the normal stress. In case of reinforced mass, increase in amount of reinforcement enhances the shear strength of blocky mass at all normal stress levels (Fig.5.3b). However, increase in spacing ratio (N) decreases the shear strength (Fig.5.3c). The shear strength enhancement due to provision of bolts occurs due to following reasons

i.   Increase in normal stress consolidates the joints in mass.

ii. Reinforcement restricts the sliding in blocky mass and induces additional normal stress on the joint surface due to development of tension in the bolts. This induced additional normal stress increases the applied normal stress (σ_n) which results in enhancement in strength.

iii. Increase in amount of reinforcement (A_r) and reduction in spacing ratio (N) develops a complex interaction between the bolts and blocks of mass. Due to development of this interaction the reinforced mass is well stitched and acts as a stiffer rigid body against the external forces.

Table 5.2 Shear stress at failure at different normal stress levels

σ_n , MPa	Shear stress at failure, MPa			
	U	R3	R5	R9
	$Ar = 0.0\%$	$Ar = 0.015\%$	$Ar = 0.025\%$	$Ar = 0.045\%$
	$N = -$	$N = 2.89$	$N = 2.24$	$N = 1.67$
0.0	0.048	0.169	0.802	1.093
0.5	0.359	0.702	1.095	1.371
1.0	0.779	0.884	1.335	1.579
2.0	1.559	1.577	1.911	2.347

.
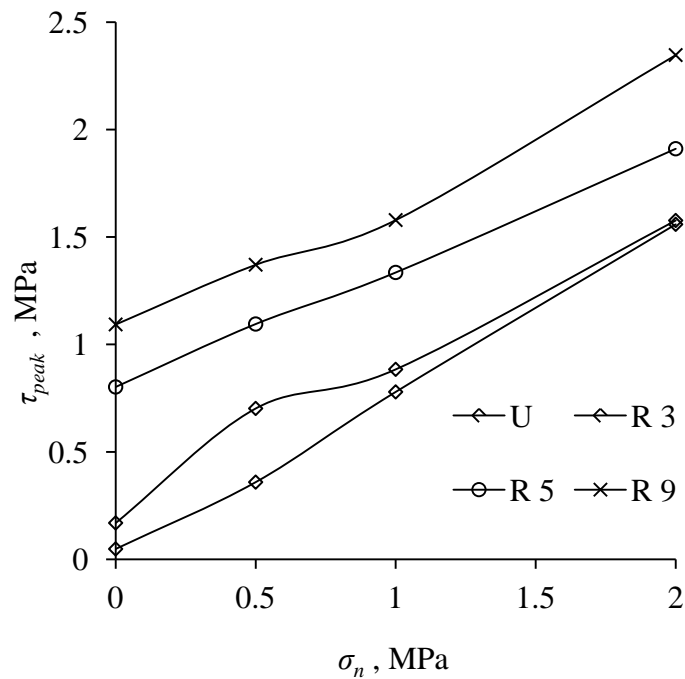
Fig. 5.2a Shear strength (τ_{peak}) vs normal stress (σ_n) plots for unreinforced and reinforced rock mass
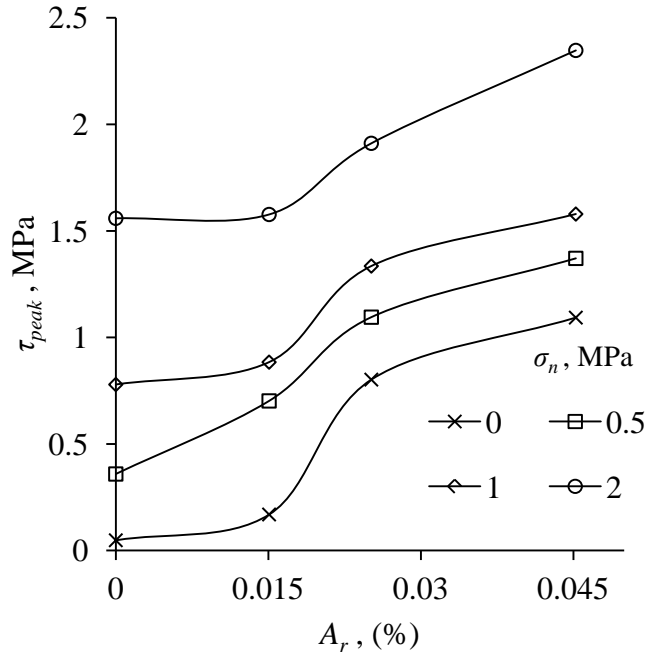
Fig. 5.2b Variation of shear strength (τ_{peak}) with area ratio (A_r)
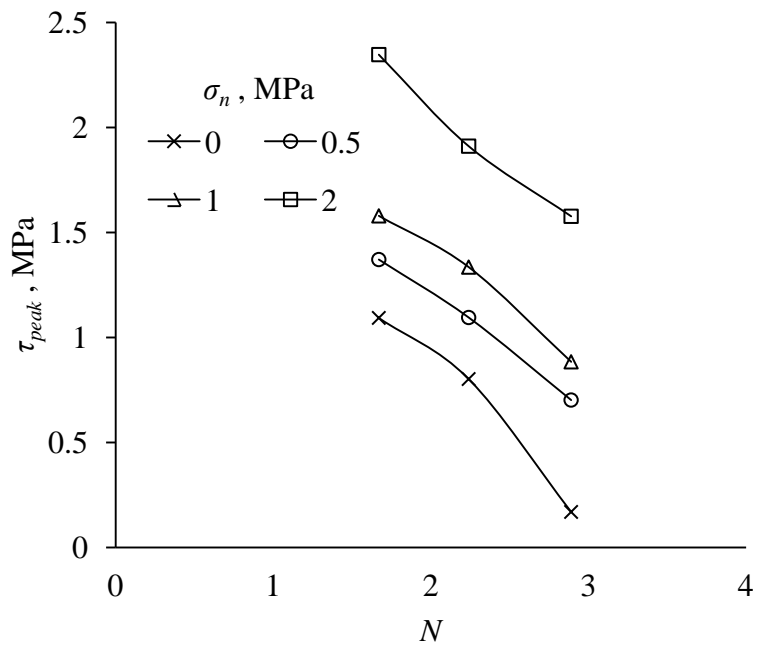
Fig. 5.2c Variation of shear strength (τ_{peak}) with spacing ratio (N)

5.3 SHEAR STIFFNESS OF BLOCKY MASS

The deformation behaviour of mass can be characterised by its shear stiffness, which is defined as the shear stress required to cause unit horizontal displacement. The shear stress vs horizontal shear displacement curves for reinforced specimens exhibit two distinct segments; the first part is relatively flat with low stiffness and, the second part is steep with high stiffness (Fig.5.3). The initial flat portion indicates the mobilization of shear stress due to the interaction of the blocks, which gives rise to the development of tensile stress in the bolts at the end of this segment. The second part indicates the mobilization of shear stress through the bolts, and the mass becomes stiffer. Table 5.3 presents the shear stiffness values for the first and second parts of the curves obtained in this study. There is a general trend of increasing shear stiffness with increasing normal stress. However, part II for the specimens with five bolts and parts I and II for specimens with nine bolts do not observe this trend. An increase in shear stiffness with increasing normal stress is as per expectation; however, if the variation of stiffness with the amount of reinforcement is observed, the stiffness increases up to five bolts and then reduces for nine bolts. It is interesting to see that the stiffness in part II with nine bolts is smaller compared to five bolts for all the normal stress values. The possible reason is explained below.

Table 5.3 Shear stiffness of joint in mass

σ_n (MPa)	Shear stiffness (MPa/m)						
	U	R3		R5		R9	
		Part I (R3_P1)	Part II (R3_P2)	Part I (R5_P1)	Part II (R5_P2)	Part I (R9_P1)	Part II (R9_P2)
0.0	5	8	21	17	248	27	144
0.5	30	13	56	40	352	49	140
1.0	32	40	90	56	240	16	102
2.0	96	88	140	119	225	56	142
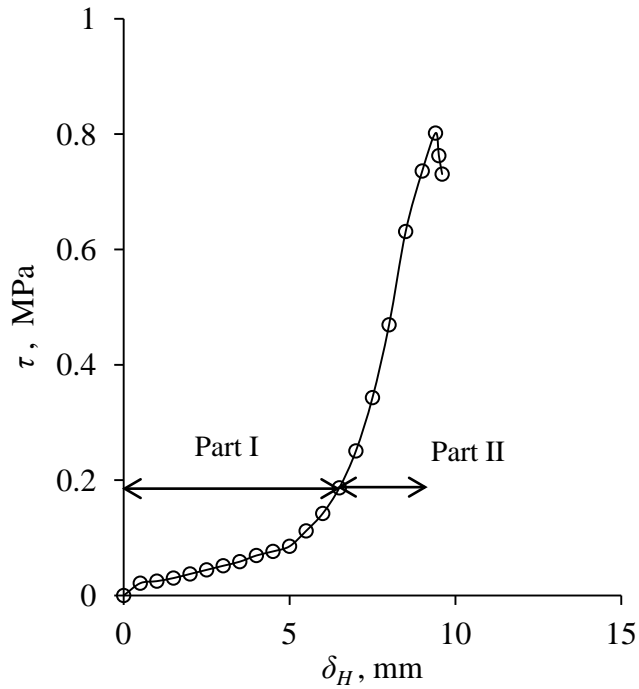
Fig.5.3 Two distinct segments of shear stress (τ) vs horizontal displacement (δ_H) plot

In the present study rock bolts act in a passive manner. They enhance the stiffness of the blocky mass by trying to prevent sliding along the shearing plane and by inducing additional normal stress due to tension in the bolts. The blocky mass therefore, becomes stiffer and stronger due to higher degree of interlocking produced by the bolts. When smaller number of bolts are installed, they introduce small degree of interlocking, enhance the stiffness of the mass, and the mass fails in a brittle manner. If a large number of rock bolts are installed, the bolts, in addition to enhancing the strength, also introduce ductility in the deformational behaviour since the bolts must yield for mobilising peak stress. With a lower number of bolts, the original character of the joint brittle failure is preserved by the mass, whereas with a large amount of steel, the ductile nature of steel starts dominating the deformational behaviour. This is the reason why in the present case the stiffness of the rock mass stiffened with 9 bolts is relatively smaller despite the fact that the shear strength is higher.

5.4 HORIZONTAL SHEAR DISPLACEMENT AT PEAK SHEAR STRESS

Horizontal shear displacement at peak stress ($\delta_{H,peak}$) at different normal stress levels is presented in Table 5.4. Figures 5.4a, 5.4b, and 5.4c show the variations of $\delta_{H,peak}$ with the normal stress, amount of reinforcement (Ar) and spacing ratio (N) respectively. It is observed that increase in normal stress first increases the $\delta_{H,peak}$ upto 1 MPa of normal stress. Further increase in normal stress decreases the $\delta_{H,peak}$. As the amount of reinforcement (Ar) increases, the $\delta_{H,peak}$ decreases and after a particular value of Ar, it increases (Fig. 5.4b). Increase in spacing ratio (N) decreases the $\delta_{H,peak}$ and after a particular value of N, $\delta_{H,peak}$ increases (Fig. 5.4c). This trend was observed for all normal stress levels. The stiffness of mass depends on $\delta_{H,peak}$. A mass with higher stiffness will show small displacements and vice-versa. This indicates that for a desired shear displacement (or for a desired stiffness) in blocky mass, there is a particular value of amount of reinforcement (A_r) and spacing ratio (N).
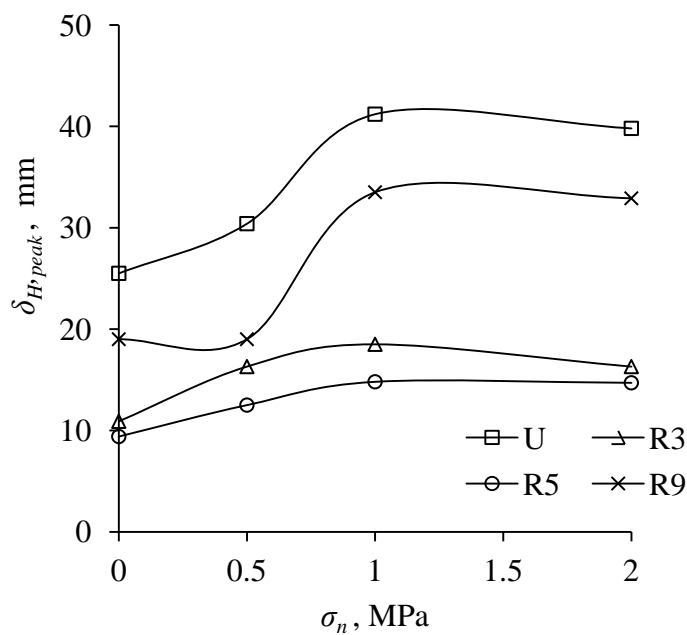
Fig. 5.4a Variation of $\delta_{H,peak}$ with normal stress (σ_n)
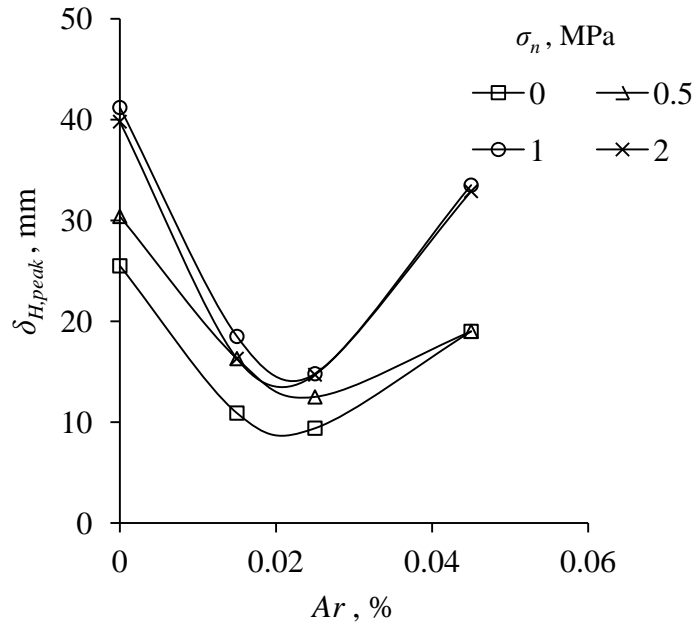
Fig. 5.4b Variation of $\delta_{H,peak}$ with area ratio (A_r)
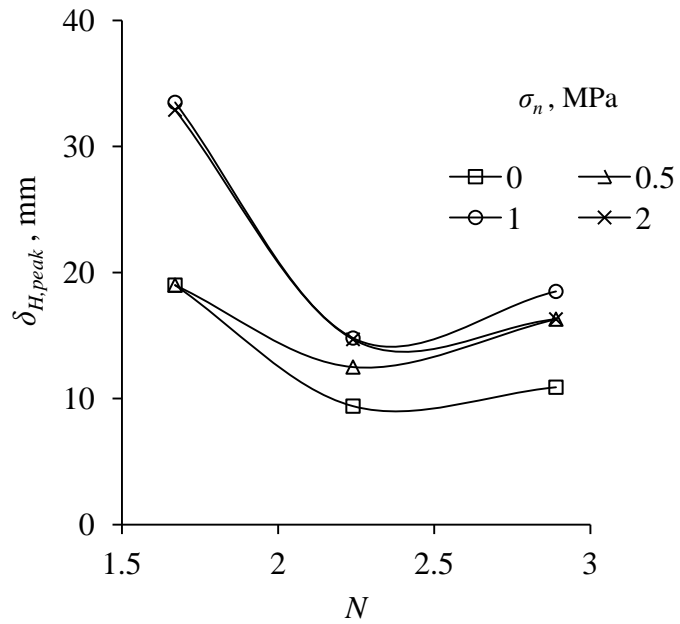
Fig. 5.4c Variation of $\delta_{H,peak}$ with spacing ratio (N)

171

Table 5.4 Horizontal shear displacement at peak stress ($\delta_{H,peak}$) at different normal stress levels

σ_n , MPa	Horizontal shear displacement at peak stress ($\delta_{H,peak}$), mm			
	U	R3	R5	R9
	$A_r = 0.0\%$	$A_r = 0.015\%$	$A_r = 0.025\%$	$A_r = 0.045\%$
	$N = -$	$N = 2.89$	$N = 2.24$	$N = 1.67$
0.0	25.5	10.9	9.4	19
0.5	30.4	16.3	12.5	19
1.0	41.2	18.5	14.8	33.5
2.0	39.8	16.3	14.7	32.9

5.5 DILATION ANGLE

The dilation angle has been taken as the ratio of volumetric strain and shear strain at the peak shear stress. It has been computed by obtaining gradient of best fitting straight line into data points of vertical displacement vs horizontal displacement plot up to peak shear stress. The values of dilation angle at different normal stress levels are presented in Table 5.5.The variations of dilation angle ($\psi°$) with normal stress (σ_n), amount of reinforcement (A_r) and spacing ratio (N) are plotted in Figs.5.5a, 5.5b and 5.5c respectively.

It is observed that dilation angle increases with increase in amount of reinforcement upto a certain value of reinforcement, beyond this dilation angle decreases. In general, dilation angle increases with increase in spacing ratio. This trend has not been observed when no normal stress ($\sigma_n = 0$ MPa) was applied to the mass.

Table 5.5 Values of dilation angle ($\psi°$) at different normal stress level

σ_n, MPa	Dilation angle ($\psi°$)			
	U	R3	R5	R9
	$Ar = 0.0\%$	$Ar = 0.015\%$	$Ar = 0.025\%$	$Ar = 0.045\%$
	$N = -$	$N = 2.89$	$N = 2.24$	$N = 1.67$
0.0	0.90	6.59	44.28	11.69
0.5	0.65	6.80	4.92	4.06
1.0	2.93	7.40	4.05	2.89
2.0	4.82	10.96	5.93	3.80
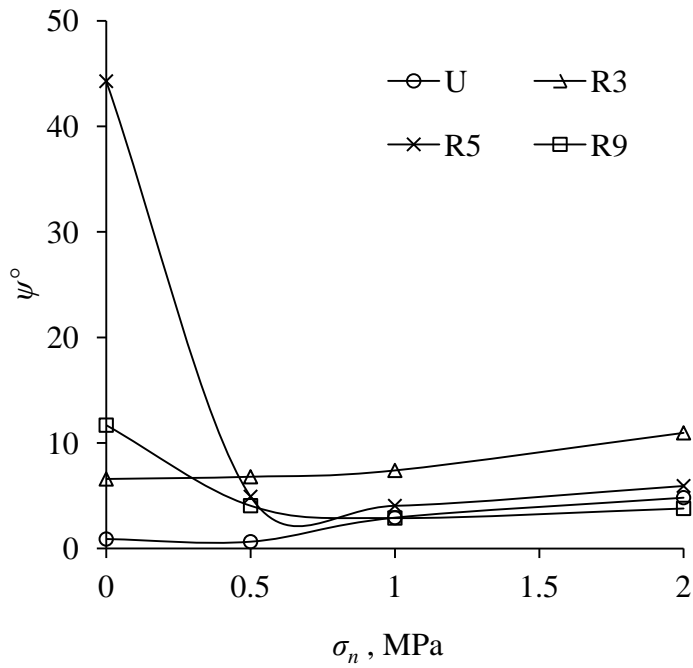
Fig.5.5a Variation of dilation angle ($\psi°$) with normal stress (σ_n)
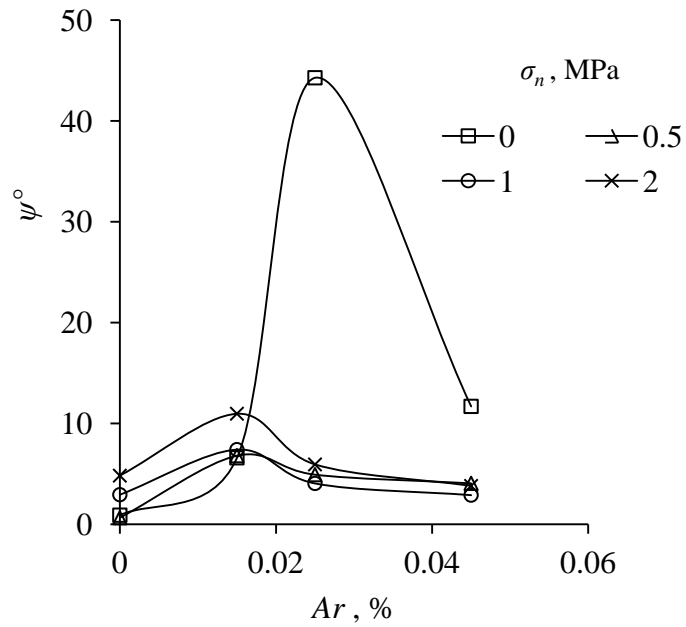
Fig.5.5b Variation of dilation angle ($\psi°$) with area ratio (A_r)
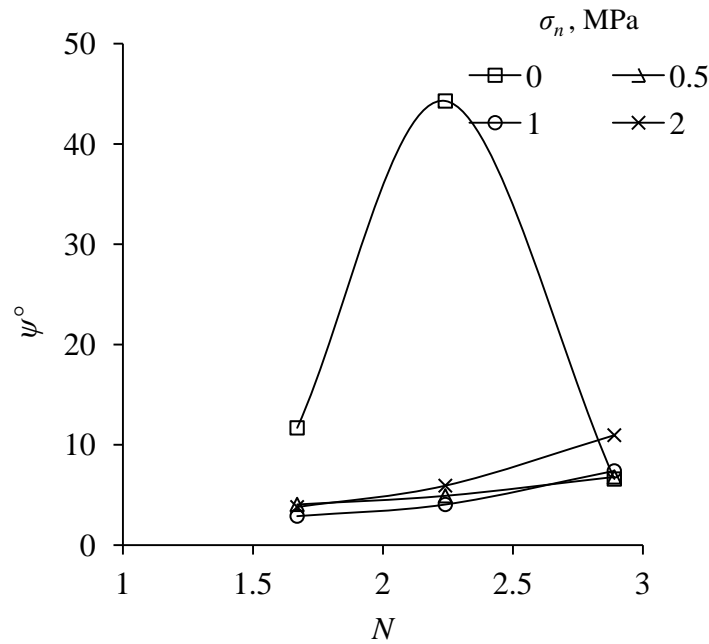
Fig.5.5c Variation of dilation angle ($\psi°$) with spacing ratio (N)

For R5 and R9 cases, the dilation angle ($\psi°$) is high at zero normal stress, and for higher normal stresses, it decreases and attains almost a constant value. For U and R3 cases, the dilation was low at zero normal stress and increased with increasing normal stress level. Both U and R3 cases, contradict the general perception that dilation should decrease with increasing normal stress level. The possible reason for this contradicting behaviour could be that U and R3 cases represent a loose assemblage of blocks with open joints. The application of normal stress consolidates the joints and makes them tightly closed. These tight joints exhibit greater dilation when sheared along the joint plane. Hence, the increase in normal stress results in higher dilation angle. For R5 and R9 cases, the mass is well stitched and dilation is less at higher normal stress levels. The reinforcement in these cases prevents sliding and blocks try to rotate. If normal stress is low, then rotation will result in higher dilation angle. If the normal stress is high it will restrict the rotation, and therefore, the dilation will be less.

5.6 SHEAR STRENGTH ENHANCEMENTS DUE TO BOLTS

Passive bolts enhance the shear strength of the mass by preventing sliding of blocks along the shearing plane. The shear strength enhancement ($\Delta\tau_f$) due to the provision of bolts in the mass at a given normal stress level is computed as:

$$\Delta\tau_f = \left(\frac{\tau_{r\_max} - \tau_{u\_max}}{\tau_{u\_max}}\right) \times 100 \ \% \tag{5.3}$$

where τ_{r_max} = Peak shear stress in reinforced case and τ_{u_max} = Peak shear stress in unreinforced case for a given normal stress level. The percent enhancement in shear strength observed in present study is given in Table 5.6.The variation of the shear strength enhancement ($\Delta\tau_f$) with normal stress (σ_n) for different types of reinforced mass specimens is also plotted in Fig. 5.6a. It is clearly observed from this figure that the shear strength enhancement decreases with increasing normal stress for each configuration of reinforced mass. The maximum shear strength enhancement has been observed when no normal stress ($\sigma_n = 0$) was applied to the mass. The figure also indicates that beyond a limiting value of normal stress, the strength enhancement due to passive rock bolts is negligibly small.
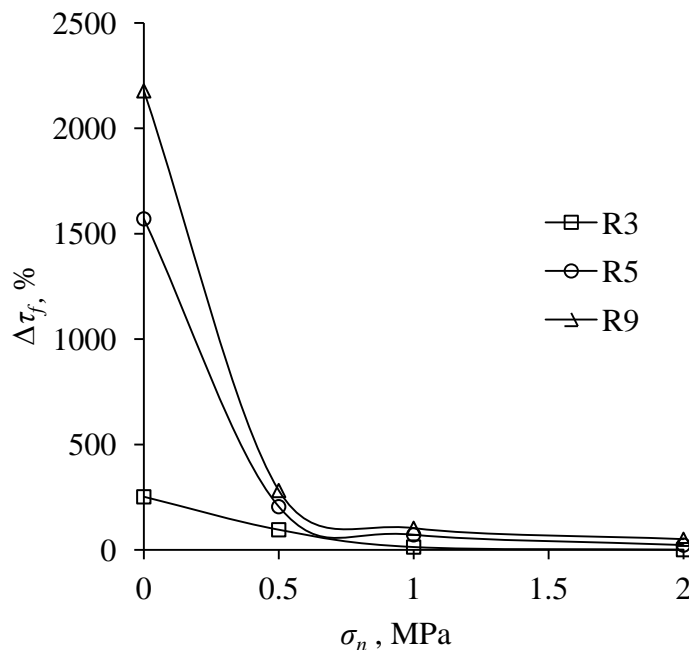
Fig.5.6a Shear strength enhancement ($\Delta\tau_f$) due to installation of rock bolt at different normal stress (σ_n) levels

Table 5.6 Shear strength enhancement due to rock bolts

σ_n (MPa)	Shear strength enhancement, $(\Delta\tau_f)$ (%)		
	R3	R5	R9
	$Ar = 0.015\%$	$Ar = 0.025\%$	$Ar = 0.045\%$
	$N = 2.89$	$N = 2.24$	$N = 1.67$
0.0	252	1570	2178
0.5	96	205	282
1.0	13	71	103
2.0	1	23	51

The strength enhancement $(\Delta\tau_f)$ due to the provision of rock bolts is plotted against area ratio, A_r (Fig.5.6b). The plot indicates that as the amount of reinforcement increases, the strength enhancement also increases. Hence, it may be inferred that strength of the reinforced mass is directly proportional to the area of reinforcement. The plots also indicate that the enhancement in shear strength reduces after a certain value of area ratio. Hence, for a particular type of a block mass, there are an optimum number of passive bolts, beyond that, the enhancement in shear strength becomes negligibly small.

The strength enhancement $(\Delta\tau_f)$ due to provision of the bolts is plotted with spacing ratio, N (Fig.5.6c). It is observed that the strength enhancement decreases with increasing value of N i.e. strength enhancement of blocky mass is inversely proportional to the spacing ratio. It is also observed that for a particular type of a block mass, there is a threshold value of spacing ratio (N) beyond that, the enhancement in shear strength decreases.

5.7 MOHR- COULOMB SHEAR STRENGTH PARAMETERS

The shear strength (τ_f) of the joint in the mass is represented as

$$\tau_f = c_{j\_mass} + \sigma_n \, tan\phi_{j\_mass} \tag{5.4}$$

where c_{j_mass} and ϕ_{j_mass} are the cohesion and friction angle along joint in the mass.
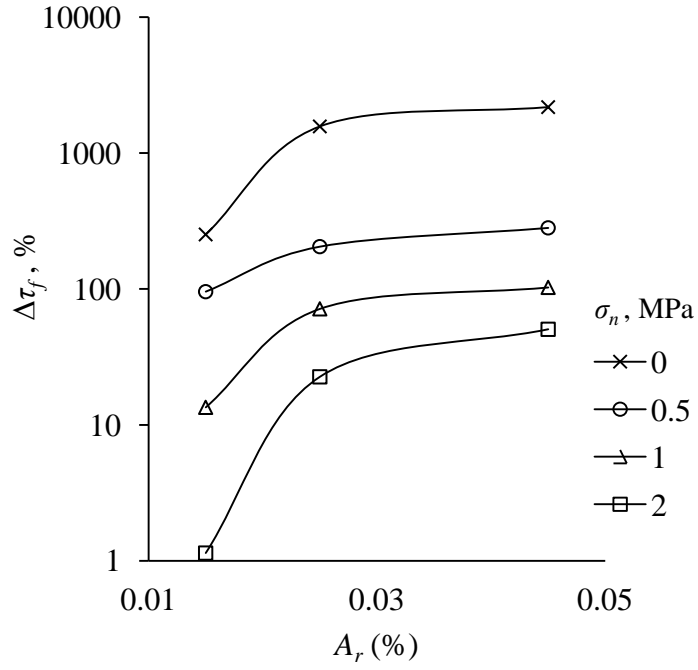
Fig. 5.6b Variation of shear strength enhancement ($\Delta\tau_f$) with area ratio (A_r)
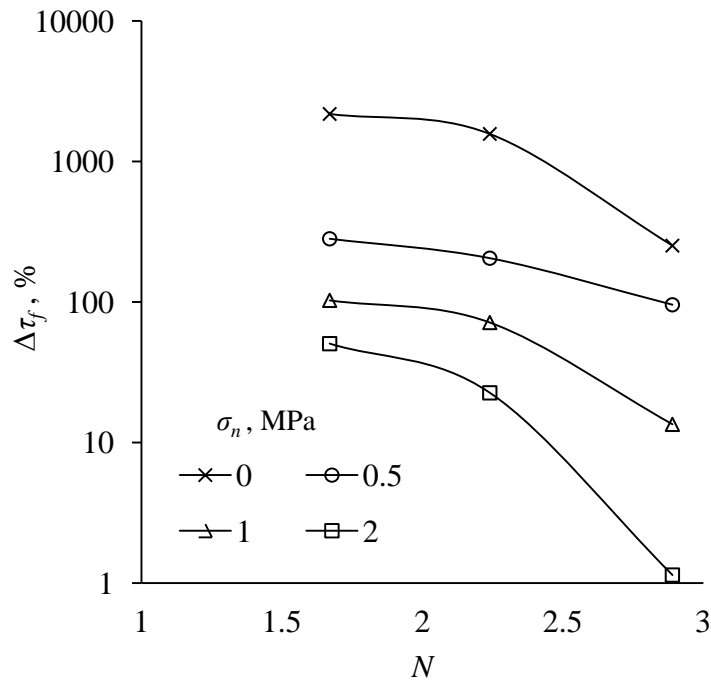
Fig.5.6c Variation of shear strength enhancement ($\Delta\tau_f$) with spacing ratio (N)

Figure 5.7 shows the shear strength (τ_f) vs normal stress (σ_n) plots for unreinforced and reinforced rock mass. The Mohr- Coulomb shear strength parameters (c_{j_mass} and ϕ_{j_mass}) for unreinforced and reinforced blocky mass as obtained from direct shear test results are presented in Table 5.7. The maximum value of cohesion was 1.056 MPa, which was observed for nine-bolts-reinforced specimen (R9) while the maximum value of friction angle was 37.43° obtained in case of unreinforced blocky mass (U).
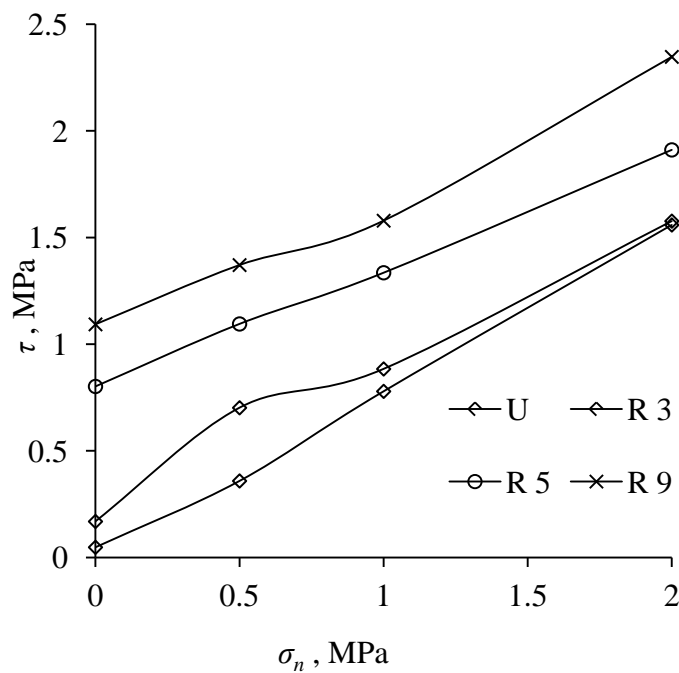
Fig.5.7 Shear strength (τ_f) vs normal stress (σ_n) plots of unreinforced and reinforced rock mass

Table 5.7 Mohr-Coulomb shear strength parameters (c_{j_mass} and ϕ_{j_mass}) for unreinforced and reinforced blocky mass

Type of reinforcement	Ar (%)	N	c_{j_mass}, MPa	ϕ_{j_mass}°
U	0.000	-	0.0164	37.43
R3	0.015	2.89	0.2436	33.96
R5	0.025	2.24	0.804	28.83
R9	0.045	1.67	1.0506	32

Installation of bolts altered the cohesion (c_{j_mass}) and friction angle (ϕ_{j_mass}) of the blocky mass. It is also observed that the cohesion increases with the amount of reinforcement (A_r) and there is very good trend of enhancement in cohesion with increasing amount of reinforcement (Fig.5.8a). However, trend in variation of friction angle with amount of reinforcement is not good (Fig.5.8b).

Variation of cohesion (c_{j_mass}) and friction angle (ϕ_{j_mass}) with spacing ratio (*N*) is plotted in Figs.5.9a and 5.9b respectively. The plot indicates that the cohesion decreases with increases in spacing ratio. However, the friction angle first decreases with spacing ratio and after a particular value of spacing ratio, friction angle increases.
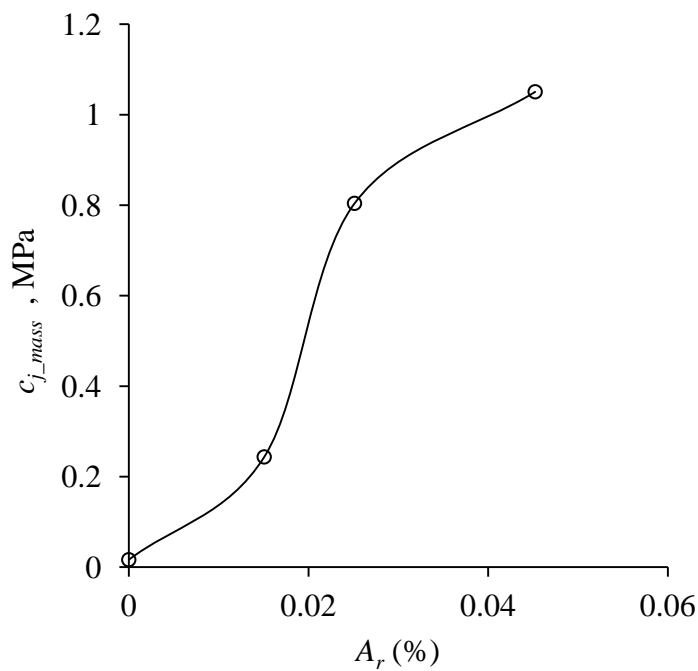
Fig.5.8a Variation of cohesion (c_{j_mass}) with area ratio (A_r)
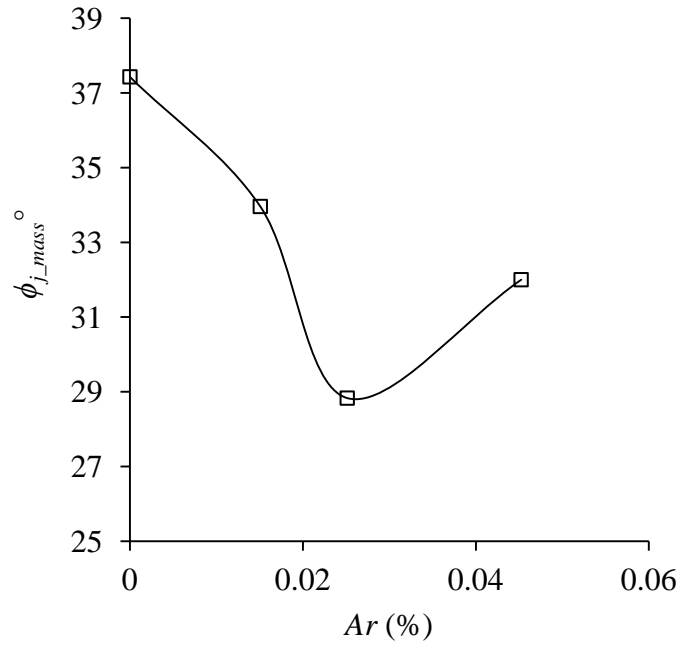
Fig.5.8b Variation of friction angle (ϕ_{j_mass}) with area ratio (A_r)
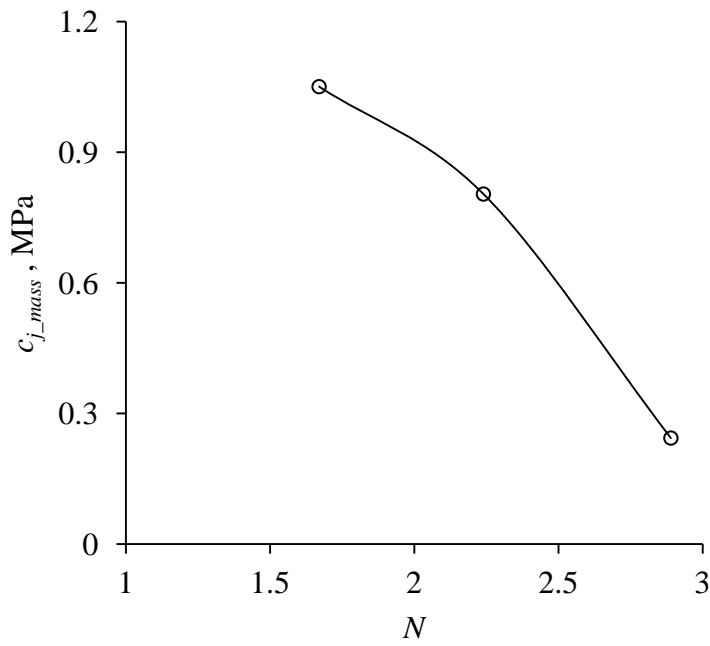
Fig.5.9a Variation of cohesion (c_{j_mass}) with spacing ratio (N)
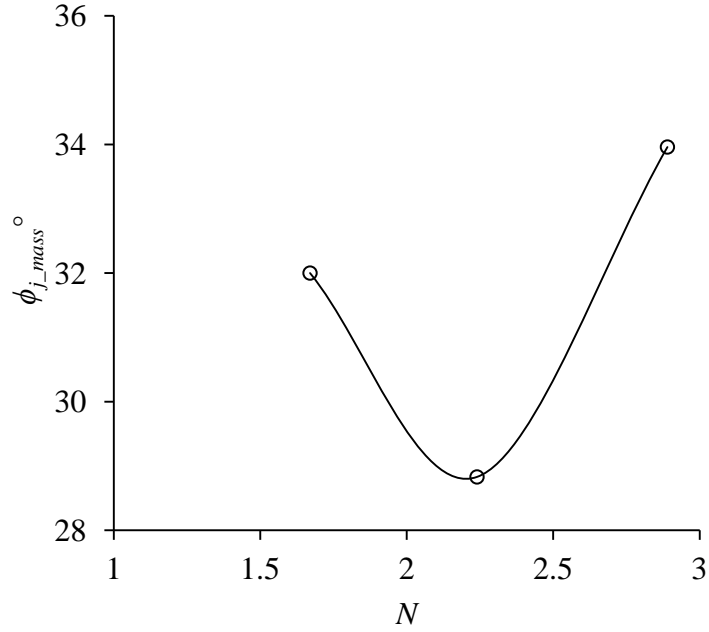
Fig.5.9b Variation of friction angle (ϕ_{j_mass}) with spacing ratio (*N*)

The percent change in cohesion (Δc_{j_mass}) and friction angle ($\Delta \phi_{j\_mass}$) is calculated as

$$\Delta c_{j\_mass} = \frac{(c_{j\_mass})_r - (c_{j\_mass})_u}{(c_{j\_mass})_u} \times 100\ \% \tag{5.5}$$

$$\Delta c_{j\_mass} = \frac{(\phi_{j\_mass})_r - (\phi_{j\_mass})_u}{(\phi_{j\_mass})_u} \times 100\ \% \tag{5.6}$$

where $(c_{j\_mass})_u$ and $(c_{j\_mass})_r$ = cohesion of unreinforced and reinforced mass respectively; $(\phi_{j\_mass})_u$ and $(\phi_{j\_mass})_r$ = friction angle of unreinforced and reinforced mass respectively. The percent change in cohesion (Δc_{j_mass}) and friction angle ($\Delta \phi_{j\_mass}$) is presented in Table 5.8.

It is observed that the percent change in cohesion is much greater than the percent change in friction angle for all configurations of reinforced blocky mass. Percent change in cohesion increases with increase in amount of reinforcement and decreases with spacing ratio. However, the percent change in friction is not consistent with amount of reinforcement and spacing ratio.

Table 5.8 Percent change in cohesion (Δc_{j_mass}) and friction angle ($\Delta \phi_{j\_mass}$)

Type of reinforcement	Ar (%)	N	(Δc_{j_mass}), %	($\Delta \phi_{j\_mass}$), %
R3	0.015	2.89	1385	-9
R5	0.025	2.24	4802	-23
R9	0.045	1.67	6306	-15

+ve sign indicates increase in value; -ve sign indicates decrease in value

For single joint, the value of the cohesion (c_j) was 0.008 MPa and the value of the friction angle (ϕ_j) was 34°. It is observed that, cohesion obtained for reinforced blocky masses (R3, R5 and R9 cases) is greater than the cohesion of unreinforced mass (U) and cohesion of single joint. In case of unreinforced mass (U), the value of ϕ_{j_mass} is higher than ϕ_j. For R5 and R9 cases, the value of ϕ_{j_mass} is lower than ϕ_j and in R3 case, the value of ϕ_{j_mass} is almost equal to ϕ_j. The percent change in cohesion of reinforced mass is much greater than the percent change in friction angle of reinforced mass. It may be noted that, the Mohr-Coulomb shear strength parameters c and ϕ are not fundamental properties of geomaterials, rather they are used as a mathematical convenience for obtaining shear strength subject to given normal stress (Duncan, 2000). Hence, to simplify the analysis, it is decided that the friction angle of reinforced mass (ϕ_{j_mass}) may be taken equal to friction angle of single joint (ϕ_j), and the overall shear strength enhancement by provision of bolts may be considered mainly due to change in cohesion of the mass (c_{j_mass}).

5.8 PREDICTION OF SHEAR STRENGTH ENHANCEMENT

By keeping ϕ_{j_mass} constant and equal to that of single joint ($\phi_j = 34°$), the cohesion values were recalculated for blocky mass specimens and are presented in Table 5.9. The recomputed cohesion (c_{j_mass}) is termed as equivalent cohesion. To incorporate the enhancement in cohesion, the cohesion enhancement (CE) is computed as

$$CE = c_{j\_mass} - c_j$$

(5.7)

where c_{j_mass} is the cohesion of a series of joints in the mass taking friction angle constant and c_j is the cohesion of a single joint. Cohesion enhancement is an overall measure of improved shear strength of joints due to the provision of passive rock bolts.

Table 5.9 Recomputed values of c_{j_mass}

σ_n (MPa)	c_{j_mass} , MPa (for $\phi_{j\_mass} = 34°$)			
	U	R3	R5	R9
0.0	0.05	0.17	0.80	1.09
0.5	0.02	0.36	0.76	1.03
1.0	0.10	0.21	0.66	0.90
2.0	0.21	0.23	0.56	1.00
Average	0.10	0.24	0.70	1.01

As discussed earlier, the strength enhancement of reinforced blocky mass is directly proportional to amount of reinforcement and inversely proportional to spacing ratio, hence a relationship is explored amongst the strength enhancement, the amount of reinforcement (A_r) and spacing ratio (*N*). The ratio CE/c_i (termed as relative cohesion enhancement) has been plotted against ratio A_r/N as shown in Fig.5.10, where c_i is the cohesion of the intact rock. The plot indicates a good correlation between relative cohesion enhancement and A_r/N. The following correlation is obtained:

$$\frac{CE}{c_i} = \frac{c_{j\_mass} - c_j}{c_i} = 0.04 \, ln\left(\frac{A_r}{N}\right) + 0.24 \tag{5.8}$$

The above correlation may be used to get cohesion enhancement due to provision of bolts. The following assumptions are implicit in the above formulation:

i. The friction angle of series of joints in mass ϕ_{j_mass} is assumed to be equal to the friction angle of a single joint ϕ_j.

ii. The value of c_{j_mass} is always less then c_i.

Based on the correlation suggested above a chart has been prepared to assess the cohesion enhancement for a given area of steel and a spacing ratio (Fig.5.11). Using this chart the value of cohesion enhancement due to provision of bolts can be calculated for application in field situations like slopes. The chart may be very helpful

in deciding optimal number of passive bolts to reinforce a situation where sliding is expected on joint planes e.g. rock slopes.
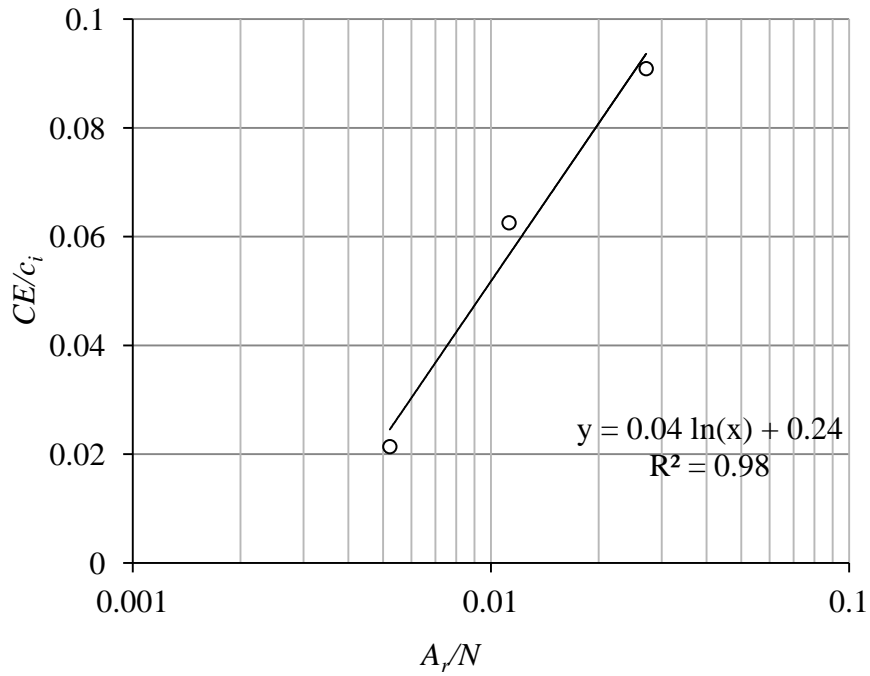
Fig. 5.10 Variation of Cohesion ratio with A_r/N
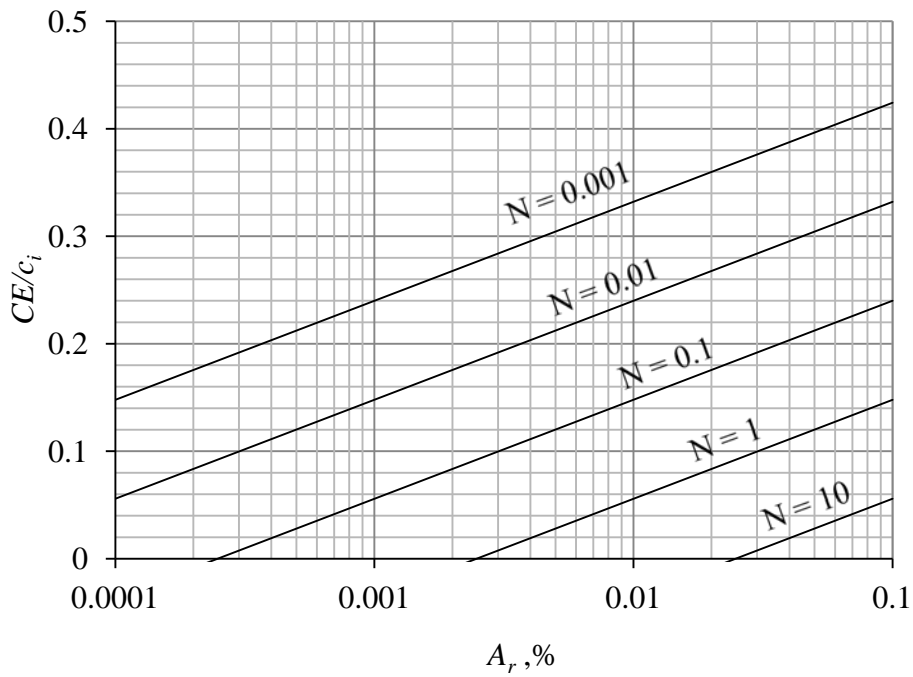
Fig.5.11 Chart for calculating the cohesion enhancement with different area ratio (A_r) and spacing ratio (N)

As the value of CE/c_i is obtained, the shear strength of a reinforced mass subjected to a given normal stress may be obtained as:

$$\tau_f = c_i \left(0.04 \; ln \left(\tfrac{A_r}{N} \right) + 0.24 \right) + c_j + \sigma_n \; tan\phi_j \tag{5.9}$$

5.9 CONCLUDING REMARKS

An experimental investigation has been carried out to study the effect of fully grouted passive bolts on shear strength parameters of joints in a blocky mass. Large size direct shear tests were conducted on a blocky mass under unreinforced and reinforced conditions. A correlation has also been established in terms of area ratio (A_r) and spacing ratio (N) to assess the enhancement in shear strength due to the provision of bolts. The main conclusions drawn from the study are as follows:

i. Rock bolts enhance the stiffness of the mass by preventing sliding along the shearing plane, and by inducing additional normal stress due to tension in the bolts. The rock mass, therefore, becomes stiffer and stronger due to the high degree of interlocking produced by the bolts.

ii. If the numbers of bolts installed are more than the threshold number, they introduce ductility in the mass.

iii. Shear strength of the mass increases with increasing numbers of bolts.

iv. In addition to normal stress, the interaction between blocks of mass and rock bolts plays significant role in governing the shear strength of the mass. In the case of reinforced mass, enhancement in shear strength due to provision of bolts decreases with an increase in normal stress.

v. With low amount of reinforcement, the dilation increases with increasing normal stress whereas with high amount of reinforcement the dilation decreases with increase in normal stress.

vi. The provision of bolts improves the cohesion of joints substantially. The effect on friction angle is low.

185

vii. The cohesion enhancement depends on the area of the bolts, spacing of the joints, spacing between the bolts and cohesion of intact material.

viii. A correlation has been established between the area ratio (A_r), spacing ratio (N) and cohesion ratio (CE/c_i). Using this correlation the enhancement in cohesion due to the provision of bolts can be assessed.

<div align="right">**Chapter 6**</div>

BEHAVIOUR OF NATURAL AND SYNTHETIC JOINTED ROCKS UNDER UNIAXIAL COMPRESSION

6.1 GENERAL

Uniaxial compression tests have been conducted on the intact, unreinforced jointed and reinforced jointed specimens of natural and synthetic rocks. The inclination of joint was varied from 0°-90° with respect to the horizontal axis. The specimens were reinforced with passive bolts. The details of results and observations are presented in chapter 4. The present chapter deals with the detailed analysis of results obtained from uniaxial compression tests. The outcome of the analysis can be used in the field situations where uniaxial compressive strength (UCS) of the mass is required. The UCS becomes a starting point in the process of analysing strength behaviour of jointed rocks though a failure criterion (Ramamurthy, 1993: Ramamurthy and Arora, 1994: Singh and Singh, 2012). It is envisaged that provision of rock bolts would bring strength enhancement in the jointed rock. If an accurate estimation of the UCS of the jointed rock reinforced with rock bolts could be made, much more reliable estimation of triaxial strength would be possible through failure criteria.

6.2 AXIAL STRESS VS AXIAL STRAIN BEHAVIOUR

Typical axial stress vs axial strain plots are presented in Figs. 6.1a, 6.1b and 6.1c respectively to highlight the difference in stress- strain behaviour of intact, unreinforced jointed and reinforced jointed specimens.
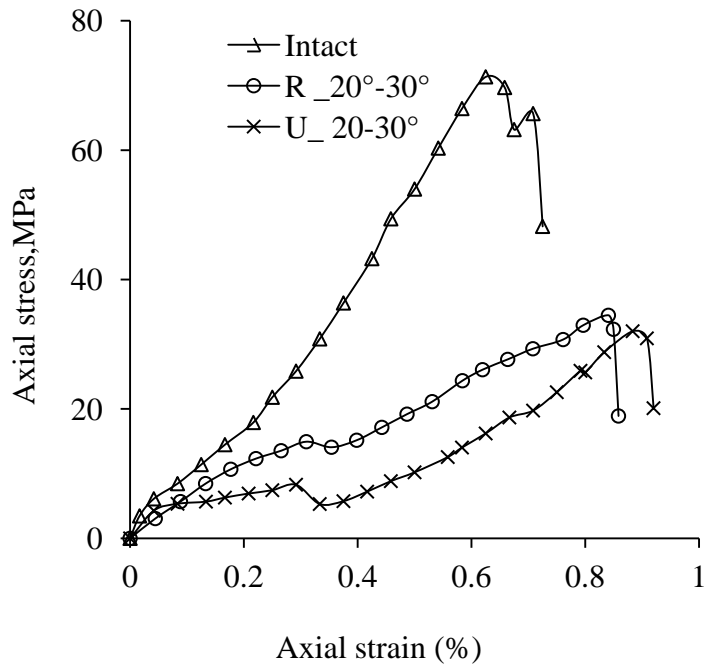
Fig.6.1a Typical axial stress vs axial strain plots for natural rock (NRC)
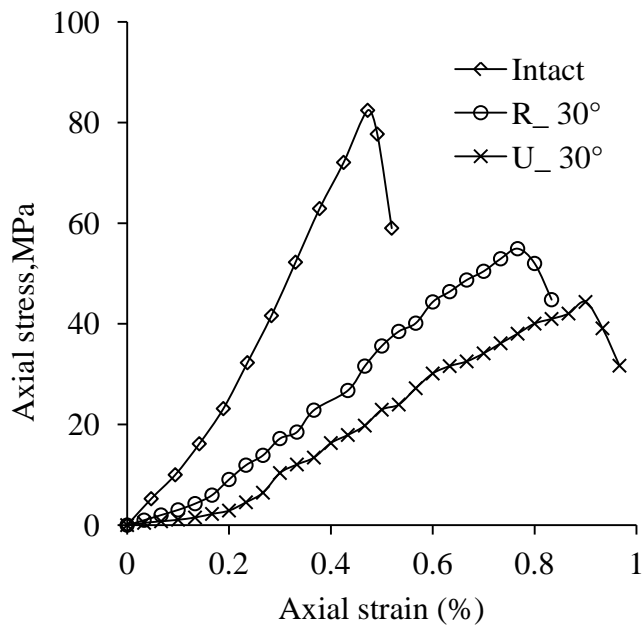
Fig.6.1b Typical axial stress vs axial strain plots for synthetic rock (T2)
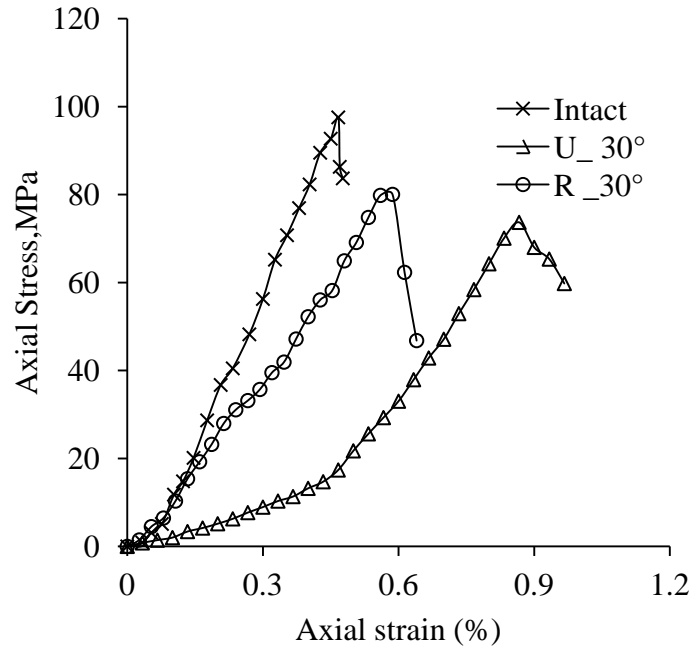
Fig.6.1c Typical axial stress vs axial strain plots for synthetic rock (T3)

For each type of the rock (both natural and synthetic), the axial stress vs axial strain plot of reinforced jointed rock is between the plots of intact and unreinforced jointed rock. The application of bolt introduces interlocking in the joints. Due to this, stress level increases for unreinforced rock at each strain level. This results in increase in strength and modulus of the jointed rock. The enhancement in strength and modulus is greatly influenced by the orientation of the joint.

6.3 ANISOTROPY IN STRENGTH AND DEFORMATIONAL BEHAVIOUR

6.3.1 Anisotropy in Strength behaviour

The variation of uniaxial compressive strength (σ_c) with joint orientation ($\theta°$) for unreinforced (NRC_U) and reinforced (NRC_R) natural rock specimens is plotted in Fig. 6.2a. For unreinforced specimens of natural rock, the uniaxial compressive strength decreases with increasing θ upto 80°, beyond this, increase in strength is observed. Very low strength (≈ 1 MPa) was observed between $\theta = 40°$ to $\theta = 80°$ (Fig.6.2a). The specimens of unreinforced natural rocks exhibit sliding mode of failure at these joint orientations. These orientations ($\theta = 40°$ to $\theta = 80°$) are termed critical joint orientations because they exhibit practically zero strength. Between $\theta =$

30° to 40°, also specimens failed due to sliding but with relatively higher strength (approximately 7 MPa). For orientation range θ = 0° to 30° and θ = 80° to 90°, the specimens failed due to splitting and showed higher strength. Provision of bolt enhances the strength of the rock and higher strength was observed between θ = 30° to 80° (Fig.6.2a). Application of reinforcement changed failure mode from sliding (for unreinforced rock) to splitting (for reinforced rock) for these joint orientations. For joint orientations θ = 0° to 30° and θ = 80° to 90°, no change of failure mode was observed and the strength enhancement is low. In case of reinforced natural rock specimens, the minimum strength (< 10 MPa) was observed between θ = 50° to 70°. Starting from θ = 20°, the strength was found to be decreasing with θ, became minimum at θ = 70°, beyond this strength was found to increase with θ.

The strength behaviour of natural jointed rock is observed to be highly anisotropic. The anisotropy ratio (ratio of maximum to minimum strength) of unreinforced natural rock is found to be 84. For reinforced case, the anisotropy ratio is 8. Provision of bolt reduces the anisotropy ratio of jointed rock and brings about 90% reduction in anisotropy ratio.
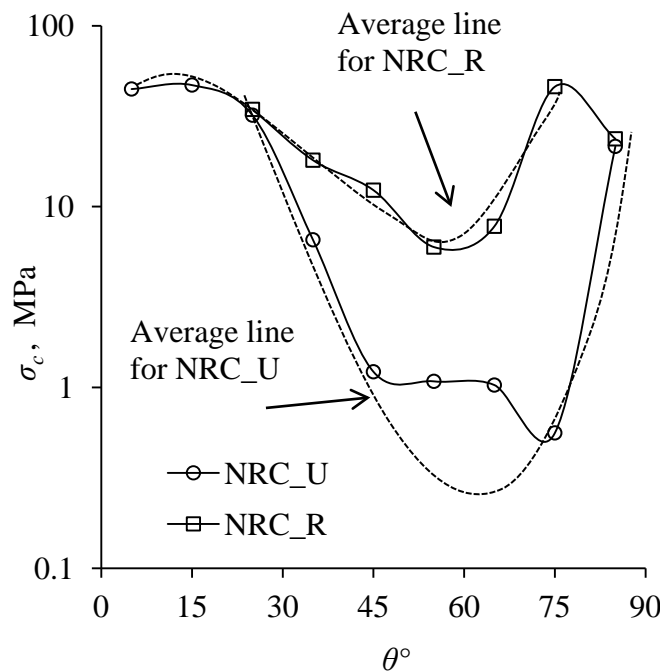
Fig.6.2a Variation of uniaxial compressive strength (σ_c) with joint orientation (θ°) for natural rock specimens

The variation of uniaxial compressive strength (σ_c) with joint orientation ($\theta°$) for T2 and T3 type of synthetic rock specimens is plotted in Fig. 6.2b and 6.2c respectively. As compared to natural rock, the results of synthetic rocks indicate more systematic variation with lesser amount of scatter.

The unreinforced specimens of synthetic rocks (T2_U and T3_U) exhibits minimum strength ($\approx$ 0.1 MPa) at critical joint orientations i.e. θ = 45° and 60°. Sliding failure was observed at theses orientations. For joint orientations other than θ = 45° and 60° splitting mode of failure was observed in unreinforced specimens and hence the strength is much higher compared to critical orientations.

For both types of synthetic rocks (T2_R and T3_R), as joint angle θ increases, the strength of unreinforced rock decreases, reaches a minimum at θ = 60°, and again increases. Similar trend was also observed for reinforced specimens (Fig.6.2b and 6.2c). Reinforced rock specimens exhibit only splitting mode of failure. The provision of bolt enhances the strength of jointed rocks for all joint orientations, however, the maximum enhancement is found for those orientations where failure mode changes due to reinforcement i.e. θ = 45° and 60°. At theses orientations, unreinforced rock exhibited sliding failure while reinforced rock exhibited splitting mode of failure. At other orientations (θ = 0° to 45° and 60° to 90°) both unreinforced and reinforced specimens exhibit splitting failure and strength enhancement due to bolt was low.

Similar to natural rocks, strength behaviour of synthetic rocks is also highly anisotropic. The anisotropy ratio of unreinforced specimens of T2 type of synthetic rock is 526 while for reinforced specimens it is 11. For T3 type of synthetic rock, the anisotropy ratio of unreinforced specimens is found to be 600. For reinforced case, it is about 8. Provision of bolt reduces the anisotropy ratio for synthetic rocks. The percent reduction in anisotropy ratio is found to be 98% and 99% for T2 and T3 types of rocks respectively.

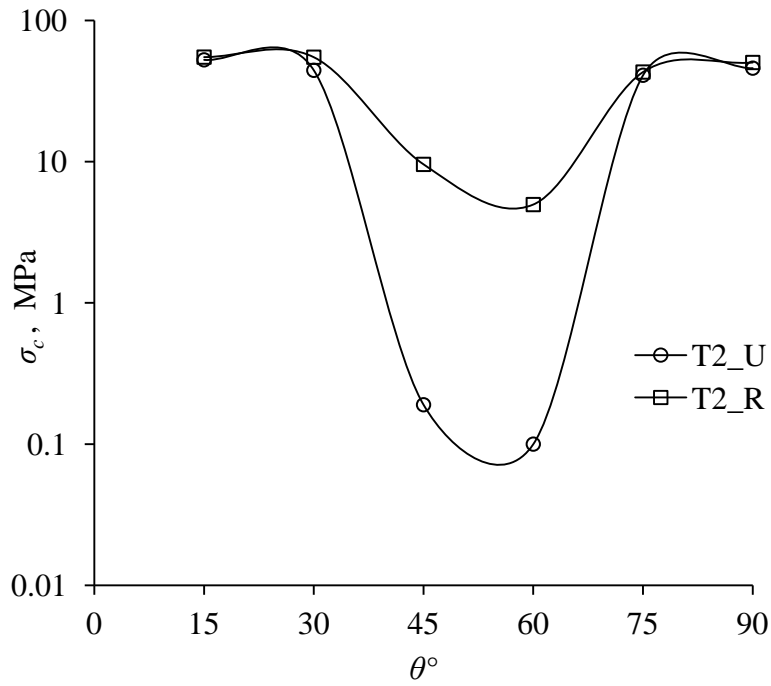**Fig.6.2b Variation of uniaxial compressive strength (σ_c) with joint orientation ($\theta°$) for synthetic rock specimens (T2)**
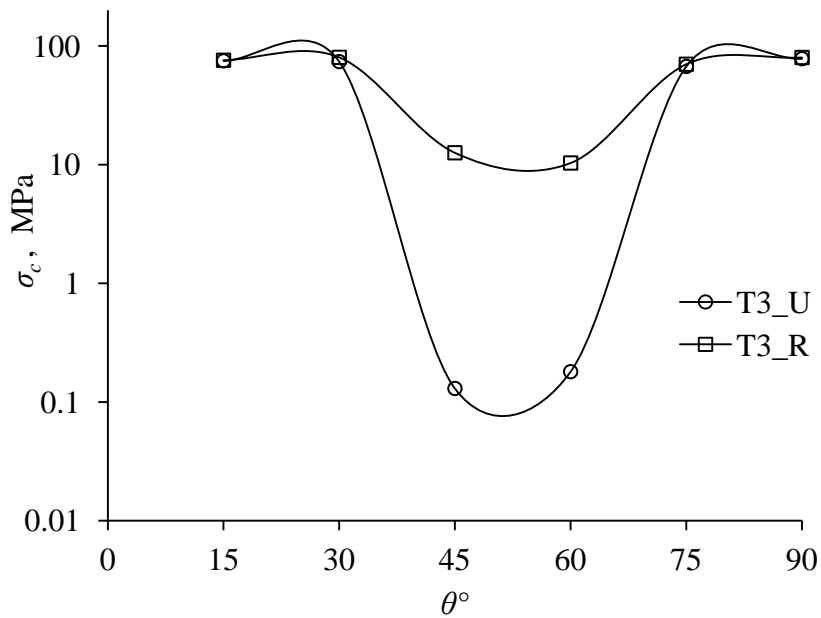
Fig.6.2c Variation of uniaxial compressive strength (σ_c) with joint orientation ($\theta°$) for synthetic rock specimens (T3)

6.3.2 Anisotropy in Deformational behaviour

The variation of tangent modulus (E_{t50}) with joint inclination ($\theta°$) for unreinforced and reinforced cases of natural and synthetic rocks is presented in Figs.6.3a, 6.3b and 6.3c respectively.

For unreinforced natural rock specimens (NRC_U), the modulus has been found to be decreasing with increasing θ from 0°. After reaching minimum values in the rage of $\theta \approx 40°$ to 80°, there is increase in tangent modulus. The values of tangent modulus between $\theta \approx 40°$ to 80° (critical joint orientations) were extremely low (< 0.5 GPa) due to sliding along joint plane. Provision of reinforcement enhances the tangent modulus, and for the same joint inclination, the tangent modulus for reinforced rock is substantially higher as compared to unreinforced cases. At orientations other than critical ones, the modulus enhancement due to bolt is low.

The variation of modulus with joint orientation (Fig.6.3a) indicates that for reinforced case also the modulus decreases with increase in θ (starting from 20°) up to a minimum and then increases. The minimum in this case has been obtained somewhere between $\theta \approx 45°$ to 65°. Figure 6.3a indicates that there is scatter in experimental data and hence an average line is plotted which shows trend of variation of the modulus.

Similar to strength, the deformational behaviour of natural jointed rock is also highly anisotropic. The anisotropy ratio (ratio of maximum to minimum modulus) of unreinforced natural rock is found to be 2800. For reinforced case, the anisotropy ratio is 11. Provision of bolt reduces the anisotropy ratio of unreinforced jointed rock. The percent reduction in anisotropy ratio is found to be about 99%.

In case of synthetic rocks (T2 and T3), the scatter is much less as compared to natural rock (Fig.6.3b and 6.3c). The tangent modulus has been found to be substantially influenced by joint orientation ($\theta°$). As one starts from $\theta = 0°$ and increases θ, the modulus decreases, reaches a minimum value near 60° and again increases. This trend is observed for both unreinforced (T2_U, T3_U) and reinforced cases (T2_R, T3_R). The values at $\theta = 75°$ are little higher than $\theta = 90°$ which is likely to be due to scatter.
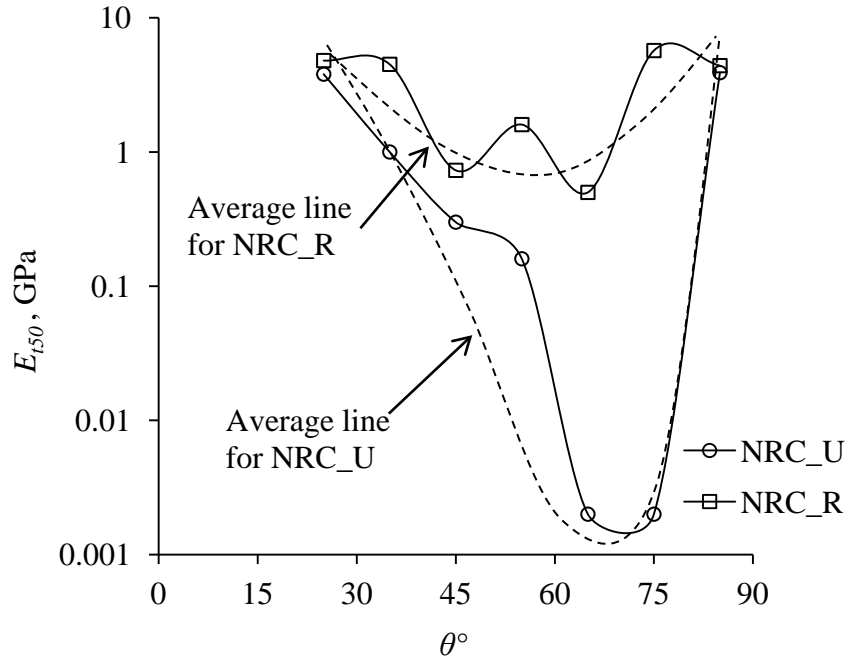
Fig.6.3a Variation of tangent modulus (E_{t50}) with joint orientation ($\theta°$) for natural rock (NRC)
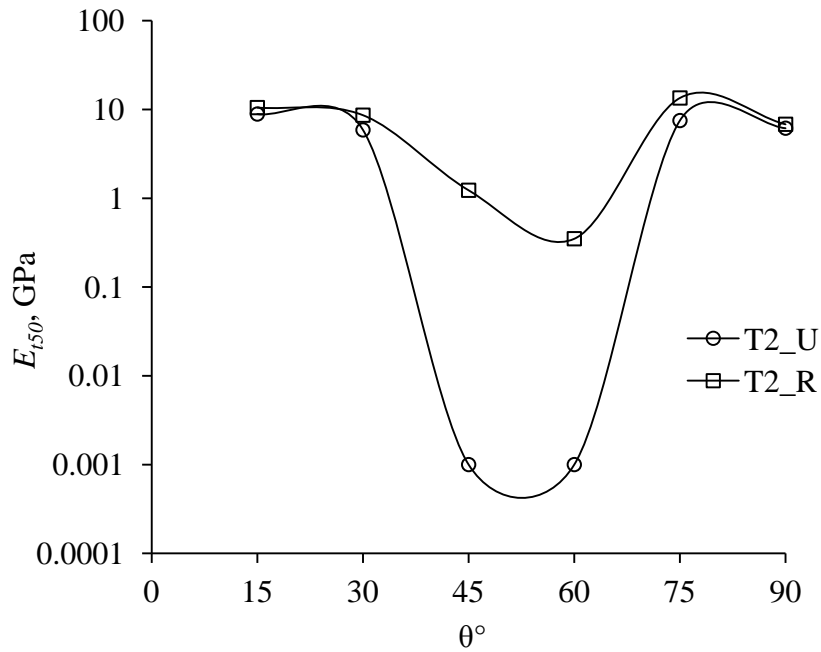
Fig.6.3b Variation of tangent modulus (E_{t50}) with joint orientation ($\theta°$) for synthetic rock (T2)

194
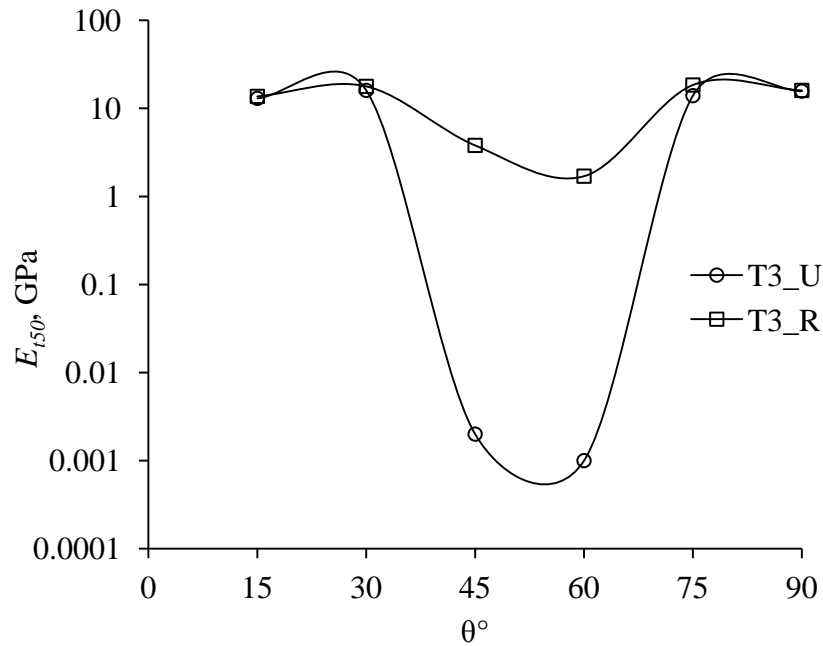
Fig.6.3c Variation of tangent modulus (E_{t50}) with joint orientation ($\theta°$) for synthetic rock (T3)

At critical joint orientations (θ = 45° and 60°), the tangent modulus of unreinforced rock is found to be very low (0.001 GPa) (Fig.6.3b and 6.3c) as compared to other orientations. Provision of bolt substantially enhances the modulus of unreinforced rock at all the orientations. At critical joint orientations, the enhancement in modulus is found to be higher as compared to other orientations.

The deformational behaviour of synthetic rocks is also highly anisotropic. In case of T2 type of synthetic rock, the anisotropy ratio is found to be 8880 and 39 for unreinforced and reinforced specimens respectively. The percent decrease in anisotropy ratio is about 99%. For T3 type of synthetic rock, the anisotropy ratio for unreinforced rock is 16000. For reinforced rock, the anisotropy ratio is reduced to 11, which is about 99 % less as compared to unreinforced specimens.

6.4 STRENGTH (UCS) AND MODULUS ENHANCEMENT DUE TO REINFORCEMENT

The provision of reinforcement has been found to enhance the strength as well as modulus values. The percent enhancement for a given joint orientation is computed as:

$$\text{Strength enhancement} = \left(\frac{\sigma_{cr} - \sigma_{cu}}{\sigma_{cu}}\right) \times 100 \text{ \%} \tag{6.1}$$

$$\text{Modulus enahncement} = \left(\frac{E_{cr} - E_{cu}}{E_{cu}}\right) \times 100 \text{ \%} \tag{6.2}$$

where σ_{cu} , $\sigma_{cr} =$ uniaxial compressive strength of unreinforced and reinforced jointed rock respectively and E_{cu} , $E_{cr} =$ tangent moduli of unreinforced and reinforced jointed rock respectively.

6.4.1 Natural rock

The effect of joint inclination ($\theta°$) on strength enhancement for the natural rock is shown in Fig. 6.4a. As there is scatter in data, the average curve is also plotted in this figure. It is observed that the strength enhancement increases with increasing θ and reaches a maximum value near 60°and thereafter decreases. Minimum enhancement in strength has been observed near $\theta = 15°$ and $\theta = 90°$. Maximum enhancement in strength is found for orientations where sliding was dominating in unreinforced specimens ($\theta \approx 40°$ to 80°).

The variation of modulus enhancement is shown in Fig.6.4b. The average curve is also shown in this figure. The trend of variation is similar to strength enhancement. Modulus enhancement increases with increasing θ and reaches a maximum value near 75° and the thereafter modulus enhancement decreases. Maximum enhancement in modulus was observed for orientations where sliding was observed in unreinforced specimens ($\theta \approx 40°$ to 80°). Minimum enhancement has been observed near $\theta = 15°$ and $\theta = 90°$. At theses orientations no change in failure mode was observed due to reinforcement.
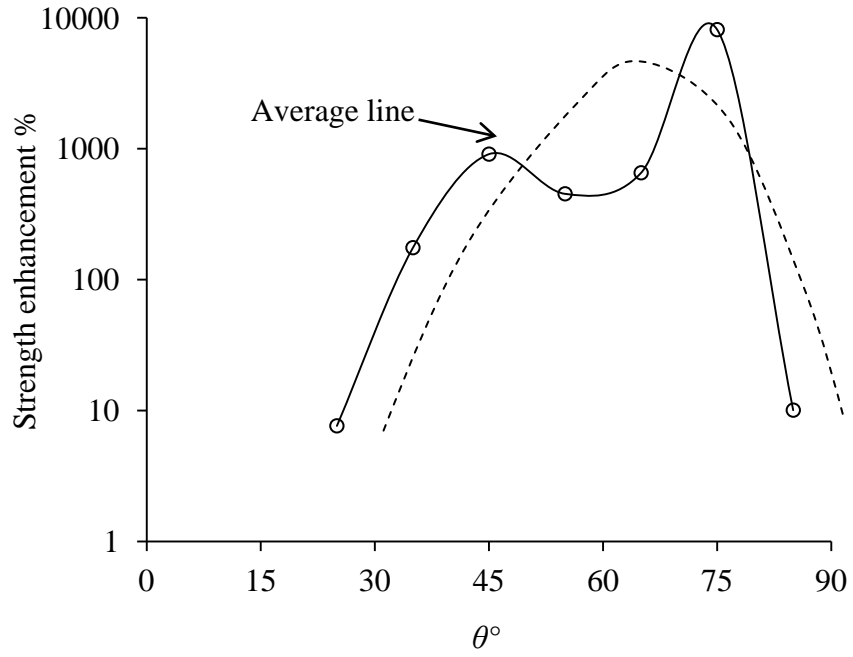
Fig.6.4a Variation of strength enhancement with joint orientation (θ°) for natural rock (NRC)
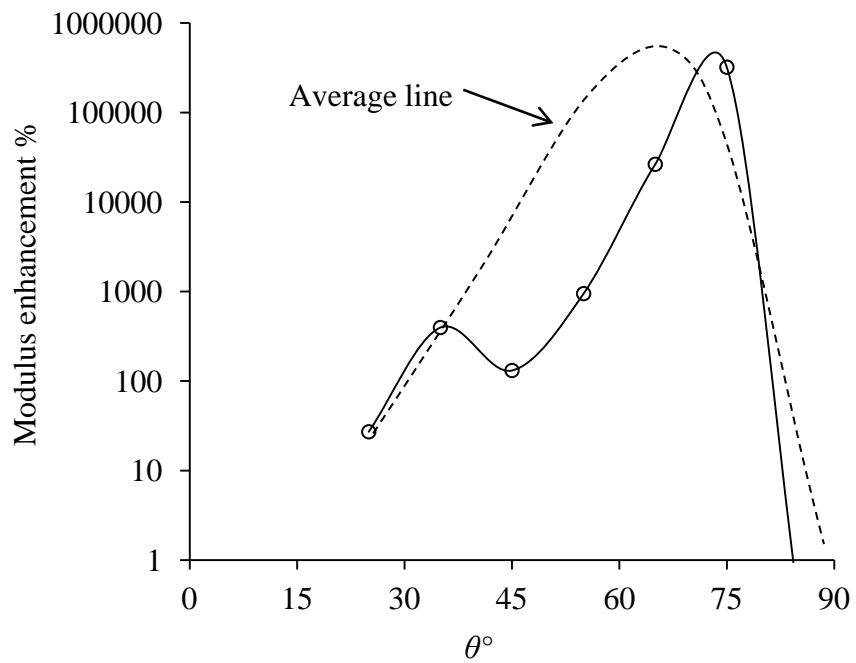
Fig.6.4b Variation of modulus enhancement with joint orientation (θ°) for natural rock (NRC)

6.4.2 Synthetic rocks

The variation of strength enhancement with joint orientation (θ) for synthetic rocks is presented in Fig. 6.5a. For critical joint orientations i.e. $\theta = 45°$ and $60°$ where change in failure mode due to reinforcement occurred, the enhancement in strength is much higher as compared to other orientations. However, the strength enhancement is greater in case of T2 type of synthetic rock as compared to T3 type of synthetic rock. For both types of synthetic rocks, increase in θ increases the strength enhancement. Between $\theta = 45° - 60°$ strength enhancement becomes maximum and after this the strength enhancement decreases.
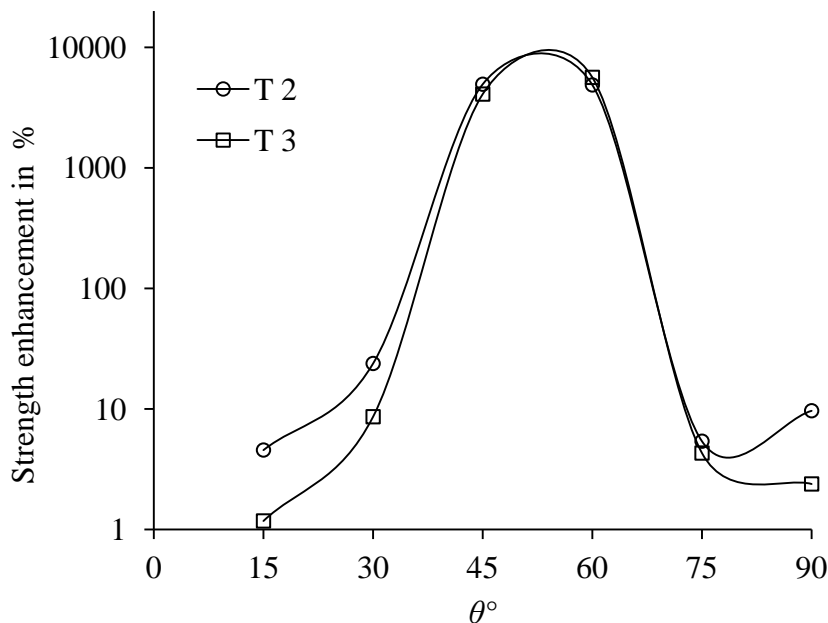
Fig.6.5a Variation of strength enhancement with joint orientation ($\theta°$) for synthetic rocks

The variation of modulus enhancement with joint orientation (θ) for synthetic rocks is presented in Fig. 6.5b. Increase in θ (starting from 0°), increases the modulus enhancement and between $\theta = 45° - 60°$ the maximum modulus enhancement was observed. After maximum, value the modulus enhancement decreases. This trend was observed for both types of synthetic rocks, but the enhancement is greater for T2 type of rock as compared to T3 type of rock. For critically oriented joints ($\theta = 45°$ and $60°$) the enhancement is maximum because of change in failure mode. At other orientations, the modulus enhancement is low.
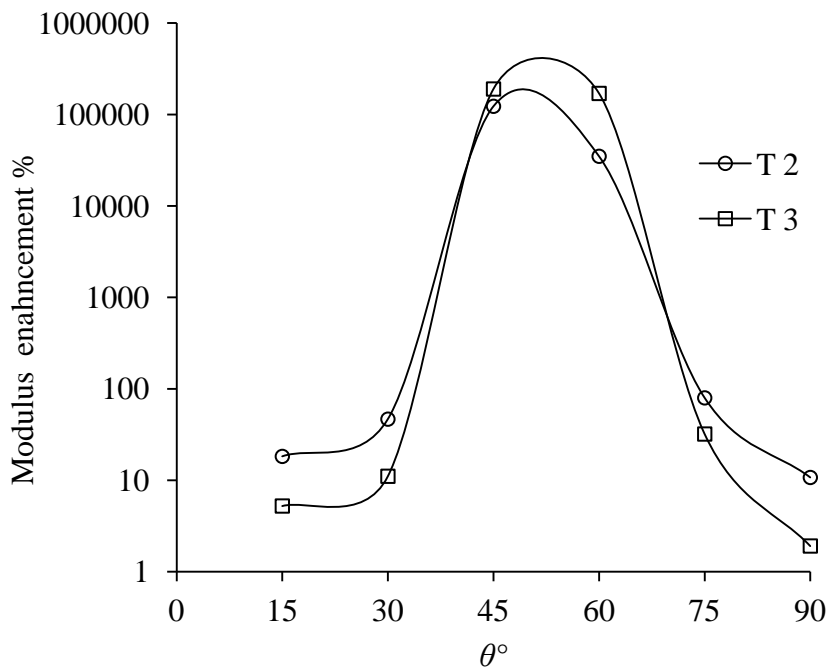
Fig.6.5b Variation of modulus enhancement with joint orientation ($\theta°$) for synthetic rocks

6.5 CORRELATIONS BETWEEN STRENGTH AND MODULUS VALUES OF INTACT, UNREINFORCED JOINTED AND REINFORCED JOINTED ROCKS

It has been observed in previous section that the strength and modulus enhancement brought by provision of rock bolts varies in systematic manner. For both strength as well as modulus, the trend with joint orientation (θ) was similar. This observation makes it prudent to explore a possibility between strength and modulus values of unreinforced and reinforced rocks. In an earlier study conducted by Singh and Rao (2005), similar successful attempt was made for jointed rocks. Singh (1997) conducted large number of tests on specimens of a jointed mass. The jointed specimens were prepared out of a synthetic rock and various configurations of joints were used (Singh, 1997; Singh et al., 2002). The tests were conducted under uniaxial loading condition and the uniaxial compressive strength (σ_{cj}) and the tangent modulus (E_{t50}) of the specimens were obtained. Four types of failure modes i.e. splitting,

shearing, sliding and rotation were observed during the study. The results, obtained were plotted on Deere-Miller (1966) classification chart (Fig.6.6).
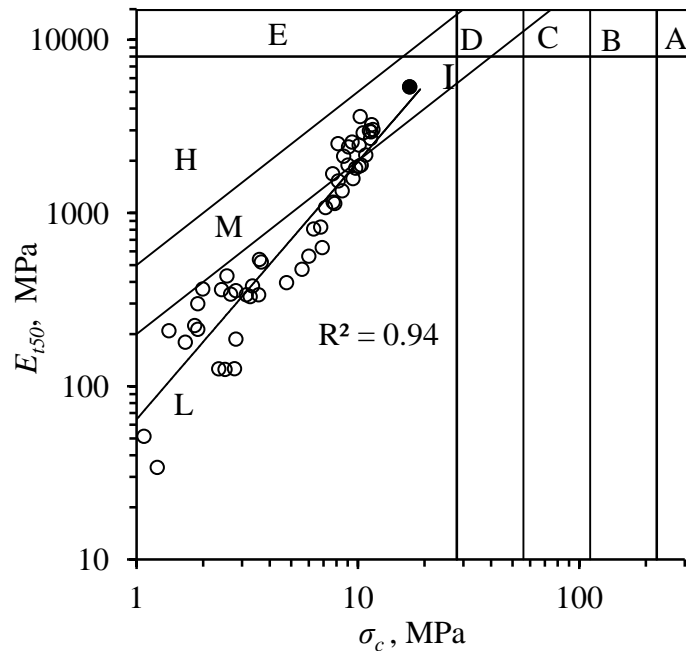
Fig.6.6 Results of tests conducted by Singh (1997) on Deere-Miller classification chart

It was observed that the points representing jointed rock were scattered around an empirical line, which started from intact rock position I. This infers that when a rock is intersected by a joint, it becomes weaker and the extent of weakness brought into strength and modulus are linked with each other. The gradient of this empirical line was used (Singh and Rao, 2005) to suggest correlation between the strength reduction and modulus reduction of the rock as given below:

Gradient of the line = log (E_j/E_i)/ log $(\sigma_{cj}/\sigma_{ci})$

$$\Rightarrow \qquad \frac{\sigma_{cj}}{\sigma_{ci}} = \left[\frac{E_j}{E_i}\right]^{1/Gradient} \tag{6.3a}$$

or   SRF = (MRF)^n (6.3b)

where, SRF = Strength Reduction Factor = σ_{cj}/σ_{ci}; MRF = Modulus Reduction Factor = E_j/E_i; σ_{cj} and σ_{ci} = UCS of jointed and intact rock respectively; E_j and E_i = modulus values of jointed and intact rock respectively.

$$n = \frac{1}{Gradient\ of\ the\ empirical\ line}$$

= 0.56 for Splitting and Shearing

= 0.66 for Sliding

= 0.72 for Rotation

= 0.63 when data points of all modes are used.

To explore relationship between the strength and the modulus values of reinforced rocks, the results obtained from UCS tests have been plotted on Deere-Miller (1966) classification chart. The results for intact, unreinforced jointed and reinforced jointed rocks are plotted in Figs.6.7. The positions of intact rock are shown by letter I_{cy} (uniaxial strength of cylindrical intact rock specimens) and I_B (uniaxial strength of prismatic intact specimens).
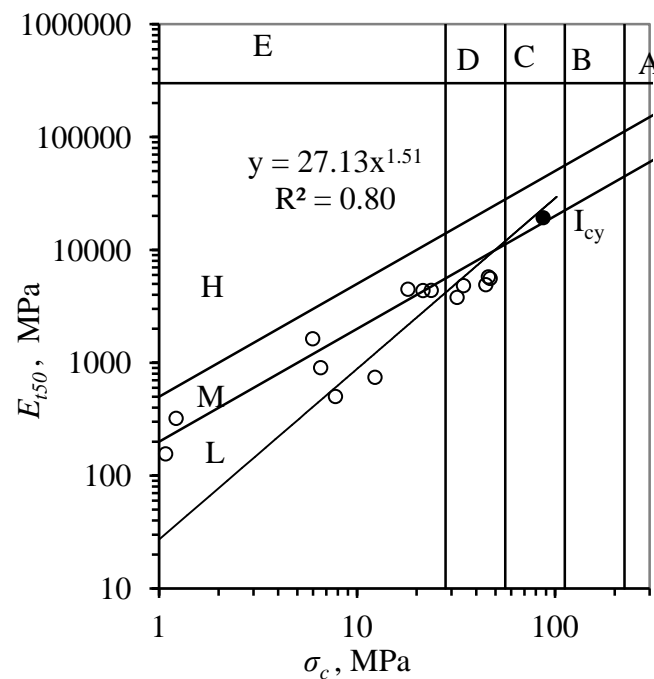
Fig.6.7a UCS test results of natural rock specimens (NRC) on Deere-Miller classification chart
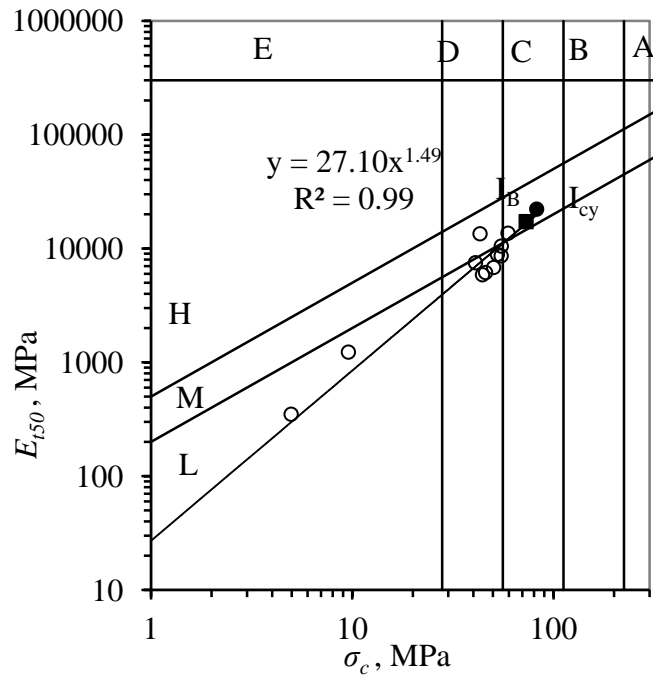
Fig.6.7b UCS test results of synthetic rock specimens (T2) on Deere-Miller classification chart
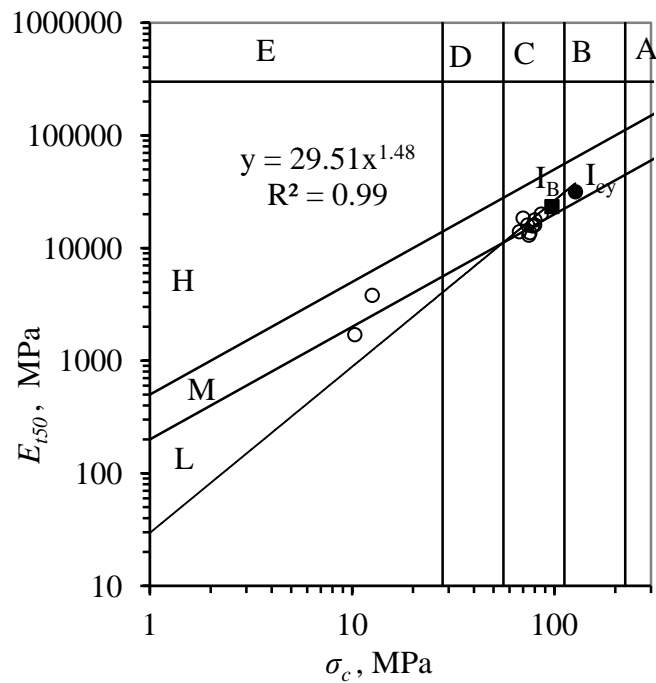
Fig.6.7c UCS test results of synthetic rock specimens (T23) on Deere-Miller classification chart

202

It is observed that the data points representing jointed rock (both unreinforced and reinforced) lie around a best fitting empirical line starting from intact rock position (I_{cy} or I_B). It is also interesting to see in Fig.6.7b and 6.7c that the points representing the intact specimens of prismatic and cylindrical shapes also lie around the same line. The gradient of the best fitting empirical line can be used to correlate the strength and modulus of unreinforced and reinforced jointed rocks to the strength and modulus of intact rock. The gradient of line is expressed as

$$Gradient\ of\ line = \frac{\log E_i - \log E_{ju}}{\log \sigma_{ci} - \log \sigma_{cju}} = \frac{\log E_i - \log E_{jr}}{\log \sigma_{ci} - \log \sigma_{cjr}} \tag{6.4}$$

where σ_{ci} and E_i = uniaxial compressive strength and modulus of intact rock; σ_{cju} and E_{ju} = uniaxial compressive strength and modulus of unreinforced jointed rock; σ_{jr} and E_{jr} = uniaxial compressive strength and modulus of reinforced jointed rock. Using the gradient of the best fitting line, the strength of unreinforced and reinforced jointed rock can be obtained by following expressions

$$\frac{\sigma_{cju}}{\sigma_{ci}} = \left[\frac{E_{ju}}{E_i} \right]^{1/\,Gradient\ of\ line} \tag{6.5}$$

$$\frac{\sigma_{cjr}}{\sigma_{ci}} = \left[\frac{E_{jr}}{E_i} \right]^{1/\,Gradient\ of\ line} \tag{6.6}$$

From Figs.6.7, the gradient of best fitting empirical line for three rock types is obtained as 1.51, 1.49, and 1.48 respectively. The gradients of the best fitting empirical lines are almost identical and an average value of 1.49 has been adopted for the gradient. Using equations 6.5 and 6.6, the strength reduction factor may be obtained as

$$\frac{\sigma_{cju}}{\sigma_{ci}} = \left[\frac{E_{ju}}{E_i} \right]^{1/1.49} = \left[\frac{E_{ju}}{E_i} \right]^{0.67} \tag{6.7a}$$

$$\Rightarrow (SRF)_u = (MRF)_u^{0.67} \tag{6.7b}$$

$$\frac{\sigma_{cjr}}{\sigma_{ci}} = \left[\frac{E_{jr}}{E_i}\right]^{1/1.49} = \left[\frac{E_{jr}}{E_i}\right]^{0.67} \tag{6.8a}$$

$$\Rightarrow (SRF)_r = (MRF)_r^{0.67} \tag{6.8b}$$

The above correlation is almost same as obtained by Singh and Rao (2005). The above expression may be used for estimation of the strength of jointed rock for unreinforced and reinforced conditions using intact rock strength and modulus. It will be shown later that the results obtained are expected to be free from scale effect.

6.6 VALIDATION OF THE PROPOSED CORRELATION THROUGH CRITICAL STRAIN CONCEPT

Sakurai (1983, 1997) compiled large number of laboratory and field test data and suggested critical strain concept for soils and rocks. The critical strain (ε_o) of laboratory specimens of a rock is expressed as:

$$\varepsilon_o = \frac{\sigma_{ci}}{E} \tag{6.9}$$

where σ_{ci} is the uniaxial compressive strength and E is the Young's modulus. The data from Sakurai (1983) has been re-plotted in Fig.6.8. The upper and lower bound as obtained by Sakurai (1983) are also shown in the figure. It is observed that the critical stain decrease with increase in uniaxial compressive strength and the relationship shown in the plot can be used to develop correlation between critical stain, UCS of the intact rock and the UCS of rock mass. It was also stated by Sakurai (1997) that critical strain concept can be used without considering the scale effect.

The critical strain was calculated for natural and synthetic rock specimens tested in present study. The plot of critical strain (ε_o) vs uniaxial compressive strength (σ_c) for combined data of all intact, unreinforced-jointed and reinforced-jointed specimens is presented in Fig.6.9. The ranges of critical strain zone obtained by Sakurai (1983) are also shown in the plot. It is observed that the majority of critical stain values calculated from laboratory uniaxial tests in the present study lie within the critical strain zone observed by Sakurai (1983).
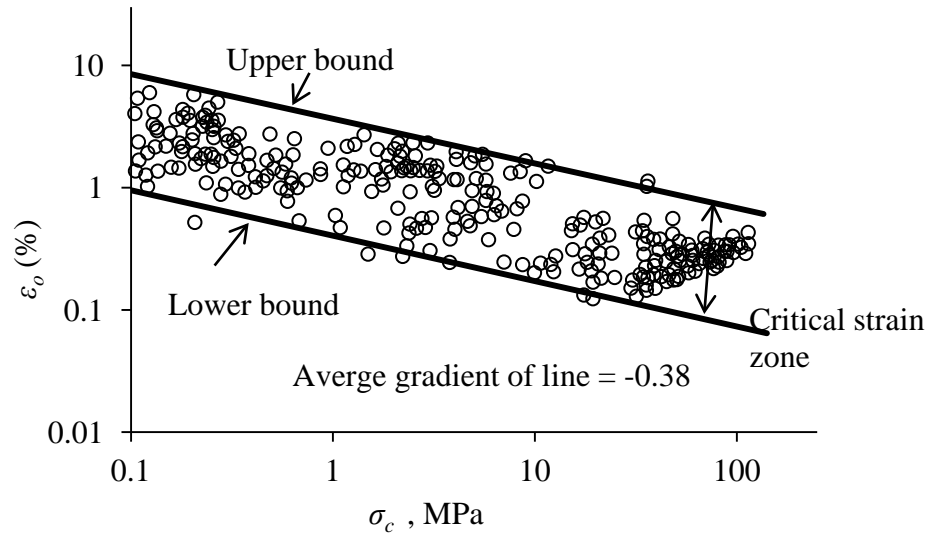
Fig.6.8 Plot of critical strain (ε_o) with uniaxial compressive strength (σ_c)
(After Sakurai, 1983)

Using data compiled by Sakurai (1983), the average gradient of strain zone can be obtained from Fig.6.8, and the same could be used to define critical strains for reinforced rocks. Considering ε_{oi}, ε_{0ju}, ε_{0jr} to be the critical strain of intact, unreinforced jointed and reinforced jointed rock, the average gradient of critical strain zone is obtained as:

$$Gradient\ of\ critical\ strain\ zone\ (G) = \frac{\log \varepsilon_{0ju} - \log \varepsilon_{0i}}{\log \sigma_{cju} - \log \sigma_{ci}} = \frac{\log \varepsilon_{0jr} - \log \varepsilon_{0i}}{\log \sigma_{cjr} - \log \sigma_{ci}} \qquad (6.10)$$

Expressing critical strain as ratio of UCS and modulus of respective rock

$$G = \frac{\log\left(\frac{\sigma_{cju}}{E_{ju}}\right) - \log\left(\frac{\sigma_{ci}}{E_i}\right)}{\log \sigma_{cju} - \log \sigma_{ci}} = \frac{\log\left(\frac{\sigma_{cjr}}{E_{jr}}\right) - \log\left(\frac{\sigma_{ci}}{E_i}\right)}{\log \sigma_{cjr} - \log \sigma_{ci}} \qquad (6.11)$$

where σ_{ci} and E_i = uniaxial compressive strength and modulus of intact rock; σ_{cju} and E_{ju} = uniaxial compressive strength and modulus of unreinforced jointed rock; σ_{jr} and E_{jr} = uniaxial compressive strength and modulus of reinforced jointed rock. From equation 6.11 the following correlations can be obtained

$$\Rightarrow \frac{\sigma_{cju}}{\sigma_{ci}} = \left[\frac{E_{ju}}{E_i}\right]^{1/(1-G)} \qquad (6.12)$$

205
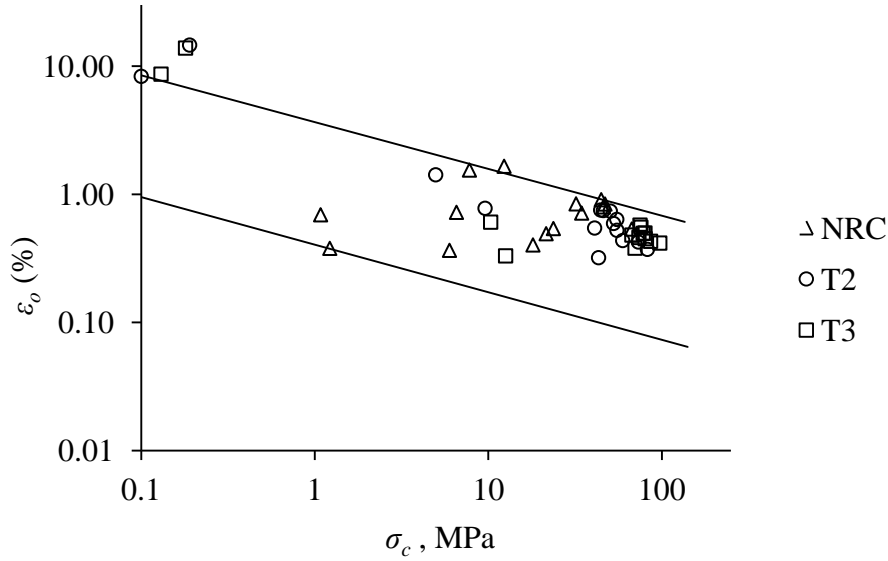
Fig.6.9 Plot of critical strain (ε_o) with uniaxial compressive strength (σ_c) for natural rock and synthetic rocks

and $\quad \dfrac{\sigma_{cjr}}{\sigma_{ci}} = \left[\dfrac{E_{jr}}{E_i}\right]^{1/(1-G)}$ $\hspace{4cm}$ (6.13)

From the plot (Fig.6.8), the average gradient of critical strain zone is observed to be about 0.38. Putting the value of gradient in equations 6.12 and 6.13 the following expressions are obtained

$$\frac{\sigma_{cju}}{\sigma_{ci}} = \left[\frac{E_{ju}}{E_i}\right]^{1/(1+0.38)} = \left[\frac{E_{ju}}{E_i}\right]^{0.72} \hspace{3cm} (6.14)$$

$$\frac{\sigma_{cjr}}{\sigma_{ci}} = \left[\frac{E_{jr}}{E_i}\right]^{1/(1+0.38)} = \left[\frac{E_{jr}}{E_i}\right]^{0.72} \hspace{3cm} (6.15)$$

The above expressions are almost identical to the correlations (equation 6.7a and 6.8a) developed in the present study. It may be noted that the equations 6 and 7 were developed through Deere-Miller classification chart by using experimental data generated in the present study; whereas the equations 6.14 and 6.15 have been developed by using independent data from Sakurai (1983) through critical stain

206

concept. The convergence of both the approaches (Deere-Miller and critical strain concept) to almost identical correlations validates the universal applicability of both the approaches. Therefore, the correlations developed in the present study can be used with confidence in design. Further, as stated by Sakurai (1997) the results obtained for critical strain concept are free from scale effect, it is envisaged that the correlations obtained from the present study should also be scale free. The proposed correlations (equation 6.7a and 6.8a) can be used in the field to find out the strength of rock bolt reinforced rock mass if the values of E_{ju}, and E_{jr} are known. The modulus of unreinforced mass (E_{ju}) can be estimated through uniaxial jacking tests (IS: 7317, 1974). In case of reinforced mass, the uniaxial jacking tests may not be feasible and back analysis of observed deformations can provide a good estimate of the modulus of reinforced rock. An example from the field is considered below to demonstrate the applicability of the proposed correlations.

6.7 EXAMPLE APPLICATION

A highway tunneling project named Chenani-Nashri project is under construction in the state of Jammu & Kashmir in India (Dwivedi, 2014). The rocks exposed at the site are sandstone, siltstone, and claystone with alternate bands. Rocks are heavily jointed having GSI ranging between 45-55 and instability is expected in structure. The height of overburden at tunnel crown is almost 87 m. The properties of rocks and rock masses are listed in Table 6.1. A section of the tunnel is shown in Fig.6.10a. The equivalent diameter of the opening is 6 m. Monitoring of displacements is being done at the site through instrumentation techniques. It is expected that in some sections, squeezing may occur and there is a need to reinforce the rock mass. Four meter long and 25 mm diameter bolts have been proposed with 1.5 m c/c spacing. The points where displacements are being measured is shown in Fig.6.10b.

Table 6.1 Rock mass properties at project site (Dwivedi, 2014)

S.No.	Properties	Rock type		
		Sandstone	**siltstone**	**claystone**
1	Unit weight (γ , kN/m^3)	27	26	26
2	UCS Intact (σ_{ci} , MPa)	50	45	20
3	Modulus Intact (Ei , MPa)	15000	10000	5000
4	Rock mass Modulus (E_{ju} ,MPa)	2625	1750	875
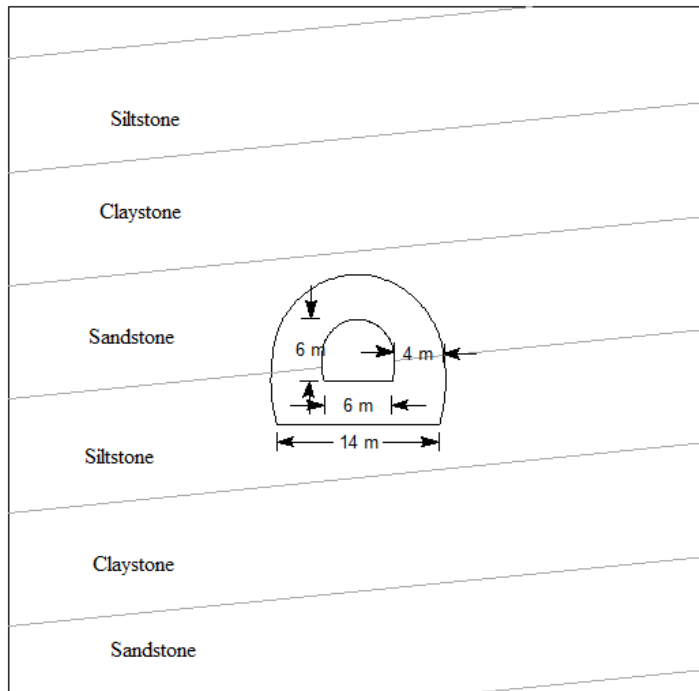
Fig.6.10 A Cross section of tunnel (after Dwivedi, 2014)
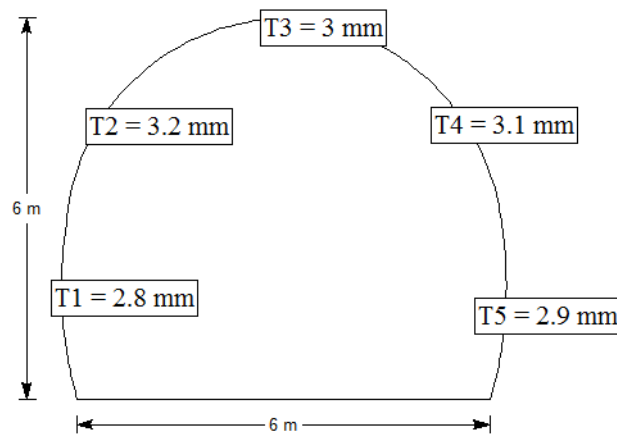
Fig.6.10b Observation points and measured displacement (after Dwivedi, 2014)

To analyse the section for different stress states due to varying overburden, the rock mass properties are required for both the unreinforced and reinforced cases. The project authorities have estimated the rock mass properties (unreinforced) using empirical approaches as given in Table 6.1. In the following section, it is shown how the strength of reinforced rocks can be estimated. The approach is based on back analysis of observed deformations of reinforced mass as suggested by Sakurai (1983). To carry out back analysis, the tunnel is analysed assuming elastic behaviour. A software package has been used which is based on finite element method. Sakurai (1983) has recommended that an equivalent continuum should be assumed in the zone where bolts are installed (Fig.6.10c). The modulus of the continuum should represent both the jointed rock and the bolts. The thickness of this equivalent continuum zone has been taken equal to the length of the bolt.
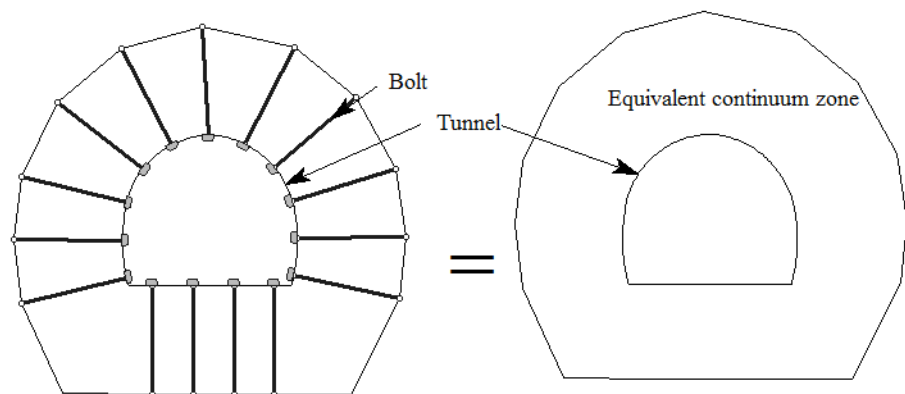
Fig.6.10c Equivalent continuum zone around tunnel periphery

A trial value of the modulus of the continuum is considered and elastic analysis is done to obtain the deformations at points T1, T2, T3, T4, and T5 respectively. In first trial, the modulus of the continuum zone was assumed to be the same as that of unreinforced rock mass, E_{ju}. The displacements obtained from the

analysis $u_i{}^c$, were compared with measured field displacements $u_i{}^m$ and following error function (ϵ) was calculated.

$$\epsilon = \sqrt{\Sigma_i^N (u_i^c - u_i^m)^2} \qquad (6.16)$$

where N is the numbers of the data points. In second trial, a small increment (about 5%) is given to the modulus values used in the first trial and the error function is calculated. The analysis was repeated a number of times and a plot of modulus vs error function was prepared (Fig.6.11).
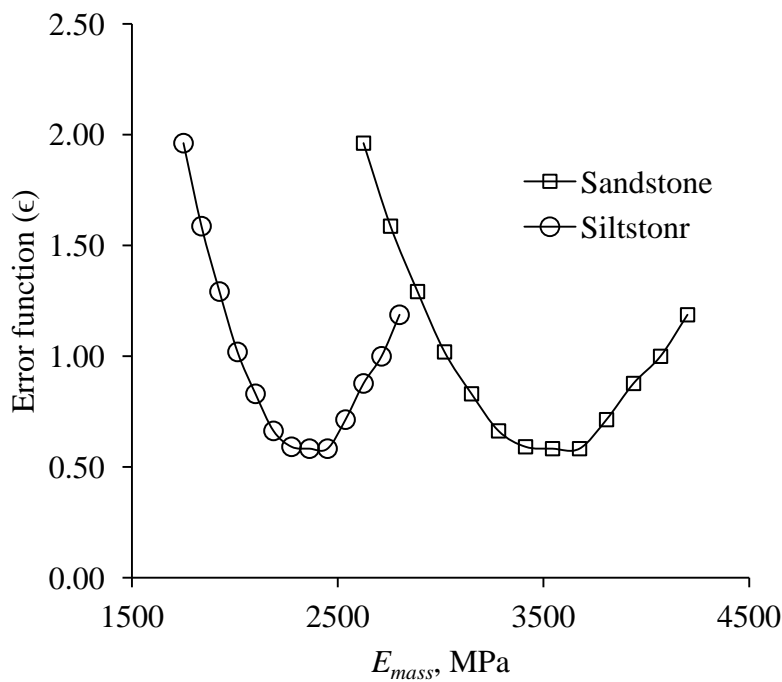
Fig.6.11Variation of error function with assumed modulus

The modulus values corresponding to the minimum error function were considered for reinforced rock. The modulus of reinforced rock corresponding to minimum value of error function is found to be 3500 and 2450 MPa for sandstone and siltstone respectively (Fig. 6.11). These values are used to assess the UCS of reinforced mass as given below

(i) Sandstone

$$\sigma_{cjr} = \sigma_{ci} \left[\frac{E_{jr}}{E_i} \right]^{0.67} = 50 \times \left[\frac{3500}{15000} \right]^{0.67} = 18.85 \text{ MPa}$$

(ii) Siltstone

$$\sigma_{cjr} = \sigma_{ci} \left[\frac{E_{jr}}{E_i} \right]^{0.67} = 45 \times \left[\frac{2450}{10000} \right]^{0.67} = 17.54 \text{ MPa}$$

The above strength value can be used to analyse the section for different stress states for the proposed reinforcement to carry further analysis.

6.8 CONCLUDING REMARKS

Results obtained from uniaxial compression tests on intact, unreinforced jointed and reinforced jointed natural and synthetic rocks were analysed in this chapter. The test results were obtained in the form of uniaxial compression strength and tangent modulus. The provision of passive bolts has been found to change the failure mode of jointed specimens and enhance strength due to improved interlocking. For critical joint conditions (θ= 45° and 60°), the enhancement in strength and modulus is found to be much higher as compared to the other joint orientations. The results, when plotted on Deere-Miller classification chart are found to be scattered around an empirical line, which starts from the intact rock position. The gradient of this empirical line helps in developing a correlation between the strength reduction factor and the modulus reduction factor of reinforced rock. Sakurai's critical stain concept was also used to find correlation between SRF and MRF for jointed rocks by using Sakurai's data. It was observed that the correlations developed in the present investigation are almost identical to what is observed for Sakurai's data. To apply correlations developed in the present study, the modulus of the reinforced rock will be required. It is suggested that deformations may be measured in the field and back analysis be done to get the optimal value of the modulus. Using modulus of the reinforced rock, strength of the reinforced mass can be obtained which can be used in the further analysis.

TRIAXIAL STRENGTH OF REINFORCED JOINTED ROCKS

7.1 GENERAL

Triaxial tests were conducted on jointed cylindrical specimens of natural rock at confining stress level of 0, 5, 20 and 40 MPa respectively. The joint orientation ($\theta°$) for theses specimens varied from 0° to 70° with respect to the base of the specimens. The passive bolt was installed perpendicular to axis of specimens. The detail results of triaxial tests have been discussed in the previous chapter. The present chapter deals with the analysis of results obtained from the triaxial tests. The outcome of the analysis is applicable in such conditions where analysis is done in σ_1, σ_3 space like underground openings. Stress conditions in the field may vary from almost uniaxial loading condition to very high confining pressure range ($\sigma_3 \gg 0$). In such situations, an appropriate strength criterion e.g. Hoek and Brown (1980), Ramamurthy (1993, 2001), Singh and Singh (2012) may be used to assess the strength of unreinforced jointed rock subjected to given σ_3 value. For designing optimal amount of reinforcement, it is essential that the strength enhancement for given σ_3 be assessed. Therefore, a strength criterion is needed for reinforced rock. In this chapter, an attempt has made to predict the strength of reinforced rock at a given σ_3 through a suitable criterion.

7.2 STRENGTH BEHAVIOUR

The variation of strength (σ_1) with confining stress (σ_3) for intact, unreinforced jointed and reinforced jointed rocks tested in this study is plotted in Figs.7.1a, through 7.1d. In general, an increase in confining pressure results in increase of strength (σ_1). The variation of σ_1 with σ_3 is found to be non-linear for all the cases investigated in present study. The installation of bolt increases the strength of jointed rocks at all confining stress levels. For each orientation of the joint, the

strength of reinforced rock has been found to lie between the strength of intact and unreinforced jointed rock. The application of bolt restricts sliding along the joint plane and hence induces interlocking in the joint. Development of tensile stress in the bolt generates additional resistance against sliding due to enhanced normal stress. Due to these reasons, the strength of reinforced rock is greater than the strength of unreinforced rock at each confining pressure.
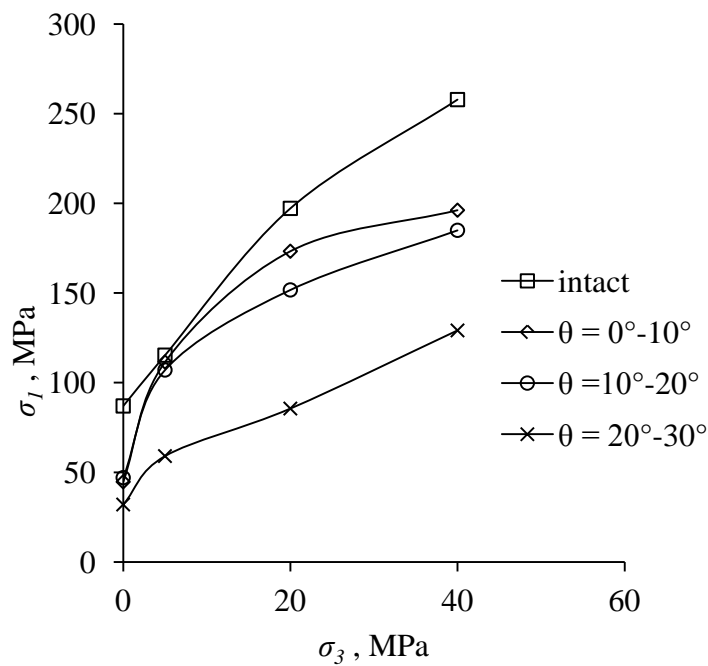
Fig.7.1a Variation of σ_1 with σ_3 for intact and unreinforced rock at $\theta = 0°\text{-}10°$, $\theta = 10°\text{-}20°$, $\theta = 20°\text{-}30°$
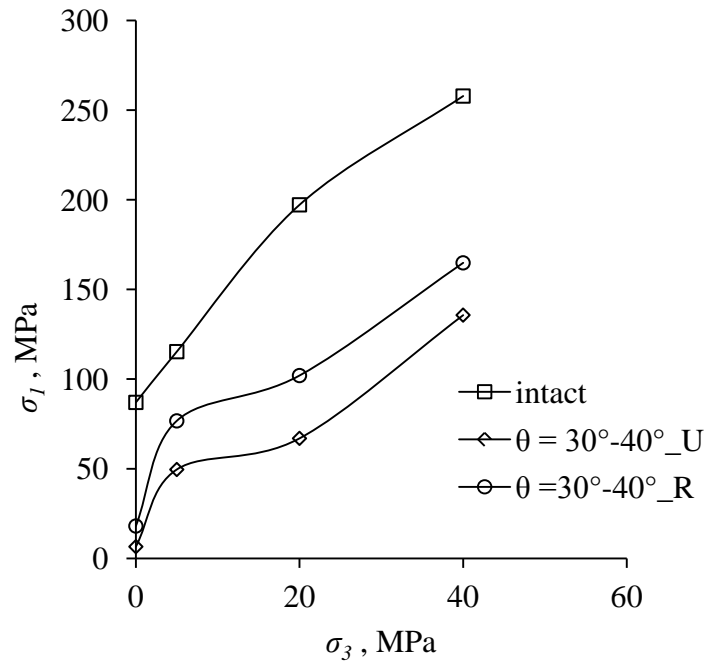
Fig.7.1b Variation of σ_1 with σ_3 for intact, unreinforced and reinforced jointed rocks at $\theta = 30°\text{-}40°$
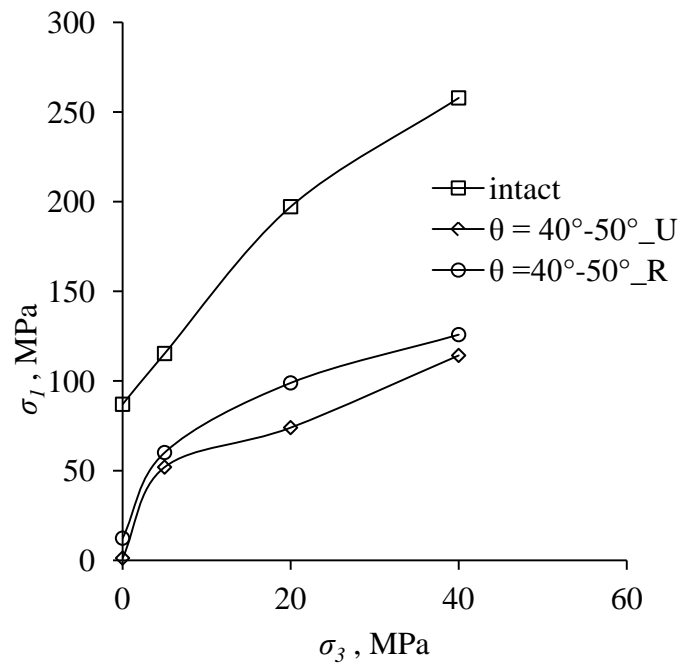
Fig.7.1c Variation of σ_1 with σ_3 for intact, unreinforced and reinforced jointed rocks at $\theta = 40°\text{-}50°$
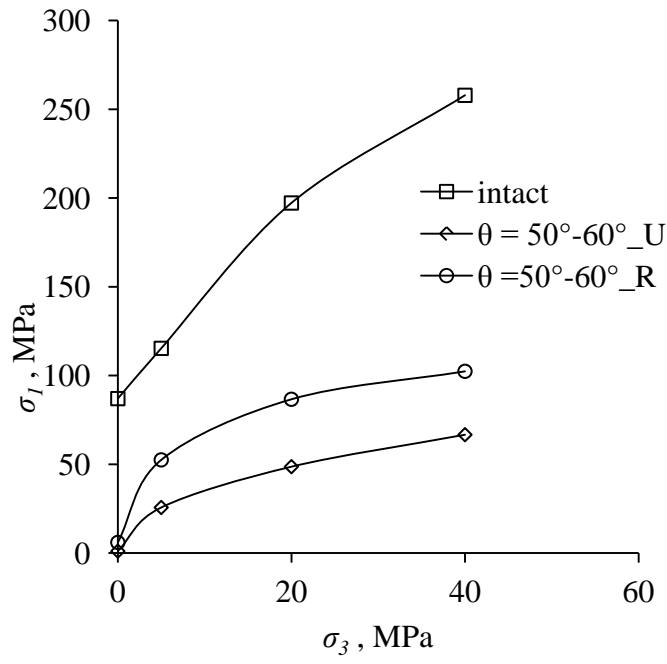
Fig.7.1d Variation of σ_1 with σ_3 for intact, unreinforced and reinforced jointed rocks at θ = 50°-60°
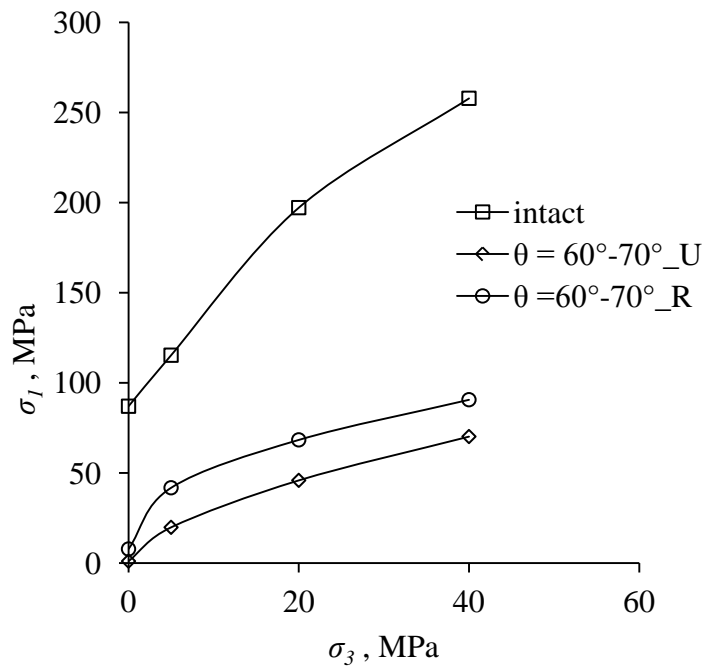
Fig.7.1e Variation with σ_1 vs σ_3 for intact, unreinforced and reinforced jointed rocks at θ = 60°-70°

7.3 ANISOTROPY IN STRENGTH BEHAVIOUR

The strength behaviour of unreinforced as well as reinforced rock has been found to be anisotropic. The anisotropy in strength behaviour is shown by plotting variation of σ_1 with joint orientation ($\theta°$) at different confining stress levels (Figs.7.2a, 7.2b, 7.2c, and 7.2d). For unreinforced specimens ($\sigma_3 = 0.0$ MPa), the strength decreases with increase in θ, reaches a minimum at about $\theta = 45°$ and remains low with further increase in θ. Due to provision of reinforcement, the mode of failure changes and enhancement occurs in strength. The behaviour still remains anisotropic. The strength decreases with increase in θ, reaches a minimum at about $\theta = 55°$ and increases with further increase in θ. For triaxial cases ($\sigma_3 = 5, 20$ and 40 MPa), the strength of unreinforced jointed rock becomes minimum between $\theta = 40°$ - 70°. The strength of reinforced rock has been found to be decreasing with increasing θ and approaching respective minimum values near $\theta = 55°$ - 65°. As natural specimens with $\theta = 90°$ were not available, the trend of strength for θ more than 65° could not be examined.
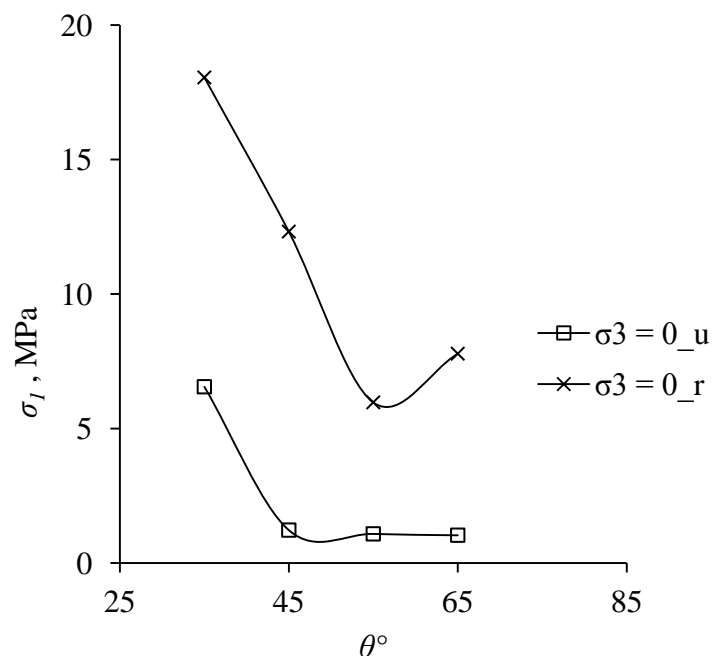
Fig.7.2a Variation of failure stress (σ_1) with joint orientation ($\theta°$) at $\sigma_3 = 0.0$ MPa

217
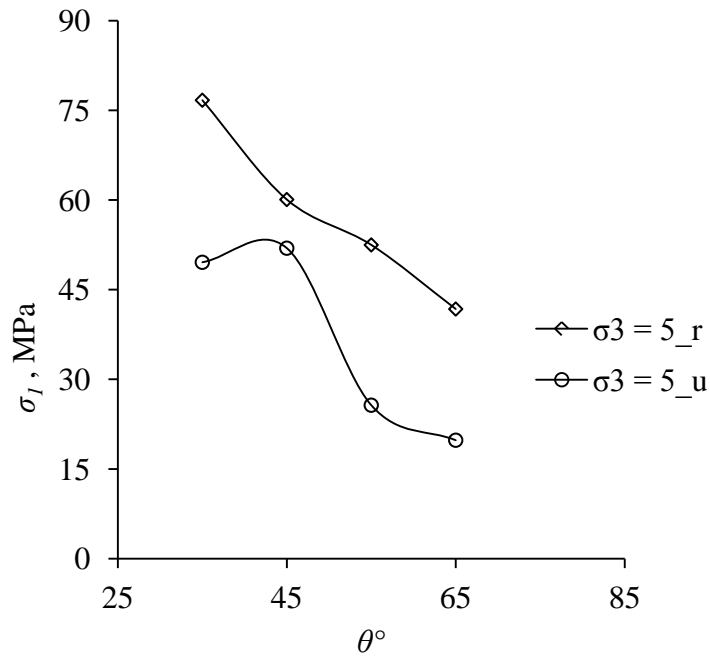
Fig.7.2b Variation of failure stress (σ_1) with joint orientation ($\theta°$) at $\sigma_3 = 5.0$ MPa
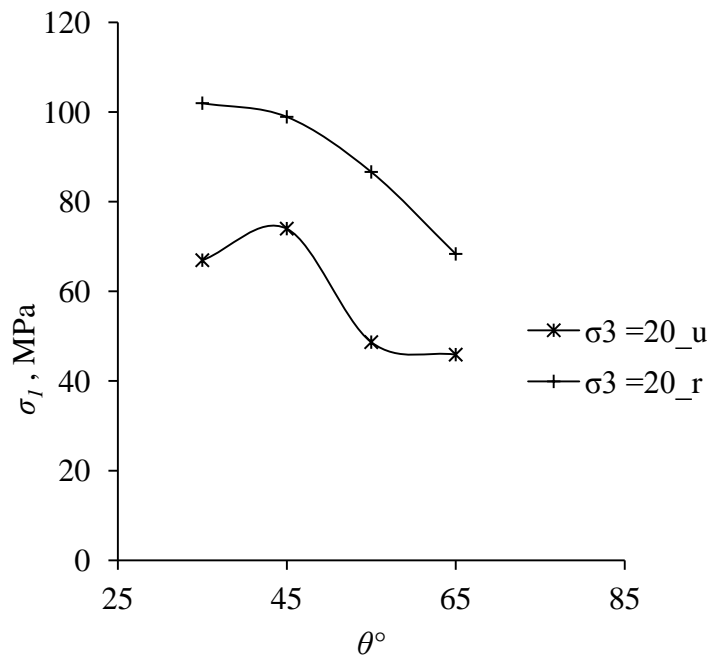
Fig.7.2c Variation of failure stress (σ_1) with joint orientation ($\theta°$) at $\sigma_3 = 20.0$ MPa

218
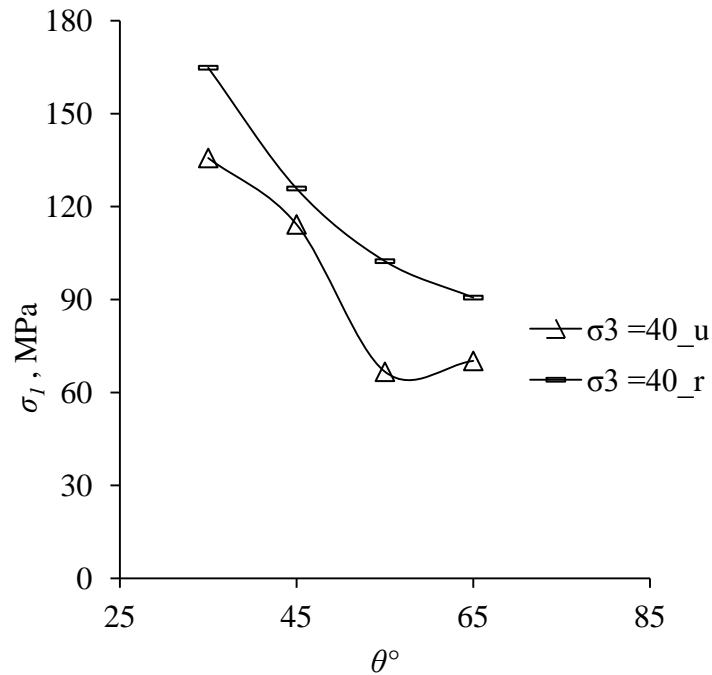
Fig.7.2d Variation of failure stress (σ_1) with joint orientation ($\theta°$) at σ_3 = 40.0 MPa

The index anisotropy ratio (AR) can be utilised to represent the extent of anisotropy (Ramamurthy, 1993). Ideally all possible orientations including $\theta = 0°$ and 90° should have been represented, however, in present case the practical limitations are that natural joints were not available for $\theta = 90°$. For calculation of anisotropy ratio, only those orientations have been considered for which the bolt were installed ($\theta = 30°$ to 70°). The variation of anisotropy ratio with confining pressure for unreinforced (AR_U) and reinforced rock (AR_R) is plotted in Fig.7.3. For unreinforced specimens, the anisotropy ratios at respective confining stress levels (0, 5, 20, and 40) are 6.4, 2.6, 1.6, and 2 respectively. The corresponding anisotropy ratios for reinforced specimens are found to be 3, 1.8, 1.5, and 1.8 respectively. For unreinforced specimens the anisotropy ratio is high and as confining pressure increases, the anisotropy ratio decreases. For 0, 5.0, 20 and 40 MPa of confining stress levels, the percent reduction in anisotropy ratio is found to be 52, 30, 7, and 10% respectively. This indicates that the provision of bolt reduces the anisotropy ratio at all confining stress levels. The anisotropy ratio for unreinforced and reinforced specimens decreases with increase in confining pressure (Fig.7.3). At higher

confining pressure, the anisotropy ratio for unreinforced and reinforced cases becomes almost identical. This indicates that an increase in confining pressure results in reduction in bolt contribution towards strength enlacement.
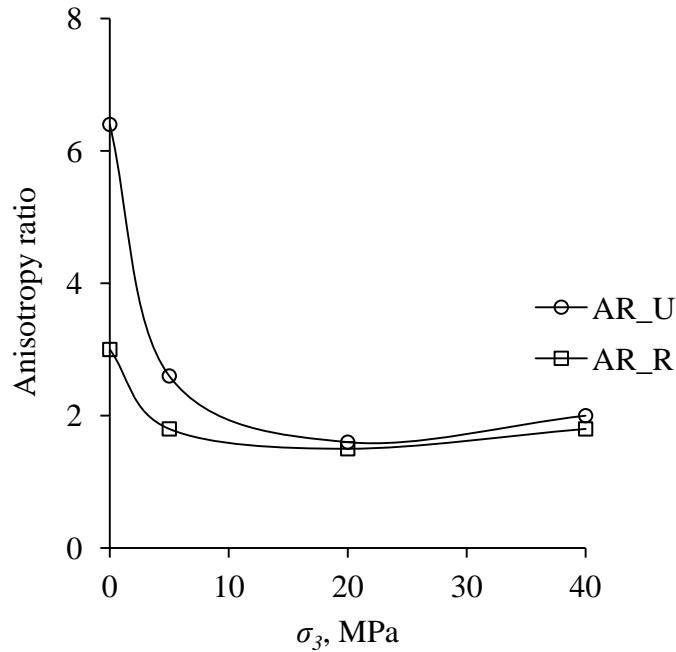
Fig.7.3 Variation of anisotropy ratio with confining pressure (σ_3) for unreinforced and reinforced rock

7.4 STRENGTH ENHANCEMENT DUE TO BOLT

As discussed earlier, the strength of jointed rock is enhanced due to provision of rock bolt. The percent strength enhancement (*SE*) due to bolt at given confining pressure σ_3, is computed as

$$SE = \left(\frac{\sigma_{1r}-\sigma_{1u}}{\sigma_{1u}}\right) \times 100 \text{ \%}$$

(7.1)

where σ_{1u} = strength of reinforced jointed rock, and σ_{1r} = strength of reinforced jointed rock. The percent strength enhancement (*SE*) obtained at all confining stress levels is presented in Table.7.1. The variations of *SE* with σ_3 at different θ are plotted in Fig.7.4a. It is observed that an increase in confining pressure results in reduction in the strength enhancement (*SE*) at all the joint orientations. Minimum strength enhancement has been observed for the maximum confining stress level ($\sigma_3 = 40$ MPa). For unconfined specimens, the joint orientations $\theta =30°\text{-}40°$, $40°\text{-}50°$, $50°\text{-}60°$,

220

and 60°-70° exhibit maximum strength enhancement due to reinforcement. The reason for this is change in failure mode due to provision of reinforcement. Sliding mode that prevailed for theses joint orientations was altered to shearing/splitting mode due to reinforcement, which brought in very high strength enhancement.

Strength enhancement also depends on joint orientation. The variation of strength enhancement (SE) with joint orientation ($\theta°$) at different confining stress levels (σ_3) is plotted in Fig.7.4b. The trend of variation is not well defined. The strength enhancement is found to be minimum between $\theta = 40°-50°$ for all the cases except $\sigma_3 = 0$.

Table 7.1 Strength enhancement due (SE) to bolt

σ_3 , MPa	Strength enhancement (SE), %			
	$\theta = 30°\text{-}40°$	$\theta = 40°\text{-}50°$	$\theta = 50°\text{-}60°$	$\theta = 60°\text{-}70°$
0	176	910	453	655
5	55	16	105	111
20	52	34	78	50
40	22	10	54	29
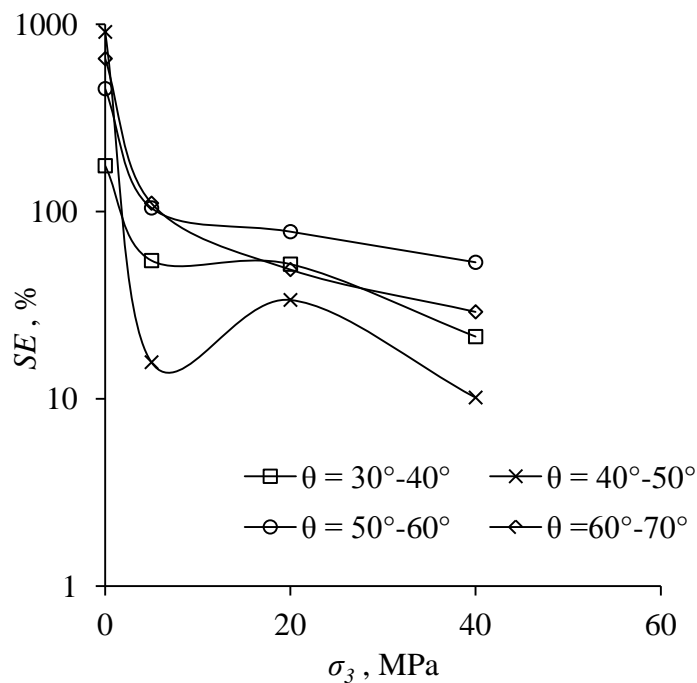
Fig.7.4a Variation of strength enhancement (SE) with confining stress (σ_3) at different joint orientation ($\theta°$)

221
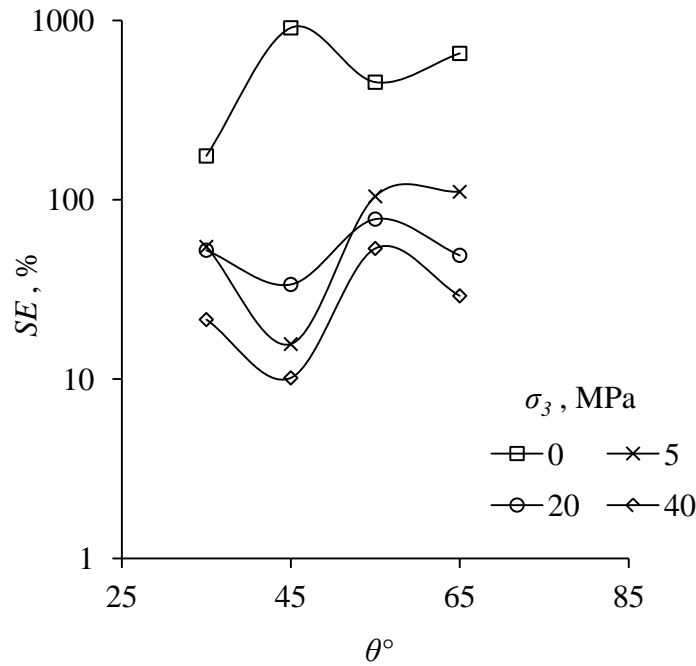
Fig.7.4b Variation of strength enhancement ($\Delta\sigma_1$) with joint orientation ($\theta°$) at different confining stress levels (σ_3)

7.5 MOHR- COULOMB SHEAR STRENGTH PARAMETERS

The Mohr circles plot of intact, jointed unreinforced and jointed reinforced rock specimens are presented in Figs.7.5a through 7.5l. Both linear and non-linear failure envelopes are shown. It is observed that the linear failure envelopes do not really capture the behaviour and the strength behaviour is better represented by non-linear failure envelopes. Scatter in data is also evident which is inherent in natural rocks.

Table 7.2 Mohr – Coulomb shear strength parameters

$\theta°$	Unreinforced rock			Reinforced rock		
	c , MPa	$\phi°$	R^2	c , MPa	$\phi°$	R^2
Intact	22.88	38.44	0.98	-	-	
0-10	20.40	33.31	0.83	-	-	
10-20	20.62	30.73	0.86	-	-	
20-30	13.10	22.90	0.98	-	-	
30-40	5.16	29.16	0.94	10.47	31.91	0.92
40-50	6.47	25.00	0.72	10.19	26.03	0.87
50-60	4.42	12.65	0.90	9.30	21.23	0.80
60-70	2.88	14.21	0.96	7.94	17.66	0.89
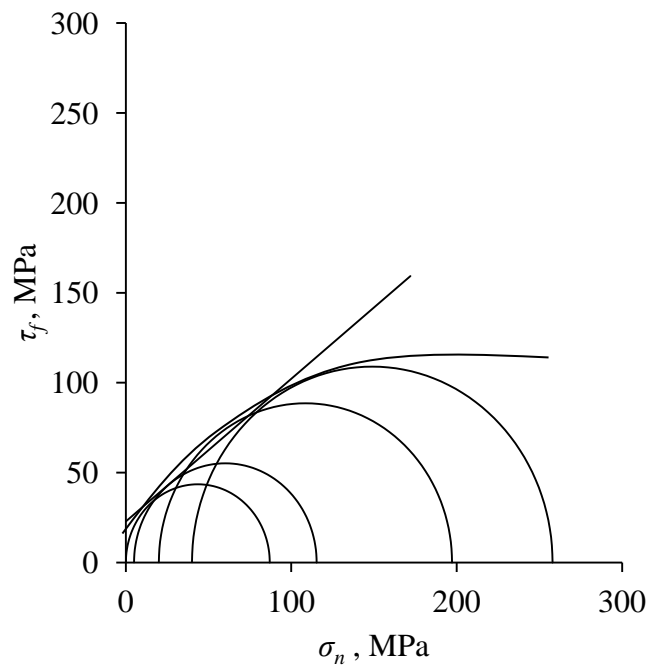
Fig.7.5a Mohr circles at failure for intact rock
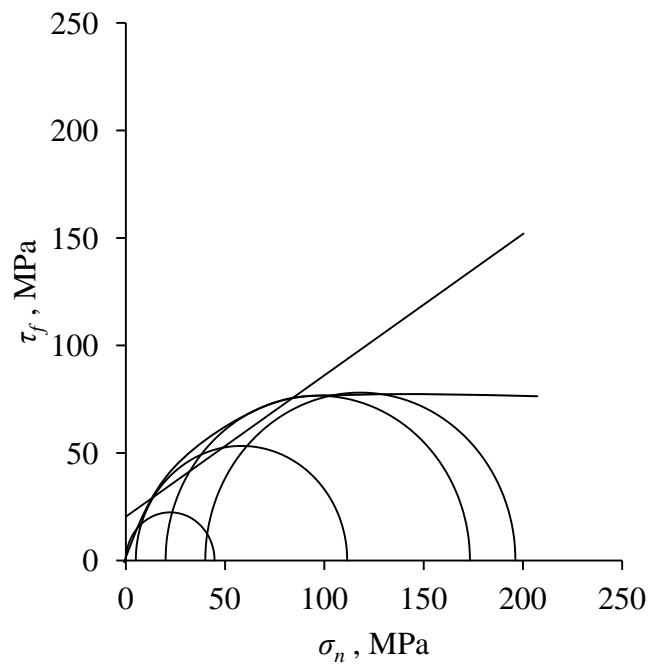
Fig.7.5b Mohr circles at failure for unreinforced jointed rock at $\theta = 0°$-$10°$
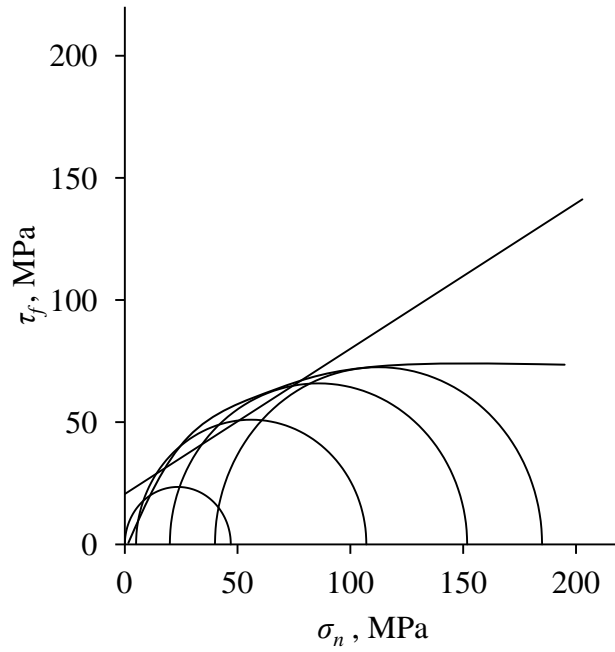
Fig.7.5c Mohr circles at failure for unreinforced jointed rock at $\theta = 10°-20°$
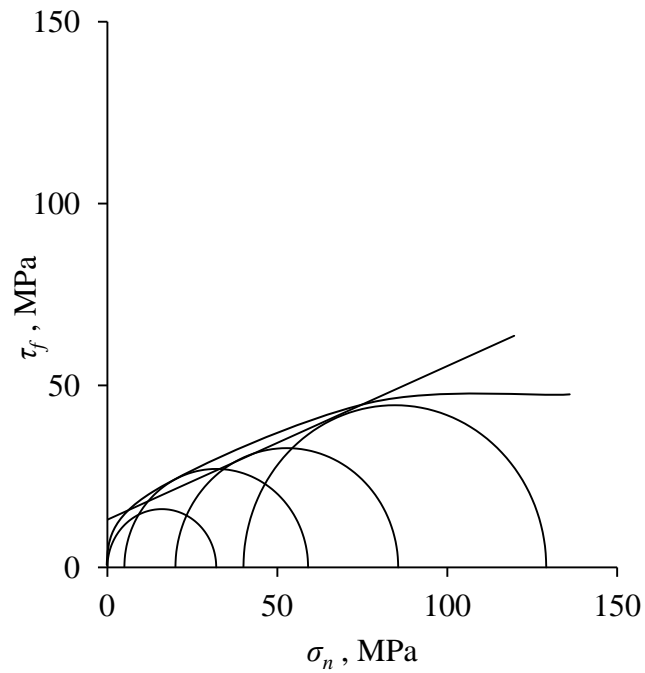
Fig.7.5d Mohr circles at failure for unreinforced jointed rock at $\theta = 20°-30°$
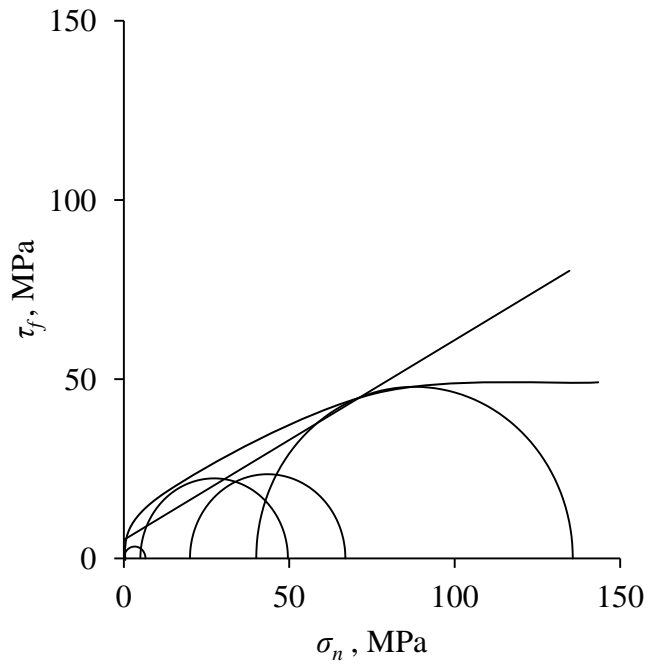
Fig.7.5e Mohr circles at failure for unreinforced jointed rock at $\theta = 30°\text{-}40°$
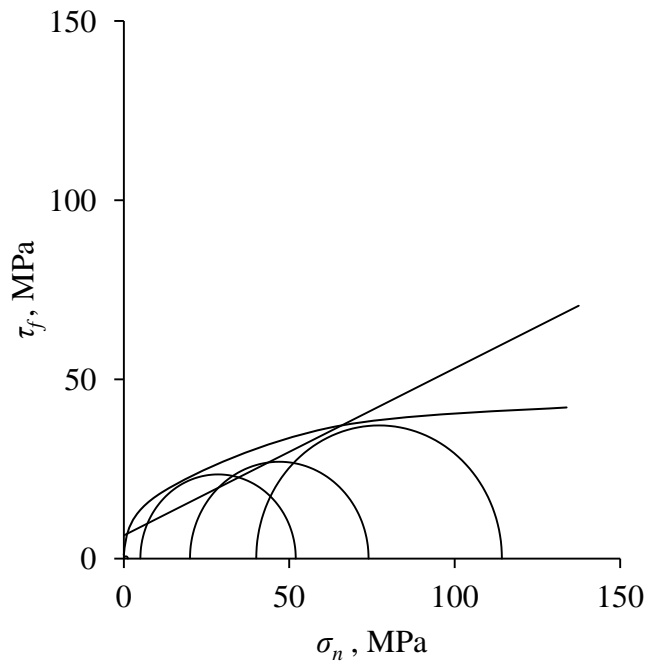
Fig.7.5f Mohr circles at failure for unreinforced jointed rock at $\theta = 40°\text{-}50°$
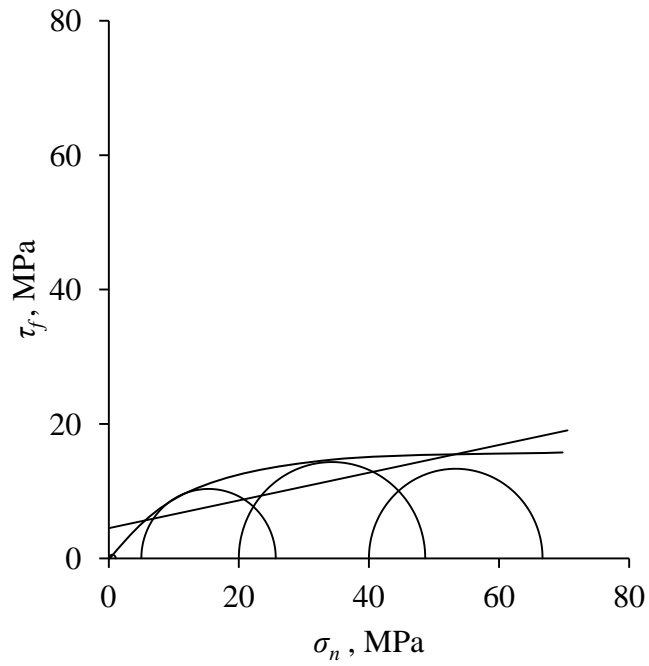
Fig.7.5g Mohr circles at failure for unreinforced jointed rock at θ = 50°-60°
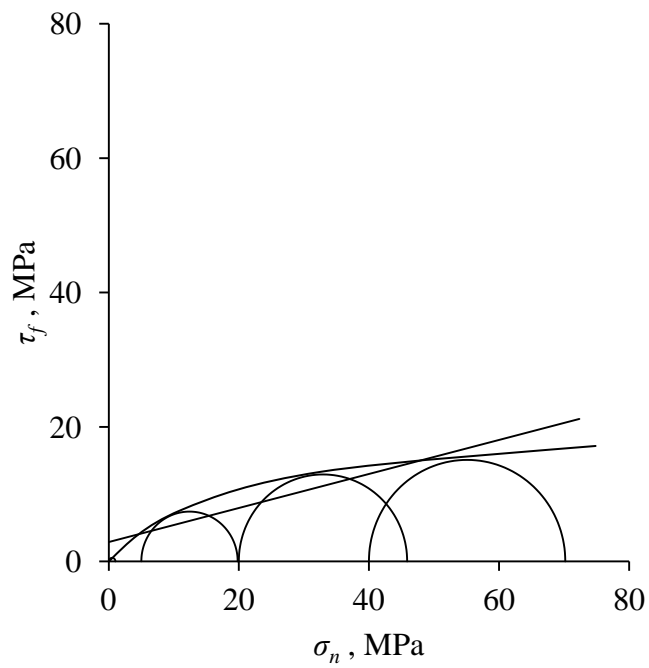
Fig.7.5h Mohr circles at failure for unreinforced jointed rock at θ = 60°-70°

Fig.7.5i Mohr circles at failure for reinforced jointed rock at $\theta = 30°\text{-}40°$
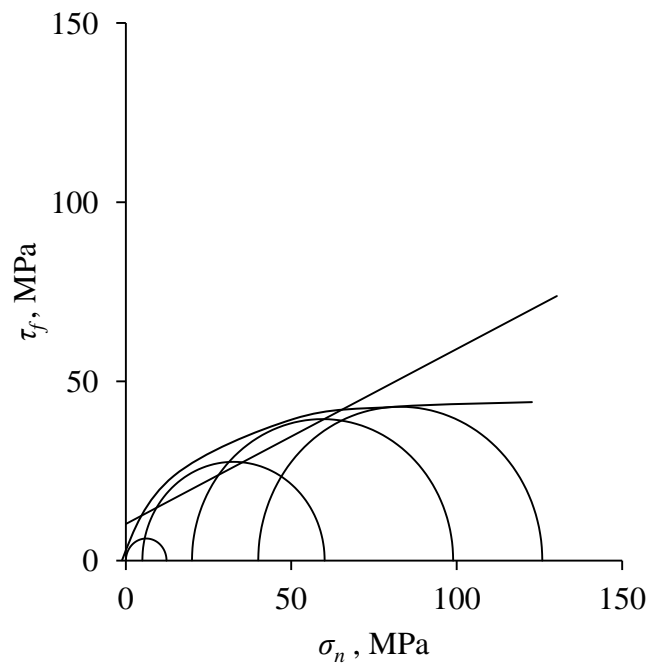
Fig.7.5j Mohr circles at failure for reinforced jointed rock at $\theta = 40°\text{-}50°$
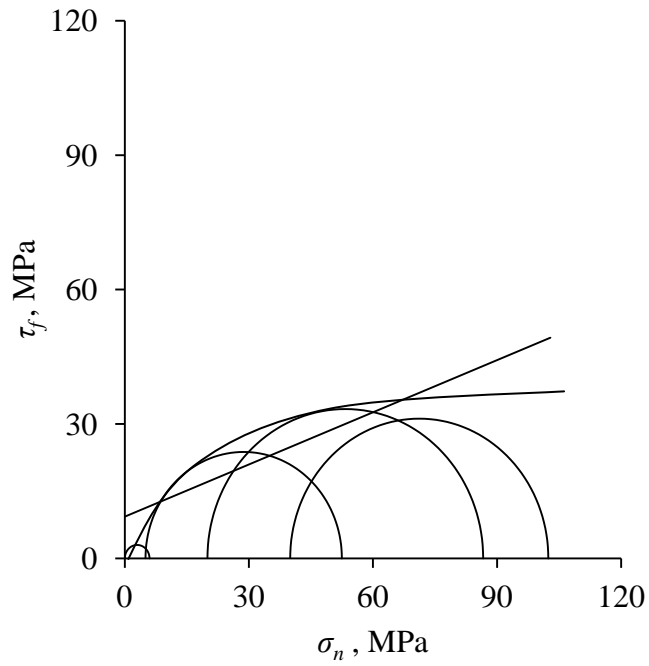
Fig.7.4k Mohr circles at failure for reinforced jointed rock at $\theta = 50°-60°$
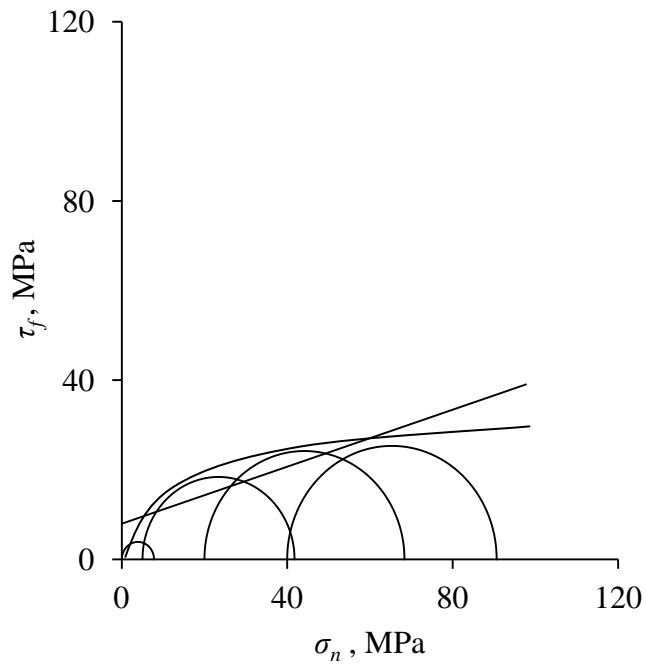
Fig.7.5l Mohr circles at failure for reinforced jointed rock at $\theta = 60°-70°$

228

The values of shear strength parameters (c and ϕ) were obtained by fitting best possible straight lines into σ_1 vs σ_3 plots. An example figure is plotted in Fig.7.6. The equation of the straight line can be written as

$$Y = mX + k \tag{7.2}$$

where m = slope of the line; k = intercept at vertical axis, X and Y = variables. The Mohr- coulomb equation in the form of σ_1 vs σ_3 is written as

$$\sigma_1 = \frac{(1+sin\phi)}{(1-sin\phi)}\,\sigma_3 + \frac{2\,c\,cos\phi}{(1-sin\phi)} \tag{7.3}$$

where c= cohesion and ϕ = friction angle which are obtained as

$$\phi = sin^{-1}\left(\frac{m-1}{m+1}\right) \qquad\qquad \text{and} \tag{7.4a}$$

$$c = \frac{k\,(1-sin\phi)}{2\,cos\phi} \tag{7.4b}$$

Using equation 7.4a and 7.4b, the values of shear strength parameters were calculated and are presented in Table 7.2.

Table 7.2 revels that the installation of bolt alters the values of the shear strength parameters. This happens due to improved interlocking of joint due to bolts. In some cases of unreinforced jointed rocks (θ = 50°-70°), very low value of friction angle has been obtained due to sliding mode of failure. In present study, the cohesion (c) and friction angle (ϕ) of the reinforced rock are observed to lie between the cohesion (c) and friction angle (ϕ) of intact and unreinforced rock respectively. The parameters c and ϕ are found to be highest for the intact rock.

The variation of c and ϕ with joint orientation (θ) is plotted in the Fig.7.7a and Fig.7.7b respectively. For unreinforced rock, cohesion (c) is high for low θ values (θ = 0° - 20°); for θ more than about 15°, cohesion intercept reduces drastically and remains almost constant (with some scatter) for higher θ values. The cohesion intercept c is directly linked with failure mode. For splitting/shearing mode, c is high whereas for sliding mode it assumes smaller value. For reinforced rock, the variation in c is less striking due to the obvious reason that the failure mode was

splitting/shearing. Further, cohesion for reinforced rock is always higher than cohesion for unreinforced rock.
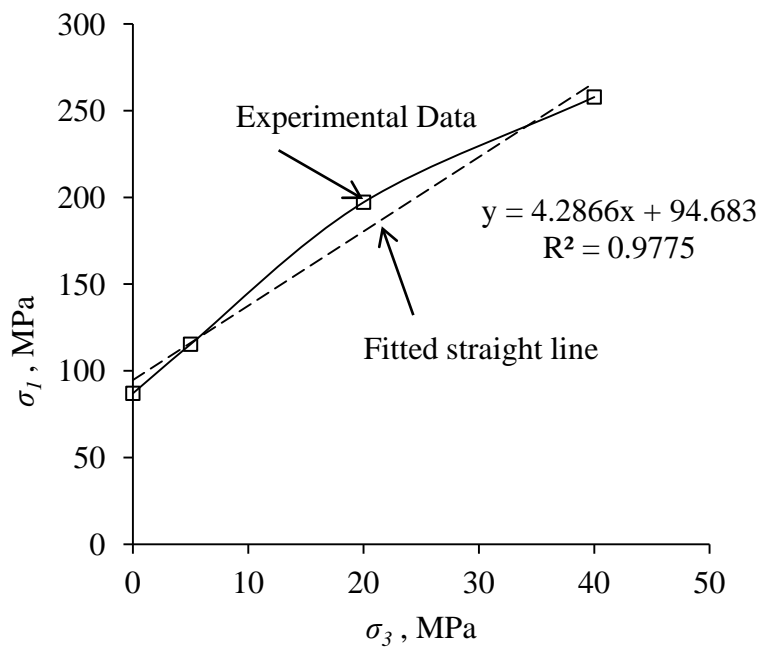
Fig.7.6 Fitting of straight line in σ_1 vs σ_3 plot for calculation of strength parameters
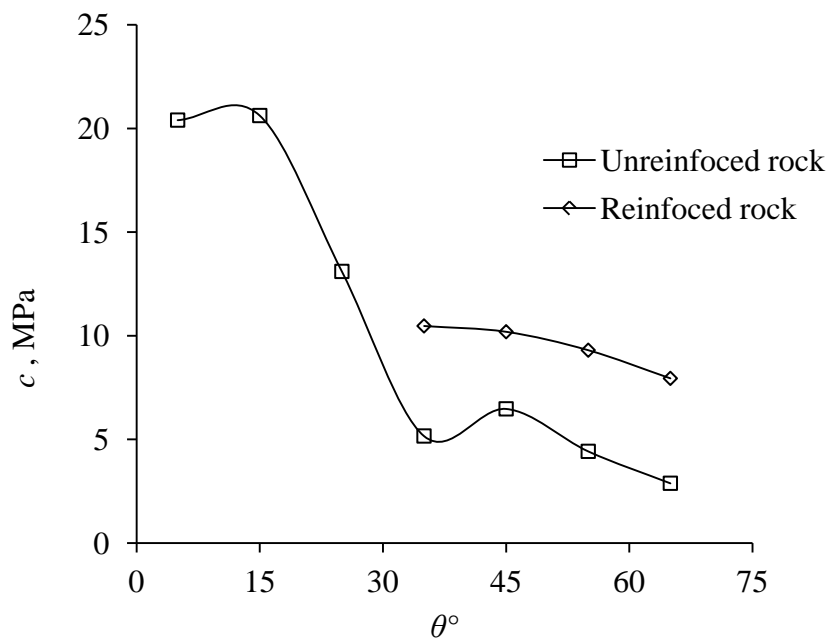
Fig.7.7a Variation of cohesion (c) with joint orientation ($\theta°$) for unreinforced and reinforced specimens

The variation of ϕ with θ for unreinforced rock is not that systematic (Fig.7.7b). Though there is a trend of decreasing ϕ with increasing θ, however, the scatter is large. For reinforced rock, at $\theta = 30°$ the value of ϕ is found to be maximum and it reduces with increasing θ upto 70°.
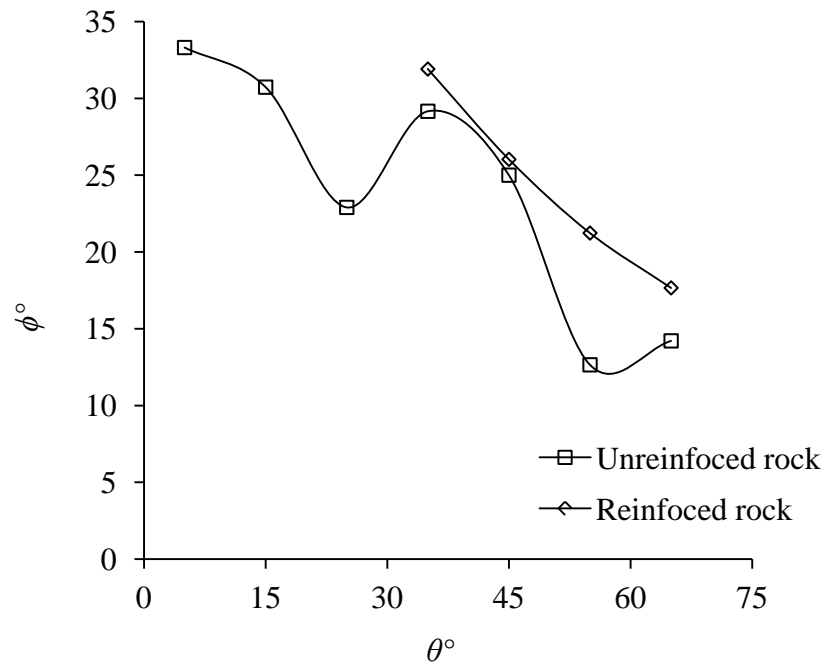
Fig.7.7b Variation of friction angle (ϕ) with joint orientation ($\theta°$) for unreinforced and reinforced specimens

The percent increase in cohesion (c) and angle of friction (ϕ) due to installation of the bolt are listed in Table 7.3. The enhancement in cohesion is greater as compared to friction angle except for one case. The percent increases in c and ϕ is found to be minimum at $\theta = 40°$-50°. The variation of percent increase in c and ϕ with joint orientation ($\theta°$) is plotted in Fig.7.8. The maximum enhancement in cohesion has been observed between for $\theta = 60°$-70° while the maximum enhancement in friction angle has been observed $\theta = 50°$-60°. It is seen that the cohesion is strongly correlated with failure mode whereas no such conclusive statement can be made about ϕ. In fact, it is prudent to assume ϕ constant and include effect of reinforcement in cohesion while designing structures.

Table 7.3 % increase in *c* and *ϕ*

θ°	% increase in *c*	% increase in *ϕ*
30-40	103	9
40-50	57	4
50-60	110	68
60-70	176	24
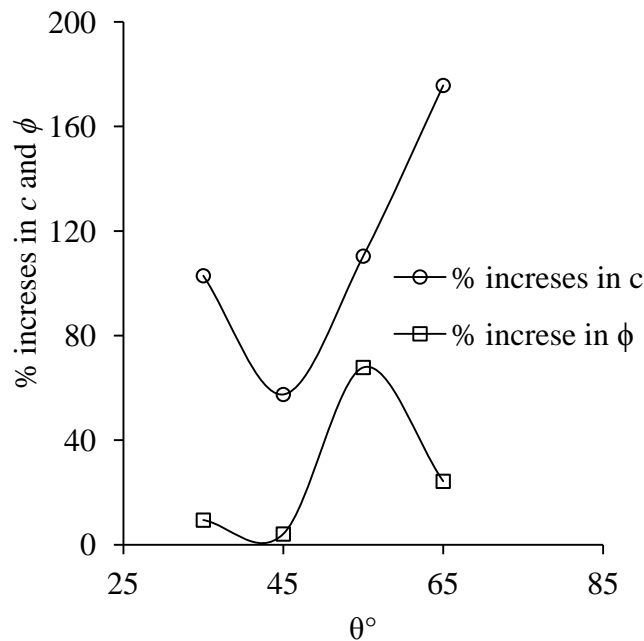
Fig.7.8 Variation of percent increase in *c* and *ϕ* with joint orientation (*θ°*)

7.6 PREDICTION OF TRIAXIAL STRENGTH

The rocks in the field are always subjected to triaxial or polyaxial stress states. Several empirical criteria have been proposed in past by various researchers to define the strength of intact rock under given confining pressure (Hoek and Brown, 1980, 2002; Ramamurthy, 1993; Singh and Singh, 2005; Singh et al., 2011). In case of jointed rocks, characteristics of the joints also come in picture and the strength behaviour is governed jointly by intact rock and joint characteristics. A number of failure criteria have been proposed for jointed rocks in past (Hoek and Brown, 1980, 2002; Ramamurthy, 2001; Singh and Rao, 2005 Singh and Singh, 2012).

The results of triaxial tests on the natural rock specimens, indicate that triaxial strength of reinforced rock varies in a non-linear fashion with increase in confining pressure. It is essential that strength criterion be suggested for non- linear strength prediction of reinforced rocks. In the following section, applicability of strength criteria to intact and jointed specimens is disused and suggestions are made for strength criterion for reinforced rock.

7.6.1 Intact Rock

The experimental values of σ_1 obtained at different confining pressure are listed in Table 7.4. To assess the applicability of strength criteria to intact rock, two empirical criteria (Hoek and Brown, 1980, 2002; and Singh et al., 2012) have been evaluated and discussed in present section. To evaluate different criteria, the percent error (*pe*) in prediction for a data point, is expressed as

$$\text{pe} = \left(\frac{\sigma_{1,cal} - \sigma_{1,exp}}{\sigma_{1,exp}} \right) \times 100 \ \% \tag{7.5}$$

where $\sigma_{1,exp}$ = experimental value of the triaxial strength and $\sigma_{1,\text{cal}}$ = predicted value of the triaxial strength through a strength criterion. The average percentage error (*avpe*) for the data set is calculated as

$$avpe = \sqrt{\frac{1}{n} \sum_{i=1}^{n} (pe)^2} \tag{7.6}$$

where *n* is the number of data points in the data set.

Table 7.4 Experimental values of σ_1 at different σ_3 (intact rock)

σ_3 , MPa	$\sigma_{1,\,exp}$ (MPa)
0	87
5	115.13
20	197.19
40	257.86

7.6.1.1 Hoek Brown (1980) Failure Criterion

The Hoek and Brown failure criterion (1980) for intact rocks is expressed as

$$\sigma_1 = \sigma_3 + \sigma_{ci}\left(m_i\frac{\sigma_3}{\sigma_{ci}} + 1\right)^{0.5} \tag{7.7}$$

where m_i and σ_{ci} are the criterion parameters. The parameter m_i is the material constant and depends upon the material type and σ_{ci} is the uniaxial compressive strength to be obtained by fitting the criterion into laboratory triaxial test data.

In present evaluation, the first two data points of Table 7.4 (including UCS) are considered for assessing parameters of the failure criterion. The results are then predicted for the other σ_3 values, and compared with experimental values. Using the first two data points, the parameters m_i and σ_{ci} are obtained as 10.48 and 87 MPa respectively. The equation 7.7 can now be written as

$$\sigma_1 = \sigma_3 + 87(0.120\,\sigma_3 + 1)^{0.5} \tag{7.8}$$

Using the failure criterion (Eq.7.8) the values of σ_1 are calculated and are presented in Table 7.5. Percent error (*pe*) for individual data points and overall average error (*avpe*) are also listed in Table 7.5. Percentage error (*pe*) varies from 0 to -9 % while *avpe* in estimating the triaxial strength is found to be 5%.

Table 7.5 Comparison of experimental and calculated triaxial strength for intact rock using Hoek and Brown failure criterion (1980)

σ_3 , MPa	$\sigma_{1,exp}$, MPa	$\sigma_{1,cal}$, MPa	*pe*
0	87.00	87.00	0
5	115.31	115.04	0
20	197.19	180.42	-9
40	257.86	249.52	-3
avpe			5

7.6.1.2 Singh et al. (2011) Failure Criterion

Singh et al. (2011) proposed the following non-linear criterion for intact rocks

$$\sigma_1 = \sigma_{ci} + \left(\frac{2\,sin\phi_{i0}}{1-sin\phi_{i0}} + 1\right)\sigma_3 - \frac{1}{\sigma_{crti}}\frac{sin\phi_{i0}}{1-sin\phi_{i0}}\sigma_3^{\,2} \;\; for\; 0 \leq \sigma_3 \leq \sigma_{crti} \tag{7.9}$$

234

where ϕ_{i0} is the Mohr-coulomb shear strength parameter obtained by conducting triaxial strength on rock specimens at low confining pressure ($\sigma_3 \rightarrow 0$) and σ_{crti} is the critical confining pressure for intact rock. Based on statistical analysis of more than 1100 data points, Singh et al. (2011) observed that the value of critical confining pressure (σ_{crti}) for an intact rock may be taken roughly equal to the uniaxial compressive strength of the intact rock (σ_{ci}). It was also suggested that the value of ϕ_{io} should be obtained by conducting triaxial strength tests on rock specimens at low confining pressure ($\sigma_3 \rightarrow 0$). Considering first two points (Table 7.4), the slope of initial portion of σ_1 - σ_3 plot is obtained which yields ϕ_{i0} to be equal to 44.41°.Considering ϕ_{io} = 44.41° and σ_{crti} = σ_{ci} = 87 MPa, the values of triaxial strength ($\sigma_{1,cal}$) were computed using equation 7.9. The experimental ($\sigma_{1,exp}$) and calculated ($\sigma_{1,cal}$) values of triaxial strength with *pe* and *avpe* are presented in Table 7.6. It is observed that the *avpe* in estimating triaxial strength is about 3%. For individual data points, the *pe* varies from 0 to -5%.

Table 7.6 Comparison of experimental and calculated triaxial strength for intact rock using Singh et al. (2011) failure criterion

σ_3 , MPa	$\sigma_{1,exp}$, MPa	$\sigma_{1,cal}$, MPa	% error
0	87	87.00	0
5	115.31	114.61	1
20	197.19	189.41	4
40	257.86	270.42	-5
avpe			3

The *avpe* as obtained using Hoek Brown (1980) criterion was about 5%. From Singh et al. (2011) criterion, the *avpe* is about 3%. The individual *pe* in Hoek Brown (1980) criterion is 0 to -9% while in Singh et al. (2011) criterion the individual *pe* is 0 to -5%. However, both the criteria give good estimation of strength. The variation of experimental and calculated triaxial strength (using both the criteria) with confining pressure (σ_3) for intact rock is shown in Fig.7.9.
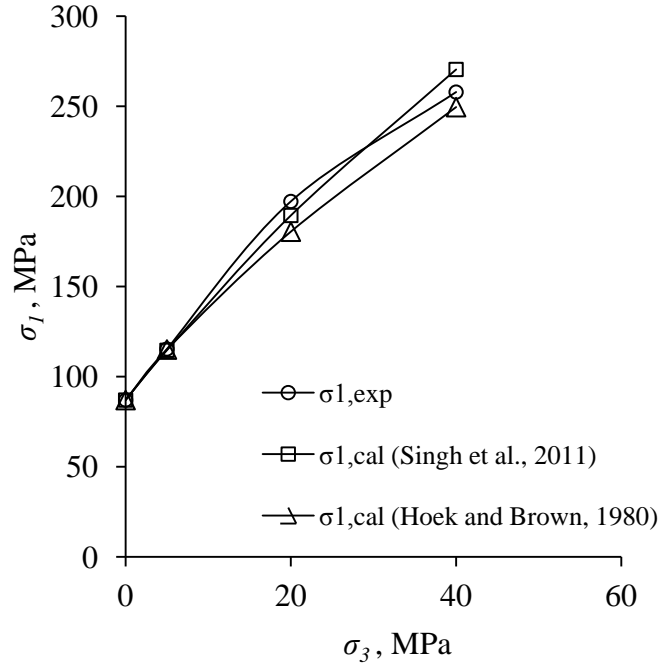
Fig.7.9 Variation of experimental and calculated triaxial strength with confining pressure (σ_3) for intact rock

7.6.2 Unreinforced and Reinforced Jointed Rocks

The uniaxial compressive strength (σ_{cj}) of jointed rocks plays an important role in governing the triaxial strength behaviour of jointed rocks (Ramamurthy, 2011; Singh and Singh, 2012). The UCS (σ_{cj}) itself is governed by characteristics of joints (Barton, 1976) and failure mode (Singh, 1997; Singh and Rao, 2005). In present section, applicability of the strength criteria to jointed unreinforced as well as for reinforced rocks is evaluated.

7.6.2.1 Ramamurthy (2001) criterion

Ramamurthy (2001) proposed a criterion for jointed rocks as

$$\frac{\sigma_1 - \sigma_3}{\sigma_3} = B_j \left(\frac{\sigma_{cj}}{\sigma_3}\right)^{\alpha_j} \tag{7.10}$$

where σ_1 and σ_3 are the major and minor principal stresses at failure respectively and σ_{cj} is the uniaxial compressive strength of the jointed rock, α_j and B_j are the criterion parameters and are obtained as

236

$$\frac{\alpha_j}{\alpha_i} = \left(\frac{\sigma_{cj}}{\sigma_{ci}}\right)^{0.5} \tag{7.11a}$$

$$\frac{B_j}{B_i} = 0.13 \exp\left[2.04 \frac{\alpha_j}{\alpha_i}\right] \tag{7.11b}$$

where α_i and B_i are the strength parameters of intact rock obtained from triaxial tests. Using triaxial test data of intact rock, the parameters α_i and B_i are found to be 0.67 and 3.26 respectively. Using value of α_i, B_i and σ_{cj} the parameters α_j and B_j are estimated and reported in Table 7.7. As the values of α_i and B_i are obtained, the strength of jointed rock is evaluated using equation 7.10.

Table 7.7 Estimation of strength parameters α_j and B_j for unreinforced and reinforced rocks

$\theta°$	σ_{cj}, MPa	α_j	B_j
Unreinforced rock			
0-10	44.69	0.48	5.81
10-20	47.01	0.49	5.60
20-30	32.02	0.41	7.27
30-40	6.55	0.18	14.33
40-50	1.22	0.08	19.70
50-60	1.08	0.07	19.98
60-70	1.03	0.07	20.08
Reinforced rock			
30-40	18.05	0.31	9.90
40-50	12.32	0.25	11.64
50-60	5.97	0.18	14.70
60-70	7.78	0.20	13.63

7.6.2.2 Single Plane of Weakness Theory (Jaeger, 1960) associated with Barton (1976) criterion

For a specimen, subjected to triaxial stress state, the shear stress (τ) and normal stress (σ_n) on a potential failure plane may be obtained as

$$\tau = \frac{\sigma_1 - \sigma_3}{2} \sin 2\theta \qquad \text{and} \tag{7.12a}$$

$$\sigma_n = \frac{\sigma_1 + \sigma_3}{2} + \frac{\sigma_1 - \sigma_3}{2} \cos 2\theta \tag{7.12b}$$

where θ is the angle of joint plane with respect to the plane on which σ_3 acts. If failure occurs due to sliding on joint plane

$$\tau \geq \tau_f \tag{7.13}$$

where τ_f is the shear strength along joint plane for given normal stress. According to the Barton (1976, 1977, 1990), the shear strength τ_f of a joint subjected to a normal stress σ_n is given by

$$\tau_f = \sigma_n \text{Tan}\left[\text{JRC}\log\left[\frac{\text{JCS}}{\sigma_n}\right] + \phi_r\right] \tag{7.14}$$

where JRC = joint roughness coefficient (geometrical component); JCS = joint wall compressive strength (asperity failure component); and ϕ_r = residual friction angle of the joint. Using Barton's equation, the condition for sliding failure can be expressed as

$$\frac{\sigma_1 - \sigma_3}{2}\sin 2\theta \geq \sigma_n \text{Tan}\left[\text{JRC}\log\left[\frac{\text{JCS}}{\sigma_n}\right] + \phi_r\right] \tag{7.15a}$$

or $\quad \dfrac{\sigma_1 - \sigma_3}{2}\sin 2\theta \geq \left[\dfrac{\sigma_1 + \sigma_3}{2} + \dfrac{\sigma_1 - \sigma_3}{2}\cos 2\theta\right]\left[\text{Tan}\left[\text{JRC}\log\left[\frac{\text{JCS}}{\sigma_n}\right] + \phi_r\right]\right]$ $\tag{7.15b}$

This equation is implicit in nature and can be solved by trial and error. For present study, the value of ϕ_r is taken as 27° and trials were performed for different cases. JRC was obtained by visually comparing the joint surface with standard JRC profiles. JCS was obtained by conducting Schmidt hammer tests on the specimens of jointed rock. Using equation 7.16b, only those cases are analysed where sliding mode of failure has been observed in uniaxial condition.

7.6.2.3 Singh and Singh (2012) criterion

Singh and Singh (2012) proposed the following non-linear criterion for jointed rocks,

$$\sigma_1 = \sigma_{cj} + \left(\frac{2\sin\phi_{j0}}{1-\sin\phi_{j0}} + 1\right)\sigma_3 - \frac{1}{\sigma_{crtj}}\frac{\sin\phi_{j0}}{1-\sin\phi_{j0}}\sigma_3{}^2 \ \ for \ 0 \leq \sigma_3 \leq \sigma_{crtj} \tag{7.16}$$

where ϕ_{j0} is the Mohr-coulomb shear strength parameter of the jointed rock at low confining pressure($\sigma_3 \rightarrow 0$), σ_{crtj} is the critical confining pressure of jointed rock and

σ_{cj} is the uniaxial compressive strength of the jointed rock. The intact and jointed rocks parameters were correlated with each other through following expressions:

$$\frac{B_j}{2} = \left(1 + \frac{B_i}{2} - SRF\right)\frac{\sigma_{ci}}{\sigma_{crtj}} \qquad (7.17a)$$

$$B_j = \frac{2\,sin\phi_{j0}}{1 - sin\phi_{j0}} \qquad (7.17b)$$

$$B_i = \frac{2\,sin\phi_{i0}}{1 - sin\phi_{i0}} \qquad (7.17c)$$

$$SRF = stregth\ reduction\ factor = \frac{\sigma_{cj}}{\sigma_{ci}} \qquad (7.17d)$$

Using equation 7.17a, the value of ϕ_{jo} was calculated for unreinforced and reinforced rock. The value of the critical confining pressure of jointed rock (σ_{crtj}) has been taken as uniaxial compressive strength of the intact rock (σ_{ci}). The calculated value of ϕ_{jo} is presented in Table 7.8.

Table 7.8 Value of ϕ_{jo} for unreinforced and reinforced rock

$\theta°$	$\phi_{j0}°$
Unreinforced rock	
0-10	47.54
10-20	47.39
20-30	48.37
30-40	49.89
40-50	50.19
50-60	50.19
60-70	50.20
Reinforced rock	
30-40	49.22
40-50	49.56
50-60	49.92
60-70	49.82

7.6.2.4 Results obtained using different criteria

The strength of unreinforced rock has been calculated using Ramamurthy (2001) criterion, Single plane of weakness theory (Jaeger, 1960) associated with Barton (1976) criterion, Singh and Singh (2012) failure criterion and are presented in

Table 7.9. Percentage error (*pe*) and *avpe* also have been calculated using equations 7.5 and 7.6 respectively (Table 7.10). It is observed that the strength values predicted by Ramamurthy (2001) and Singh and Singh (2012) failure criteria are much higher than those obtained from experimental results. For sliding mode of failure, the SPWT gives better results. The *avpe* obtained for SPWT varies from 19% to 35% in case of sliding failure (θ=30°-70°). Ramamurthy (2001) criterion gives the maximum *avpe* for both sliding and non-sliding cases as compared to SPWT and Singh and Singh (2012) criteria. The *avpe* in Ramamurthy (2001) criterion is found to be 90% to 269%. In Singh and Singh (2012) criterion, the *avpe* varies from 44% to 118%.

Table 7.9 Comparison of the results obtained from the different criteria

σ_3 , MPa	σ_{cj}, MPa	Failure Mode observed	JCS , MPa	JRC	$\sigma_{1,exp}$, MPa	Ramamurthy (2001)	Jaeger (1960)	Singh and Singh (2012)
Unreinforced rock								
θ=0°-10°								
5		SP	42	14	111.52	88.19	-	77.02
20	44.69	SP	47	12	173.29	191.00	-	164.32
40		SP	44	12	196.18	285.17	-	258.07
θ=10°-20°								
5		SP	47	14	107.5	89.39	-	79.08
20	47.01	SP	48	10	151.71	190.55	-	165.69
40		SP+SH	48	12	184.96	282.46	-	258.75
θ=20°-30°								
5		SP	25	8	59.05	82.38	-	65.77
20	32.02	SP+SH	22	10	85.55	196.14	-	156.80
40		SP	32	14	129.12	305.74	-	254.37
θ=30°-40°								
5		SP	35	10	49.58	80.29	30.13	43.14
20	6.55	SP	22	10	66.94	253.39	63.44	141.70
40		SP	36	12	135.69	450.94	132.73	246.94
θ=40°-50°								
5		SP+SH	39	12	51.94	93.05	23.1	38.41
20	1.22	SL+SH	28	14	73.98	335.51	57.78	138.54
40		SP	35	12	114.24	637.26	99.83	245.38

θ=50°-60°								
5		SP+SH	42	8	25.67	94.09	17.25	38.28
20	1.08	SL+SH	20	14	48.66	341.34	48.73	138.45
40		SP	25	16	66.68	650.27	87.23	245.34
θ=60°-70°								
5		SL+SH	35	10	19.81	94.50	18.11	38.24
20	1.03	SL+SH	22	10	45.87	343.59	52.85	138.43
40		SP+SH	27	14	70.18	655.29	89.75	245.33
Reinforced rock								
θ=30°-40°								
5		SP	40	12	76.7	78.25	-	53.36
20	18.05	SP	38	10	101.97	211.94	-	148.52
40		SP	45	8	164.83	350.69	-	250.30
θ=40°-50°								
5		SP+SH	28	12	60.08	78.05	-	48.27
20	12.32	SP+SH	44	12	98.92	225.99	-	145.12
40		SP+SH	35	14	125.84	385.93	-	248.62
θ=50°-60°								
5		SP+SH	45	12	52.49	80.80	-	42.63
20	5.97	SP+SH	43	14	86.63	257.72	-	141.35
40		SP+SH	30	10	102.38	460.98	-	246.77
θ=60°-70°								
5		SP+SH	27	8	41.76	79.43	-	44.23
20	7.78	SP	22	8	68.34	245.53	-	142.43
40		SP+SH	28	10	90.62	432.58	-	247.30

SP =Splitting; SH = Shearing; SL = Sliding.

Table 7.10 Percent error obtained in different criteria

σ_3 , MPa	σ_{cj}, MPa	Failure Mode observed	Ramamurthy (2001)	Jaeger (1960)	Singh and Singh (2012)
Unreinforced rock					
θ=0°-10°					
5		SP	-21	-	-31
20	44.69	SP	10	-	-5
40		SP	45	-	32
avpe			29	-	26
θ=10°-20°					
5		SP	-16	-	-26
20	47.01	SP	26	-	9
40		SP+SH	53	-	40

	avpe		35	-	28
θ=20°-30°					
5		SP	40	-	11
20	32.02	SP+SH	129	-	83
40		SP	137	-	97
	avpe		111	-	74
θ=30°-40°					
5		SP	62	-39	-13
20	6.55	SP	279	-5	112
40		SP	232	-2	82
	avpe		212	23	81
θ=40°-50°					
5		SP+SH	79	-55	-26
20	1.22	SL+SH	354	-22	87
40		SP	458	-13	115
	avpe		337	35	85
θ=50°-60°					
5		SP+SH	267	-33	49
20	1.08	SL+SH	601	0	185
40		SP	875	31	268
	avpe		632	26	190
θ=60°-70°					
5		SL+SH	377	-9	93
20	1.03	SL+SH	649	15	202
40		SP+SH	834	28	250
	avpe		648	19	193
Reinforced rock					
θ=30°-40°					
5		SP	2	-	-30
20	18.05	SP	108	-	46
40		SP	113	-	52
	avpe		90	-	44
θ=40°-50°					
5		SP+SH	30	-	-20
20	12.32	SP+SH	128	-	47
40		SP+SH	207	-	98
	avpe		142	-	64
θ=50°-60°					
5		SP+SH	54	-	-19
20	5.97	SP+SH	197	-	63
40		SP+SH	350	-	141
	avpe		234	-	90

θ=60°-70°					
5		SP+SH	90	-	6
20	7.78	SP	259	-	108
40		SP+SH	377	-	173
avpe			269	-	118

For better comparison, the values of experimental triaxial strength ($\sigma_{1,exp}$) are plotted against calculated triaxial strength ($\sigma_{1,cal}$) values (Fig.7.10). An index, coefficient of accordance (*COA*) is calculated as

$$COA = \frac{\Sigma(\sigma_{1,exp}-\sigma_{1,cal})^2}{\Sigma(\sigma_{1,exp}-\sigma_{1,av})^2} \tag{7.18}$$

$\sigma_{1,exp}$ = experimental triaxial strength; $\sigma_{1,cal}$ = calculated triaxial strength; $\sigma_{1,av}$ = average of experimental σ_1 values for data points under consideration. Lower value of COA indicates the better prediction. Comparison of $\sigma_{1,cal}$ by using different criteria and $\sigma_{1,exp}$ values considering all modes of failure (for both unreinforced and reinforced cases) are plotted in Fig.7.10a to 7.10c. Comparisons of *COA* obtained from different criteria are presented in Table 7.11.
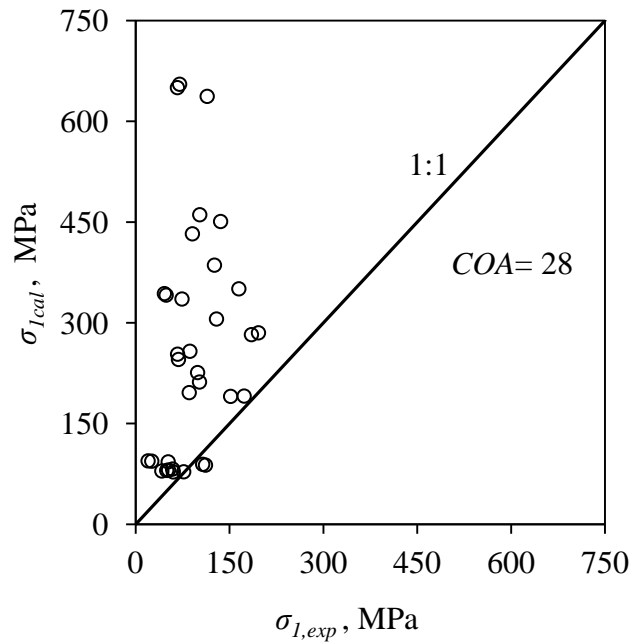
Fig.7.10a Comparison of $\sigma_{1,cal}$ by Ramamurthy (2001) criterion and $\sigma_{1,exp}$ values (all failure modes)

243
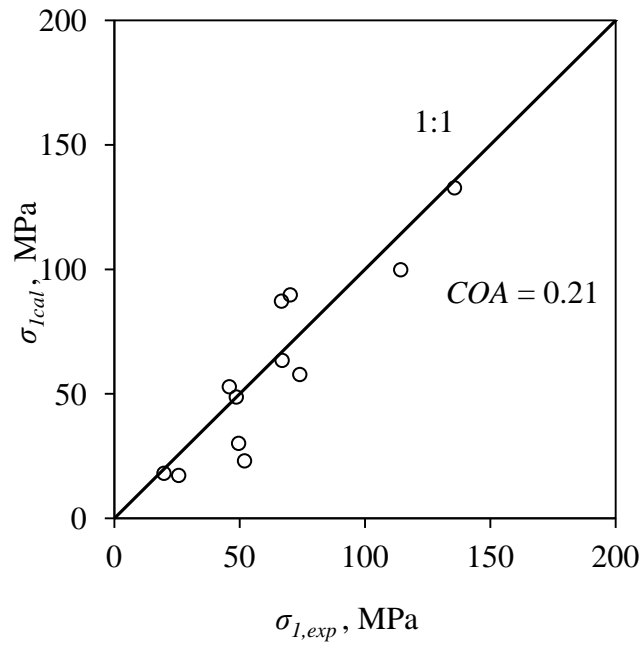
Fig.7.10b Comparison of $\sigma_{1,cal}$ by Jaeger (1960) criterion and $\sigma_{1,exp}$ values (only sliding failure mode)
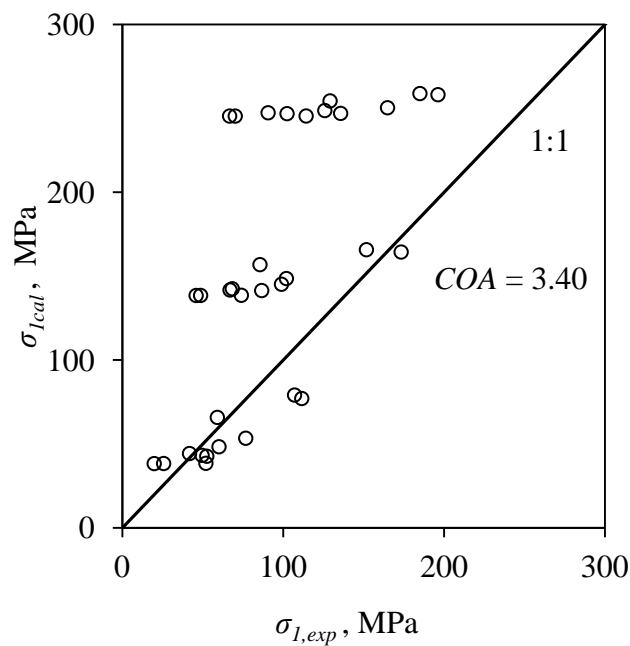
Fig.7.10c Comparison of $\sigma_{1,cal}$ by Singh and Singh (2012) criterion ($\sigma_{crtj} = \sigma_{ci}$) and $\sigma_{1,exp}$ values (all failure modes)

Table 7.11 Comparisons of *COA* obtained from different criteria

Criterion	Non-sliding failure		Sliding failure	All modes of failure (both unreinforced and reinforced)
	Unreinforced	Reinforced	Unreinforced	
Ramamurthy (2001)	4	35	111	28
Jaeger (1960)	-	-	0.2	-
Singh and Singh (2012) criterion	1.8	6.5	9.8	3.4

It is observed that for sliding cases, the coefficient of accordance (*COA*) is found to be minimum for single plane of weakness theory (Jaeger, 1960). For non-sliding cases (both unreinforced and reinforced), the lower value of *COA* is observed for Singh and Singh (2012) criterion. For Ramamurthy (2001) criterion, *COA* is found to be 111 for sliding cases. For non-sliding, *COA* is found to be 4 and 35 for unreinforced and reinforced cases respectively. When all failure modes are considered the *COA* using Ramamurthy (2001) criterion is 28. From Singh and Singh (2012) criterion the *COA* is 3.40 for all failure modes. For non-sliding cases of unreinforced and reinforced rock the COA is found to be 1.8 and 6.5 respectively.

Based on the analysis of results, it is found that for sliding failure, the criterion proposed by Barton (1976) when used in single plane of weakness theory (Jaeger, 1960) gives the better results (*COA* = 0.2). Singh and Singh (2012) suggested that for critical joint orientation where sliding occurred along joint plane the criterion proposed by them is not applicable. It was suggested by Singh and Singh (2012) that for such cases analysis should be done through a more appropriate criterion. It is seen that error in prediction for non-sliding cases is also high. A criterion needs to be suggested for reinforced rocks.

7.7. PROPOSED CRITERION FOR NON SLIDING FAILURE

As discussed earlier, the variation of σ_1 with σ_3 for unreinforced and reinforced jointed rocks is found to be non-linear in all the cases (section 7.2:Fig.7.1b, 7.1c, and 7.1d). In case of non-sliding failure, the intact rock properties as well as the characteristics of joint will govern the failure. Joint characteristics can be defined in the terms of *JRC* and *JCS*. In present analysis, an attempt has been made to modify Sing and Singh (2012) criterion by incorporating JRC and JCS in its expression.

In first trial (Trial I), to incorporate the characteristics of joints and intact material it is assumed that the value of ϕ_{jo} is equal to ϕ_{io} plus *JRC*

$$\phi_{jo} = \phi_{io} + JRC \tag{7.19}$$

Singh and Singh (2012) suggested, "*The failure envelope of jointed rock may merge with the failure envelope of intact rock either at a confining pressure less than σ_{ci} or more than σ_{ci} and strength of intact and jointed rocks will be nearly equal in critical state.*" Hence, the critical confining pressure (σ_{crtj}) for jointed rocks can be taken nearly equal to σ_{ci}. Now considering ϕ_{jo} equal to ϕ_{io} plus *JRC*, and $\sigma_{crtj} = \sigma_{ci} = 87$ MPa, the strength of jointed rock for both unreinforced and reinforced rock was calculated using equation 7.16 and presented in Table 7.12. The value of σ_{cj} is taken as obtained from experimental results. The *pe* and *avpe* is calculated by equation 7.5 and 7.6.

Table 7.12a Comparison of experimental and calculated triaxial strength for unreinforced jointed rock ($\theta=0°$-$10°$) ($\phi_{jo} = \phi_{io} + JRC$ and $\sigma_{crtj} = \sigma_{ci}$)

σ_3, MPa	Failure Mode observed	*JRC*	$\sigma_{1,exp}$, MPa	$\sigma_{1,cal}$, MPa	*pe*
0	SP	12	44.69	44.69	0
5	SP	14	111.52	105.44	5
20	SP	12	173.29	241.07	-39
40	SP	12	196.18	391.64	-100
avpe					54

SP =Splitting; SH = Shearing; SL = Sliding

Table 7.12b Comparison of experimental and calculated triaxial strength for unreinforced jointed rock ($\theta=10°\text{-}20°$) ($\phi_{jo} = \phi_{io} + JRC$ and $\sigma_{crtj} = \sigma_{ci}$)

σ_3, MPa	Failure Mode observed	JRC	$\sigma_{1,exp}$, MPa	$\sigma_{1,cal}$, MPa	pe
0	SP	12	47.01	47.01	0
5	SP	14	107.5	107.76	0
20	SP	10	151.71	220.95	-46
40	SP+SH	12	184.96	393.96	-113
avpe					61

Table 7.12c Comparison of experimental and calculated triaxial strength for unreinforced jointed rock ($\theta=20°\text{-}30°$) ($\phi_{jo} = \phi_{io} + JRC$ and $\sigma_{crtj} = \sigma_{ci}$)

σ_3, MPa	Failure Mode observed	JRC	$\sigma_{1,exp}$, MPa	$\sigma_{1,cal}$, MPa	pe
0	SP	12	32.02	32.02	0
5	SP	8	59.05	74.05	-25
20	SP+SH	10	85.55	205.96	-141
40	SP	14	129.12	425.68	-230
avpe					135

Table 7.12d Comparison of experimental and calculated triaxial strength for reinforced jointed rock ($\theta=30°\text{-}40°$) ($\phi_{jo} = \phi_{io} + JRC$ and $\sigma_{crtj} = \sigma_{ci}$)

σ_3, MPa	Failure Mode observed	JRC	$\sigma_{1,exp}$, MPa	$\sigma_{1,cal}$, MPa	pe
0	SP	10	18.05	18.05	0
5	SP	12	76.7	71.44	7
20	SP	10	101.97	191.99	-88
40	SP	8	164.83	292.95	-78
avpe					59

Table 7.12e Comparison of experimental and calculated triaxial strength for reinforced jointed rock ($\theta=40°\text{-}50°$) ($\phi_{jo} = \phi_{io} + JRC$ and $\sigma_{crtj} = \sigma_{ci}$)

σ_3, MPa	Failure Mode observed	JRC	$\sigma_{1,exp}$, MPa	$\sigma_{1,cal}$, MPa	pe
0	SP+SH	10	12.32	12.32	0
5	SP+SH	12	60.08	65.71	-9
20	SP+SH	12	98.92	208.70	-111
40	SP+SH	14	125.84	405.98	-223
avpe					124

Table 7.12f Comparison of experimental and calculated triaxial strength for reinforced jointed rock (θ=50°-60°) ($\phi_{jo} = \phi_{io} + JRC$ and $\sigma_{crtj} = \sigma_{ci}$)

σ_3, MPa	Failure Mode observed	JRC	$\sigma_{1,exp}$, MPa	$\sigma_{1,cal}$, MPa	pe
0	SP+SH	10	5.97	5.97	0
5	SP+SH	12	52.49	59.36	-13
20	SP+SH	14	86.63	229.19	-165
40	SP+SH	10	102.38	313.86	-207
avpe					132

Table 7.12g Comparison of experimental and calculated triaxial strength for reinforced jointed rock (θ=60°-70°) ($\phi_{jo} = \phi_{io} + JRC$ and $\sigma_{crtj} = \sigma_{ci}$)

σ_3, MPa	Failure Mode observed	JRC	$\sigma_{1,exp}$, MPa	$\sigma_{1,cal}$, MPa	pe
0	SP+SH	12	7.78	7.78	0
5	SP+SH	8	41.76	49.81	-19
20	SP	8	68.34	162.76	-138
40	SP+SH	10	90.62	315.69	-248
avpe					142

It is observed that the if $\phi_{jo} = \phi_{io} + JRC$ and $\sigma_{crtj} = \sigma_{ci}$, the *avpe* for calculating the strength for both unreinforced and reinforced cases varies from 54% to 142% which is very high. It is found that the at $\sigma_3 = 20$ and 40 MPa, the individual *pe* for estimating the strength is very high, while at $\sigma_3 = 0$ and 5 MPa the individual *pe* is quite low (< 25%). This indicates that the either the value of ϕ_{jo} or σ_{crtj} or both parameters are wrongly estimated. Now a second trial (Trial II) has been performed with following assumption

i. At $\sigma_3 = 0$ and 5 MPa the value of ϕ_{jo} is equal to $\phi_{io} + JRC$
ii. At $\sigma_3 = 20$ and 40 MPa the value of ϕ_{jo} is equal to ϕ_{io}.

Using above assumption and taking $\sigma_{crtj} = \sigma_{ci}$, the strength of jointed rocks (both unreinforced and reinforced) is calculated using equation 7.16 and is presented in Table 7.13.

Table 7.13a Comparison of experimental and calculated triaxial strength for unreinforced jointed rock ($\theta=0°$-$10°$) ($\phi_{jo} = \phi_{io} + JRC$ or $\phi_{jo} = \phi_{io}$ and $\sigma_{crtj} = \sigma_{ci}$)

σ_3, MPa	Failure Mode observed	JRC	$\phi_{jo}°$	$\sigma_{1,exp}$, MPa	$\sigma_{1,cal}$, MPa	pe
0	SP	12	56.41	44.69	44.69	0
5	SP	14	58.41	111.52	105.44	5
20	SP	12	44.41	173.29	147.15	15
40	SP	12	44.41	196.18	228.19	-16
avpe						11

Table 7.13b Comparison of experimental and calculated triaxial strength for unreinforced jointed rock ($\theta=10°$-$20°$) ($\phi_{jo} = \phi_{io} + JRC$ or $\phi_{jo} = \phi_{io}$ and $\sigma_{crtj} = \sigma_{ci}$)

σ_3, MPa	Failure Mode observed	JRC	$\phi_{jo}°$	$\sigma_{1,exp}$, MPa	$\sigma_{1,cal}$, MPa	pe
0	SP	12	56.41	47.01	47.01	0
5	SP	14	58.41	107.5	107.76	0
20	SP	10	44.41	151.71	149.47	1
40	SP+SH	12	44.41	184.96	230.51	-25
avpe						12

Table 7.13c Comparison of experimental and calculated triaxial strength for unreinforced jointed rock ($\theta=20°$-$30°$) ($\phi_{jo} = \phi_{io} + JRC$ or $\phi_{jo} = \phi_{io}$ and $\sigma_{crtj} = \sigma_{ci}$)

σ_3, MPa	Failure Mode observed	JRC	$\phi_{jo}°$	$\sigma_{1,exp}$, MPa	$\sigma_{1,cal}$, MPa	pe
0	SP	12	56.41	32.02	32.02	0
5	SP	8	52.41	59.05	74.05	-25
20	SP+SH	10	44.41	85.55	134.48	-57
40	SP	14	44.41	129.12	215.52	-67
avpe						46

Table 7.13d Comparison of experimental and calculated triaxial strength for reinforced jointed rock (θ=30°-40°) ($\phi_{jo} = \phi_{io} + JRC$ or $\phi_{jo} = \phi_{io}$ and $\sigma_{crtj} = \sigma_{ci}$)

σ_3, MPa	Failure Mode observed	JRC	$\phi_{jo}°$	$\sigma_{1,exp}$, MPa	$\sigma_{1,cal}$, MPa	pe
0	SP	10	54.41	18.05	18.05	0
5	SP	12	56.41	76.7	71.44	7
20	SP	10	44.41	101.97	120.51	-18
40	SP	8	44.41	164.83	201.55	-22
avpe						15

Table 7.13e Comparison of experimental and calculated triaxial strength for reinforced jointed rock (θ=40°-50°) ($\phi_{jo} = \phi_{io} + JRC$ or $\phi_{jo} = \phi_{io}$ and $\sigma_{crtj} = \sigma_{ci}$)

σ_3, MPa	Failure Mode observed	JRC	$\phi_{jo}°$	$\sigma_{1,exp}$, MPa	$\sigma_{1,cal}$, MPa	pe
0	SP+SH	10	54.41	12.32	12.32	0
5	SP+SH	12	56.41	60.08	65.71	-9
20	SP+SH	12	44.41	98.92	114.78	-16
40	SP+SH	14	44.41	125.84	195.82	-56
avpe						29

Table 7.13f Comparison of experimental and calculated triaxial strength for reinforced jointed rock (θ=50°-60°) ($\phi_{jo} = \phi_{io} + JRC$ or $\phi_{jo} = \phi_{io}$ and $\sigma_{crtj} = \sigma_{ci}$)

σ_3, MPa	Failure Mode observed	JRC	$\phi_{jo}°$	$\sigma_{1,exp}$, MPa	$\sigma_{1,cal}$, MPa	pe
0	SP+SH	12	56.41	5.97	5.97	0
5	SP+SH	12	56.41	52.49	59.36	-13
20	SP+SH	14	44.41	86.63	108.43	-25
40	SP+SH	10	44.41	102.38	189.47	-85
avpe						45

Table 7.13g Comparison of experimental and calculated triaxial strength for reinforced jointed rock ($\theta=60°$-$70°$) ($\phi_{jo} = \phi_{io} + JRC$ or $\phi_{jo} = \phi_{io}$ and $\sigma_{crtj} = \sigma_{ci}$)

σ_3, MPa	Failure Mode observed	JRC	$\phi_{jo}°$	$\sigma_{1,exp}$, MPa	$\sigma_{1,cal}$, MPa	pe
0	SP+SH	12	56.41	7.78	7.78	0
5	SP+SH	8	52.41	41.76	49.81	-19
20	SP	8	44.41	68.34	110.24	-61
40	SP+SH	10	44.41	90.62	191.30	-111
avpe						64

It is observed that the individual *pe* and *avpe* in all the cases reduced considerably as compared to first trial. In most of the cases, the *avpe* is less than 50%. This indicates that the after a particular value of σ_3, there is a reduction in ϕ_{jo} and it may be taken as ϕ_{io}. However, there are still uncertainties to predict the strength using equation 7.16. Barton and Chaubey (1977) suggested that the *JCS* value of rock influences the strength of discontinuity present in jointed rock. To incorporate the effect of *JCS* the following assumptions are made in third trial

i. At $\sigma_3 = 0$ and 5 MPa the value of ϕ_{jo} is equal to $\phi_{io} + JRC$
ii. At $\sigma_3 = 20$ and 40 MPa the value of ϕ_{jo} is equal to ϕ_{io}.
iii. Critical confining pressure (σ_{crtj}) for jointed rocks is equal to *JCS* of rock.

Using above assumption the strength of unreinforced and reinforced jointed rocks is calculated using equation 7.16 and presented in Table 7.14.

Table 7.14a Comparison of experimental and calculated triaxial strength for unreinforced jointed rock ($\theta=0°$-$10°$) ($\phi_{jo} = \phi_{io} + JRC$ or $\phi_{jo} = \phi_{io}$ and $\sigma_{crtj} = JCS$)

σ_3, MPa	Failure Mode observed	JCS, MPa	σ_3/JCS	JRC	$\phi_{jo}°$	$\sigma_{1,exp}$, MPa	$\sigma_{1,cal}$, MPa	pe
0	SP	43	0	12	56.41	44.69	44.69	0
5	SP	42	0.12	14	58.41	111.52	103.68	7
20	SP	47	0.43	12	44.41	173.29	138.04	20
40	SP	44	0.91	12	44.41	196.18	186.33	5
avpe								11

Table 7.14b Comparison of experimental and calculated triaxial strength for unreinforced jointed rock (θ=10°-20°) ($\phi_{jo} = \phi_{io} + JRC$ or $\phi_{jo} = \phi_{io}$ and $\sigma_{crtj} = JCS$)

σ_3, MPa	Failure Mode observed	JCS, MPa	σ_3/JCS	JRC	$\phi_{jo}°$	$\sigma_{1,exp}$, MPa	$\sigma_{1,cal}$, MPa	pe
0	SP	40	0	12	56.41	47.01	47.01	0
5	SP	47	0.1	14	58.41	107.5	106.36	1
20	SP	48	0.4	10	44.41	151.71	140.77	7
40	SP+SH	48	0.8	12	44.41	184.96	195.71	-6
avpe								5

Table 7.14c Comparison of experimental and calculated triaxial strength for unreinforced jointed rock (θ=20°-30°) ($\phi_{jo} = \phi_{io} + JRC$ or $\phi_{jo} = \phi_{io}$ and $\sigma_{crtj} = JCS$)

σ_3, MPa	Failure Mode observed	JCS, MPa	σ_3/JCS	JRC	$\phi_{jo}°$	$\sigma_{1,exp}$, MPa	$\sigma_{1,cal}$, MPa	pe
0	SP	40	0	12	56.41	32.02	32.02	0
5	SP	25	0.2	8	52.41	59.05	71.33	-21
20	SP+SH	22	1.0	10	44.41	85.55	102.84	-20
40	SP	32	1.25	14	44.41	129.12	141.90	-10
avpe								15

Table 7.14d Comparison of experimental and calculated triaxial strength for reinforced jointed rock (θ=30°-40°) ($\phi_{jo} = \phi_{io} + JRC$ or $\phi_{jo} = \phi_{io}$ and $\sigma_{crtj} = JCS$)

σ_3, MPa	Failure Mode observed	JCS, MPa	σ_3/JCS	JRC	$\phi_{jo}°$	$\sigma_{1,exp}$, MPa	$\sigma_{1,cal}$, MPa	pe
0	SP	45	0	10	54.41	18.05	18.05	0
5	SP	40	0.1	12	56.41	76.7	69.76	9
20	SP	38	0.5	10	44.41	101.97	106.70	-5
40	SP	45	0.9	8	44.41	164.83	161.57	2
avpe								5

Table 7.14e Comparison of experimental and calculated triaxial strength for reinforced jointed rock ($\theta=40°-50°$) ($\phi_{jo} = \phi_{io} + JRC$ or $\phi_{jo} = \phi_{io}$ and $\sigma_{crtj} = JCS$)

σ_3 , MPa	Failure Mode observed	JCS , MPa	σ_3/JCS	JRC	$\phi_{jo}°$	$\sigma_{1,exp}$, MPa	$\sigma_{1,cal}$, MPa	pe
0	SP+SH	28	0	10	54.41	12.32	12.32	0
5	SP+SH	28	0.2	12	56.41	60.08	62.69	-4
20	SP+SH	44	0.5	12	44.41	98.92	104.31	-5
40	SP+SH	35	1.1	14	44.41	125.84	132.18	-5
avpe								4

Table 7.14f Comparison of experimental and calculated triaxial strength for reinforced jointed rock ($\theta=50°-60°$) ($\phi_{jo} = \phi_{io} + JRC$ or $\phi_{jo} = \phi_{io}$ and $\sigma_{crtj} = JCS$)

σ_3 , MPa	Failure Mode observed	JCS , MPa	σ_3/JCS	JRC	$\phi_{jo}°$	$\sigma_{1,exp}$, MPa	$\sigma_{1,cal}$, MPa	pe
0	SP+SH	32	0	12	56.41	5.97	5.97	0
5	SP+SH	45	0.1	12	56.41	52.49	58.02	-11
20	SP+SH	43	0.5	14	44.41	86.63	97.47	-13
40	SP+SH	30	1.3	10	44.41	102.38	108.08	-6
avpe								9

Table 7.14g Comparison of experimental and calculated triaxial strength for reinforced jointed rock ($\theta=60°-70°$) ($\phi_{jo} = \phi_{io} + JRC$ or $\phi_{jo} = \phi_{io}$ and $\sigma_{crtj} = JCS$)

σ_3 , MPa	Failure Mode observed	JCS , MPa	σ_3/JCS	JRC	$\phi_{jo}°$	$\sigma_{1,exp}$, MPa	$\sigma_{1,cal}$, MPa	pe
0	SP+SH	36	0	12	56.41	7.78	7.78	0
5	SP+SH	27	0.2	8	52.41	41.76	47.38	-13
20	SP	22	0.9	8	44.41	68.34	78.60	-15
40	SP+SH	28	1.4	10	44.41	90.62	101.04	-11
avpe								12

It is observed that the *avpe* for predicting the strength reduced considerably as compared to Trial II. *avpe* for unreinforced jointed rocks varies between 5 to 15% and the maximum individual *pe* is -21%. For reinforced cases, the maximum *pe* for individual case is -15%. The *avpe* for reinforced cases varies between 4 to 12%, which indicates a good estimation of strength. Compared to unreinforced cases, the *avpe* in reinforced case is less. A comparison of *avpe* for all three trials is presented in Table 7.15, which indicates that in Trial III the value of *avpe* is minimum as compared to others. It can be seen that when the value of σ_3/JCS is ≤ 0.2, best results are obtained when ϕ_{io}, *JRC* and *JCS* are considered in the criterion; if σ_3/JCS is ≥ 0.4, the best results are obtained by incorporating ϕ_{io} and *JCS* in the criterion. This indicates that if applied confining pressure is very small as compared to *JCS* of the rock, *JRC* of joint plays major role in governing the triaxial strength whereas at higher confining pressure the JRC plays no role.

Table 7.15 avpe (%) in all the trails

$\theta°$	Trial I $(\phi_{jo} = \phi_{io} + JRC$ and $\sigma_{crtj} = \sigma_{ci})$	Trial II $(\phi_{jo} = \phi_{io} + JRC$ or $\phi_{jo} = \phi_{io}$ and $\sigma_{crtj} = \sigma_{ci})$	Trial III $(\phi_{jo} = \phi_{io} + JRC$ or $\phi_{jo} = \phi_{io}$ and $\sigma_{crtj} = JCS)$
Unreinforced rock			
0-10	54	11	11
10-20	61	12	5
20-30	135	45	15
Reinforced rock			
30-40	59	15	5
40-50	124	29	4
50-60	132	45	9
60-70	142	64	12

COA obtained in different trials is listed in Table 7.16. For unreinforced and reinforced rock cases, the minimum value of *COA* is found in trial III. However, in case of reinforced rocks the COA is less as compared to unreinforced rock. This suggests that if the joint is perfectly interlocked (due to provision of bolt), the error in predicting the triaxial strength using assumption made in trial III will be small.

Table 7.16 *COA* obtained in different trials

$\theta°$	Trial I	Trial II	Trial III
Unreinforced rock	11.06	0.79	0.12
Reinforced rock	19.12	2.15	0.04
Overall (considering unreinforced and reinforced cases)	10.84	1.02	0.07

Tables 7.14, 7.15 and 7.16, indicate that the equation 7.16 can be used for predicting the strength of reinforced rocks as well as for unreinforced rocks where non-sliding failure (splitting and shearing) is observed. However, in equation 7.16 some modifications are required. Considering all the factors, which influence the strength, the following modifications are suggested in equation 7.16 for unreinforced and reinforced rock having non-sliding failure;

i. At low confining stress level ($\sigma_3/JCS = 0.3$), the value of ϕ_{jo} is assumed to be equal to ϕ_{io} plus *JRC* of the joint. For $\sigma_3/JCS > 0.3$, the value of ϕ_{jo} can be taken equal to ϕ_{io}.

ii. The critical confining pressure (σ_{crtj}) of jointed rock is assumed to be equal to *JCS* of rock.

Now the equation 7.16 can be modified for unreinforced rocks as;

$$\sigma_1 = \sigma_{cj} + \left(\frac{2\sin(\phi_{i0}+JRC)}{1-\sin(\phi_{i0}+JRC)} + 1\right)\sigma_3 - \frac{1}{JCS}\frac{\sin(\phi_{i0}+JRC)}{1-\sin(\phi_{i0}+JRC)}\sigma_3{}^2 \quad for \ \frac{\sigma_3}{JCS} \leq 0.3 \quad (7.20a)$$

$$\sigma_1 = \sigma_{cj} + \left(\frac{2\sin(\phi_{i0})}{1-\sin(\phi_{i0})} + 1\right)\sigma_3 - \frac{1}{JCS}\frac{\sin(\phi_{i0})}{1-\sin(\phi_{i0})}\sigma_3{}^2 \qquad for \ \frac{\sigma_3}{JCS} > 0.3 \quad (7.20b)$$

Similar to unreinforced jointed rock the triaxial strength of reinforced rock can be predicted by using equation 7.16. The analysis on reinforced specimens indicates that the *JRC* and *JCS* influence the triaxial strength of reinforced jointed rocks. For reinforced jointed, the equation 7.16 can be written as

$$\sigma_1 = \sigma_{cr} + \left(\frac{2\sin(\phi_{i0}+JRC)}{1-\sin(\phi_{i0}+JRC)} + 1\right)\sigma_3 - \frac{1}{JCS}\frac{\sin(\phi_{i0}+JRC)}{1-\sin(\phi_{i0}+JRC)}\sigma_3{}^2 \quad for \ \frac{\sigma_3}{JCS} \leq 0.3 \quad (7.21a)$$

$$\sigma_1 = \sigma_{cr} + \left(\frac{2\,sin(\phi_{i0})}{1-sin(\phi_{i0})} + 1\right)\sigma_3 - \frac{1}{JCS}\frac{sin(\phi_{i0})}{1-sin(\phi_{i0})}\sigma_3{}^2 \qquad for\,\frac{\sigma_3}{JCS} > 0.3 \qquad (7.21b)$$

where σ_{cr} is the uniaxial compressive strength of reinforced jointed rock. Using equation 7.22 the strength of reinforced jointed rock can be predicted using *JCS* and *JRC* values if the value of σ_{cr} is known. To assess the value of σ_{cr} the correlations suggested in chapter 6 can be used. The variations of experimental and calculated triaxial strength with confining pressure (σ_3) using equations 7.20 and 7.21 for unreinforced and reinforced jointed rock are presented in Fig 7.11.
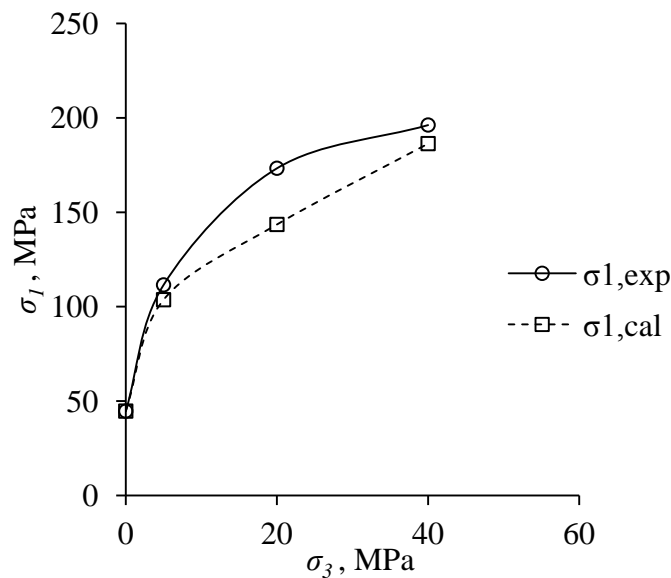
Fig.7.11a Variation of experimental and calculated triaxial strength with confining pressure (σ_3) for unreinforced jointed rock ($\theta=0°$-$10°$)
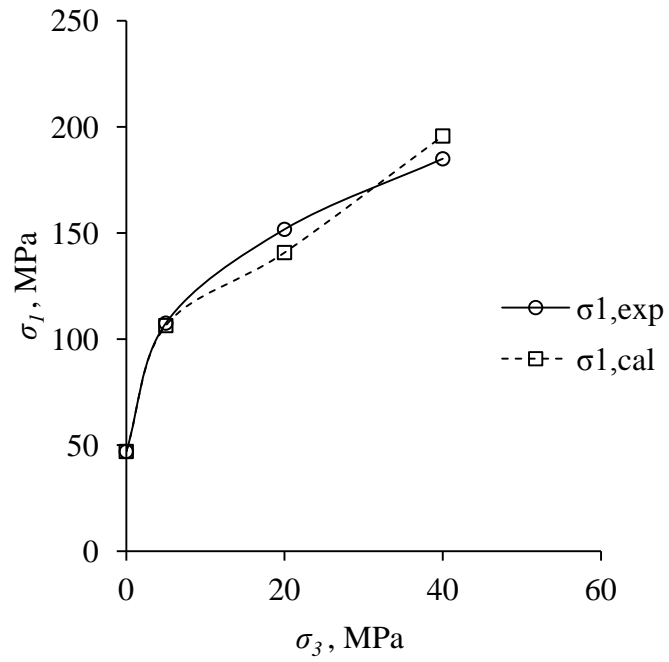
Fig.7.11b Variation of experimental and calculated triaxial strength with confining pressure (σ_3) for unreinforced jointed rock (θ=10°-20°)
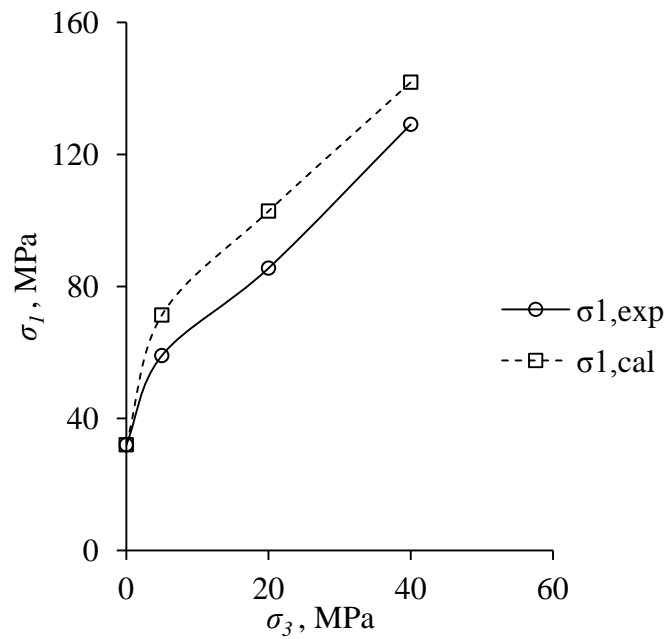
Fig.7.11c Variation of experimental and calculated triaxial strength with confining pressure (σ_3) for unreinforced jointed rock (θ=20°-30°)

Fig.7.11d Variation of experimental and calculated triaxial strength with confining pressure (σ_3) for reinforced jointed rock ($\theta=30°-40°$)

Fig.7.11e Variation of experimental and calculated triaxial strength with confining pressure (σ_3) for reinforced jointed rock ($\theta=40°-50°$)

258

Fig.7.11f Variation of experimental and calculated triaxial strength with confining pressure (σ_3) for reinforced jointed rock (θ=50°-60°)

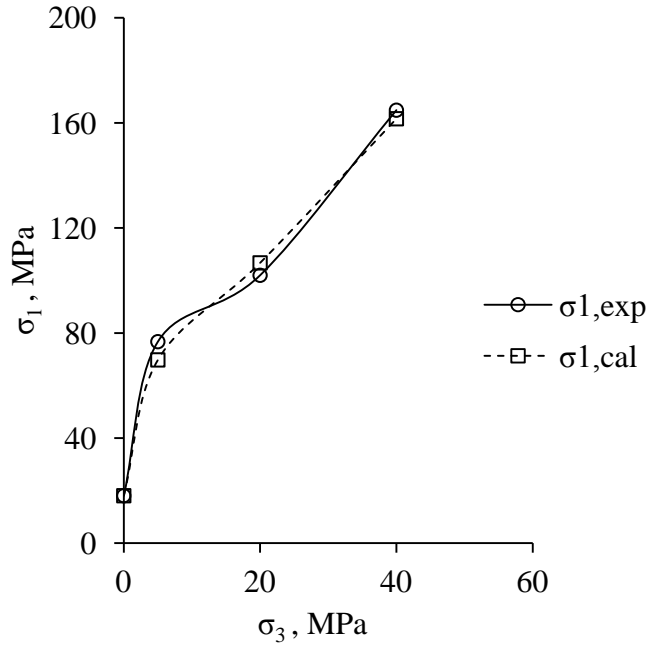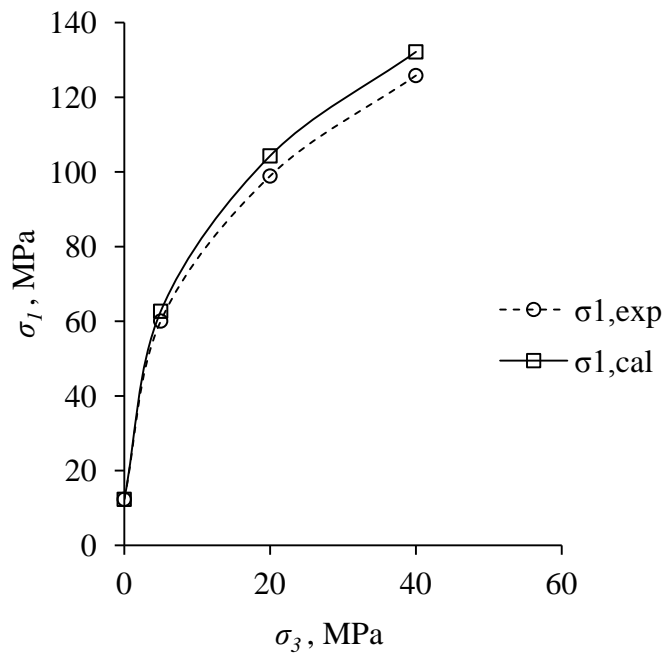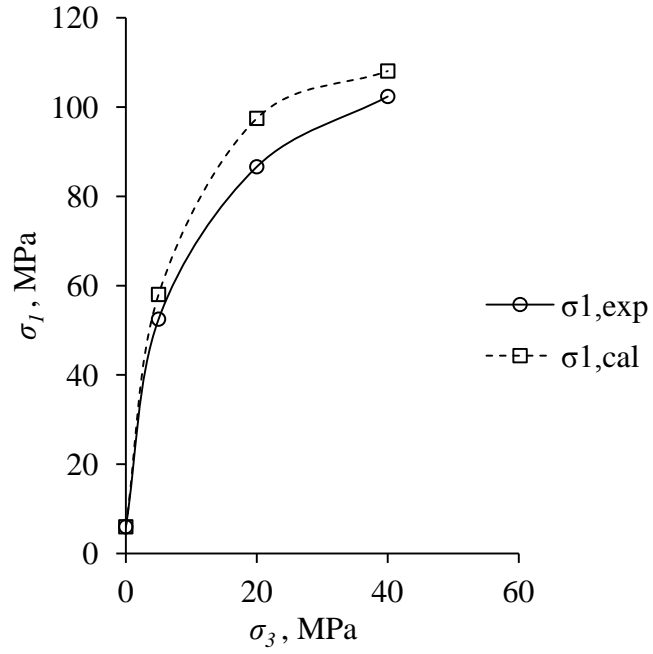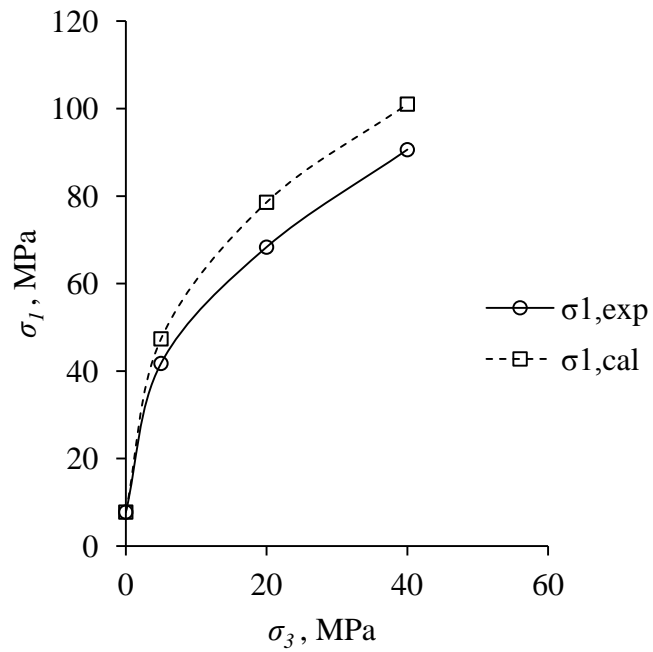
Fig.7.11g Variation of experimental and calculated triaxial strength with confining pressure (σ_3) for reinforced jointed rock (θ=60°-70°)

7.8 CONCLUDING REMARKS

Based on the results of triaxial tests on intact, unreinforced and reinforced jointed rocks it is found that the properties of intact rock and properties of joints (*JCS* and *JRC*) influence the strength behaviour of unreinforced and reinforced jointed rocks. It is also observed that the failure mode plays very important role in governing the strength of jointed rocks. Results indicate that the where splitting/shearing or combinations of these modes are observed, the criterion proposed by Singh and Singh (2012) is the most suitable criterion for predicting the strength. In case failure is governed by sliding along joint, Barton (1976) model in Single plane of weakness theory gives better results. For reinforced rocks the criterion proposed by Singh and Singh (2012) gives good results. However, the some modifications are suggested. The conclusions of the analysis are listed below.

i.   Strength of unreinforced and reinforced rock increase with increase in confining pressure. The variation of σ_1 with σ_3 is found to be non-linear. At low confining pressure, the increase in strength per unit increase in confining pressure is high. At higher confining pressure, the increase in strength per unit increase in confining pressure becomes smaller.

ii. Strength of jointed rocks enhances due to installation of bolt. The application of bolt restricts sliding along joint plane and induces interlocking in the joint. For critical joint orientation where failure mode of unreinforced rock is sliding, the failure mode alters to splitting or shearing due to bolt resulting in very high gain in strength. At low confining pressure, the strength enhancement is high and at high confining pressure, strength enhancement becomes smaller.

iii. Unreinforced jointed rocks, in general are anisotropic in strength behaviour with high anisotropy ratio. Provision of bolt reduces the anisotropy ratio at all confining stress levels. The anisotropy ratio reduces with increase in confining stress.

iv. Installation of bolt alters the value of strength parameters. Enhancement in cohesion is greater as compared friction angle.

v.   Criterion proposed by Singh and Singh (2012) can be used for predicting the strength of unreinforced and reinforced rocks where non-sliding (splitting and

shearing) failure is observed. Following modifications are suggested in the criterion.

At low confining stress level ($\sigma_3/JCS = 0.3$), the value of ϕ_{jo} is assumed to be equal to ϕ_{io} plus *JRC* of the joint. For $\sigma_3/JCS > 0.3$, the value of ϕ_{jo} can be taken equal to ϕ_{io} and the critical confining pressure (σ_{crtj}) of jointed rock is assumed to be equal to *JCS* of rock.

SUMMARY AND CONCLUSIONS

8.1 GENERAL

Rock bolts are frequently used for reinforcing rock mass in the field. Bolts act as an integral part of the rock and make the rock mass stiff against external forces. The engineering behaviour of reinforced rocks is substantially different from unreinforced rocks due to complex interaction between intact material, joints and bolts. As a consequence, the strength assessment of reinforced rock is a difficult task. The main objectives of the present research have been

   i.   To investigate shear strength response of a large blocky mass through direct shear tests under different normal stresses and different amount of reinforcement (passive bolts), and suggest approach for assessing strength enhancement due to provision of passive bolts.

   ii.   To investigate effect of passive rock bolts on uniaxial compression strength of natural and synthetic rocks. The outcome of this part has been used to suggest correlations between strength and modulus of intact, unreinforced jointed and reinforced jointed rocks.

   iii.   To investigate effect of confining pressure on strength of natural jointed reinforced rocks. Applicability of strength criteria for reinforced rocks has been investigated.

To achieve the above-mentioned objectives, laboratory tests were performed on the synthetic and natural rock specimens without and with bolts.

8.2 EXPERIMENTAL STUDY

It was planned to conduct experimental study on the specimens of unreinforced and reinforced jointed rocks. Passive rock bolts were used as reinforcement. The experimental investigation was divided into three parts as follows.

8.2.1 Direct Shear Tests on Large Sized Specimens of Blocky Mass

Direct shear tests, using a special apparatus (shear box size 750 mm x 750mm x 1000 mm (height)), were conducted on large size specimens of blocky mass. Concrete was used as a model material to simulate the intact rock. The blocky unreinforced mass (U) specimens were prepared by piling elemental cubical concrete blocks of size 150 mm x150 mm x150 mm. The size of the prepared blocky mass was 750 mm x 750mm x 900 mm (height). The formed jointed mass consisted of three orthogonal joint sets having spacing of 150 mm each. Six mm diameter steel bars (tensile strength 550 MPa) were used as bolts to reinforce the blocky mass. The bolts were installed perpendicular to the shearing direction, and were grouted with cement mortar. Three configurations of bolts were used. In the first case (R3), three rock bolts were installed in the middle columns of blocks with a centre-to-centre spacing of 300 mm. In the second case (R5), five rock bolts were installed in the mass; one at the centre and the others in the four outermost corners of the mass. The centre-to-centre spacing for the staggered pattern was 300 mm. In the third case (R9), nine bolts were installed; in square grid pattern with a centre-to-centre spacing of 300 mm. Direct shear tests were conducted at normal stress levels ranging between 0 to 2 MPa (0.0, 0.5, 1.0, and 2.0 MPa respectively). For each configuration, four tests were performed, one at each normal stress level. The shearing was continued until the shear load dropped substantially after reaching its peak value.

8.2.2 Uniaxial Compression Tests on Synthetic Rock specimens

Uniaxial compression tests were performed on the specimens of jointed rock to investigate effect of reinforcement on UCS of jointed rock. Two different grades of concrete (referred to T2 and T3) were used as model material. The size of the specimens was 150 mm x 150 mm x 300 mm (height). The prepared specimens carried one joint having orientation 0° to 90° with the base of the specimen. Two steel bars of diameter 6 mm were installed in the specimens perpendicular to loading

direction and were grouted with cement. For each test axial load and axial displacement were recorded.

8.2.3 Triaxial Compression Tests on Natural Rock Cores (NRC)

Triaxial compression tests were performed on the specimens of natural jointed rocks (size NX) without and with bolts. The height to diameter ratio of prepared specimens was about 2. The joint orientation (θ) was varied from 0° to 90° with respect to base of the specimens. For bolted specimens, a 6 mm diameter hole was drilled and 4 mm diameter bolt was installed and grouted with cement mortar. The specimens were tested at confining pressure of 0, 5, 20, and 40MPa respectively. For each test, axial load and axial displacement were recorded.

8.3 SUMMERY OF OBSERVATIONS AND CONCLUSIONS

8.3.1 Strength Behaviour of Blocky Mass

During direct shear testing of blocky mass, sliding of blocks were observed in case of unreinforced blocky mass at all the normal stress levels. In reinforced cases, provision of bolts restricted the sliding along the joint plane. Shear stress (τ) vs horizontal shear displacement (δ_H), and vertical displacement (δ_v) vs horizontal shear displacement plots were prepared for all cases of blocky mass. From theses plots, peak shear stress at failure, horizontal shear displacement at failure and dilation angle were obtained. During shearing, the shear stress increased with increasing shear displacement and exhibited a clearly defined peak in the majority of cases (except for unreinforced mass at 0.0 and 0.5 MPa of normal stress). The horizontal shear displacement at failure was found to be minimum when five bolts were used to reinforce the mass (R5 case). The shear stress vs the horizontal shear displacement plots of reinforced blocky mass exhibit two distinct segments. The first part of the plot is relatively flat which indicates the mobilization of shear stress due to the interaction of the blocks. The second part of the plot is steep which indicates the mobilization of shear stress through the bolts.

In all the cases of unreinforced and reinforced blocky mass, an increase in the normal stress results in increase in the peak shear stress (shear strength). It is found

that for all the normal stress levels, the provision of bolts enhances the shear strength of blocky mass. The enhancement in shear strength occurs due to the following reasons;

i. Bolts improve interlocking of the joints in the mass. In addition, development of tensile stress in the bolt induces additional normal stress on the joint surface in the blocky mass. This additional normal stress increases "effective normal stress" on the joint surfaces in the mass, which contributes in the strength enhancement due to provision of bolts.

ii. Due to improved interlocking produced by the bolts, the stiffness of the mass enhances. The rock mass, therefore, becomes stiffer and stronger.

The enhancement in shear strength is greatly influenced by the amount of reinforcement, spacing between joints, and spacing between the bolts. Installation of bolts altered the cohesion (c_{j_mass}) and friction angle (ϕ_{j_mass}) of the blocky mass. The provision of bolts improves the cohesion of joints substantially but the effect on friction angle is low. To simplify the analysis, it is decided that the friction angle of reinforced mass (ϕ_{j_mass}) should be taken equal to friction angle of single joint (ϕ_j). Further, it is assumed that the overall shear strength enhancement by provision of bolts is mainly due to change in cohesion value of mass (c_{j_mass}). Analysis of results, suggested the following correlation to assess the shear strength of a reinforced mass subjected to a given normal stress (σ_n)

$$\tau_f = c_i \left(0.04 \ ln \left(\frac{A_r}{N} \right) + \ 0.24 \right) + c_j + \sigma_n \ tan\phi_j \tag{8.1}$$

where τ_f = shear strength of reinforced mass; c_i = cohesion of intact rock material; A_r = percent area ratio; N = spacing ratio; c_j = cohesion of a single joint and; ϕ_j = friction angle of single joint. The parameters percent area ratio (A_r) and spacing ratio (N) can be calculated as

$$A_r = \frac{A_b}{A} \times 100 \ \% \tag{8.2}$$

$$N = \frac{S_b}{D_b} \tag{8.3}$$

where A_b= total cross section area of bolts on shearing plane; A = area of mass on shearing plane; D_b = equivalent block size and S_b = equivalent spacing between bolts.

$$S_b = \sqrt{\frac{Area\ of\ shearing\ plane}{numbers\ of\ bolts}} \qquad \text{(8.4a)}$$

$$D_b = \sqrt[3]{volume\ of\ representative\ block} \qquad \text{(8.4b)}$$

The proposed correlation can be used in the field to find out the shear strength of rock mass due to provision of rock bolts.

8.3.2 Strength and Deformational Behaviour of Natural and Synthetic Jointed Rocks under Uniaxial Compression

The unreinforced jointed rock specimens under uniaxial compression exhibited three different types of failure modes i.e. splitting, shearing, and sliding or a combination of these depending upon joint orientation. Sliding mode dominated the failure mechanism for joint orientation ranging between θ =30° to 80° for unreinforced natural rock specimens. In case of reinforced natural rock specimens, the sliding was restricted and the failure occurred only due to splitting and shearing. The restriction imposed by the bolt on relative displacement enhances interlocking and alters sliding mode into shearing/splitting modes of failure. For orientations $\theta < 30°$ and $\theta > 80°$, both the unreinforced and reinforced natural rock specimens exhibited splitting/shearing modes.

The majority of the unreinforced and reinforced jointed specimens of synthetic rock (both T2 and T3) failed due to splitting. Very few specimens of unreinforced jointed synthetic rocks failed due to sliding (θ =45° and 60°). Installation of bolts altered the sliding failure mode into splitting mode of failure. At other orientations, both unreinforced and reinforced specimens of synthetic rocks show splitting mode of failure.

Axial stress vs axial stain curves were plotted for each specimen of natural and synthetic rock. Results were obtained in form of uniaxial compressive strength (σ_c) and modulus (E_{t50}). Strength and modulus values of reinforced specimens lie between those of jointed unreinforced and intact specimens. Both natural and synthetic rocks exhibit this trend. The provision of the bolts enhances the strength and modulus value

of unreinforced jointed rock (both natural and synthetic rocks). For orientations, $\theta = 40°$ to $80°$ for natural rock and $\theta = 45°$ and $60°$ for synthetic rocks, the unreinforced specimens showed practically nil strength due to sliding. Theses orientations are termed as critical orientation. However, at theses orientations, provision of bolts brought substantial strength and modulus enhancement. At other orientations, the strength and modulus enhancement due to bolt is low.

To obtain relationship between the strength and the modulus values of reinforced rocks, the results obtained from UCS tests were plotted on Deere-Miller (1966) classification chart. It is observed that the data points representing jointed rock (both unreinforced and reinforced) lie around a best fitting empirical line starting from intact rock position. The gradient of the best fitting empirical line was used to correlate the strength and modulus of unreinforced and reinforced jointed rocks to the strength and modulus of intact rock.

The following correlations were obtained from the Deere-Miller classification chart for unreinforced and reinforced rock respectively.

$$\frac{\sigma_{cju}}{\sigma_{ci}} = \left[\frac{E_{ju}}{E_i}\right]^{0.67} \tag{8.5}$$

$$\frac{\sigma_{cjr}}{\sigma_{ci}} = \left[\frac{E_{jr}}{E_i}\right]^{0.67} \tag{8.6}$$

where σ_{ci} and E_i = uniaxial compressive strength and modulus of intact rock; σ_{cju} and E_{ju} = uniaxial compressive strength and modulus of unreinforced jointed rock; σ_{jr} and E_{jr} = uniaxial compressive strength and modulus of reinforced jointed rock. The above correlations may be used for estimation of the strength of jointed rock for unreinforced and reinforced conditions using intact rock strength and modulus.

Sakurai's critical stain concept (1983) was also used to find correlation between strength and modulus of intact, unreinforced and reinforced jointed rocks. Independent data from Sakurai (1983) was used for analysis. It was observed that the correlations obtained by using Sakurai's critical stain concept (1983) were almost identical to correlations developed in present study using Deere-Miller classification chart. This indicates universal applicability of the proposed correlations. Further, as

stated by Sakurai (1997) the results obtained from critical strain concept are free from scale effect, it is envisaged that the correlations obtained from the present study should also be scale free.

The proposed correlations (equation 8.5 and 8.6) can be used in the field to find out the strength of rock bolt reinforced rock mass if the values of E_{ju}, and E_{jr} are known. The modulus of unreinforced mass (E_{ju}) can be estimated through uniaxial jacking tests (IS: 7317 (1974)). In case of reinforced mass, the uniaxial jacking tests may not be applicable. Therefore, it is suggested that deformations may be measured in the field (after installation of bolts) and back analysis be done to get the optimal value of the modulus of reinforced rock. Using modulus of the reinforced rock, the strength of the reinforced mass may be obtained which can be used in the further analysis.

8.3.3 Triaxial Strength of Reinforced Natural Rocks

Most of the specimens of unreinforced and reinforced natural rocks tested under triaxial condition failed due splitting. For unreinforced natural rock (at $\sigma_3 = 5$, 20 and 40 MPa) splitting failure mode combined with shearing or sliding was observed. At $\sigma_3 = 5$, 20 and 40 MPa, the reinforced natural rock exhibited splitting failure combined with shearing failure. However, not well defined trend of failure modes with joint inclination was observed. The results of triaxial tests indicated that for unreinforced and reinforced rock, an increase in confining stress increases the σ_1 at all joint orientations. The strength of reinforced rock was found to be more as compared to unreinforced rock. Provision of bolt introduces interlocking in the joint, which enhances the strength. At higher confining stress levels, the strength enhancement due to bolt was low. Provision of bolt also reduces the anisotropy ratio at all confining stress levels. The anisotropy ratio reduces with increase in confining stress. This indicates that at higher confining stress levels, bolt contribution towards strength enlacement is low.

Installation of bolt alters the value of strength parameters (c and ϕ) by introducing interlocking in the joint. The enhancement in cohesion and friction angle was found to be minimum at $\theta° = 40°-50°$.

The variation of σ_1 with σ_3 is found to be non-linear for all the cases investigated in present study. Results obtained from triaxial tests were analysed using Single plane of weakness theory associated with Barton (1976) criterion, Ramamurthy (2001) criterion and Singh and Singh (2012) criterion. The applicability of these criteria in case of reinforced rocks was also investigated. From the analysis it was found that the for sliding cases Barton (1976) failure criterion with Single plane of weakness theory can be used with confidence. However for non-sliding failure, criterion proposed by Singh and Singh (2012) can be used for predicting the strength of unreinforced and reinforced rocks if effect of *JCS* and *JRC* was incorporated. Based on the analysis the following criterion was proposed for reinforced rocks

$$\sigma_1 = \sigma_{cr} + \left(\frac{2\sin(\phi_{i0}+JRC)}{1-\sin(\phi_{i0}+JRC)} + 1\right)\sigma_3 - \frac{1}{JCS}\frac{\sin(\phi_{i0}+JRC)}{1-\sin(\phi_{i0}+JRC)}\sigma_3{}^2 \quad for \ \frac{\sigma_3}{JCS} \leq 0.3 \quad (8.7a)$$

$$\sigma_1 = \sigma_{cr} + \left(\frac{2\sin(\phi_{i0})}{1-\sin(\phi_{i0})} + 1\right)\sigma_3 - \frac{1}{JCS}\frac{\sin(\phi_{i0})}{1-\sin(\phi_{i0})}\sigma_3{}^2 \qquad for \ \frac{\sigma_3}{JCS} > 0.3 \quad (8.7b)$$

where σ_{cr} is the uniaxial compressive strength of reinforced jointed rock. The critical confining pressure of jointed rock (σ_{crtj}) is assumed to be equal to *JCS* of rock. Using equation 8.7 the strength of reinforced jointed rock can be predicted if the value of σ_{cr} is known. To assess the value of σ_{cr} the equation 8.6 can be used.

8.4 CONCLUDING REMARKS

Extensive experimental study has been carried out to understand the behaviour of bolt reinforced blocky mass/jointed rock. Different types of tests were performed on the specimens of natural and synthetic rock without and with passive bolts. The results indicated that the provision of bolts substantially affect the engineering response of jointed rocks. Bolt improves the interlocking of joint and enhances the strength of unreinforced rock. Based on the results, correlations have been suggested to assess the strength of reinforced rock for the different situations in the field. The proposed correlations can be useful for designing the rock bolt support system in the field.

8.5 LIMITATIONS AND SCOPE OF FUTURE WORK

The present study has been limited to behaviour of passive bolts only. Effect of pretensioning has been not considered in the present study. Further, the properties of the bolt and the grout were kept same throughout the experimental investigations. Tests should also be performed by varying the properties of bolts and grout. In case of blocky mass, the joint spacing was kept constant and the joint surfaces were smooth. For general applicability in the field, investigations should be done by varying theses parameters. In the present study, the normal stress was limited to 2 MPa (5% of UCS of intact material). Higher range of normal stress may be used in future study.